uOttawa

L'Université canadienne
Canada's university

FACULTÉ DES ÉTUDES SUPÉRIEURES ET POSTOCTORALES

uOttawa

L'Université canadienne
Canada's university

FACULTY OF GRADUATE AND POSDOCTORAL STUDIES

Sean Langley
AUTEUR DE LA THÈSE / AUTHOR OF THESIS

Ph.D. (Earth Sciences)
GRADE / DEGREE

Department of Earth Sciences
FACULTÉ, ÉCOLE, DÉPARTEMENT / FACULTY, SCHOOL, DEPARTMENT

Characterization and Microbial Reduction of Bacteriogenic Iron Oxides

TITRE DE LA THÈSE / TITLE OF THESIS

Danielle Fortin
DIRECTEUR (DIRECTRICE) DE LA THÈSE / THESIS SUPERVISOR

CO-DIRECTEUR (CO-DIRECTRICE) DE LA THÈSE / THESIS CO-SUPERVISOR

EXAMINATEURS (EXAMINATRICES) DE LA THÈSE / THESIS EXAMINERS

André Lalonde

Frederick Michel

David Lean

Kenneth Nealson

Gary W. Slater
Le Doyen de la Faculté des études supérieures et postdoctorales / Dean of the Faculty of Graduate and Postdoctoral Studies

Characterization and Microbial Reduction of Bacteriogenic Iron Oxides

Roger Sean Langley

Thesis submitted to the Faculty of Graduate and Postdoctoral Studies, University of Ottawa, in partial fulfillment of the requirements for the PhD degree in the Earth Sciences

Ottawa-Carleton Geoscience Centre

and

University of Ottawa

Ottawa, Canada

Your file Votre référence
ISBN: 978-0-494-51815-1
Our file Notre référence
ISBN: 978-0-494-51815-1

Table of Contents

List of Tables

Section 2

Section 3

Section 4

Section 4 (continued)

Section 5

List of Figures

Section 1

Section 2

Section 3

Section 4

Section 4 (continued)

Section 5

Section 5 (continued)

Résumé

La présente étude s'intéresse dans un premier lieu, à la caractérisation minéralogique d'oxydes de fer bactériogeniques, ainsi qu'à leur capacité de sorption (notamment le Sr), et finalement à leur stabilité en présence de bactéries ferro-réductrices. Les oxydes de fer bactériogeniques ont été échantillonnés dans des environnements terrestres marécageux près de Deep River en Ontario, près de sources hydrothermales marines le long de l'arc Kermadec entre la Nouvelle-Zélande et Fidji, ainsi que dans le Tunnel Äspö en Suède. Les analyses par diffraction X et par diffraction des électrons ont démontré que tous les oxydes de fer bactériogeniques étaient essentiellement composés de ferrihydrite. La spectroscopie Mössbauer a aussi confirmé que les oxydes de fer marins hydrothermaux contenaient de la ferrihydrite, ainsi qu'une très petite quantité d'oxydes de fer plus cristallins. Tous les échantillons étudiés contenaient aussi des structures cellulaires s'apparentant aux espèces *Gallionella*, *Leptothrix* et parfois *Mariprofundus*, lesquelles sont des bactéries capables d'oxyder le Fe(II) en Fe(III). Les observations par microscopie électronique ont révélé des phases minérales amorphes encroûtant (épaisseur: 100-200 nm) les bactéries, mais les échantillons d'oxydes de fer marins contenaient aussi quelques minéraux plus cristallisés. Les expériences de sorption de Sr en présence d'oxydes de fer bactériogeniques ont démontré que le métal était immobilisé sous forme de complexe externe, suggérant une sorption réversible. Les analyses EXAFS ont confirmé l'attachement du Sr^{2+} hydraté, mais la technique n'a pas permis de déterminer si la sorption se produisait sur les sites de sorption des oxydes de fer ou sur les sites des cellules bactériennes. Les expériences de réduction en présence de la bactérie ferro-reductrice *Shewanella putrefaciens* CN32 ont indiqué que tous les oxydes de fer bactériogeniques étaient plus susceptibles à la réduction microbienne que la

ferrihydrite synthétique. Ceci suggère que les oxydes de fer bactériogeniques ne sont pas stabilisés lors de leur précipitation sur des surfaces microbiennes. Finalement, tout le Sr sorbé à la surface des oxydes de fer bactériogeniques a été remis en solution lors de leur réduction microbienne, indiquant que le Sr est principalement sorbé sur les oxydes de fer et non pas sur la matière organique. L'utilisation d'oxydes de fer biogéniques pour atténuer le transport de métaux lourds (comme Sr) dans l'environnement devra donc prendre en compte leur réactivité sous des conditions réductrices.

Abstract

The main objectives of the present study were to first determine the chemical and mineralogical composition of bacteriogenic iron oxides (BIOS) collected from various locations (i.e., wetlands near Deep River, Ontario, hydrothermal sea vents along the Kermadec Arc between New-Zealand and Fiji, and from the Äspö tunnel in Sweden), to assess their sorptive capacity for Sr and to measure their rates of reduction in the presence of a well known iron-reducing bacterium. X-ray diffraction (XRD) and selected area electron diffraction indicated that both marine and freshwater BIOS were composed of the iron mineral, 2-line ferrihydrite, in combination with cellular structures of known iron-oxidizing microbes such as *Gallionella* spp., *Leptothrix* spp., and *Mariprofundus* spp. Mössbauer spectroscopy of marine BIOS confirmed 2-line ferrihydrite as the dominant mineral phase, but a small fraction of more crystalline oxides may also have been present (as detected by XRD). Using electron microscopy, the mineral phases were typically observed as 100-200 nm thick crusts of poorly structured material, attached to the surfaces of the associated microbial debris. Some well-defined crystal habits were observed in one marine sample.

Sorption experiments showed that BIOS were effective adsorbents of dissolved strontium. Sorption isotherms indicated that Sr was bound to the BIOS via reversible outer-sphere complexation. Extended X-ray absorption fine structure (EXAFS) confirmed binding of hydrated Sr^{2+} but failed to elucidate whether sorption occurred to sites specific to the iron or organic component of the BIOS. All BIOS samples were more susceptible to microbial Fe(III) reduction than was synthetic 2-line ferrihydrite. This suggests that BIOS are not stabilized by precipitation along microbial surfaces, and that the use of synthetic analogs to model BIOS reactivity is insufficient. Reduction of BIOS resulted in the complete dissolution of the iron mineral phase, and a nearly complete solubilization of the sorbed Sr. This suggests that sorption occurs primarily to sites within the iron oxide component. In a natural BIOS deposit, levels of dissolved Sr in BIOS porewaters were elevated at depths where Fe(II) was also elevated, and levels of dissolved Sr were 2 to 3 times higher in aquifer waters that did not contain BIOS. These data suggest that BIOS may represent a natural means of Sr attenuation, provided oxidizing conditions are maintained.

Acknowledgements

I would like to dedicate this thesis to the memory of my MSc supervisor, Dr. Terry J. Beveridge. Terry's enthusiasm for science and research started me down this path, and he helped to guide my first steps along it. He will be deeply missed by the many researchers whose careers he influenced.

Completion of this degree would not have been possible without the love and support of my wife, Amanda. Throughout our years together she has been a constant source of strength and inspiration. I only hope that I can provide the same for her in the years to come. We would both like to express appreciation to our families for their support and understanding during our many long absences from "home".

A special *gros merci* to my friend and supervisor (in that order), Dr. Danielle Fortin, first for her always upbeat and positive attitude, and also for her years of support and encouragement (even as I depleted her travel budget – *arigato gozaimasu Fortin-sensei!*). I would also be remiss if I did not thank her husband, Keith Anderson, first for selling Ottawa, but also for dropping creamy beats and co-hosting the coolest lab meetings ever.

I am indebted to all the members of the Fortin Lab (past and present), often for their help, but mainly for their friendship. Four years would have seemed much longer if not for their presence in the lab. I hope our friendship and collaborations will continue well into the future.

Finally, I would like to acknowledge the generous financial support of the Natural Sciences and Engineering Research Council of Canada, the Ontario Graduate Scholarship Program, and the University of Ottawa.

Introduction

The research described in this thesis examines the reactivity of bacteriogenic iron oxides (BIOS), which are fine-grained oxides of ferric iron, formed as a result of ferrous iron oxidation in the presence of microbial cells and cell surfaces. Fine-grained iron oxides are often reported as a reactive component in soils and sediments at the Earth's surface (Drever, 1997). In oxygenated waters, these nano- and micro-scale minerals can have an effect on contaminant flow, by adsorbing dissolved chemical species, thereby limiting their migration (Langmuir, 1997; Cornell and Schwertmann, 2003). Under anoxic conditions, however, iron oxides are susceptible to reductive dissolution by dissimilatory iron-reducing bacteria (DIRB), which may cause a release of adsorbed contaminants back into the aqueous (mobile) phase. Reduction of Fe(III) oxides and hydroxides is often modeled in vitro using various synthetic, hydrated ferric oxides (HFO) such as ferrihydrite and goethite (Glasauer et al., 2003). These minerals are assumed to comprise the bulk of iron oxides in soils and sediments, often being present as coatings on larger mineral grains such as sand (Drever, 1997). More crystalline iron oxides, such as hematite, have also been studied (Roden, 2003). In addition to synthetic forms, geogenic iron oxides are also commercially available as standard reference materials. While much literature exists on the reactivity of synthetic and geogenic iron oxides, very little exists on the study of BIOS. Due to differences in the precipitation of the mineral, and the large amounts of organic material associated with BIOS, it seems reasonable to suggest that the bulk material might exhibit markedly different physico-chemical properties, hence making the use of synthetic and geogenic analogs invalid for extrapolation to BIOS systems.

Reports of known or suspected marine BIOS deposits have been published for Loihi Seamount, Axial Seamount, and Volcano 19 of the Tonga-Kermadec Arc (Emerson and Moyer, 2002; Kennedy et al., 2003; Stoffers et al., 2006). However, while most work has focused on elaborating the microbial community structure within the BIOS, only one analysis (Kennedy et al., 2003) on the reactivity of the iron oxide phase has been published, to date. With respect to freshwater environments, there are several reports describing the deposition of BIOS in both groundwater and surface water flow systems (James and Ferris, 2004). However, all but one of these studies focuses on BIOS deposits of the Stråssa mine complex and Äspö Hardrock Research Laboratory in Sweden, and only two of these (Ferris et al., 1999, 2000) have examined the reactivity of the BIOS (specifically, as it pertains to metal ion sorption). No literature is currently available on the anaerobic reduction of BIOS, nor on the effect of BIOS reduction on contaminant desorption. Consequently, the research presented here represents the first data available on the microbial reduction of various natural BIOS samples (both marine and freshwater), and on the effect of BIOS reduction on the release of a sorbed contaminant (i.e., strontium). It is also the first research to examine the mechanisms of Sr sorption to BIOS.

The thesis is divided into five sections. The first is a broad introduction to the available literature on biogenic iron oxides. The following four sections represent separate submissions made to peer-reviewed journals, based on original research conducted over the course of study. Each submission covers a particular aspect of BIOS reactivity, and the specific objectives of each are outlined in detail in their respective introductory sections. However, to serve as a brief outline to the organization of the entire thesis, the overall objectives and hypotheses are briefly described as follows:

1) to characterize various known BIOS with respect to their mineralogy, with particular emphasis on the iron oxide phase(s); it was hypothesized (based on available literature) that BIOS are composed primarily of amorphous or poorly ordered iron oxyhydroxides.
2) to determine the sorptive properties of BIOS with respect to strontium (Sr), a contaminant of interest at the primary study site; it was hypothesized that BIOS would be effective sorbents of dissolved Sr.
3) to determine the stability of various BIOS when subjected to anaerobic, dissimilatory Fe(III) reduction, and to compare the reduction rates of BIOS to those of mineralogically similar, synthetic analogs; it was hypothesized that the precipitation of the BIOS on microbial cell surfaces would act to stabilize the BIOS and make them less susceptible to reduction than similar oxide minerals precipitated from chemically pure solutions.
4) to determine the effect of dissimilatory Fe(III) reduction in BIOS on the retention of adsorbed Sr; it was hypothesized that reduction of the BIOS would lead to partial dissolution of the iron oxide component, possibly resulting in the release of adsorbed Sr.
5) to provide a preliminary characterization of putative BIOS from two previously unstudied submarine hydrothermal systems, with particular emphasis on the mineralogy and microbiology of the sediments, and to determine rates of Fe(III) reduction in those sediments; it was hypothesized that differences in the depositional environment between the two sites would lead to differences in iron oxide crystallinity and, therefore, reduction rate.

References

Cornell, R.M., and Schwertmann, U. 2003. The iron oxides: structure, properties, reactions, occurrence and uses. VCH, Weinheim, Germany.

Drever, J.I. 1997. The geochemistry of natural waters: surface and groundwater environments. Prentice-Hall, Inc., New Jersey, USA.

Emerson, D., Moyer, C.L. 2002. Neutrophilic Fe-oxidizing bacteria are abundant at the Loihi seamount hydrothermal vents and play a major role in Fe oxide deposition. Appl. Environ. Microbiol. 68:3085-3093.

Ferris, F.G., Konhauser, K.O., Lyvén, B., Pedersen, K. 1999. Accumulation of metals by bacteriogenic iron oxides in a subterranean environment. Geomicrobiol. J. 16:181-192.

Ferris, F.G., Hallberg, R.O., Lyvén, B., Pedersen, K. 2000. Retention of strontium, cesium, lead and uranium by bacterial iron oxides from a subterranean environment. Appl. Geochem. 15:1035-1042.

Glasauer, S., Weidler, P.G., Langley, S., Beveridge, T.J. 2003. Controls on Fe reduction and mineral formation by a subsurface bacterium. Geochim. Cosmochim. Acta. 67:1277-1288.

James, R., Ferris, F.G. 2004. Evidence for microbial-mediated iron oxidation at a neutrophilic groundwater spring. Chem. Geol. 212:301-311.

Kennedy, C.B., Martinez, R.E., Scott, S.D., Ferris, F.G. 2003. Surface chemistry and reactivity of bacteriogenic iron oxides from Axial Volcano, Juan de Fuca Ridge, north-east Pacific Ocean. Geobiology. 1:59-69.

Langmuir, D. 1997. Aqueous environmental geochemistry. Prentice-Hall, Inc., New Jersey, USA.

Roden, E.E. 2003. Fe(III) oxide reactivity toward biological versus chemical reduction. Environ. Sci. Technol. 37:1319-1324.

Stoffers, P., Worthington, T.J., Schwarz-Schampera, U., Hannington, M.D., Massoth, G.J., Heknian, R., Schmidt, M., Lundsten, L.J., Evans, L.J., Vaiomo'unga, R., Kerby, T. 2006. Submarine volcanoes and high-temperature hydrothermal venting on the Tonga Arc, southwest Pacific. Geology. 34:453-456.

Section 1

Formation and occurrence of biogenic iron-rich minerals

A previous version of this manuscript has been published in *Earth Science Reviews*[1].

It has been updated for the purposes of this dissertation to include the most recent literature.

[1] Fortin, D., Langley, S. 2005. Formation and occurrence of biogenic iron-rich minerals. Earth Sci. Rev. 72:1-19.

Abstract

Iron cycling in the Earth's crust depends on redox reactions, which often trigger the precipitation and dissolution of Fe-rich minerals. Microbial activity is also an integral part of iron cycling, through carbon fixation, respiration and passive sorption reactions. Iron oxides formed in close association with bacteria (either as internal or external precipitates) are referred to as biogenic minerals. They form in several types of environments on Earth, from freshwater to marine systems, aquifers, soils and mining impacted systems. Biogenic iron oxides generally occur as nano-crystals and show a wide range of morphology and mineralogy. These minerals form as a result of the direct metabolic activity of bacteria or as a result of passive sorption and nucleation reactions. The metabolic activity of acidophilic and neutrophilic iron-oxidizing bacteria under oxic conditions promotes the oxidation of Fe(II) to Fe(III) and the precipitation of biogenic iron oxides as extracellular precipitates near or on the bacterial cells. Iron oxidation under anoxic conditions can also occur, as a result of the activity of nitrate-reducers and photoautotrophic bacteria using Fe(II) as an electron donor. Secondary Fe-oxide formation has also been reported during the microbial reduction of iron oxides. Passive Fe sorption and nucleation onto bacterial cell walls represents another important mechanism leading to iron oxide formation. The surface reactivity of the bacterial surface under environmental pH conditions confers a net negative charge to the cell wall, which leads to the binding of soluble iron and eventually to the precipitation of iron oxides under saturation conditions. Extracellular polymers produced by bacteria can also act as a template for iron sorption and Fe-oxide nucleation. Intracellular iron oxide formation has also been observed in natural environments. Magnetotactic bacteria produce intracellular magnetosomes, occurring as chains of magnetite crystals within the

cells. An unidentified iron-rich mineral phase also forms inside *Shewanella* cells during the anaerobic reduction of ferrihydrite. Several studies have clearly shown that biogenic iron oxides form in present-day environments, but they might also be important components of ancient geological formations, such as banded-iron formations (BIF). BIF formation is still being debated, but there is now strong evidence that bacteria, more specifically, phototrophic iron oxidizers and possibly iron reducers might have been involved. Thus, iron oxides represent a potential tool in the search for past and present life on Earth and other planetary systems. Despite the promising use of Fe-isotopes and magnetosomes, there is still no clear proof that they can form only as a result of biological activity. In fact, Fe isotope fractionation of abiotic iron oxides is often similar to that of biogenic oxides and the specific mineralogical characteristics of magnetite crystals present inside magnetotactic bacteria can be reproduced under abiotic conditions. In summary, the role of bacteria in iron cycling has been the focus of several studies in the last few decades, but clearly, more research is needed in order to fully assess the role of microorganisms in their formation.

Keywords: iron oxides, bacteria, biosignatures, ferrihydrite, lepidocrocite, magnetite

1 Introduction

Iron, which represents the fourth most abundant element in the earth's crust, has been the focus of several studies in recent years, because of its importance in biogeochemical redox reactions in marine and freshwater environments (Edwards et al., 2004; Emerson and Weiss, 2004; Kappler and Newman, 2004; Roden et al., 2004; Bach and Edwards, 2003; Straub et al., 2001, etc.). Global iron cycling is driven by both abiotic and biotic reactions. In the presence of oxygen and at circumneutral pH conditions, ferrous iron is quickly oxidized to Fe(III) and precipitates as iron oxides (Stumm and Morgan, 1996). Under the same pH conditions, but also at low pH, several microorganisms can oxidize Fe(II) to Fe(III) and gain energy from the reaction (see reviews by Baker and Banfield, 2003; Emerson, 2000). Recently, there has also been a lot of interest in the role of bacteria in Fe(II) oxidation under anoxic conditions (Widdel et al., 1993; Straub et al., 1996; 2004; Kappler and Newman, 2004) and in their role in the rapid cycling of iron at oxic-anoxic interfaces in sediments (Roden et al., 2004). Under anoxic conditions, some iron oxides undergo reduction as a result of abiotic reactions (Poulton et al., 2004) or microbial anaerobic respiration (Lovley, 2000; Emerson and Weiss, 2004). These oxidation and reduction reactions take place in marine and freshwater environments, such as lake sediments, aquifers, soils, wetlands, deep-sea vent environments and in man-made settings, like mine tailings impoundments. In addition to these oxidation-reduction reactions, several studies have also reported the presence of intracellular Fe-rich minerals inside bacterial cells in aquatic environments (Blakemore, 1975; Bazylinski et al., 1988; 1993).

In natural environments, iron oxides include poorly ordered minerals (i.e., green-rust and ferrihydrite) and more crystalline forms, such as goethite, lepidocrocite, hematite and

magnetite (Fortin and Chatellier, 2003). They accumulate in sediments and are thought to play an important role in the sorption of trace elements, including heavy metals and nutrients (Fortin et al., 1993; Tessier et al., 1996).

Several studies have documented the formation and occurrence of iron oxides formed as a result of both biotic and abiotic pathways in natural environments (Bazylinski et al., 1988; 1993; Fortin et al., 1993; 1998; Emerson et al., 1999; Banfield et al., 2000; Kennedy et al., 2003a; 2003b; James and Ferris, 2004). Given the fact that biogenic iron oxides, i.e., iron oxides found in close association with microorganisms, display physico-chemical characteristics that are similar to their abiotic counterparts, it however remains difficult to ascertain the exact role of microbes in their formation (Fortin, 2004). This paper is divided into 5 sections, i.e., the characteristics, formation and involvement of bacteria in extracellular (section 2) and intracellular (section 3) iron oxide formation, the occurrence of iron oxides in ancient geological formations (section 4) and a brief discussion of the potential use of biogenic iron oxides as biosignatures (section 5). While the focus of this paper is on iron oxides, it is clear that other iron-rich minerals (such as iron silicates, sulfides, carbonates and phosphates) exist in natural environments and that they also occur in close association with microorganisms (Fortin and Beveridge, 1997; Brown et al., 1999; Ueshima and Tazaki, 2001, Ueshima et al., 2004). These minerals are however not discussed in this paper.

2 Extracellular iron-rich minerals

In natural sediments, iron oxide particulates often occur in the close vicinity of bacterial cell walls (Fig. 1a) and bacterial exopolymers (Fig. 1b). These minerals are referred

to as extracellular biogenic iron oxides. Iron oxides forming inside bacterial cells are referred to as intracellular biogenic minerals and are discussed in section 3.

2.1 Occurrence and mineralogy of extracellular biogenic iron oxides

The most common iron oxides include oxides (e.g., hematite, magnetite), oxyhydroxides (e.g., goethite, lepidocrocite, akaganeite) and amorphous to poorly ordered phases (e.g., 2-line and 6-line ferrihydrite) (Cornell and Schwertmann, 1996). Natural biogenic iron oxides generally occur as small crystals (2-500 nm) and contain "impurities", such as sorbed or structural Si, PO_4^{3-}, SO_4^{2-}, Mn^{4+}, Al^{3+}, etc. (Fortin and Châtellier, 2003 and references therein). In freshwater lakes (sediments and water column), amorphous iron oxides, 2-line ferrihydrite and lepidocrocite have been identified on bacterial cell walls and extracellular exopolymers (Fig 1a) (Tipping et al., 1989; Fortin et al., 1993). The same bacterial-iron oxide associations have also been observed near the roots (in the iron plaque) of aquatic plants in wetlands (St-Cyr et al., 1993; Emerson et al., 1999). In Fe-rich seepage areas, amorphous Fe-oxides and ferrihydrite closely associated with neutrophilic Fe-oxidizing bacteria have also been identified (Fig. 2) (James and Ferris, 2004). In deep aquifers, Brown et al. (1999) reported the presence of poorly ordered iron oxides, ferrihydrite and hematite, in close association with bacteria within a biofilm, whereas poorly ordered iron oxides, and possibly hematite, were intimately associated with neutrophilic iron-oxidizing bacteria in a seepage zone in an underground tunnel (Ferris et al., 1999; Hallberg and Ferris, 2004). In the ocean, the oxidation of reduced iron originating from deep-sea vents provides energy for several lithoautrophic bacteria (Edwards et al., 2004; Emerson et al., 2007), which often leads to the precipitation of biogenic iron oxides. Several

studies of various vent systems around the world (see review article by Little et al., 2004 and references therein) have reported the presence of amorphous Fe-oxides and ferrihydrite, as the dominant iron oxides associated with bacteria. In anoxic environments, ferrihydrite and magnetite might also form as a result of bacteria capable of coupling Fe(II) oxidation to nitrate reduction (Benz et al., 1998; Chaudhuri et al., 2001). Magnetite is also a common by-product of iron reduction by dissimilatory iron-reducing bacteria in anaerobic environments (Lovley et al., 1986; Johnson et al., 2005). In addition, the activity of photoautotrophic bacteria using Fe(II) as an electron donor during anoxygenic photosynthesis produces ferrihydrite which transforms upon aging to more crystalline iron oxides, such as goethite and lepidocrocite (Kappler and Newman, 2004). In acidic hot-spring environments, microbes can become mineralized in iron-rich precipitates including jarosite and hydrous ferric oxides (Jones and Renaut, 2007). Finally, in environments impacted by mining activity, where iron is often abundant, amorphous iron oxides often encrust bacterial cells in mine tailings (Fig. 1a) (Fortin et al, 1995); whereas biogenic schwertmannite-like minerals have been identified in acidic mine drainage streams (Akai et al., 2001). Chan et al. (2004) also recently reported that akaganeite and ferrihydrite formed on the surface of bacterial exopolymers in the water of a submerged mine and showed that the exopolymers acted as a template for Fe-oxide nucleation. At the same site, Banfield et al. (2000) identified nano-crystals of 2-line ferrihydrite on the sheath and stalk of neutrophilic iron-oxidizing bacteria.

2.2 Role of bacteria in biogenic iron oxide formation

Biotic reactions responsible for the formation of biogenic iron oxides include the microbial oxidation of Fe(II) to Fe(III) by a wide range of microorganisms under both acidic

and neutral pH and oxic and anoxic conditions. Iron oxide formation also occurs as a result of passive reactions, whereby *in situ* chemical conditions favour the precipitation of the minerals on biological surfaces, namely bacterial cell walls and extracellular material. These reactions are considered passive because the microbes do not gain energy from the oxidation and nucleation processes, but simply act as binding and nucleation surfaces (Châtellier et al., 2001; 2004; Châtellier and Fortin, 2004). pH changes triggered by microbial metabolic activity and the production of certain bacterial exudates might also favour Fe-oxide formation (Ehrlich, 2002). These reactions are considered passive as well.

2.2.1 Biotic reactions

The chemical and microbial oxidation of Fe(II) to Fe(III) depends on the pH and the O_2 concentration. *Gallionella* spp. and *Leptothrix* spp. are the most commonly observed bacteria in association with biogenic iron oxides in neutral pH environments (Emerson and Weiss, 2004). They are considered microaerophilic bacteria, i.e., they are gradient bacteria with regard to oxygen concentration (Hallberg and Ferris, 2004). Other neutrophilic Fe-oxidizing bacteria have recently been discovered in groundwater and hydrothermal vents (Emerson and Moyer, 1997; 2002; Emerson et al., 2007), on the seafloor near deep-sea vents (Edwards et al., 2003; 2004) and in wetland sediments (Sobolev and Roden, 2004). The ability of these bacteria to derive energy from the oxidation of Fe(II) at neutral pH has always been somehow a controversial issue (Sobolev and Roden; 2004), because the microorganisms have to compete with the rapid abiotic oxidation of Fe(II). However, evidence of chemolithotrophy with bacteria associated with Fe(II) oxidation at neutral pH have been reported (Hallbeck and Pedersen, 1991; Emerson and Moyer, 1997). Moreover,

the novel organism *Mariprofundus ferrooxydans* has been shown to be an obligate iron-oxidizer, such that Fe(II) and Fe(0) are the only energy sources capable of supporting growth of the organism (Emerson et al., 2007). Passive sorption of Fe-oxides (as on the sheath of *Leptothrix* spp.) is also possible, along with dissolved iron sorption and precipitation (Emerson and Weiss, 2004). At the present time, it remains very difficult to clearly differentiate between true biogenic Fe-oxides and those formed as a result of abiotic reactions in natural samples containing neutrophilic Fe-oxidizers.

In acidic environments, where the oxidation rate of Fe(II) is nearly pH-independent (Stumm and Morgan, 1996), iron oxidation is catalyzed by a wide range of iron-oxidizing bacteria. However, the free energy yield of the Fe(II) oxidation under acidic conditions is barely sufficient to synthesize ATP and large quantities of iron must be oxidized to sustain growth (Ehrlich, 2002). *Acidithiobacillus* spp. (γ-Proteobacteria) is by far the most studied group of bacteria capable of gaining energy from the oxidation of Fe(II) to Fe(III) at very low pH (Baker and Banfield, 2003). For example, Jones and Renaut (2007) recently attributed the formation of goethite and lepidocrocite within an acidic hot-spring to *Acidithiobacillus*-like cells, and *A. ferrooxidans* has been implicated in the formation of unusual iron-oxide nodules from sedimentary deposits in Japan (Yoshida et al., 2006). However, *Acidithiobacillus* might not be the most relevant bacterium in acidic environments, as shown by the study of Schrenk et al. (1998) at Iron Mountain, California. These authors reported that at very low pH (0.7 to 1.0), *Leptospirillum ferrooxidans* could be the key player in the catalysis of sulfide oxidation by ferric iron. At the same site, but under extremely acidic conditions (pH = - 0.5), Edwards et al. (2000) isolated an archean Fe-oxidzing bacteria closely related to *Thermoplasmales*. In other acidic environments, α-, β-,

and γ-Proteobacteria have also been identified and are thought to play a role in either iron or sulfur oxidation (see review by Baker and Banfield, 2003).

Recent studies have also shown that microbial Fe(II) oxidation is not limited to oxygenated environments, but also occurs under anoxic pH-neutral conditions (Kappler and Newman, 2004; Sobolev and Roden, 2004; Straub et al., 2001; 2004). Photoautotrophic bacteria gain energy from the oxidation of Fe(II) and use light energy for CO_2 fixation (Widdel et al., 1993). These bacteria include sulfur bacteria, purple non-sulfur and sulfur bacteria (Kappler and Newman, 2004 and references therein). It is thought that Fe(II) oxidation takes place on the cell surface and that Fe(III) is released as a soluble inorganic or colloidal entity (Kappler and Newman, 2004). Iron oxide nucleation likely happens in the vicinity of the cell wall. Fe(II) oxidation under anoxic conditions can also be coupled to nitrate reduction, according to Straub et al. (2001, 2004), who showed that the ability to oxidize iron with nitrate is widespread amongst the Proteobacteria. The same studies have also indicated that the ferrihydrite formed during the reduction of nitrate is rapidly reduced by iron reducing bacteria, creating a rapid Fe redox cycling in anoxic natural sediments (Roden et al., 2004). Microbial Fe(II) oxidation can also be coupled to perchlorate reduction (Lack et al., 2002).

Finally, Pósfai et al. (2006) have reported the unusual production of extracellular, cell-bound hematite particles by a weakly magnetotactic bacterium, *Desulfovibrio magneticus* RS-1. The particles are actually aggregates of smaller (5 to 10 nm) grains of hematite. Each particle is surrounded by an organic polymeric substance, which implies a biogenic mineralization process, although the precise mechanism of formation is still unknown.

The precipitation of iron oxides on or near the cell wall of bacteria brings up two interesting questions. What do microorganisms gain from promoting mineral nucleation? And how to they cope with it? It seems possible that mineral precipitation on the cell wall likely acts as a barrier to the transport of metabolic material through the cell membrane. In the case of neutrophilic Fe-oxidizers (such as *Leptothrix* and *Gallionella*), the production of layers of exopolysaccharides (i.e., sheath) or twisted stalks around the cells protects the cell itself from encrustation (Hallberg and Ferris, 2004). Another explanation is that bacteria favour or promote mineral formation to prevent cell entombment and death by mineral metabolic by-products (Fortin, 2004 and references therein). Recently, a novel explanation has been proposed by Chan et al. (2004). According to these authors, neutrophilic iron-oxidizing bacteria promote Fe-oxide formation onto extracellular polymers in order to enhance metabolic energy generation. The oxidation of Fe(II) increases the pH gradient across the cell membrane, which in return increases the proton motive force and the energy generating potential of the cells (Chan et al., 2004). This suggests that mineral precipitation on bacterial cells might represent a survival mechanism (Fortin, 2004).

2.2.2 Abiotic passive reactions

Passive reactions linked to biogenic Fe-oxide formation are related to the reactivity of the bacterial cell wall. Most bacteria possess a net negative surface charge resulting from the deprotonation of the components of the cell wall and extracellular material (Fortin et al., 1997, Daughney and Fortin, 2002 and references therein). Electrostatic attraction between negatively charged bacteria and positively charged minerals (like iron oxides), along with the hydrophobicity of either substrate, often lead to the sorption of minerals onto the cell

wall (Glasauer et al., 2001). Bacterial cell walls (Gram-negative and Gram-positive bacteria) and extracellular exopolymers possess several types of surface reactive sites that can also bind soluble Fe and other metals (Fein et al., 1997; Yee and Fein, 2001; Daughney et al., 2001; Châtellier and Fortin, 2004). Laboratory experiments with pure bacterial cultures have shown that Fe(III) sorption onto bacterial cell walls can lead to Fe-oxide nucleation under saturation conditions (Warren and Ferris, 1998). Châtellier et al. (2001; 2004) have also shown that the rapid abiotic oxidation of Fe(II) at pH 7 in the presence of various bacteria promotes the formation of lepidocrocite and ferrihydrite near and on the bacterial cell wall (Fig. 3). In simple systems containing only Fe and cells, the presence of bacteria affected the morphology of the lepidocrocite crystals when compared to abiotic systems (Châtellier et al., 2001). However, in systems containing iron and bacteria, along with Si, SO_4^{2-} or PO_4^{3-} in concentrations typically found in freshwater sediments, the presence of bacteria had very little effect on the morphology of the iron oxides, suggesting that the anionic species were the dominant factor controlling the nucleation and precipitation of the oxides. These studies indicate that it is very difficult to determine whether bacterial surfaces actually serve as templates for iron oxide formation in the environment. Evidence of bacterial templating has, however, been demonstrated by Chan et al. (2004) in their study of Fe-oxide formation on bacterial exopolymers in pH-neutral Fe-rich waters. With the use of high-resolution transmission electron microscopy (HRTEM) observations and X-ray absorption near-edge spectroscopy (XANES) analyses, these authors showed that a microbially-derived organic rich template promoted the formation of elongated crystals of akaganeite. Laboratory experiments with alginate as a synthetic template also led to the development of similar akaganeite crystals. Such results represent an important step in the understanding of bacterial

involvement in iron oxide formation and might lead to the development of better characterization tools to assess the true origin of iron oxides in present and past environments.

3 Intracellular Iron-Rich Minerals

3.1 Introduction – magnetotactic bacteria

Bacteria produce a variety of organic and inorganic intracellular polymers, including polyphosphate granules (Chavez et al., 2004), polyhydroxybutyrate granules (James et al., 1999), sulfur granules (Rosetti et al., 2003), and selenium nanospheres (Oremland et al., 2004). However, the production of inorganic, metal-rich, intracellular minerals is remarkably rare among prokaryotic genera. The first indication that bacteria may be capable of producing intracellular minerals came with the discovery of magnetotaxis by Richard Blakemore (1975). Using optical microscopy of marine marsh mud samples, Blakemore observed microorganisms that rapidly swam toward one side of the mud droplet he had placed on his microscope slides. He noted that the direction in which the cells swam changed when he placed small magnets near the slides, and concluded that the cells' migration was being directed by the earth's geomagnetic field – a process he termed magnetotaxis (Blakemore, 1975). Transmission electron microscopy, coupled with energy dispersive X-ray spectroscopy, revealed that the magnetotactic cells contained intracellular chains of 5-10 membrane-bound, crystal-like particles that were electron-opaque and rich in iron. The phenomenon of intracellular mineral production by bacteria was confirmed when Frankel et al. (1979) provided the first proof of the production of intracellular magnetite in magnetotactic bacteria. The small, magnetic particles originally discovered by Blakemore

(1975) are today known as magnetosomes (Balkwill et al., 1980), and they are the defining characteristic of all magnetotactic bacteria.

3.1.1 Occurrence – magnetotactic bacteria and their environments

The term "magnetotactic bacteria" encompasses a range of prokaryotes including anaerobic, sulfate-reducing bacteria such as *Desulfovibrio magneticus* (Sakaguchi et al., 1993), microaerophilic species such as *Magnetotacticum bavaricum* (Spring et al., 1993) and *Magnetospirillum gryphiswaldense* (Schleifer et al., 1991), and even multicellular bacterial aggregates (Farina et al., 1990, Mann et al., 1990). While the majority of magnetotactic species belong to the α-subclass of the Proteobacteria, representative species have also been ascribed to the δ-subclass, and also to the phylum Nitrospira (DeLong et al., 1993). All of the species and strains described to date are members of the domain Bacteria (i.e., there are, as yet, no reports of magnetotactic members of the domain Archaea). They are all motile by means of flagella, with Gram-negative cell wall architecture (i.e., a cytoplasmic membrane and an outer membrane, separated by a layer of peptidoglycan), and they all possess a respiratory metabolism requiring anaerobic or microaerophilic environments (Bazylinski and Frankel, 2004).

Microaerophilic species are commonly found in soils (Fassbinder et al., 1990) and freshwater and marine sediments (Sparks et al., 1986), or suspended within the water column of chemically stratified freshwater environments. In such environments, they are present in highest abundance at the so-called oxic-anoxic transition zone (OATZ; Bazylinski et al., 1993). This zone typically forms at the sediment/water interface in freshwater environments, or in marine environments at depths where oxygen diffusion becomes limited. Spring et al.

(1993) determined that a particular genus (*Magnetotacticum bavaricum*) was the dominant organism in this region of their sampling site, with cell densities approaching 7×10^5 cells cm^{-3}, as measured using flow cytometry, DAPI (4',6-diamidino-2-phenylindole) staining and fluorescent in situ hybridization (FISH). *M. bavaricum* represented as much as 30% of the entire microbial volume within the OATZ (Spring et al., 1993).

One of the first examples of anaerobic magnetosome production was reported by Bazylinski et al. (1988), but the organism was also capable of microaerophilic growth and therefore is not considered a strict anaerobe. However, in 1993, Sakaguchi and co-workers isolated an obligately anaerobic strain from sulfide-rich mud. The cells exhibited strong negative taxis from dissolved oxygen, and accumulated only within anoxic regions of cell suspensions (Sakaguchi et al., 1993). Further, Petermann and Bleil (1993) determined that, for marine environments, maximum concentrations of magnetotactic bacteria occur in the anaerobic zones of sediments collected at depths of about 3000 m below sea level. Here, the distribution of cells within various strata of the sediments suggested a metabolic dependence on the reduction of nitrate or other nitrous oxides (Petermann and Bleil, 1993). This finding is consistent with laboratory results, which have implicated a role for nitrate reduction in the growth of magnetotactic bacteria (Guerin and Blakemore, 1992). The findings of Petermann and Bleil (1993) also show that, despite their dominance in the freshwater OATZ, the majority of magnetotactic bacteria residing within ocean sediments are likely anaerobes.

3.1.2 Magnetosomes – Mineralogy and Morphology

Most single magnetosome crystals are approximately 35-120 nm long (Bazylinski et al., 1994). This places magnetosomes into the theoretical size range of single domain

magnets with permanent dipole moments (Diaz-Ricci and Kirschvink, 1992; Moskowitz, 1995; Fabian et al., 1996). Larger magnetosomes (greater than 120 - 200 nm long) have been described (Farina et al., 1994; Spring et al., 1998), however their magnetic properties have yet to be fully elucidated.

Two types of magnetosome mineral have been reported. The first to be described (Frankel et al., 1979) was the iron oxide, magnetite (Fe_3O_4). Later it was discovered that magnetotactic cells were also capable of synthesizing greigite, an iron sulfide mineral that is analogous (Fe_3S_4) to magnetite (Farina et al., 1990; Mann et al., 1990). In addition, several other (non-magnetic) intracellular, iron-rich mineral phases have been reported, including mackinawite (FeS; Pósfai et al., 1998) and unidentified iron hydroxides (Lins and Farina, 2001; Taylor and Barry, 2004). However, each of these non-magnetic phases is believed to be only a transient precursor to the final, magnetic mineral. Pyrite (FeS_2) has been described in cells of a greigite-producing strain (Mann et al., 1990), as has pyrrhotite (Farina et al., 1990). However these minerals may have been incorrectly identified due to inaccuracies with the electron diffraction used to characterize them (Lins and Farina, 2001). While important to mention, the iron sulfide magnetosomes fall outside the scope of this paper and we will therefore attempt to limit our discussion to magnetite-containing magnetosomes.

To date, three general classes of crystal morphology have been reported for magnetite magnetosomes. The first type includes cuboidal or cubo-octahedral, which have been described in *Magnetospirillum magnetotacticum* (Balkwill et al., 1980) and other species (Mann et al., 1990). This is the simplest of the three magnetosome crystal types, and it retains the cubic crystal geometry characteristic of abiotic magnetite. The second crystal type is elongated hexa- or octahedral. This crystal type appears rectangular, has been

reported in a variety of magnetotactic cells (Lins and Farina, 1998), and was thought to be distinct from inorganic magnetite in that it displays elongation along the [111] crystal axis (Meldrum et al., 1993). Finally, a variety of elongated, cubo-octahedral forms exist that are all geometrically irregular (Bazylinski et al., 1993; Schüler and Frankel, 1999; Taylor and Barry, 2004), but similar in appearance (such as tooth-, arrowhead- and bullet-shaped crystals). While species-to-species variations in crystal morphology exist, the production of a particular type appears to be biochemically regulated, such that cells of the same species will only produce magnetosomes of the same morphological type (Bazylinski et al., 1994). The apparently unique physico-chemical properties of some bacterial magnetite crystals has led to speculation (McKay et al., 1996; Thomas-Keprta et al., 2001) that they can be used as potential biomarkers in the search for past life on Earth and other planets (see section 5).

3.1.3 Magnetosome formation

Within most magnetotactic cells, magnetite production is strictly confined to the lumens of magnetosome vesicles (Balkwill et al., 1980; Gorby et al., 1988). Gorby et al. (1988) found evidence of some empty magnetosome vesicles, and some which were only partially filled with an amorphous iron phase, suggesting that the vesicle is formed first, and is later filled in as iron is deposited within it. Nakamura et al. (1995a; 1995b) have identified a proton-Fe(II) antiporter protein which may be involved in transporting ferrous iron across the vesicle membrane in *Magnetospirillum* (strain AMB-1) cells. Genes encoding similar proteins have been identified in other magnetotactic species (Grünberg et al., 2001), so it is possible that ferrous iron is transported into the vesicle lumen, where it is subsequently oxidized to form magnetite. In contrast, the uptake of ferric iron by a number of strains

(Schüler and Baeuerlein, 1996; 1998) would first necessitate the reduction of the metal prior to its transport into the vesicle, and there is evidence for a cytoplasmic Fe(III) reductase protein in at least one species (Noguchi et al., 1999). Alternatively, ferric iron may be transported directly across the vesicle membrane but, as yet, no mechanism indicative of such transport has been elucidated.

Enzymatic processing of iron by dissimilatory iron-reducing bacteria has been shown to result in isotopic fractionation of the metal, such that the biologically produced ferrous iron is isotopically lighter than the ferric iron on which the cells were grown (Beard et al., 1999). Since enzymatic processing of iron appears to be involved in magnetosome production (Nakamura et al., 1995a; 1995b), it is possible that a similar fractionation may take place. However, for the two magnetotactic strains studied to date (*M. magnetotacticum* strains MS-1 and MV-1), the processing of iron during the production of their magnetosomes did not result in any significant isotopic fractionation (Mandernack et al., 1999).

Magnetite formation by magnetotactic bacteria requires oxygen. While magnetotactic strains can grow aerobically, the cells tend to be non-magnetic, with the production of magnetite being induced only after the establishment of microaerophilic or anaerobic conditions (Blakemore et al., 1985; Bazylinski et al., 1988; Matsunaga et al., 1991; Matsunaga and Tsujimura, 1993; Yang et al., 2001). Schüler and Baeuerlein (1998) report magnetite production at O_2 values of 2 to 7 μM. Similarly, Heyen and Schüler (2003) determined that magnetosome production was induced only when the partial pressure of oxygen (pO_2) was maintained below 20 mbar (2 kPa), with maximum magnetosome production occurring at pO_2 of only 0.25 mbar (25 Pa).

Despite the obvious effects of atmospheric O_2 concentration on magnetite production, isotope fractionation experiments have shown that the oxygen which is incorporated into the magnetosome crystals is largely derived from the water surrounding the cells, and not from dissolved, molecular O_2 (Mandernack et al., 1999). Molecular O_2 may still play a role in magnetosome formation, however, perhaps by affecting the physicochemical conditions (e.g., E_h) within the magnetosome vesicle, as suggested by Schüler and Baeuerlein (1998). Alternatively, it may influence the expression of specific proteins required for magnetite synthesis (Bazylinski and Frankel, 2004).

Within the magnetosome vesicle, the exact reaction mechanism by which the magnetite is generated is still largely unknown, however crystallization of the nascent magnetite particle, and the expression of different crystal faces upon it appear to be influenced by environmental factors and cell growth conditions, in particular iron limitation. This implies a high level of biological control over mineral formation (Faivre et al., 2008). Frankel et al. (1983) found evidence for intracellular low- and high-density hydrous iron oxides, similar to the mineral ferrihydrite. They proposed that chelated ferric iron is reduced as it is transported into the cytoplasm. The ferrous iron might then be re-oxidized in the vesicle lumen to form a ferrihydrite-like mineral precursor. This precursor would then undergo subsequent chemical modification (dehydration and partial reduction of some of the ferric iron) to form magnetite (Frankel et al., 1983). More recently, it was proposed that a magnetosome vesicle may not be required for magnetosome synthesis at all. Taylor and Barry (2004) calculated that the inter-magnetosomal spacing was too narrow to allow for the presence of two biological membranes and suggested that the bacteria used in their study likely did not produce magnetosome vesicles. Instead, they found that the magnetosomes

were surrounded by a semi-crystalline organic (possibly polysaccharide) matrix, which they termed the "magnetosome matrix". The matrix extended 20 to 70 nm (depending on the type of cell) beyond the surface of the magnetosomes and exhibited lattice fringes that were aligned parallel with the {111} crystal lattice planes of the encapsulated magnetosome. Within the matrix, and surrounding the growing magnetosomes, was an iron mineral phase which the authors termed "pre-magnetite", and which had lattice d-spacing values distinct from either two-line or six-line ferrihydrite. The authors propose that the magnetosome matrix is a semicrystalline gel that may provide an oxidizing environment, favourable to the production of magnetite, possibly through the transfer of electrons to the closely-associated electron transport system (Taylor and Barry, 2004). Alternatively, the matrix may nucleate formation of pre-magnetite and control the infiltration of additional ferrous iron into the growing magnetosome via chelation. Such "templating" of mineral phases along organic polymers has also been noted in other systems (Chan et al., 2004). Lins and Farina (2001), also found evidence of amorphous iron-rich mineral phases which were not membrane-bound. The significance of these iron-rich amorphous phases remains to be elucidated.

3.2 A Novel Bacterial Intracellular Iron Mineral

Recently, it was discovered that cells of the iron-reducing bacterium *Shewanella putrefaciens* (strain CN32) also produce intracellular particles of an iron-rich mineral (Glasauer et al., 2002). While *Shewanella* is not a magnetotactic genus, it does share a number of traits in common with its magnetotactic relatives. 1) it is a member of the domain Bacteria, within the gamma subdivision of the Proteobacteria; 2) it has Gram-negative cell wall architecture; 3) it is motile by means of polar flagella; 4) it possesses respiratory

metabolism and is also capable of anaerobic respiration, using a wide variety of terminal electron acceptors, including ferric iron (Balashova and Zavarzin, 1980).

Glasauer et al. (2002) grew *S. putrefaciens* CN32 anaerobically by supplying the cells with a hydrous ferric oxide mineral (HFO, or two-line ferrihydrite) to serve as terminal electron acceptor. At about the same time that Fe(II) could be detected in the cultures, the authors noticed the presence of small (30-50 nm wide) electron-dense particles associated with the cells, and apparently forming within the cytoplasm (Fig. 4). The number of particles per cell increased with the age of the culture. Selected area electron diffraction of the particles revealed an amorphous (though sometimes slightly ordered) structure, but did not indicate the crystallinity that would be expected for a highly ordered mineral phase such as magnetite (Bazylinski et al., 1993). Additionally, the diffraction data obtained from the intracellular particles was different from that obtained from the surrounding HFO mineral phase (Glasauer et al., 2002), indicating that the intracellular mineral was being formed *de novo*. More recent analyses of these novel inclusions using synchrotron X-ray fluorescence and XANES have shown them to be a mixed-valence form of iron, intermediate between green rust and magnetite. While their precise function is still unknown, they appear to play a role in anaerobic iron respiration (Glasauer et al., 2007).

4 Banded Iron Formations - Ancient Biogenic Iron Minerals?

4.1 Characterization and Geochemical Formation

The Archean and Proterozoic eras in Earth's early history are marked by the deposition of banded iron formations (BIFs). These are large deposits of iron-rich mineral layers (including, but not limited to, hematite, magnetite, chamosite, siderite and pyrite;

Garrels et al., 1973) alternating with iron-deplete, but silicon-rich layers (typically chert-like minerals). They are often uniformly deposited and can cover thousands of square kilometers and range in thickness from just a few to several hundred meters (Lundgren and Dean, 1979). As ore bodies, they represent the largest concentrations of iron resources in the world. Typical BIF ore contains between 25% and 35% iron (James and Sims, 1973) and individual deposits can hold tens of billions of tons of iron (Cloud, 1973). The chemical composition of BIFs is highly variable, and their models of deposition are numerous. However, for maintaining the brevity of this paper we have limited our discussion to the iron layers, while focusing primarily on only one popular model of BIF deposition.

The period of maximum deposition of the BIFs is thought to have occurred primarily between 1.8 and 2.7 billion years (Ga) ago (Goldich, 1973), although the oldest known BIF (a member of the Isua Supracrustal Group of West Greenland) has been dated at 3.8 Ga (Appel, 1980). One possible explanation of BIF deposition suggests that they were formed by silica precipitation concurrent with alternating periods of iron-rich and iron-poor precipitation, occurring within shallow, partially-isolated depositional basins of Archean cratons (Morris and Horwitz, 1983; Morris 1993). The massive amounts of iron are thought to have been transported onto the depositional basin in the form of reduced (ferrous) iron. Since the waters and atmosphere of the time are generally believed to be anoxic (Rasmussen and Buick, 1999), ferrous iron could be delivered over long geographic and temporal spans without precipitation.

Holland (1973) proposed that volcanism and terrestrial run-off were inadequate sources of the vast amount of iron (he calculated as much as 2×10^{10} kg Fe/year) needed to produce a BIF, and instead promoted an oceanic origin for the iron. More recent studies

(Jacobsen and Pimentel-Klose, 1988; Isley, 1995) have supported Holland's model, suggesting that the iron was likely produced at sites along mid-ocean spreading ridges, and at oceanic hotspots and hydrothermal plumes. However, the possibility also exists that the oceanic iron could have been supplemented by normal continental drainage, as suggested by Konhuaser et al. (2002). More recently, Hamade et al. (2003) measured Ge/Si ratios in various mesobands of BIFs from the Hamersley Group (Western Australia) and found that as Si decreased (and Fe increased) in their samples, the Ge/Si ratios trended similar to those associated with mid-ocean-ridge solutions and metalliferous sediments. While not definitive, the results add additional weight to the argument that the iron source for BIFs was oceanic water rich in ferrous iron. Upwelling currents may have delivered this iron-rich water onto the depositional basin (Klein and Beukes, 1989), allowing for uniform precipitation and sedimentation on vast scales (e.g., the Hamersley Group in Western Australia may cover 100,000 km^2 or more; Walker et al., 1983).

For iron deposition to have taken place, a source of oxidizing power must have been present, although most researchers suggest an anoxic environment at the time. Purely geochemical models of BIF deposition must therefore account for the extensive primary precipitation of ferric iron minerals in the absence of large concentrations of atmospheric and dissolved O_2. Iron oxidation via sulfate reduction is one possibility, however in some BIFs (e.g., in the Dales Gorge Member) sulfide minerals tend not to be as abundant as their oxide counterparts (Walker, 1984). Many geochemical models instead favour the photo-oxidation of ferrous iron by solar ultraviolet (UV) radiation (Cairns-Smith, 1978), which may have precipitated as much as 100 mg Fe cm^{-2} yr^{-1} in waters with a total dissolved iron concentration of 10-100 μM (Braterman et al., 1983; Francois, 1986). This high yield could

account for the oxidized iron required for the formation of the Hamersley Basin deposits (Anbar and Holland, 1992).

4.2 Potential Roles for Microorganisms in the Formation of BIFs

4.2.1 Photosynthesis and the production of molecular oxygen

In 1987, Schopf and Packer provided compelling evidence for the occurrence of ancient (as old as 3.5 Ga) cyanobacteria-like microfossils embedded within carbonaceous cherts from two different sampling sites in the Warrawoona Group (Australia). These findings have recently been questioned by Brasier et al. (2002), however these authors do not definitively rule out the possible microbial origin of the "microfossils". A more recent study on stromatolites of the Zimbabwe Craton (Kamber et al., 2004) suggests that established microbial communities were extant in both the open oceans and in continental basins as long ago as 2.8 Ga. Briefly, stromatolites are laminated assemblages of sediment (or sedimentary rock). The various layers of a stromatolite are created, in part, by the trapping of sediment by organisms, typically filamentous mats of cyanobacteria, algae, diatoms and bacteria (Lundgren and Dean, 1979). Stromatolites are still being formed and studied today (e.g., Brake et al., 2004). However, similar microbial communities may have had the potential to affect local redox conditions in their ancient ecosystems (Kamber et al., 2004). While the results of Schopf and Packer (1987) and Kamber et al. (2004) are not derived from BIFs, their findings suggest that microbial life was well established (and, possibly, metabolically well advanced) during the time of BIF deposition. Richardson et al. (1988) demonstrated that the metabolic activity of *Microcystis* spp. led to steep gradients in pH and O_2 within the microenvirnments surrounding pelagic aggregates of the cells. More

recently, Pierson et al. (1999) have found that cyanobacteria growing near the surface of present-day microbial mats are able to increase the local oxygen level to more than 200% of air saturation during periods of active photosynthesis, resulting in the total oxidation of ferrous groundwater iron within the top few millimeters of the mat. The authors also found that ferrous iron was able to stimulate photosynthesis (measured by ^{14}C-bicarbonate uptake) by as much as 500 to 600%, relative to control levels (Pierson et al., 1999).

Therefore, it is possible that oxygenic photoautotrophs contributed (via the production of molecular oxygen and the uptake of CO_2) to the oxidation of ferrous iron in ancient depositional basins. Cloud (1973) suggested that early (anaerobic) photosynthetic life forms would not yet have evolved the biochemical pathways necessary for dealing with molecular oxygen (a highly damaging molecule to all biological systems). As a result, early oxygenic phototrophs would have depended on the abundance of ferrous iron to immediately react with the toxic oxygen they produced. Alternatively, as discussed by Nealson and Myers (1990) and Pierson et al. (1999), ferrous iron may also have been oxidized by serving as the electron donor in early, anaerobic photosynthetic systems. Present-day analogues to such organisms might include the so-called purple and green bacteria (Widdel et al., 1993; Heising and Schink, 1998). In any event, the presence of photosynthetic organisms (as suggested by the fossil record) would have necessarily impacted on the surrounding ferrous iron.

4.2.2 Iron-oxidizing bacteria

Photosynthetic production of O_2 is not the only way in which microbial life might have contributed to iron oxidation and deposition. As discussed in section 2.2.1, acidophilic

and neutrophilic iron-oxidizing bacteria gain energy from the oxidation of ferrous iron. Holm (1987) reported that surface layers of sediment collected near the exhalative zone of a shallow, hydrothermal vent near the island of Santorini contained "anomalous concentrations" (i.e., 35 to 40%) of iron, relative to the sediments of the shelf zone (about 2.7%). Microscopic analysis of the "anomalous" sediments revealed that they consisted almost entirely of bacterial stalks and iron oxide hydroxide particles, with no crystalline iron phases (Holm, 1987). Similar results (bacterial stalks and cells mixed with iron oxide hydroxide) were also obtained for sediments collected near a cooler (12°C) hydrothermal outflow in Iceland (Holm, 1987). Holm (1989) consequently proposed that iron oxidation by microaerophilic species (e.g., *Gallionella*, or *Gallionella*-like organisms) growing in seas with limited O_2 may have been responsible for the widespread deposition of ferric iron found in BIFs.

Based on available data (Trendall, 2000) for depositional rates in the Hamersley basin (Australia), Konhauser et al. (2002) estimated an annual iron accumulation rate of 1 mm (as hematite) in iron-rich bands, which corresponded to 45.3 mol Fe m^{-2}, during periods of peak deposition. Using previously published (Emerson and Revsbech, 1994b; Ehrenreich and Widdel, 1994) rates of iron oxidation for two model organisms (*Gallionella* and *Chromatium*), theoretical cell densities were calculated which showed that minimum required densities of 4.3×10^4 cells cm^{-3} for *Gallionella*, and 5.7×10^4 cells cm^{-3} for *Chromatium* were needed to account for BIF layer deposition (Konhauser et al., 2002). As discussed by the authors, these theoretical values are 1 to 2 orders of magnitude lower than typical cell densities observed in present-day ecosystems, and (in the case of *Gallionella*) up to 5 orders of magnitude lower than densities observed in some present-day, ferrous-iron-

rich mat communities (Emerson and Revsbech, 1994a). Clearly, microbial cells display (even today) the oxidative capacity and population sizes required to achieve significant precipitation of ferrous iron.

4.2.3 Iron-reducing bacteria

It is usually assumed that the alternating of iron-rich and iron-poor layers in BIFs represents cyclical fluctuations in the amount of iron delivered to the sedimentary basin over time (Morris, 1993; Konhauser et al., 2002). However, Becker and Clayton (1972) and Baur et al. (1985), reported isotopic fractionation of the carbon within carbonate rocks of iron-poor layers, such that the carbonate was isotopically light. This led to the hypothesis that iron-reducing bacteria may also have been involved in the creation of BIFs (Baur et al., 1985; Nealson and Myers, 1990). Iron-reducing organisms living in the sedimentary layers could use organic detritus as a carbon source, coupled to the reduction of ferric iron oxides (or hydroxides), while at the same time producing isotopically light CO_2, which was subsequently incorporated into the carbonate mineral (Nealson and Myers, 1990). These authors proposed that the source of isotopically light organic carbon may have been the remains of dead phototrophic organisms (known to fractionate carbon; Erez et al., 1998) which accumulated on the surface of the oxidized iron layers. Therefore, as the phototrophic organisms went through cycles of growth and decline, the availability of organic carbon to the iron-reducers would also cycle, leading to variations in the iron-content of the sediment layers (Nealson and Myers, 1990). More recently, Johnson et al. (2008) have reported that iron isotope fractionation within siderite and magnetite facies BIFs indicates complete reduction of the precursor Fe(III) oxides and hydroxides, in addition to reactions occurring

between those precursors and excess, isotopically light, Fe(II) produced by microbial reduction. Iron-reducing bacteria, therefore, may have also played a major role in the cycling and diagenetic processing of iron in ancient sediments.

4.3 Summary – Toward an Integrated Approach

We have seen in the preceding sections how microbial cells can induce potent effects on their geochemical environments. With respect to BIFs, recent theoretical calculations (Konhauser et al., 2002) have shown the ability of iron-oxidizing cells to precipitate the extraordinary amounts of iron needed to produce iron-rich sediments on a vast scale. In combination with the photoautotrophs, they also fixed environmental CO_2 (Widdel et al., 1993), thereby making the carbon biologically available for heterotrophic organisms living within the same consortium. The newly created ferric iron could, in turn, be metabolized by iron-reducing cells, leading to the formation of a variety of secondary iron oxide minerals (Glasauer et al., 2003), as well as metabolism of the available fixed carbon present in the sedimentary layers. Certainly, this is not to say that microbes were solely responsible for the creation of BIFs. In developing working geochemical and biological models to explain any geological process, we must be careful not to fall into an "either-or" mentality. Not only does this introduce the potential for bias in interpreting observations, it could preclude the formation of some very useful collaborations between earth scientists and biologists. Given our current (and still emerging) knowledge of the numerous and complex interactions that exist between present-day biological communities and their geological environments, it is not unreasonable to assume that similar biological and geochemical interactions took place during the early formation of the earth. The presence of putative microfossils in 3.3-billion-

year-old rock facies (Schopf and Packer, 1987), and ancient fossil stromatolites (Brake et al., 2004) leaves little doubt that microbial life was extant at the time. The model that should arise, therefore, is a necessarily complex one that should seek to integrate the numerous interactions between processes such as (but not limited to): volcanism and tectonics, hydrology, photochemistry, sedimentation and diagenesis, photosynthesis, and microbial oxidation and reduction processes. To expect anything simpler is probably unreasonable. Clearly, geological processes were responsible for providing the raw materials (and some or all of the processes) needed for the deposition of the BIFs. However, their diverse metabolic processes, and potential for enormous population size, mean that microbes could certainly have had a profound impact on the ancient environment. It is not totally unreasonable, therefore, to hypothesize that BIFs may represent the oldest known iron "biominerals".

5 Iron-rich minerals as biosignatures?

According to the NASA, a biosignature is an object, substance and/or pattern whose origin specifically requires a biological agent (http://astrobiology.arc.nasa.gov). Iron oxides, more specifically magnetite, have been identified as potential biosignatures. The study of McKay et al. (1996) started the whole debate on whether or not magnetite crystals present in the ALH84001 Martian meteorite had a biological origin. It was proposed that the unique chemical, physical and mineralogical features of the magnetite crystals in the meteorite were similar to the ones of biogenic magnetite produced by magnetotactic bacteria (see section 3) (Thomas-Keprta et al., 2000; 2001). The magnetite crystals produced by the magnetotactic strain MV-1 are elongated on a [111] crystallographic axis in a so-called "truncated hexa-octahedral" shape (Meldrum et al., 1993; Golden et al. 2004). Such morphology was thought

to be indicative of a biological origin, but Golden et al. (2004) recently showed that such characteristics were most likely exclusively inorganic in origin. Previous work by Barber and Scott (2002) had also pointed out that the magnetite crystals in the Martian meteorite were abiogenic in origin and that they formed because of shock-heating. Finally, Weiss et al. (2004b) have indicated that magnetite grains within ALH84001 are not aligned in chains (one of the factors thought to be indicative of microbial magnetofossils).

Even though the door is almost closed on the use of magnetite crystals as potential bioindicators of life, research continues on other aspects and characteristics of iron oxides. The use of high spatial resolution tools (HRTEM, XANES, etc.) and powerful mineralogical analysis to characterize samples containing mineralized organic structures should improve our understanding of biomineralization mechanisms and help identify true biosignatures. Indeed, recent studies have continued to assert that biogenic magnetite displays unique physico-chemical properties that are advantageous for its use as a biomarker. These factors include iron isotope fractionations (see below), transition temperature measurements, magnetic remanence values, and distribution measurements such as crystal-size and shape-factor distributions (Weiss et al., 2004a; Arato et al., 2005; Pan et al., 2005a,b).

The use of Fe isotopes represents another potential tool to discriminate between abiotic and biogenic iron oxide minerals (Beard et al., 1999; Paasche et al., 2004; Pan et al., 2005b). Several studies have measured Fe isotope fractionation in biological experimental systems in order to detect metabolic processing of Fe. (Croal et al., 2004 and references therein). According to Beard et al. (2003), most igneous rock and some sedimentary rocks display similar Fe isotopic characteristics, but significant variations ($\sim 4\ ^{0}/_{00}$) in Fe isotope compositions have been measured in late Archean BIF (Johnson et al. 2003, 2008). The Fe

isotope fractionation (~1.5 $^{0}/_{00}$ +/- 0.2 %) during the oxidation of Fe(II) by photoautotrophic bacteria is in fact comparable to that observed for iron-reducing bacteria (Croal et al., 2003). However, the same authors pointed out that the fractionation observed in their biological systems was also similar to that measured for abiotic Fe(II) oxidation by oxygen. This implies that that Fe isotopes might only represent a useful tool when studying biogenic Fe-rich samples formed in the near absence of oxygen (Croal et al., 2004; Johnson et al., 2005). Given the relatively new interest in Fe isotopes, it is clear that additional studies on various natural and synthetic biogenic and abiotic Fe-oxides are required before one can ascertain that a specific Fe isotope signature is indeed indicative of past or present biological activity.

6 Conclusion

Iron oxides formed in close association with bacteria form as a result of several different metabolic activities, passive reactions and internal biomineralization processes. Despite the fact that these oxides have been widely studied and that they possess unique features in terms of size, morphology and mineralogy, we are still left with the task of finding specific characteristics that could only be ascribed to a biological origin. The development of new genetic, biochemical and genomic approaches designed to study the diversity of microbial life in geological systems is very promising (Newman and Banfield, 2002). This, combined with culture-independent analyses of microbial communities should shed more light on the role of bacteria in global iron cycling and in their role in the formation of biogenic iron oxides. However, biomineralization processes are certainly not confined to bacteria and as a result, other living entities, including eukaryotes and viruses should be investigated. Recent work by Daughney et al. (2004) showed that marine viruses

(i.e., bacteriophage), which are often more abundant than bacteria in aquatic and terrestrial systems, possess surface binding sites which can bind soluble Fe and act as nucleation surfaces for Fe-oxide formation (Fig. 5). This laboratory study remains preliminary, but it certainly opens the door for the search of biogenic iron oxides resembling mineralized viruses in present and ancient geological formations. Finally, despite the fact that the role of bacteria in Fe cycling is well known, we might just be scratching the surface, knowing that most bacteria in the Earth's crust remain to be identified and studied.

7 Acknowledgements

We are very grateful to former graduate students and post-doctoral fellows, who generated some of the data presented in this paper. We also thank S. Glasauer, X. Châtellier and R. James for providing us with electron micrographs of biogenic iron oxides. Finally, we thank K. Anderson for preparing the figures.

References

Akai, J., Akai, K., Ito, M., Nakano, S., Maki, Y., Sasagawa, I., 2001. Biologically induced iron ore at Gunma iron mine, Japan. Am. Mineral. 84, 171-182.

Anbar, A.D., Holland, H.D., 1992. The photochemistry of manganese and the origin of banded iron formations. Geochim. Cosmochim. Acta. 56, 2595-2603.

Appel, P.W.U., 1980. On the early Archean Isua iron-formation, West Greenland. Precambrian Res. 11, 73-87.

Arato, B., Szanyi, Z., Flies, C., Schueler, D., Frankel, R.B., Buseck, P.R., Pósfai, M., 2005. Crystal-size and shape distributions of magnetite from uncultured magnetotactic bacteria as a potential biomarker. Amer. Mineral. 90, 1233-1240.

Bach, W., Edwards, K.J., 2003. Iron and sulfide oxidation within the basaltic ocean crust: Implications for chemolithoautotrophic microbial biomass production. Geochim. Cosmochim. Acta. 67, 3871-3887.

Baker, B.J., Banfield, J.F., 2003. Microbial communities in acid mine drainage. FEMS Microbiol. Ecol. 44, 139-152.

Balashova, V.V., Zavarzin, G.A., 1980. Anaerobic reduction of ferric iron by hydrogen bacteria. Microbiology. 48, 635-639.

Balkwill, D.L., Maratea, D., Blakemore, R.P., 1980. Ultrastructure of a magnetotactic spirillum. J. Bacteriol. 141, 1399-1408.

Banfield, J.F., Welch, S.A., Zhang, H., Ebert, T.T., Penn, L.P., 2000. Aggregation-based crystal growth and microstructure development in natural iron oxyhydroxide biomineralization products. Science 289, 751-754.

Barber, D.J., Scott, E.R.D., 2002. Origin of supposedly biogenic magnetite in the Martian meteorite Allan Hills 84001. PNAS. 99, 6556–6561.

Baur, M., Hayes, J., Studley, S., Walter, M., 1985. Millimeter-scale variations of stable isotope abundances in carbonates from banded iron formations in the Hamersley group of Western Australia. Econ. Geol. 80, 270-282.

Bazylinski, D.A., Frankel, R.B., 2004. Magnetosome formation in prokaryotes. Nature Rev. 2, 217-230.

Bazylinski, D.A., Frankel, R.B., Jannasch, H.W., 1988. Anaerobic magnetite production by a marine magnetotactic bacterium. Nature. 334, 518-519.

Bazylinski, D.A., Heywood, B.R., Mann, S., Frankel, R.B., 1993. Fe_3O_4 and Fe_3S_4 in a bacterium. Nature. 366, 218.

Bazylinski, D.A., Garratt-Reed, A.J., Frankel, R.B., 1994. Electron microscopic studies of magnetosomes in magnetotactic bacteria. Microsc. Res. Tech. 27, 389-401.

Beard, B.L., Johnson, C.M., Cox, L., Sun, H., Nealson, K.H., Aguilar, C., 1999. Iron isotope biosignatures. Science. 285, 1889-1892.

Beard, B.L., Johnson, C.M., Von Damm, K.L., 2003. Iron isotope constraints on Fe cycling and mass balance in the oxygenated Earth oceans. Geology. 31,629-632.

Becker, R., Clayton, R., 1972. Carbon isotopic evidence for the origin of a banded iron-formation in Western Australia. Geochim. Cosmochim. Acta. 36, 577-595.

Benz, M., Brune, A., Schink, B., 1998. Anaerobic and aerobic oxidation of ferrous iron at neutral pH by chemoheterotrophic nitrate-reducing bacteria. Arch. Microbiol. 169, 159-165.

Blakemore, R.P., 1975. Magnetotactic bacteria. Science. 190, 377-379.

Blakemore, R.P., Short, K.A., Bazylinski, D.A., Rosenblatt, C., Frankel, R.B., 1985. Microaerobic conditions are required for magnetite formation within *Aquaspirillum magnetotacticum*. Geomicrobiol. J. 4, 53-72.

Brake, S.S., Hasiotis, S.T., Dannelly, H.K., 2004. Diatoms in acid mine drainage and their role in the formation of iron-rich stromatolites. Geomicrobiol. J. 21, 331-340.

Brasier, M.D., Green, O.R., Jephcoat, A.P., Kleppe, A.K., van Kranendonk, M.J., Lindsay, J.F., Steele, A., Grassineau, N.V., 2002. Questioning the evidence for Earth's oldest fossils. Nature. 416, 76-81.

Braterman, P.S., Cairns-Smith, A.G., and Sloper, R.W., 1983. Photo-oxidation of hydrated Fe^{2+}: significance for banded iron formations. Nature. 303, 163-164.

Brown, A.D., Sherriff, B.L., Sawicki, J.A., Sparling, R., 1999. Precipitation of iron minerals by a natural microbial consortium Geochim. Cosmochim. Acta. 63, 2163-2169.

Cairns-Smith, A.G., 1978. Precambrian solution photochemistry-inverse segregation and banded iron formations. Nature. 276, 807-808.

Chan, C.S., De Stasio, G., Welch, S.A., Girasole, M., Frazer, B.H., Nesterova, M.V., Fakra, S., Banfield, J.F., 2004. Microbial polysaccharides template assembly of nanocrystal fibers. Science. 303, 1656-1658.

Châtellier, X., Fortin, D., 2004. Adsorption of ferrous ions onto *Bacillus subtilis* cells. Chem. Geol. (in press).

Châtellier, X., Fortin, D., West, M., Leppard, G.G., Ferris, F.G., 2001. Effect of the presence of bacterial surfaces during the synthesis of Fe-oxides by oxidation of ferrous ions. Eur. J. Mineralogy. 13, 705-714.

Châtellier, X., West, M., Rose, J., Fortin, D., Leppard, G.G., Ferris, F.G., 2004. Oxidation of ferrous ions in the presence of various bacterial strains and inorganic ligands. Geomicrobiol. J. 21, 99-112.

Chaudhuri, S.K., Lack, J.G., Coates, J.D., 2001. Biogenic magnetite formation through anaerobic biooxidation of Fe(II). Appl. Environ. Microbiol. 67, 2844-2848.

Chavez, F.P., Lunsdorf, H., Jerez, C.A., 2004. Growth of polychlorinated-biphenyl-degrading bacteria in the presence of biphenyl and chlorobiphenyls generates oxidative stress and massive accumulation of inorganic polyphosphate. Appl. Environ. Microbiol. 70, 3064-3072.

Cloud, P., 1973. Paleoecological significance of the banded iron-formation. Econ. Geol. 68, 1135-1143.

Cornell, R.M., Schwertmann, U., 2003. The iron oxides: Structure, Properties, Reactions, Occurrences and Uses, 2nd, Completely Revised and Extended Edition. Wiley-VCH Verlag, Weinheim, Germany, p. 703.

Croal, L.R., Johnson, C.M., Beard, B.L., Newman, D.K., 2004. Iron isotope fractionation by Fe(II)-oxidizing photoautotrophic bacteria. Geochim. Cosmochim. Acta. 68, 1227-1242.

Daughney, C.J., Fowle D., Fortin, D., 2001. The effect of growth phase on proton and metal adsorption by *Bacillus subtilus.* Geochim. Cosmochim. Acta. 65, 1025-1035.

Daughney, C.J., Fortin, D., 2002. Mineral Adsorption and Absorption by Biological Cells. In: Hubbard, A. (Ed.), Encyclopedia of Surface and Colloid Science. Marcel Dekker Inc., New York, NY, pp. 3430-3446.

Daughney, C.D., Châtellier, X., Chan, A., Kenward, P., Fortin, D., Suttle, C.A., Fowle, D., 2004. Adsorption and Precipitation of Iron from Seawater by a Marine Bacteriophage (PWH3a-P1). Marine Chemistry (in press).

DeLong, E.F., Frankel, R.B., Bazylinski, D.A., 1993. Multiple evolutionary origins of magnetotaxis in bacteria. Science. 259, 803-806.

Diaz-Ricci, J.C., Kirschvink, J.L., 1992. Magnetic domain state and coercivity predictions for biogenic greigite (Fe_3S_4): a comparison of theory with magnetosome observations. J. Geophys. Res. 97, 17309-17315.

Edwards, K.J., Bond, P.L., Gihring, T.M., J.F. Banfield, 2000. An archaeal iron-oxidizing extreme acidophile important in acid mine drainage. Science. 287, 1796-1799.

Edwards, K.J., Rogers, D.R., Wirsen, C.O., McCollom, T.M., 2003. Isolation and characterization of novel psychrophilic neutrophilic, Fe-oxidizing, chemolithoautotrophic α- and γ-Proteobacteria from the deep sea. Appl. Environ. Microbiol. 69, 2906-2913.

Edwards, K.J., Bach, W., McCollom, T.M., Rogers, D.R., 2004. Neutrophilic iron-oxidizing bacteria in the ocean: their habitats, diversity, and roles in mineral deposition, rock alteration, and biomass production in the deep-sea. Geomicrobiol. J. 21, 393-404.

Ehrenreich, A., Widdel, F., 1994. Anaerobic oxidation of ferrous iron by purple bacteria, a new type of phototrophic metabolism. Appl. Environ. Microbiol. 60, 4517-4526.

Ehrlich, H.L., 2002. Geomicrobiology of iron. In: Ehrlich, H.L. (Ed.), Geomicrobiology. Marcel Dekker, Inc., New York, NY, pp. 345-428.

Emerson, D., 2000. Microbial oxidation of Fe(II) at circumneutral pH. In: Lovley D.R., (Ed.), Environmental Microbe-Metal Interactions. ASM Press, Washington DC, pp. 31-52.

Emerson, D., Revsbech, N.P., 1994a. Investigation of an iron-oxidizing microbial mat community located near Aarhus, Denmark: field studies. Appl. Environ. Microbiol. 60, 4020-4031.

Emerson, D., Revsbech, N.P., 1994b. Investigation of an iron-oxidizing microbial mat community located near Aarhus, Denmark: laboratory studies. Appl. Environ. Microbiol. 60, 4032-4038.

Emerson, D., Moyer, C.L., 1997. Isolation and characterization of novel iron-oxidizing bacteria that grow at circumneutral pH. Appl. Environ. Microbiol. 63, 4784-4792.

Emerson, D., Moyer, C.L., 2002. Neutrphilic Fe-oxidizing bacteria are abundant and play a major role in Fe-oxide deposition at the Loihi Seamount hydrothermal vent system. Appl. Environ. Microbiol. 68, 3085-3093.

Emerson, D., Weiss, J.V., 2004. Bacterial iron oxidation in circumneutral freshwater habitats: Findings from the field and the laboratory. Geomicrobiol. J. 21, 405-414.

Emerson, D., Weiss, J.V., Megonigal, J.P., 1999. Iron-oxidizing bacteria are associated with ferric hydroxide precipitates (Fe-plaque) on the roots of wetland plants. Appl. Environ. Microbiol. 65, 2758-2761.

Emerson, D., Rentz, J.A., Lilburn, T.G., Davis, R.E., Aldrich, A., Chan, C., Moyer, C.L., 2007. A novel lineage of Proteobacteria involved in formation of marine Fe-oxidizing microbial mat communities. PLoS ONE. 2, e667.

Erez, J., Bouevitch A., Kaplan, A., 1998. Carbon isotope fractionation by photosynthetic aquatic microorganisms: experiments with *Synechococcus* PCC7942, and a simple carbon flux model. Can. J. Bot. 76, 1109-1118.

Fabian, K., Kirchner, A., Williams, W., Heider, F., Leibl, T., Hubert, A., 1996. Three-dimensional micromagnetic calculations for magnetite using fft. Geophys. J. Int. 124, 89-104.

Faivre, D., Menguy, N., Pósfai, M., Schueler, D., 2008. Environmental parameters affect the physical properties of fast-growing magnetosomes. Amer. Mineral. 93, 463-469.

Farina, M., Esquivel, D.M.S., Lins de Barros, H.G.P., 1990. Magnetic iron-sulphur crystals from a magnetotactic microorganism. Nature. 343, 256-258.

Farina, M., Kachar, B., Lins, U., Broderick, R., Lins de Barros, H., 1994. The observation of large magnetite (Fe_3O_4) crystals from magnetotactic bacteria by electron and atomic force microscopy. J. Microsc. 173. 1-8.

Fassbinder, J.W.E., Stanjek, H., Vali, H., 1990. Occurrence of magnetic bacteria in soil. Nature. 343, 161-163.

Fein, J.B., Daughney, C.J., Yee, N., Davis, T.A., 1997. A chemical equilibrium model for metal adsorption onto bacterial surfaces. Geochim. Cosmochim Acta. 61, 3319-3328.

Ferris, F.G., Konhauser, K.O., Lyven, B., Pedersen, K., 1999. Accumulation of metals by bacteriogenic iron oxides in a subterranean environment. Geomicrobiol. J. 16, 181-192.

Fortin, D., 2004. What biogenic minerals tell us. Science. 303, 1618-1619.

Fortin, D., Beveridge, T.J., 1997. Microbial sulfate reduction within mine tailings: formation of diagenetic Fe-sulfides. Geomicrobiol. J. 14, 1-21.

Fortin, D., Châtellier, X., 2003. Biogenic iron oxides. In: Pandalai, S.G. (Ed.), Recent Research Developments in Mineralogy, vol. 3. Research Signpost, Trivandrum, Kerala, India, pp. 47-63.

Fortin, D., Tessier, A., Leppard, G.G., 1993. Characteristics of lacustrine iron oxyhydroxides. Geochim. Cosmochim. Acta. 57, 4391-4404.

Fortin, D., Davis, B, Southam, G., Beveridge, T.J., 1995. Biogeochemical phenomena induced by bacteria in sulfidic mine tailings. J. Industrial Microbiol. 14, 178-185.

Fortin, D., Ferris F.G., Beveridge, T.J., 1997. Surface-mediated mineral development by bacteria. In: Banfield, J.F., Nealson, K.H. (Eds.), Reviews in Mineralogy, MSA, vol. 35, Washington DC, USA, pp. 161-180.

Fortin, D., Ferris, F.G., Scott, S.D., 1998. Formation of Fe-silicates and Fe-oxides on bacterial surfaces in hydrothermal deposits collected near the Southern Explorer Ridge in the Northeast Pacific Ocean. Am. Mineralogist. 83, 1399-1408.

Francois, L.M., 1986. Extensive deposition of banded iron formations was possible without photosynthesis. Nature. 320, 352-354.

Frankel, R.B., Blakemore, R.P., 1980. Navigational compass in magnetic bacteria. J. Magnet. Magnet. Mater. 15-18, 1562-1564.

Frankel, R.B., Blakemore, R.P., Wolfe, R.S., 1979. Magnetite in freshwater magnetotactic bacteria. Science. 203, 1355-1356.

Frankel, R.B., Papaefthymiou, G.C., Blakemore, R.P., O'Brien, W., 1983. Fe_3O_4 precipitation in magnetotactic bacteria. Biochim. Biophys. Acta. 763, 147-159.

Garrels, R.M., Perry, E.A., Mackenzie, F.T., 1973. Genesis of Precambrian iron-formations and the development of atmospheric oxygen. Econ. Geol. 68, 1173-1179.

Glasauer, S., Langley, S., Beveridge, T.J., 2001. Sorption of Fe (hydr)oxides to the surface of *Shewanella putrefaciens*: Cell-bound fine-grained minerals are not always formed de novo. Appl. Environ. Microbiol. 67, 5544-5550.

Glasauer, S., Langley, S., Beveridge, T.J., 2002. Intracellular iron minerals in a dissimilatory iron-reducing bacterium. Science. 295, 117-119.

Glasauer, S., Weidler, P.G., Langley, S., Beveridge, T.J., 2003. Controls on Fe reduction and mineral formation by a subsurface bacterium. Geochim. Cosmochim. Acta. 67, 1277-1288.

Glasauer, S., Langley, S., Boyanov, M., Lai, B., Kemner, K., Beveridge, T.J., 2007. Mixed-valence cytoplasmic iron granules are linked to anaerobic respiration. Appl. Environ. Microbiol. 73, 993-996.

Golden, D.C., Ming, D.W., Morris, R.V., Brearley, A.J., Lauer, H.V. Jr., Treiman, A.H., Zolensky, M.E., Schwandt, C.S., Lofgren, G.E., McKay, G.A., 2004. Evidence for exclusively inorganic formation of magnetite in Martian meterorite ALH84001. Am. Mineral. 89, 681-695.

Goldich, S.S., 1973. Ages of Precambrian banded iron-formations. Econ. Geol. 68, 1126-1134.

Gorby, Y.A., Beveridge, T.J., Blakemore, R.P., 1988. Characterization of the bacterial magnetosome membrane. J. Bacteriol. 170, 834-841.

Grünberg, K., Wawer, C., Tebo., B.M., Schüler, D., 2001. A large gene cluster encoding several magnetosome proteins is conserved in different species of magnetotactic bacteria. Appl. Environ. Microbiol. 67, 4573-4582.

Guerin, W.F., Blakemore, R.P., 1992. Redox cycling of iron supports growth and magnetite synthesis by *Aquaspirillum magnetotacticum*. Appl. Environ. Microbiol. 58, 1102-1109.

Hallbeck, L., Pedersen, K., 1991. Autotrophic and mixotrophic growth of *Gallionella ferruginea*. J. Gen. Microbiol. 137, 2657-2661.

Hallberg, R., Ferris, F.G., 2004. Biomineralization by *Gallionella*. Geomicrobiol. J. 21, 325-330.

Hamade, T., Konhauser, K.O., Raiswell, R., Goldsmith, S., Morris, R.C., 2003. Using Ge/Si ratios to decouple iron and silica fluxes in Precambrian banded iron formations. Geology. 31, 35-38.

Heising, S., Schink, B., 1998. Phototrophic oxidation of ferrous iron by a *Rhodomicrobium vannielii* strain. Microbiology. 144, 2263-2269.

Heyen, U., Schüler, D., 2003. Growth and magnetosome formation by microaerophilic *Magnetospirillum* strains in an oxygen-controlled fermentor. Appl. Microbiol. Biotechnol. 61, 536-544.

Holland, H.D., 1973. The oceans: a possible source of iron in iron-formations. Econ. Geol. 68, 1169-1172.

Holm, N.G., 1987. Possible biological origin of banded iron-formations from hydrothermal solutions. Orig. Life. 17, 229-250.

Holm, N.G., 1989. The $^{13}C/^{12}C$ ratios of siderite and organic matter of a modern metalliferous hydrothermal sediment and their implications for banded iron formations. Chem. Geol. 77, 41-45.

Isley, A.E., 1995. Hydrothermal plumes and the delivery of iron to banded iron formation. J. Geol. 103, 169-185.

Jacobsen, S.B., Pimentel-Klose, M.R., 1988. A Nd isotopic study of the Hamersley and Michipicoten banded iron formations: the source of REE and Fe in Archean oceans. Earth Planet. Sci. Lett. 87, 29-44.

James, H.L., Sims, P.K., 1973. Precambrian iron-formations of the world. Econ. Geol. 68, 913-914.

James, R., Ferris, F.G., 2004. Evidence for Microbial-Mediated Iron Oxidation at a Neutrophilic Groundwater Spring. Chem. Geol. (in press).

James, B.W., Mauchline, W.S., Dennis, P.J., Keevil, C.W., Wait, R., 1999. Poly-3-hydroxybutyrate in *Legionella pneumophila*, an energy source for survival in low-nutrient environments. Appl. Environ. Microbiol. 65, 822-827.

Jones, B., Renaut, R.W., 2007. Selective mineralization of microbes in Fe-rich precipitates (jarosite, hydrous ferric oxides) from acid hot springs in the Waiotapu geothermal area, North Island, New Zealand. Sediment. Geol. 194, 77-98.

Jonhson, C.M., Beard, B.L., Beukes, N.J., Klein, C., O'Leary, J.M., 2003.Ancient geochemical cycling in the Earth as inferred from Fe isotope studies of banded iron formations from Transvaal Craton. Contrib. Mineral. Petrol.144, 523-547.

Johnson, C.M., Roden, E.E., Welch, S.A., Beard, B.L., 2005. Experimental constraints on Fe isotope fractionation during magnetite and Fe carbonate formation coupled to dissimilatory hydrous ferric oxide reduction. Geochim. Cosmochim. Acta. 69, 963-993.

Johnson, C.M., Beard, B.L., Klein, C., Beukes, N.J., Roden, E.E., 2008. Iron isotopes constrain biologic and abiologic processes in banded iron formation genesis. Geochim. Cosmochim. Acta. 72, 151-169.

Kamber, B.S., Bolhar, R., Webb, G.E., 2004. Geochemistry of late Archean stromatolites from Zimbabwe: evidence for microbial life in restricted epicontinental seas. Precambrian Res. 132, 379-399.

Kappler, A., Newman, D.K., 2004. Formation of Fe(III)-minerals by Fe(II)-oxidizing photoautotrophic bacteria. Geochim. Cosmochim. Acta. 68, 1217-1226.

Kennedy C.B., Scott S.D., Ferris F.G., 2003a. Characterization of bacteriogenic iron oxide deposits from Axial Volcano, Juan de Fuca Ridge, Northeast Pacific Ocean. Geomicrobiol. J. 20, 199-214.

Kennedy, C.B., Martinez, R.E., Scott, S.D., F. G. Ferris, 2003b. Surface chemistry and reactivity of bacteriogenic iron oxides from Axial Volcano, Juan de Fuca Ridge, north-east Pacific Ocean. Geobiology. 1, 59-66.

Klein, C., Beukes, N.J., 1989. Geochemistry and sedimentology of a facies transition from limestone to iron-formation deposition in the Early Proterozoic Transvaal Supergroup, South Africa. Econ. Geol. 84, 1733-1774.

Konhauser, K.O., Hamade, T., Raiswell, R., Morris, R.C., Ferris, F.G., Southam, G., Canfield, D.E., 2002. Could bacteria have formed the Precambrian banded iron formations? Geology. 30, 1079-1082.

Lack, J.G., Chaudhuri, S.K., Chakraborty, R., Achebach, L.A., Coates, J.D., 2002. Anaerobic biooxidation of Fe(II) by *Dechlorosoma suillum.* Microb. Ecol. 43, 424-431.

Lins, U., Farina, M., 1998. Magnetosome size distribution in uncultured rod-shaped bacteria as determined by electron microscopy and electron spectroscopic imaging. J. Microsc. Res. Tech. 42, 459-464.

Lins, U., Farina, M., 2001. Amorphous mineral phases in magnetotactic multicellular aggregates. Arch. Microbiol. 176, 323-328.

Little, C.T.S., Glynn, S.E.J. and Mills, R.A., 2004. Four-hundred-and ninety-million-year record of bacteriogenic iron oxide precipitation at sea-floor hydrothermal vents. Geomicrobiol. J. 21, 415-429.

Lovley, D.R., Stolz, J.F., Nord Jr., G.L., Phillips, E. J.P., 1986. Anaerobic production of magnetite by a dissimilatory iron-reducing microorganism. Nature 330, 252-254.

Lovley, D.R., 2000. Fe(III) and Mn(IV) reduction. In: Lovley, D.R. (Ed.), Environmental Microbe-Metal Interactions. ASM Press, Washington DC, pp. 3-30.

Lundgren, D.G., Dean, W., 1979. Biogeochemistry of iron. In: Trudinger, P.A., Swaine, D.J. (Eds.), Biogeochemical Cycling of Mineral-Forming Elements. Elsevier Scientific Publishing Company, New York, NY, pp. 211-251

Mandernack, K.W., Bazylinski, D.A., Shanks, W.C., Bullen, T.D., 1999. Oxygen and iron isotope studies of magnetite produced by magnetotactic bacteria. Science. 285, 1892-1896.

Mann, S., Sparks, N.H.C., Frankel, R.B., Bazylinski, D.A., Jannasch, H.W., 1990. Biomineralization of ferrimagnetic greigite (Fe_3S_4) and iron pyrite (FeS_2) in a magnetotactic bacterium. Nature. 343, 258-261.

Matsunaga, T., Tsujimura, N., 1993. Respiratory inhibitors of a magnetic bacterium *Magnetospirillum* sp. AMB-1 capable of growing aerobically. Appl. Microbiol. Biotechnol. 39, 368-371.

Matsunaga, T., Sakaguchi, T, Tadokoro, F., 1991. Magnetite formation by a magnetic bacterium capable of growing aerobically. Appl. Microbiol. Biotechnol. 35, 651-655.

McKay, D.S., Gibson, E.K. Jr, Thomas-Keprta, K.L., Vali, H., Romanek, C.S., Clemett, S.J., Chillier, X.D., Maechling, C.R., Zare, R.N., 1996. Search for past life on Mars: possible relic biogenic activity in martian meteorite ALH84001. Science. 273, 924-930.

Meldrum, F.C., Mann, S., Heywood, B.R., Frankel, R.B., Bazylinski, D.A., 1993. Electron microscopy study of magnetosomes in two cultured vibroid magnetotactic bacteria. Proc.R. Soc. Lond. [Biol]. 251, 237-242.

Morris, R.C., 1993. Genetic modeling for banded iron formation of the Hamersley Group, Pilbara Craton, Western Australia. Precambrian Res. 60, 243-286.

Morris, R.C., Horwitz, R.C., 1983. The origin of the iron-formation-rich Hamersley Group of Western Australia – deposition on a platform. Precambrian Res. 21, 273-297.

Moskowitz, B.M., 1995. Biomineralization of magnetic minerals. Rev. Geophysics. 33, 123-128.

Nakamura, C., Burgess, J.G., Sode, K., Matsunaga, T., 1995a. An iron-regulated gene, *magA*, encoding an iron transport protein of *Magnetospirillum* AMB-1. J. Biol. Chem. 270, 28392-28396.

Nakamura, C., Kikuchi, T., Burgess, J.G., Matsunaga, T., 1995b. Iron-regulated expression and membrane localization of the MagA protein in *Magnetospirillum* sp. strain AMB-1. J. Biochem. 118, 23-27.

Nealson, K.H., Myers, C.R., 1990. Iron reduction by bacteria: a potential role in the genesis of banded iron formations. Am. J. Science. 290-A, 35-45.

Newman, D.K., Banfield, J.F., 2002. Geomicrobiology: Molecular-scale interactions underpin biogeochemical systems. Science. 296, 1071-1077.

Noguchi, Y., Fujiwara, T., Yoshimatsu, K., Fukumori, Y., 1999. Iron reductase for magnetite synthesis in the magnetotactic bacterium Magnetospirillum magnetotacticum. J. Bacteriol. 181, 2142-2147.

Oremland, R.S., Herbel, M.J., Switzer Blum, J., Langley, S., Beveridge, T.J., Ajayan, P.M., Sutto, T., Ellis, A.V., Curran, S., 2004. Structural and spectral features of selenium nanospheres produced by Se-respiring bacteria. Appl. Environ. Microbiol. 70, 52-60.

Paasche, O., Lovlie, R., Dahl, S.O., Bakke, J., Nesje, A., 2004. Bacterial magnetite in lake sediments; late glacial to Holocene climate and sedimentary changes in Northern Norway. Earth Planet. Sci. Lett. 223, 319-333.

Pan Y., Petersen, N., Winklhofer, M., Davila, A.F., Liu, Q., Frederichs, T., Hanzlik, M., Zhu, R., 2005a. Rock magnetic properties of uncultured magnetotactic bacteria. Earth Planet. Sci. Lett. 237, 311-325.

Pan, Y., Petersen, N., Davila, A.F., Zhang, L., Winklhofer, M., Liu, Q., Hanzlik, M., Zhu, R., 2005b. The detection of bacterial magnetite in recent sediments of Lake Chiemsee (southern Germany). Earth Planet. Sci. Lett. 232, 109-123.

Petermann, H., Bleil, U., 1993. Detection of live magnetotactic bacteria in South Atlantic deep-sea sediments. Earth. Planet. Sci. Lett. 117, 223-228.

Pierson, B.K., Parenteau, M.N., Griffin, B.M., 1999. Phototrophs in high-iron-concentration microbial mats: physiological ecology of phototrophs in an iron-depositing hot spring. Appl. Environ. Microbiol. 65, 5474-5483.

Pósfai, M., Buseck, P.R., Bazylinski, D.A., Frankel, R.B., 1998. Reaction sequence of iron sulfide minerals in bacteria and their use as biomarkers. Science. 280, 880-883.

Pósfai, M., Moskowitz, B.M., Arato, B., Schuler, D., Flies, C., Bazylinski, D.A., Frankel, R.B., 2006. Properties of intracellular magnetite crystals produced by *Desulfovibrio magneticus* strain RS-1. Earth Planet. Sci. Lett. 249, 444-455.

Poulton, S.W., Krom, M.D., Raiswell, R., 2004. A revised scheme for the reactivity of iron (oxyhydr)oxide minerals towards dissolved sulfide. Geochim. Cosmochim. Acta. 68, 3703-3715.

Rasmussen, B., Buick, R., 1999. Redox state of the Archean atmosphere: evidence from detrital heavy metals in ca. 3250-2750 Ma sandstone from the Pilbara Craton, Australia. Geology. 27, 115-118.

Richardson, L., Aguilar, C., Nealson, K., 1988. Manganese oxidation in pH and O_2 microenvironments produced by phytoplankton. Limnol. Oceanogr. 33, 352-366.

Roden, E.E., Sobolev, D., Glazer, B., Luther III, G.W., 2004. Potential for microscale bacterial Fe redox cycling at the aerobic-anaerobic interface. Geomicrobiol. J. 21, 379-391.

Rosetti, S., Blackall, L.L., Levantesi, C., Uccelletti, D., Tandoi, V., 2003. Phylogenetic and physiological characterization of a heterotrophic, chemolithoautotrophic *Thiothrix* strain isolated from activated sludge. Int. J. Syst. Evol. Microbiol. 53, 1271-1276.

Sakaguchi, T., Burgess, J.G., Matsunaga, T., 1993 Magnetite formation by a sulphate-reducing bacterium. Nature. 365, 47-49.

Schleifer, K.H., Schüler, D., Spring, S., Weizenegger, M., Amann, R., Ludwig, W., Köhler, M., 1991. The genus *Magnetospirillum* gen. nov., description of *Magnetospirillum gryphiswaldense* sp. nov. and transfer of *Aquaspirillum magnetotacticum* to *Magnetospirillum magnetotacticum* comb. nov. Syst. Appl. Microbiol. 14, 379-385.

Schopf, J.W., Packer, B.M., 1987. Early Archean (3.3-billion to 3.5-billion-year-old) microfossils from Warrawoona Group, Australia. Science. 237, 70-73.

Schrenk, M.O., Edwards, K.J., Goodman, R.M., Hamers, R.J., Banfield, J.F., 1998. Distribution of *Thiobacillus ferrooxidans* and *Leptospirillum ferrooxidans*: Implications for generation of acid mine drainage. Science. 279, 1519-1522.

Schüler, D., Baeuerlein, E., 1996. Iron-limited growth and kinetics of iron uptake in *Magnetospirillum gryphiswaldense*. Arch. Microbiol. 166, 301-307.

Schüler, D., Baeuerlein, E., 1998. Dynamics of iron uptake and Fe_3O_4 biomineralization during aerobic and microaerobic growth of *Magnetospirillum gryphiswladense*. J. Bacteriol. 180, 159-162.

Schüler, D., Frankel, R.B., 1999. Bacterial magnetosomes: microbiology, biomineralization and biotechnological applications. Appl. Microbiol. Biotechnol. 52, 464-473.

Sobolev, D., Roden, E.E., 2004. Characterization of a neutrophilic, chemolithoautotrophic Fe(II)-β-proteobacterium from freshwater wetland sediments. Geomicrobiol. J. 21, 1-10.

Sparks, N.H.C., Courtaux, L., Mann, S., Board, R.G., 1986. Magnetotactic bacteria are widely distributed in sediments in the U.K. FEMS Microbiol. Lett. 37, 305-308.

Spring, S., Amann, R., Ludwig, W., Schleifer, K.-H., van Gemerden, H., Petersen, N., 1993. Dominating role of an unusual magnetotactic bacterium in the microaerobic zone of a freshwater sediment. Appl. Environ. Microbiol. 59, 2397-2403.

Spring, S., Lins, U., Amann, R., Schleifer, K.-H., Ferreira, L.C.S., Esquivel, D.M.S., Farina, M., 1998. Phylogenetic affiliation and ultrastructure of uncultured magnetic bacteria with unusually large magnetosomes. Arch. Microbiol. 169, 136-147.

St-Cyr, L., Fortin, D., Campbell, P.G.C., 1993. Microscopic observations of the iron plaque of a sumerged aquatic plant (*Vallisneria americana Michx*). Aquatic Botany. 46, 155-167.

Straub, K.L., Benz, M., Schink, B., Widdel, F., 1996. Anaerobic, nitrate-dependent microbial oxidation of ferrous iron. Appl. Environ. Microbiol. 62, 1458-1460.

Straub, K.L., Benz, M., Schink, B., 2001. Iron metabolism in anoxic environments at near neutral pH. FEMS Microbiol. Ecol. 34, 181-186.

Straub, K.L., Schonhuber, W.A., Buchlolz-Cleven, B.E.E., Schink, B., 2004. Diversity of ferrous iron-oxidizing , nitrate-reducing bacteria and their involvement in oxygen-independent iron cycling. Geomicrobiol. J. 21, 371-378.

Stumm, W., Morgan, J.J., 1996. Aquatic chemistry: Chemical Equilibria and Rates in Natural Waters, 3rd Edition. Wiley-Interscience, New York, N.Y., p. 1040.

Taylor, A.P., Barry, J.C., 2004. Magnetosomal matrix: ultrafine structure may template biomineralization of magnetosomes. J. Microsc. 213, 180-197.

Tessier, A., Fortin, D., Belzile, N., DeVitre, R., Leppard, G.G., 1996. Trace metal-sediment interactions in two shield lakes: narrowing the gap between field and laboratory experiments. Geochim. Cosmochim. Acta. 60, 387-404.

Thomas-Keprta, K. L., Bazylinski, D. A., Kirschvink, J. L., Clement, S. J., McKay, D. S., Wentworth, S. J., Vali, H., Gibson, E. K., Jr., Romanek, C. S., 2000. Elongated prismatic magnetite crystals in ALH84001 carbonate globules: potential Martian magnetofossils. Geochim. Cosmochim. Acta. 64, 4049-4081.

Thomas-Keprta, K. L., Clemett, S.J., Bazylinski, D. A., Kirschvink, J. L., McKay, D.S., Wentworth, S. J., Vali, H., Gibson, E. K., Jr., McKay, M.F., Romanek, C. S., 2001. Truncated hexa-octahedral magnetite crystals in ALH84001: Presumptive biosignatures. PNAS. 98, 2164-2169.

Tipping, E., Thompson, D.W., Woof, C., 1989. Iron oxides particulates formed by the oxygenation of natural and model lakewaters containing Fe(II). Arch. Hydrobiol. 115, 59-70.

Trendall, A., 2000. The significance of banded iron formation (BIF) in the Precambrian stratigraphic record. Geoscientist. 10, 4-7.

Ueshima, M., Tazaki, K., 2001. Possible role of microbial polysaccharides in montronite formation. Clays and Clay Minerals, 49, 292-299.

Ueshima, M., Fortin, D., Kalin, M., 2004. Biogeochemical stability of iron phosphate minerals for attenuation of acid mine wastes. Geomicrobiol. J. 21, 313-323.

Walker, J.C.G., 1984. Suboxic diagenesis in banded iron formations. Nature. 309, 340-342.

Walker, J.C.G., Klein, C., Schidlowski, M., Schopf, J.W., Stevenson, D.J., Walter, M.R., 1983. Environmental evolution of the Archean-Early Proterozoic earth. In: Schopf, J.W. (Ed.), Earth's Earliest Biosphere: it's Origin and Evolution. Princeton University Press, Princeton, NJ, pp. 260-290.

Warren, L.A., Ferris, G.F., 1998. Continuum between sorption and precipitation of Fe(III) on microbial surfaces. Environ. Sci. and Technol. 32, 2331-2337.

Weiss, B.P., Sam Kim, S., Kirschvink, J.L., Kopp, R.E., Sankaran, M., Kobayashi, A., Komeili, A., 2004a. Ferromagnetic resonance and low-temperature magnetic tests for biogenic magnetite. Earth Planet. Sci. Lett. 224, 73-89.

Weiss, B.P., Kim, S.S., Kirschvink, J.L., Kopp, R.E., Sankaran, M., Kobayashi, A., Komeili, A., 2004b. Magnetic tests for magnetosome chains in Martian meteorite ALH84001. PNAS. 101, 8281-8284.

Widdel, F., Schnell, S., Heising, S., Ehrenreich, A., Assmus, B., Schink, B., 1993. Ferrous iron oxidation by anoxygenic phototrophic bacteria. Nature. 362, 834-836.

Yang, C.D., Takeyama, H., Tanaka, T., Matsunaga, T., 2001. Effects of growth medium composition, iron sources and atmospheric oxygen concentrations on production of luciferase-bacterial magnetic particle complex by a recombinant *Magnetospirillum magneticum* AMB-1. Enzyme Microb. Technol. 29, 13-19.

Yee, N., Fein, J.B., 2001. Cd adsorption onto bacterial surfaces: A universal adsorption edge? Geochim. Cosmochim. Acta. 65, 2037-2042.

Yoshida, H.D., Yamamoto, K., Murakami, Y., Matsuoka, K., 2006. Formation of biogenic iron-oxide nodules in reducing sediments as an analogue of near-field redox reaction products. Phys. Chem. Earth. 31, 593-599.

Figure captions

Fig. 1. Transmission electron micrographs of a mineralized bacterium in oxidized and acidic Cu-Zn mine tailings, showing fine Fe-rich minerals (see arrows) on the cell wall (A) and Fe-rich filaments (F) and nodules (N) in neutral-pH freshwater lake sediments (B).

Fig. 2. Neutrophilic Fe-oxidizing bacteria closely associated with iron oxides (see arrow) in an Fe(II)-rich discharge area (scanning electron micrograph).

Fig. 3. Transmission electron micrographs showing the presence of nanocrystals of lepidocrocite on and away from the cell wall of *Bacillus subtilis,* during the oxidation of Fe(II) in the presence of SO_4 (A) and ferrihydrite, in the presence of Si (B).

Fig. 4. Transmission electron micrograph showing a cell of *Shewanella putrefaciens* CN32 in whole mount. Anaerobic respiration with extracellular ferrihydrite (large arrow) produced intracellular iron-rich minerals (small arrow) that are distinct from the external ferrihydrite (see Glasauer et al., 2002).

Fig. 5. Transmission electron micrograph showing individual lepidocrocite crystals (see arrows) attached to the surface of viruses (marine bacteriophage PWH3a-P1) during the oxidation of Fe(II) at pH 7 (see Daughney et al., 2004).

Figure 1

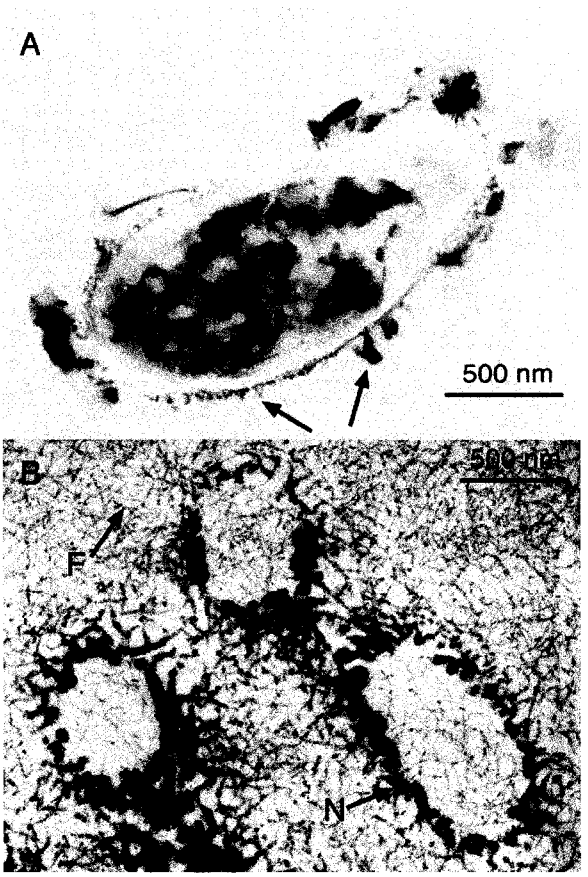

Figure 2

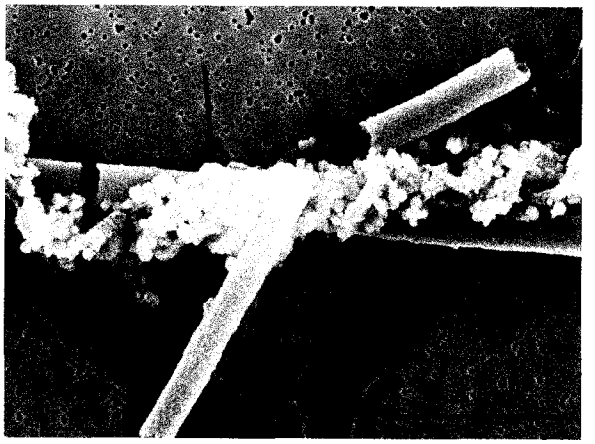

Figure 3

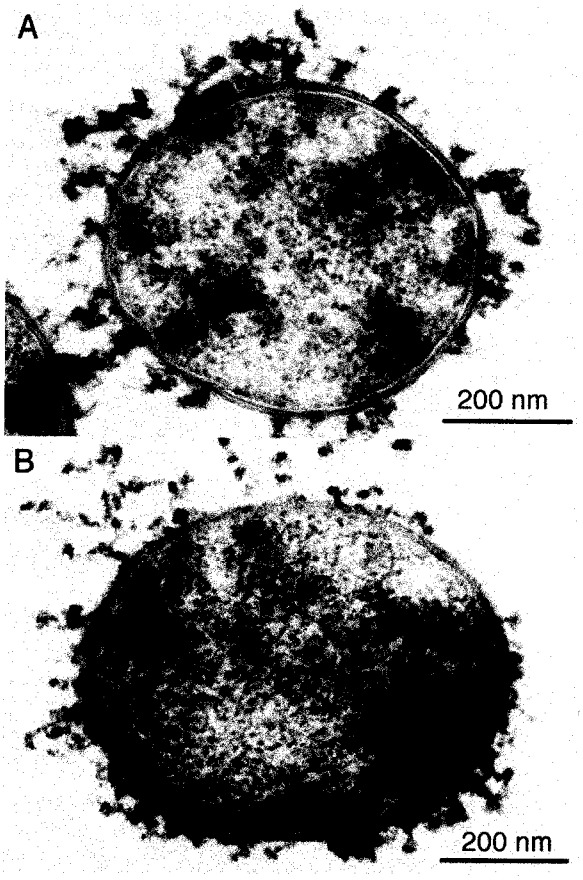

Figure 4

Figure 5

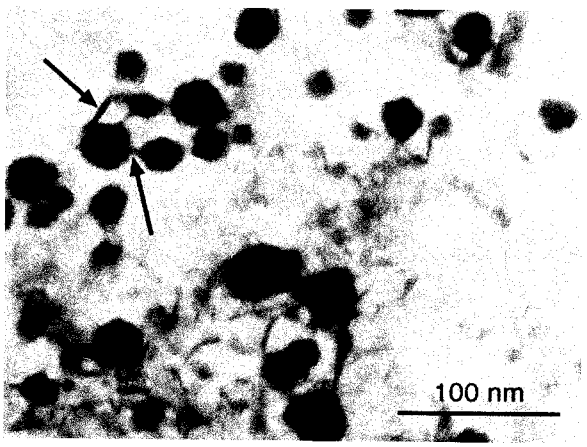

As highlighted in the preceding literature review, the broadly defined term "biogenic iron oxides" can refer to a variety of solid iron phases, including amorphous iron precipitates, poorly ordered oxyhydroxides such as ferrihydrite, and crystalline oxides such as hematite. The term "biogenic" also implies that these phases can be formed in the presence of a variety of organisms, not just iron-oxidizing bacteria (FeOB). However, the sample sites described in this thesis are dominated primarily by bacterial cells and bacterial cellular detritus. Furthermore, the majority of cellular forms display characteristic structural morphologies similar to those produced by known or suspected iron-oxidizing genera. As a result, the term "biogenic" has been replaced by the more specific term "bacteriogenic", even though it is likely that other organisms and organic polymers still comprise some fraction of the total BIOS mass. Nevertheless, despite evidence for an abundance of (FeOB) within the samples, the term "bacteriogenic" should not be interpreted here as implying only active (i.e., metabolic) oxidation of ferrous iron in these environments, since it is unlikely that the cells can fully compete against the rapid autooxidation of Fe^{2+} in such oxygenated, circumneutral waters.

Literature on fine-grained iron oxides have also highlighted their reactive surfaces and large surface area-to-mass ratios, two factors which make them effective sorbents of dissolved chemical species. As detailed below, an important groundwater contaminant of interest to the Canadian nuclear industry is strontium. Due to this interest, Sr was chosen as a means of examining the sorptive capacity of a natural BIOS deposit, currently forming on the grounds of Atomic Energy of Canada Limited's Chalk River Laboratories (an area impacted by radioactive ^{90}Sr contamination). The results of this work are presented, below, in Section 2.

Section 2

Sorption of strontium onto bacteriogenic iron oxides

A revised version of this manuscript has been accepted for publication in *Environmental Science and Technology*[1]

[1] Langley, S., Gault, A.G., Ibrahim, A., Takahashi, Y., Renaud, R., Fortin, D., Clark, I.D., Ferris, F.G. 2008. Sorption of strontium onto bacteriogenic iron oxides. Environ. Sci. Technol. In press.

Abstract

Bacteriogenic iron oxides (BIOS) were obtained from a dilute, circumneutral groundwater seep, characterized with respect to mineralogy, and examined for their ability to sorb aqueous Sr^{2+}. BIOS were composed of microbial sheaths encrusted in 2-line ferrihydrite. Sorption experiments indicated that Sr remained completely unbound at pH < 4.5, but sorption increased with increasing pH (maximum of 95% at pH > 7.6). EXAFS analysis of Sr-loaded BIOS failed to elucidate whether Sr sorption occurred on sites specific to the mineral or microbial fraction, but indicated that sorption likely occurred by outer-sphere complexation between BIOS and hydrated Sr^{2+}. Isotherm experiments showed that, at low ionic strength (I = 0.001 M), sorption followed a Langmuir distribution (S_{max} = 3.41 mol Sr g Fe^{-1}, K_{ads} = 1.26). At higher ionic strength (I = 0.1 M), there was significant inhibition of Sr sorption (S_{max} = 1.06 mol Sr g Fe^{-1}, K_{ads} = 1.23), confirming that sorption to BIOS occurs by outer-sphere complexation. The results indicate that, under dilute circumneutral conditions, BIOS deposits should efficiently sorb dissolved Sr from groundwater flow systems where such deposits exist. This finding has particular relevance to sites impacted by radioactive ^{90}Sr groundwater contamination.

Introduction

Bacteriogenic iron oxides (BIOS) are minerals precipitated by metabolic oxidation of ferrous iron by acidophilic (*1, 2*) and neutrophilic (*3, 4*) bacteria. BIOS can also refer to iron oxides precipitated chemically in association with cellular surfaces. BIOS accumulations can cover several thousand square metres, at depths up to several metres (*5, 6*). They have been described in marine and freshwater systems, fed by iron-rich sources such as springs, seeps,

and hydrothermal upwelling (*5, 6, 7, 8, 9*). The iron precipitates on cell surfaces as nanometre-scale aggregates of oxide minerals (*10*). Such small-scale iron oxides display large surface area-to-mass ratios (several hundred $m^2\ g^{-1}$), with highly reactive surfaces. These properties make them effective sorbents of aqueous chemical moieties including organic contaminants, heavy metals, and radionuclides (*11*). BIOS are also comprised of bacterial cells and cellular debris, and this organic component provides additional reactive surfaces, which are also effective sorbents of dissolved compounds (*12*).

A contaminant of concern to the nuclear industry is strontium-90 (^{90}Sr). While naturally-occurring levels of ^{90}Sr are virtually non-existent, concentrations in groundwater are typically elevated in areas involved with nuclear weapons development and detonations (*13*). ^{90}Sr is also produced within nuclear reactors and is partially responsible for the heat and luminescence of high-level radioactive waste (*14*). ^{90}Sr can substitute for calcium in bones, leading to increased risk of leukemia and other diseases (*15*). Attenuation of ^{90}Sr migration is, therefore, a major concern for any affected ecosystem.

^{90}Sr is more mobile than most radionuclides (*16*), however Sr^{2+} readily adsorbs to bacterial cells (*17*) and a variety of inorganic solids, including oxide minerals (*18, 19, 20*). Consequently, adsorption to mineral phases exerts a major control on Sr^{2+} migration, and some remediation strategies have employed adsorption onto silicates, oxides and iron oxide-coated particles. However, these strategies often require extensive human management and intervention (*21, 22, 23*). In contrast, BIOS deposits constitute large volumes of naturally occurring, adsorptive material directly within the flow path of affected aquifers and, thus, may represent a means of natural attenuation in ecosystems impacted by Sr contamination.

While several studies have examined the sorptive behaviour of bacteria-iron oxide composites, these employed artificial mixtures of synthetic oxides with laboratory cultures (*24, 25*). Natural iron oxides such as BIOS are less ordered than synthetic forms and their precipitation in association with microbial cell structures may lead to significantly different sorptive properties (*26*). Ferris et al. (*12, 27*) examined metal sorption onto BIOS and reported distribution coefficients (K_d) and surface complexation constants for various dissolved metals, including Sr. However, these studies did not address the mechanism(s) by which sorption to BIOS occurred, or the effect of pH on Sr uptake. Also, K_d values are sensitive to the composition of heterogeneous sorbents (*12*), and assume an infinite number of non-reacted sorption sites. Further, they must be measured experimentally for each system and are, therefore, not readily transferable from one site to another (*28*).

Our goals in this research were to: 1) characterize (mineralogically and biologically) a naturally occurring BIOS deposit, 2) use EXAFS to determine the mechanism and binding sites involved in Sr sorption, 3) assess the effect of pH on Sr sorption, and 4) model Sr sorption on BIOS using a Langmuir model, which should accurately account for a finite number of sorption sites, providing a more transferable measurement of sorption (i.e., the maximum binding capacity, S_{max}, of the solid). While copious literature exists on the study of synthetic and geogenic iron oxides for remediative applications, this study is one of the first to examine the potential remediative capacity of natural BIOS.

Materials and Methods

Site Description, Sample Collection and Storage. Samples were collected from a pH-neutral groundwater seep on the grounds of Atomic Energy of Canada Limited's (AECL)

Chalk River Laboratories, Ontario, Canada (latitude: 46°03'04"N, longitude: 77°25'11"W). The site is not currently impacted by ^{90}Sr, however other aquifers on the AECL grounds are, and in situ physical remediation strategies have been employed to retard contaminant migration (*22*). Groundwater at the site is recharged from a freshwater lake and flows through a 10,000 year-old aeolian sand dune. Several points of discharge occur along the dune base, flowing into a wetland that covers approximately 26,000 m^2. The BIOS form within these surface discharges, at a depth from 1 mm to over 1 m. Physical variables at the discharge sites were measured using a YSI 650MDS datalogger with 600QS probe.

Surface water (i.e., groundwater discharge) was collected using 20 mL sterile syringes and was placed into 60 mL, acid-washed plastic bottles. Oxygen-sensitive measurements were measured immediately on-site, using a HACH spectrophotometer and colorimetric reagents. Remaining samples were acidified (0.02 M HCl) and stored (4°C) until return to the laboratory, where they were analyzed for elemental composition using inductively-coupled plasma – optical emission spectrometry (ICP-OES). Samples for analysis of soluble-phase components were filtered (0.22 μm) on-site prior to analysis.

Samples of solid BIOS were collected by immersing 500 mL acid-washed, plastic bottles into the sediment. In the laboratory, BIOS were sieved (200-mesh) and centrifuged (14,000 × g), to remove as much detrital material and water as possible. Subsamples (0.5 g) were acid digested by addition of 2 mL concentrated, trace metal-grade HNO_3, and 4 mL 30% H_2O_2, for 12 hours at 70°C (*29*). Digests were analyzed by ICP-OES as described above. To prevent mineralogical transformations by the native microbial community during storage, BIOS were sterilized by gamma irradiation using a Nordion Gammacell 220 (48 kGray). Irradiated samples were stored at 4°C.

Preparation of synthetic iron oxide. Synthetic hydrated ferric oxide (HFO) was prepared as described previously (*30*), by addition of 1 M NaOH to 2 M $FeCl_3 \cdot 6H_2O$ to a pH of 7.0. The resulting precipitate was washed 10 times in ultrapure water (UPW) and stored at 4°C.

Electron Microscopy. 0.5 mL of BIOS was chemically fixed by addition of 15 μL 50% (aq) glutaraldehyde (electron microscopy grade). Fixed samples were used for the preparation of thin sections, as described previously (*31*). Transmission electron microscopy and energy-dispersive X-ray spectroscopy (EDS) of thin sections were performed using a Philips CM-10 electron microscope operating at 80 kV. The microscope was coupled to a Soft-imaging Systems (SiS) Morada CCD camera, controlled by SiS iTEM software, and an EDAX Sapphire X-ray detector which collected spectra over 100 seconds (live count) at a beam diameter of 200 nm. Scanning electron microscopy was performed using a JEOL JSM-6400 scanning electron microscope operating at 20 kV.

Mineralogy. Mineralogy was determined using powder X-ray diffraction (XRD). Native and Sr-loaded BIOS samples and synthetic HFO were freeze-dried, then ground using a mortar-and-pestle. XRD was performed using a Philips PW 1830 X-ray diffractometer, with a Cu-Kα X-ray source, operating at 45 kV with a current of 40 mA. Continuous scans were run from 5° to 80° (2θ).

Extended X-ray Absorption Fine Structure (EXAFS). In an attempt to determine precise Sr binding sites within BIOS, samples were prepared by sorbing aqueous Sr^{2+} onto washed suspensions of: a) BIOS, b) a pure culture of microbial cells (*Shewanella putrefaciens* CN32, without any Fe mineral added), and c) synthetic HFO (without any microbial cells added). Strontium loading was performed by suspending 5 g of each sorbent material in 50 mL 0.4 M $Sr(NO_3)_2$ at pH 8.0 for 2 hours at 22°C. The material was then washed 5 times in UPW at

pH 8.0, to remove any excess soluble Sr^{2+}. Hydrated Sr^{2+} ion, in the form of a $Sr(NO_3)_2$ solution (1000 mg L^{-1} Sr), served as a reference standard. Approximately 200 mg of each Sr-loaded material were packed in polyethylene bags for measurement. For sorption samples, a minimal amount of water remained in the samples, reducing the possibility of detection of signals from Sr^{2+} in solution. Strontium K-edge (16.105 keV) EXAFS spectra were collected at beamline BL01B1 of SPring-8 (Hyogo, Japan). A Si(111) double-crystal monochromator was used to obtain the incident X-ray beam. All the spectra were measured in fluorescence mode using a 19-element Ge semiconductor detector. Data analysis was performed using REX2000 ver.2.3 (Rigaku) with parameters generated by FEFF7.02 (*32, 33*). EXAFS spectra were Fourier transformed to real (*R*) space, and back-transformed to *k* space for spectral simulation.

Strontium Sorption. Sorption edge experiments were performed following the protocol of Small et al. (*24*), with minor modifications. Nine 100 mL beakers were loaded with 0.5 g of BIOS suspended in 50 mL 0.001 M KNO_3 and sparged with N_2 for 2 hours at 22°C within an anaerobic chamber (atmosphere: 100% N_2). After sparging, each beaker was adjusted to a specific initial pH, ranging from 4.0 to 8.0, in increments of 0.5 pH units. All beakers were then spiked with a concentrated $Sr(NO_3)_2$ solution to a final concentration of 50 mg L^{-1} Sr. Suspensions were equilibrated for 2 hours at 22°C while sparging. After equilibration, each beaker was sampled as follows. A 6 mL aliquot was removed and filtered (0.2 μm) for analysis of soluble-phase Sr and Fe. Another 6 mL aliquot was removed, without filtration, for analysis of total Sr and Fe. Both aliquots were acid digested for analysis by ICP-OES.

For sorption isotherms (*29*), eight 100 mL beakers were loaded with BIOS suspensions and sparged as described above. After sparging, the pH of all beakers was

adjusted to 8.0. Using a concentrated $Sr(NO_3)_2$ solution, the final Sr concentration in the beakers was then adjusted to: 25, 50, 100, and 500 μg L^{-1}, and 1.0, 5.0, 10, and 50 mg L^{-1}. Suspensions were equilibrated for 2 hours at 22°C while sparging, then sampled, digested and analyzed as described above. The procedure was repeated using 0.1 M KNO_3 as the background electrolyte, to elucidate the effect of ionic strength on sorption. Experimental data were fit to a single-site Langmuir sorption model using unconstrained non-linear regression and a Levenberg-Marquardt optimization routine for variable estimation (STATISTICA v 6.0). Tests for false local minima were performed by adjusting the initial variable estimates. Results with the highest correlation coefficients (i.e., r^2 value) were accepted as the global minima for the residual variance (i.e., sum of squared residuals) about the regression line. All analyses converged to the same final result, regardless of the initial variable estimates, as expected for optimal minimization of the deviation between observed experimental and predicted values.

Results

Site parameters and BIOS digestions. Physicochemical measurements at the sample site displayed spatial and seasonal variations. For mean values and ranges see Table S1, Supporting Information. The groundwater was predominantly circumneutral, with some sites becoming acidic. Low conductivity values indicated low ionic strength. Low concentrations of ferrous Fe reflected precipitation of the BIOS within the deposit, prior to emergence of the groundwater at the surface. Strontium concentrations were typically low. Elemental analyses of BIOS digests are presented in Table S2, Supporting Information. The elemental composition of BIOS was dominated by iron, however significant quantities of calcium,

silicon and phosphorus were detected, likely derived from detrital weathering minerals and organic components. Drying of BIOS for X-ray diffraction resulted in a loss of mass on the order of 95-99%, indicating a high degree of hydration in the cellular-mineral phase.

Electron microscopy. BIOS were dominated by tubular structures, morphologically similar to the sheaths produced by the iron-oxidizing bacterium *Leptothrix*. (Figure 1a). Occasionally, twisted stalk structures were also observed (See Figure S1a, Supporting Information), characteristic of the iron-oxidizing bacterium *Gallionella*. In thin section preparations, these structures were encrusted in an iron-rich mineral precipitate, 100-200 nm thick (Figure 1b). Attempts to obtain electron diffraction patterns from the precipitates were unsuccessful, suggesting a lack of crystallinity. EDS analysis confirmed that the precipitates were rich in iron and oxygen, with trace amounts of silicon and calcium (See Figure S1b, Supporting Information), which were also detected in the BIOS digests.

Mineralogy. X-ray diffraction of all samples yielded two broad features centred at approximately 1.5 Å and 2.5 Å (See Figure S2, Supporting Information). These are characteristic of the poorly ordered iron oxyhydroxide, 2-line ferrihydrite. Minor sharp peaks were also observed in BIOS samples, but not HFO. These peaks corresponded to d-spacings of quartz and other silicate weathering products (feldspars and micas) present in the sand aquifer.

EXAFS. The EXAFS spectra and radial structure functions (RSF) are shown in Figure 2. Although Sr^{2+} was sorbed on different solid samples, all spectra were almost identical to that of hydrated Sr^{2+}, suggesting that Sr^{2+} was sorbed as a hydrated species onto every solid medium. The peak at $R + \Delta R = 2.0$ Å in the RSF for Sr^{2+} sorbed on HFO (Figure 2) corresponds to the distance between Sr^{2+} and oxygen as first neighboring atom. By the

simulation based on the parameters generated by FEFF, the interatomic distance between Sr and O was determined as $R_{Sr-O} = 2.59 \pm 0.02$ Å, identical to that of hydrated Sr^{2+} species with $R_{Sr-O} = 2.58 \pm 0.02$ Å (see Table S3, Supporting Information). For Sr sorbed on bacteria alone and on BIOS, the spectra both in k and R space were identical to those of hydrated Sr^{2+} and Sr^{2+} sorbed on HFO alone.

Strontium Sorption Edge. Sorption edge data are presented in Figure 3. The solid line indicates a line of best fit to the average of three replicates. At equilibrium pH values lower than 4.5, all of the available Sr existed in an unbound state. Sorption increased, with increasing pH, to a maximum of approximately 95% at an equilibrium pH of 7.6 or higher. The sorption edge (the pH at which 50% of the Sr was sorbed) for BIOS was 6.06.

Strontium Sorption Isotherms. Sorption isotherms for the low ionic strength (0.001 M KNO_3) system are shown in Figure 4a. Isotherms for the high ionic strength (0.1 M KNO_3) system are displayed in Figure 4b. The data in each followed a typical Langmuir model distribution (solid line). For physical parameters (S_{max}, K_{ads}) and correlation coefficients of the curves see Table S4, Supporting Information. It is apparent from these data that increased ionic strength led to decreased sorption of Sr, indicating competition between the Sr^{2+} and background electrolyte ions for available binding sites within the BIOS.

Discussion

BIOS formations of the type described here arise from chemical oxidation of ferrous iron by molecular O_2 combined with enzymatic oxidation performed by iron-oxidizing bacteria (*3, 4*). Influx of fresh dissolved ferrous iron in this case is dependent on the perennial flow of the groundwater. The combination of biotic and abiotic Fe^{2+} oxidation

results in a massive precipitation of highly hydrated, amorphous ferric iron, and a concomitant decrease in the concentration of dissolved Fe^{2+}. With little or no dissolved solids in the groundwater, the resulting deposit consists of essentially pure iron oxyhydroxide precipitated on a microbial matrix, with only trace levels of natural weathering elements present.

In pH-neutral solutions, poorly ordered ferrihydrite is often one of the first solid phases to precipitate upon oxidation of ferrous iron (*11*). It is also one of the more common minerals found in association with active microbial iron oxidation in circumneutral freshwater systems (5, *34*). When analyzed by powder XRD, synthetic 2-line ferrihydrite is characterized by two broad reflections occurring at d-spacings of 2.50 Å and 1.51 Å. Continued oxidation and hydrolysis of the iron can result in ordering of the atomic lattice, producing more crystalline iron oxides, including goethite and lepidocrocite (*11*). In the present study, the reflections obtained from XRD analysis of BIOS correspond well to those of 2-line ferrihydrite. There was a slight shift in the precise d-spacings, however this may be due to organic components (and other constituents), which would not be present in chemically pure, synthetic ferrihydrite. Regardless, the lack of sharp peaks in the diffraction pattern (see Figure S2, Supporting Information) indicate that the BIOS are composed primarily of a poorly ordered mineral phase. This suggests that more crystalline oxides (e.g., goethite or lepidocrocite), if present, are at levels below the detection limits of the technique (< ~5 wt %), or that conversion of the ferrihydrite to a more crystalline mineral is inhibited within BIOS, perhaps due to a stabilizing influence brought on by precipitation of the mineral on the microbial surfaces, as has been suggested for similar biogenic deposits in marine environments (*35*).

Figure 1 demonstrates that the BIOS are dominated by tubular structures, morphologically similar to the sheaths produced by the known iron-oxidizing genus *Leptothrix* (*36*). The spiral stalks (suggestive of another iron oxidizer, *Gallionella*; see Figure S1a, Supporting Information) were much less common, perhaps representing 1% or less of the microbial forms we observed. Similar BIOS deposits have been described elsewhere, often displaying the same mineralogy and cellular morphologies, although with different relative abundances of the organisms involved (*5, 7, 27*). Since morphology alone is insufficient for assigning organisms to a particular genus, work is currently underway in our laboratory to characterize the microbiota using 16S rRNA sequencing and molecular biological approaches. Regardless of their exact metabolism, it is clear from TEM thin sections that the iron phase appears to be cell-surface associated, as 100-200 nm thick crusts, completely encasing the microbial sheaths. Energy dispersive X-ray analysis confirmed the elemental composition of the crust as being rich in iron and oxygen (See Figure S1b, Supporting Information). The presence of peaks generated by silicon and calcium within the EDS spectra is not surprising, given that the BIOS form at the base of a sand aquifer, and that quartz (SiO_2) and silicate weathering minerals (such as feldspars and micas, both rich in Si and Ca) were also occasionally observed by XRD and ICP-OES.

The inability of the BIOS to generate an electron diffraction pattern further suggests a lack of crystallinity, and serves to confirm the XRD findings. As noted, powder XRD requires a detection limit of about 5% (w/w of the sample) in order to elucidate crystalline structure. Electron diffraction is much more sensitive and is, therefore, better suited to the detection of nano- and micro-scale crystallites which may not be present in abundance. The fact that no diffraction pattern could be obtained from the BIOS suggests that the material is

in fact a poorly ordered iron oxide such as ferrihydrite, and likely does not contain more crystalline phases. Nevertheless, we are aware that production of an electron diffraction pattern is dependent upon the optimal 3-dimensional alignment of a crystal to the incident electron beam, and it is possible that such alignment was not achieved in the present study.

Glasauer et al. (*37*) have noted that association between microbial cell surfaces and fine-grained mineral phases in natural samples does not necessarily reflect a microbial origin for the mineral phase. However, given the morphological similarities between the organisms in the present study and those of known iron-oxidizing genera, as well as the complete encrustation of the microbial sheaths with iron oxide, we feel confident that the mineral phase is being microbially precipitated. Furthermore, biogenic iron oxides can also form in vitro, via passive nucleation and precipitation of iron by chemical groups within microbial cell wall polymers (*10*). Therefore, regardless of whether there is active iron oxidation occurring, it seems likely that the iron oxide observed in the present study was precipitated primarily in association with microbial cell surfaces and, therefore, constitutes a true bacteriogenic deposit.

In metal sorption experiments involving both bacteria and iron oxide minerals, the extent to which a particular metal will sorb to the surface of either a microbial cell or a mineral is dependent upon the availability of specific surface complexation sites (*29, 38*). These sites are susceptible to protonation and deprotonation and pH will, therefore, play a large role in determining the sorptive behaviour of a particular solid phase. The sorption edge displayed in Figure 3 indicates that Sr sorption to BIOS is highly pH-dependent through a narrow pH range (from 5.0 to 7.0) with the edge occurring at pH 6.06. To the best of our knowledge, this study represents only the third time that natural BIOS have been

examined with respect to Sr sorption, and the first time that Sr sorption edge data have been generated. Consequently, no literature is available for direct comparison of the edge data presented. However, Small et al. (*24*) examined Sr sorption to synthetic HFO, bacterial cells, and bacteria-HFO mixtures. The Sr sorption edge for two species of bacteria (without iron) were 5.5 and 5.8, while for HFO alone it was 7.6 (*24*). For the composite mixture, however, the Sr sorption edge shifted to 5.9, significantly different from either of the other three systems. In light of the present study, this finding is important, because the bacteria-HFO composite used by Small et al. can be seen as an artificial analogue to a BIOS system. As such, it is significant that the BIOS sorption edge is much closer to that of a bacteria-HFO composite, than it is to either bacteria or HFO alone. It also suggests that, at circumneutral pH, with low concentrations of dissolved Sr, a higher proportion of the metal should be removed by BIOS than by HFO alone. This likely reflects an overall increase in the number of available reactive sorption sites (provided by the organic component). Direct comparison with the results of Small et al. (*24*) is complicated by the fact that an artificial system is easily defined with respect to relative amounts of iron oxide and cellular material present in the system. In contrast, the ratio of Fe:cells in BIOS is more difficult to quantify.

Due to the low ionic strength of the aquifer, Sr sorption to BIOS was initially modeled in a dilute electrolyte (0.001 M KNO_3). Sorption followed a Langmuir distribution, indicating saturation (S_{max}) of the available binding sites at a value of 3.41 μmol g^{-1}. This value is higher than the S_{max} value of HFO alone (1 μmol g^{-1}) reported in previous work (*24, 25*). Again, this finding likely reflects the contribution of additional sorption sites provided by the organic component. However, it is interesting to note that BIOS exhibit a 10-fold lower S_{max}, when compared to the artificial bacteria-HFO composite (34 μmol g^{-1}) used by

Small et al. (*24*). This may be due to the fact that the composite consisted of individual cells (or small clumps) of rod-shaped bacteria coated with HFO. In contrast, the organic component of BIOS consists of longer (tens of microns) filaments. Smaller particle size in the artificial composite likely provided a higher surface area than would be expected for an equivalent volume of material with larger particle size. This may explain the observed decrease in the sorptive capacity of BIOS relative to the artificial bacteria-HFO composite.

When examined by EXAFS, strontium sorbed onto microbial cells, HFO, or BIOS displayed the same atomic coordination as that of hydrated Sr^{2+} (see Table S3, Supporting Information). This finding prevented us from accurately determining whether Sr was sorbing preferentially to sites within the Fe component of the BIOS (as opposed to sites within the microbial fraction). Strontium bound to HFO by inner-sphere compelxation can generate a Sr-Fe shell as a second shell in radial structural function (RSF), which was not the case in our data (Figure 2). Due to the overall negative charge density of most microbial cell surfaces, it seems likely that Fe^{3+} (whether actively precipitated or passively sorbed) would saturate the high affinity, inner sphere complexation sites within BIOS and limit Sr sorption to lower affinity, outer sphere complexation sites within the organic and mineral phases, as suggested by Small et al. (*25*). At this point, we believe that both fractions contribute to sorption, but we are unable to state what proportion of the metal is sorbed by each fraction.

The interatomic distance between Sr and O was determined as $R_{Sr\text{-}O} = 2.59 \pm 0.02$ Å for Sr-HFO (see Table S3, Supporting Information). This was identical to that of hydrated Sr^{2+}, with $R_{Sr\text{-}O} = 2.58 \pm 0.02$ Å. The distances were also similar to those for hydrated Sr^{2+} sorbed on HFO, kaolinite, and silica by outer-sphere complexation, reported by Sahai et al. (*16*). Sahai et al. (*16*) also indicated that there are two species for Sr sorbed on HFO;

hydrated Sr^{2+} (an outer-sphere complex), and $SrCO_3$ (precipitated at the surface of HFO). For the latter, a peak corresponding to a Sr-Sr shell should be found in the RSF around R + ΔR = 3.7 Å, however, such a peak was not found in the RSF of Sr^{2+} sorbed on HFO in our analyses. Thus, it is suggested that Sr^{2+} was sorbed as a hydrated species by outer-sphere complexation on HFO in our samples, and not as a carbonate precipitate. In the cases of Sr sorbed on bacterial cells and on BIOS, the EXAFS spectra were identical to those of hydrated Sr^{2+} and Sr^{2+} sorbed on HFO. These spectra could be well fitted by a Sr-O shell (indicated as solid curves in Figure 2), showing that other shells are not needed to explain the EXAFS spectra. For the Sr-O shell, EXAFS measurements such as $R_{Sr\text{-}O}$, coordination number (CN), and Debye-Waller factors (σ^2) were similar between the Sr species considered in this study. Hence, we suggest that Sr species sorbed on the solid media were primarily hydrated Sr^{2+}, sorbed via outer sphere complexation.

Outer sphere complexation is a reversible phenomenon that is susceptible to changes in ionic strength, such that high concentrations of competing cations should decrease the observed S_{max} of the sorbent. This appears to be the case when dealing with bacterial cells alone. Small et al. (*25*) reported that Sr^{2+} complexation to *Shewanella alga* appeared to be largely electrostatic in nature, with inner sphere complexation to high affinity sites occurring only under conditions of increased ionic strength. In contrast, Sr^{2+} sorption to HFO appeared to be controlled more by inner sphere complexation (being relatively independent of ionic strength), while mixtures of the cells with HFO resulted in sorption behaviour that was intermediate between inner and outer sphere complexation (*25*). In the present study, when sorption was modeled under high ionic strength (0.1 M KNO_3), we observed a three-fold decrease in the S_{max} of the BIOS, indicating that, at high ionic strength (and at low

concentrations of dissolved Sr), Sr^{2+} was effectively excluded from sorption onto low affinity sites within the BIOS. This occurred despite the fact that divalent Sr^{2+} would normally be expected to sorb more strongly to the available reactive sites than would monovalent K^+ (*39*). Sorption of Sr at high ionic strength was only detected when the initial dissolved [Sr] surpassed 500 $\mu g\ L^{-1}$, possibly indicating binding to higher affinity sites when Sr concentrations become elevated.

In summary, the mobility of Sr^{2+} through ground and surface water systems is governed by sorption reactions on solid phases such as iron oxide minerals. In flow systems impacted by ^{90}Sr contamination, sorption reactions are of paramount importance in limiting the spread of the radionuclide. Sorption of strontium onto BIOS appears to be governed almost entirely by outer sphere complexation of hydrated Sr^{2+} to low affinity sites within the BIOS matrix. Correspondingly, the sorption is highly dependent on the pH and ionic strength of the surrounding aqueous milieu. Under the conditions of circumneutral pH and low ionic strength in which these BIOS are formed, it is likely that significant sorption of Sr^{2+} will occur. However, the reversible nature of outer sphere complexation means that Sr^{2+} would be remobilized into the flow system following either a decrease in pH or increase in ionic strength of the groundwater. De-sorption is also likely to occur when deeper layers of the BIOS become susceptible to anaerobic microbial reduction, which will solubilize the iron and release any sorbed contaminants back into solution.

Acknowledgments

SL was supported by the Natural Sciences and Engineering Research Council of Canada (NSERC), Ontario Graduate Scholarship (OGS) program, and the University of

Ottawa. This work was funded by an NSERC Strategic Project grant to GF. We thank Dragica Bogdanovic (National HIV Laboratories, Health Canada) for assistance with sample irradiation. We also thank Dianne Moyles and Bob Harris (University of Guelph, Canada) and Xavier Châtellier (University of Rennes, France) for assistance with electron microscopy.

Supplementary Information

Table S1: Physicochemical measurements of groundwater overflowing the BIOS

Table S2: Elemental analysis of acid-digested BIOS.

Table S3: Measurements obtained from fitting Sr K-edge EXAFS spectra

Table S4: Isotherm measurements for Sr sorption on BIOS.

Figure S1: Scanning electron micrograph of a *Gallionella*-like helical stalk, and elemental analysis of the mineral highlighted in Figure 1b.

Figure S2: X-ray diffractograms produced from HFO and BIOS.

Literature Cited

(1) Edwards, K.J.; Bond, P.L.; Gihring, T.M.; Banfield, J.F. An archaeal iron-oxidizing extreme acidophile important in acid mine drainage. *Science.* **2000**, *287*, 1796-1799.

(2) Baker, B.J.; Banfield, J.F. Microbial communities in acid mine drainage. *FEMS Microbiol. Ecol.* **2003**, *44*, 139-152.

(3) Hallbeck, L.; Pedersen, K. Culture parameters regulating stalk formation and growth rate of *Gallionella ferruginea*. *J. Gen. Microbiol.* **1990**, *136*, 1675-1680.

(4) Hallbeck, L.; Pedersen, K. Autotrophic and mixotrophic growth of *Gallionella ferruginea*. *J. Gen. Microbiol.* **1991**, *137*, 2657-2661.

(5) James, R.E.; Ferris, F.G. Evidence for microbial-mediated iron oxidation at a neutrophilic groundwater spring. *Chem. Geol.* **2004**, *212*, 301-311.

(6) Stoffers, P.; Worthington, T.J.; Schwarz-Schampera, U.; Hannington, M.D.; Massoth, G.J.; Heknian, R.; Schmidt, M.; Lundsten, L.J.; Evans, L.J.; Vaiomo'unga, R.; Kerby, T. Submarine volcanoes and high-temperature hydrothermal venting on the Tonga Arc, southwest Pacific. *Geology.* **2006**, *34*, 453-456.

(7) Pedersen, K. Microbial life in deep granitic rock. *FEMS Microbiol. Lett.* **1997**, *20*, 399-414.

(8) Kennedy, C.B.; Martinez, R.E.; Scott, S.D.; Ferris, F.G. Surface chemistry and reactivity of bacteriogenic iron oxides from Axial Volcano, Juan de Fuca Ridge, north-east Pacific Ocean. *Geobiology.* **2003**, *1*, 59-69.

(9) Kennedy, C.B.; Scott, S.D.; Ferris, F.G. Characterization of bacteriogenic iron oxide deposits from Axial Volcano, Juan de Fuca Ridge, Northeast Pacific Ocean. *Geomicrobiol. J.* **2003**, *20*, 199-214.

(10) Fortin, D.; Langley, S. Formation and occurrence of biogenic iron-rich minerals. *Earth Sci. Rev.* **2005**, *72*, 1-19.

(11) Cornell, R.M.; Schwertmann, U. In *The iron oxides: structure, properties, reactions, occurrence and uses*, 2nd ed.; Wiley-VCH: Weinheim, 2003; Chapters 5, 10, 11, 13.

(12) Ferris, F.G.; Konhauser, K.O.; Lyvén, B.; Pedersen, K. Accumulation of metals by bacteriogenic iron oxides in a subterranean environment. *Geomicrobiol. J.* **1999**, *16*, 181-192.

(13) Um, W.; Papelis, C. Sorption mechanisms of Sr and Pb on zeolitized tuffs from the Nevada test site as a function of pH and ionic strength. *Amer. Mineral.* **2003**, *88*, 2028-2039.

(14) Bruno, J.; Ewing, R.C. Spent nuclear fuel. *Elements.* **2006**, *2*, 343-349.

(15) Nielsen, P. The biological role of strontium. *Bone.* **2004**, *35*, 583-588.

(16) Sahai, N.; Carroll, S.A.; Roberts, S.; O'Day, P.A. X-ray absorption spectroscopy of strontium(II) coordination II: sorption and precipitation at kaolinite, amorphous silica and goethite surfaces. *J. Colloid. Interface Sci.* **2000**, *222*, 198-212.

(17) Schultze-Lam, S.; Beveridge, T.J. Nucleation of celestite and strontianite on a cyanobacterial S-layer. *Appl. Environ. Microbiol.* **1994**, *60*, 447-453.

(18) Axe, L.; Bunker, G.B.; Anderson, P.R.; Tyson, T.A. An XAFS analysis of strontium at the hydrous ferric oxide surface. *J. Colloid. Interface Sci.* **1998**, *199*, 44-52.

(19) Parkman, R.H; Charnock, J.M.; Livens, F.R.; Vaughan, D.J. A study of the interaction of strontium ions in aqueous solution with the surfaces of calcite and kaolinite. *Geochim. Cosmochim. Acta.* **1998**, *62*, 1481-1492.

(20) Palmer, J.L.; Gunter, M.E. The effects of time, temperature, and concentration on Sr2+ exchange in clinoptilolite in aqueous solutions. *Amer. Mineral.* **2001**, *86*, 431-437.

(21) Fuhrmann, M.; Aloysius, D.; Zhou, H. Permeable subsurface sorbent barrier for ^{90}Sr: laboratory studies of natural and synthetic materials. *Waste Management.* **1995**, *15*, 485-493.

(22) Lee, D.R.; Smyth, D.J.A.; Shikaze, S.G.; Jowett, R.; Hartwig, D.S.; Milloy, C. Wall and curtain for passive collection/treatment of contaminant plumes. First

International Conference on Remediation of Chlorinated and Recalcitrant Compounds, Monterey, CA, USA. **1998**.

(23) Hansen, B.Ø.; Kwan, P.; Benjamin, M.M.; Li, C.-W.; Korshin, G.V. Use of iron oxide-coated sand to remove strontium from simulated Hanford tank wastes. *Environ. sci. technol.* **2001**, *35*, 4905-4909.

(24) Small, T.D; Warren, L.A.; Roden, E.E.; Ferris, F.G. Sorption of strontium by bacteria, Fe(III) oxide, and bacteria-Fe(III) oxide composites. *Environ. Sci. Technol.* **1999**, *33*, 4465-4470.

(25) Small, T.D.; Warren, L.A.; Ferris, F.G. Influence of ionic strength on strontium sorption to bacteria, Fe(III) oxide, and composite bacteria-Fe(III) oxide surfaces. *Appl. Geochem.* **2001**, *16*, 939-946.

(26) Tessier, A.; Fortin, D.; Belzile, N.; DeVitre, R.R.; Leppard, G.G. Metal sorption to diagenetic iron and manganese oxyhydroxides and associated organic matter: narrowing the gap between field and laboratory measurements. *Geochim. Cosmochim. Acta.* **1996**, *60*, 387-404.

(27) Ferris, F.G.; Hallberg, R.O.; Lyvén, B.; Pedersen, K. Retention of strontium, cesium, lead and uranium by bacterial iron oxides from a subterranean environment. *Appl. Geochem.* **2000**, *15*, 1035-1042.

(28) Drever, I. In *The geochemistry of natural waters: surface and groundwater environments*, 3rd ed.; Prentice Hall: New Jersey, 1997; Chapter 5.

(29) Kulczycki, E.; Ferris, F.G.; Fortin, D. Impact of cell wall structure on the behavior of bacterial cells as sorbents of cadmium and lead. *Geomicrobiol. J.* **2002**, *19*, 553-565.

(30) Glasauer, S.; Weidler, P.G.; Langley, S.; Beveridge, T.J. Controls on Fe reduction and mineral formation by a subsurface bacterium. *Geochim. Cosmochim. Acta.* **2003**, *67*, 1277-1288.

(31) Langley, S.; Beveridge, T.J. Effect of O-side-chain-lipopolysaccharide chemistry on metal binding. *Appl. Environ. Microbiol.* **1999**, *65*, 489-498.

(32) Zavinsky, S. I.; Rehr, J. J.; Ankudinov, A.; Albers, R. C.; Eller, M. J. Multiple Scattering Calculations of X-ray Absorption Spectra. *Phys. Rev.* **1995**, *B52*, 2995-3009.

(33) Ankudinov, A. L.; Rehr, J. J. Relativistic calculations of spin-dependent x-ray absorption spectra. *Phys. Rev.* **1997**, *B56*, 1712-1716.

(34) Hallberg, R.; Ferris, F.G. Biomineralization by *Gallionella*. *Geomicrobiol. J.* **2004**, *21*, 325-330.

(35) Kennedy, C.B.; Scott, S.D.; Ferris, F.G. Hydrothermal phase stabilization of 2-line ferrihydrite by bacteria. *Chem. Geol.* **2004**, *212*, 269-277.

(36) Emerson, D.; Ghiorse, W.C. Ultrastructure and chemical composition of the sheath of *Leptothrix discophora* SP-6. *J. Bacteriol.* **1993**, 175, 7819-7827.

(37) Glasauer, S.; Langley, S.; Beveridge, T.J. Sorption of Fe (hydr)oxides to the surface of *Shewanella putrefaciens*: cell-bound fine-grained minerals are not always formed de novo. *Appl. Environ. Microbiol.* **2001**, *67*, 5544-5550.

(38) Kulczycki, E.; Fowle, D.A.; Fortin, D.; Ferris, F.G. Sorption of cadmium and lead by bacteria-ferrihydrite composites. *Geomicrobiol. J.* **2005**, *22*, 299-310.

(39) Dzombak, D.A.; Morel, F.M.M. In *Surface complexation modeling: hydrous ferric oxide*, 1st ed.; Wiley Inter Science: New York, 1990; Chapter 1.

(40) Stookey, L.L. Ferrozine – a new spectrophotometric reagent for iron. *Anal. Chem.* **1970**, *42*, 779-781.

Figure Legends

Figure 1. **a)** Scanning electron micrograph of BIOS showing abundant filamentous microbial sheaths. **b)** Unstained transmission electron micrograph of BIOS showing mineral-encrusted sheaths in cross-section and one (arrow) in longitudinal section.

Figure 2. EXAFS spectra and radial structure functions (RSFs) of hydrated Sr^{2+} and Sr^{2+} sorbed to: HFO alone, bacterial cells alone, and BIOS. Solid lines are non-linear least-squares fits with k-range of 2.5 to 10.0 $Å^{-1}$.

Figure 3. Strontium sorption edge data for BIOS. Symbols represent data points from three independent replicates. 50% sorption of strontium (i.e., the characteristic sorption edge) occurs at pH 6.06.

Figure 4. Isotherm data for strontium sorption under conditions of **a)** low ionic strength (0.001 M KNO_3) and **b)** high ionic strength (0.1 M KNO_3). Symbols represent data points from three independent replicates. The data follow a Langmuir model (solid line) with high correlation.

Figure 1

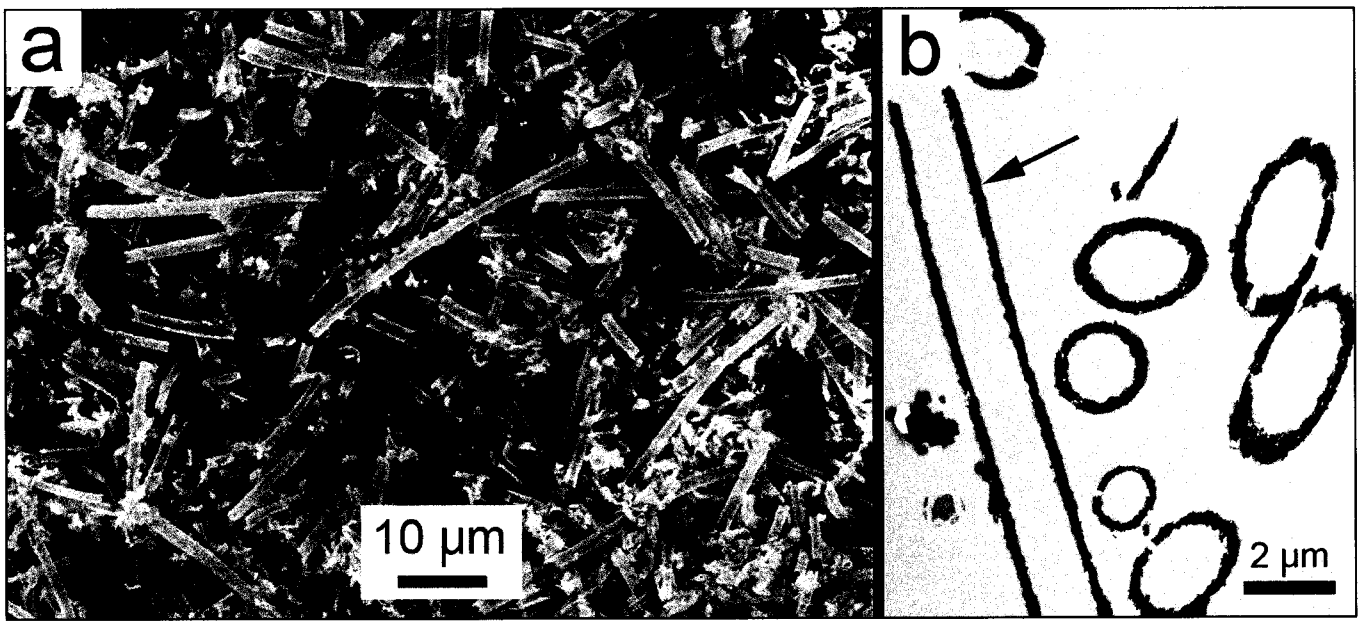

Figure 2

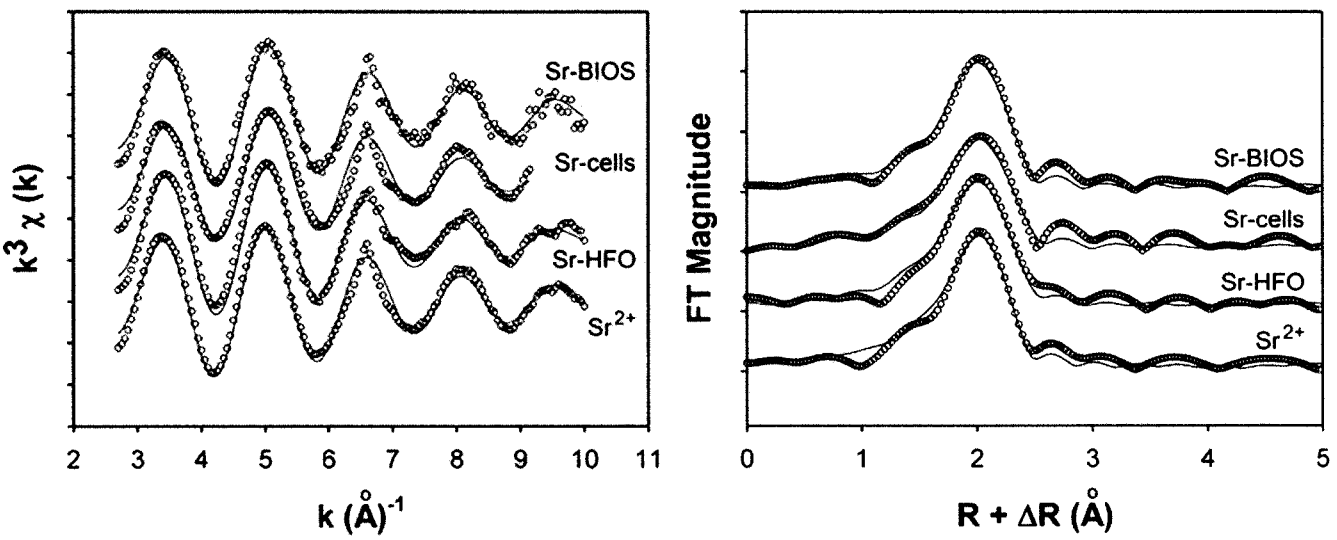

Figure 3

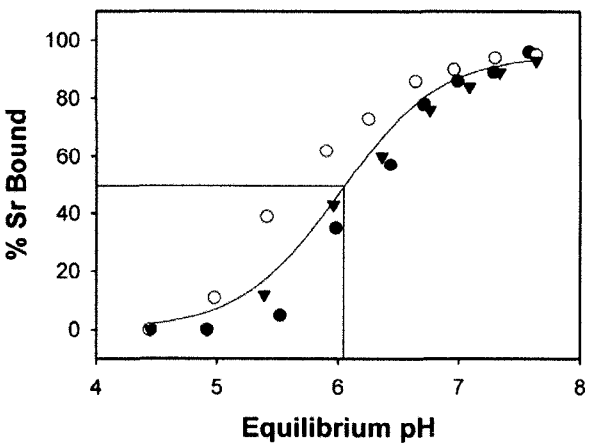

Figure 4

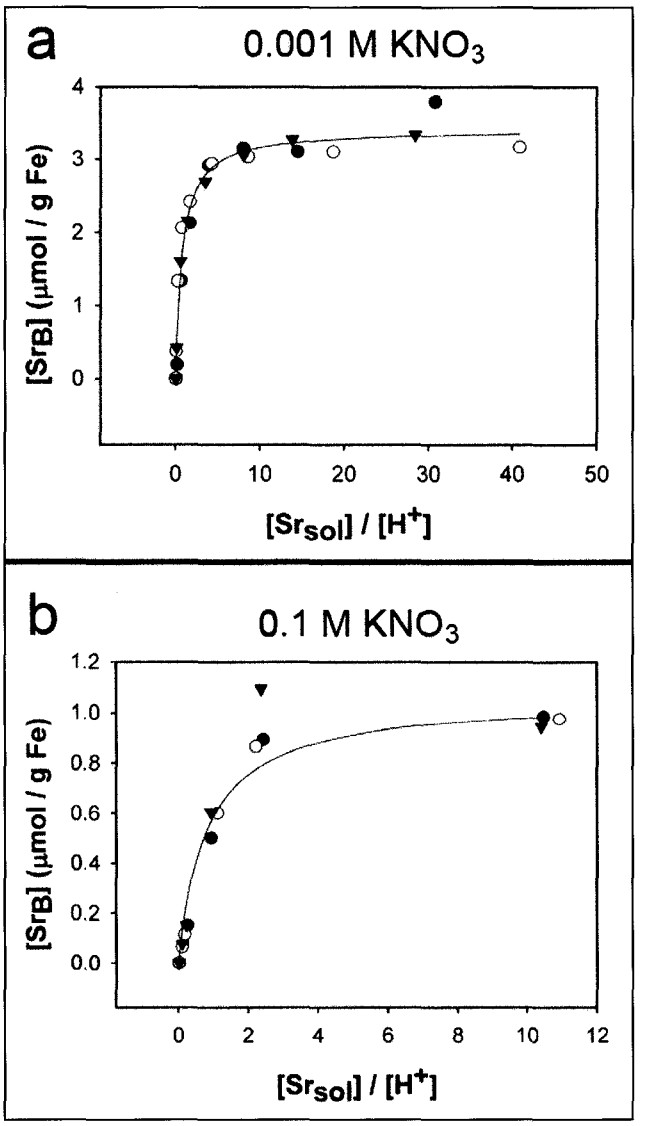

Table S1. Selected physicochemical measurements of the groundwater overflowing the Chalk River BIOS deposit. Data include values from 11 sample sites situated 0.5 – 40 m from a diffuse groundwater discharge zone, and measured seasonally over a span of one year.

Measurement	**Mean (*n* = 39)**	**Minimum**	**Maximum**
pH	5.92	5.41	6.61
Eh (mV)	282.0	211.6	381.0
T (°C)	7.95	1.43	13.01
Dissolved Oxygen (mg L^{-1})	5.12	0.05	13.84
Conductivity (μS cm^{-1})	29	ND[c]	51
Total Fe(II) (mg L^{-1})[a]	2.47	ND[c]	12.25
Soluble Fe(II) (mg L^{-1})[a,b]	1.66	ND[c]	5.25
Total soluble Fe (mg L^{-1})[b]	1.77	1.44	2.18
Total Fe (mg L^{-1})	7.62	4.17	8.82
Soluble Sr (mg L^{-1})[b]	0.04	0.03	0.04
Total Sr (mg L^{-1})	0.04	0.03	0.06

[a] Fe(II) measured using ferrozine (*40*)

[b] refers to samples filtered through 0.22 μm syringe filters prior to analysis by ICP-OES

[c] ND = none detected

Table S2. Major and selected trace element composition of the BIOS following acid digestion. All values are mg L^{-1}.

Element[a]	Mean (n = 6)	Minimum	Maximum
Ba	0.13	0.04	0.31
Ca	6.23	1.49	14.77
Fe	152.33	128.81	183.64
K	0.37	0.31	0.47
Mg	0.98	0.39	1.86
Mn	0.47	0.06	1.07
Mo	0.29	ND[b]	1.75
Na	0.73	0.39	1.34
P	2.12	1.35	2.95
S	0.30	0.12	0.85
Si	6.19	5.43	6.64
Sr	0.18	0.01	0.52

[a] values for Al were omitted due to inadvertent corrosion of Al-foil cap liners during the sample digestion procedure, while all values for Cd, Co, Cr, Cu, Ni and Zn were below the limits of detection.

[b] ND = none detected.

Table S3. Measurements obtained from fitting Sr K-edge EXAFS spectra

	Shell	N	R (Å)	ΔE_0 (eV)	σ^2 (Å^2)
Aqueous Sr^{2+}	Sr-O	8.0 ± 1.3	2.580 ± 0.015	-2.6 ± 1.5	0.013 ± 0.001
Sr-BIOS	Sr-O	7.6 ± 1.3	2.576 ± 0.018	-1.4 ± 1.7	0.013 ± 0.001
Sr-cells	Sr-O	7.2 ± 1.4	2.584 ± 0.019	-0.7 ± 1.7	0.013 ± 0.001
Sr-HFO	Sr-O	8.9 ± 1.6	2.585 ± 0.018	-1.3 ± 1.7	0.015 ± 0.001

Table S4. Isotherm measurements for Sr sorption on BIOS under conditions of low and high ionic strength. The values displayed represent the means and standard deviations from three independent replicates. R^2 values refer to the correlation of the experimental data with the Langmuir model.

Ionic strength	**S_{max} (μmol Sr g Fe^{-1})**	**K_{ads}**	**R^2**
Low (0.001 M KNO_3)	3.41 ± 0.11	1.26 ± 0.06	0.99
High (0.1 M KNO_3)	1.06 ± 0.11	1.23 ± 0.44	0.96

Supporting Information Figure Legends

Figure S1. **a)** High magnification scanning electron micrograph of BIOS, showing tubular sheath structures and a twisted stalk, resembling structures produced by *Leptothrix* spp. (L) and *Gallionella* spp. (G), respectively. **b)** Elemental analysis of the mineral phase confirmed it was composed largely of iron and oxygen, with traces of silicon and calcium. The large phosphorus signal reflects the high-phosphate buffer solution in which the material was suspended. The carbon and copper peaks were generated by the specimen support grid.

Figure S2. X-ray diffraction patterns produced from untreated and Sr-loaded HFO and BIOS. The broad features centred at 1.5 Å and 2.5 Å are characteristic of 2-line ferrihydrite. Sharper peaks in the BIOS patterns are derived from silicate weathering minerals (quartz, feldspar, mica). For clarity, patterns have been vertically separated on an arbitrary y-axis.

Figure S1

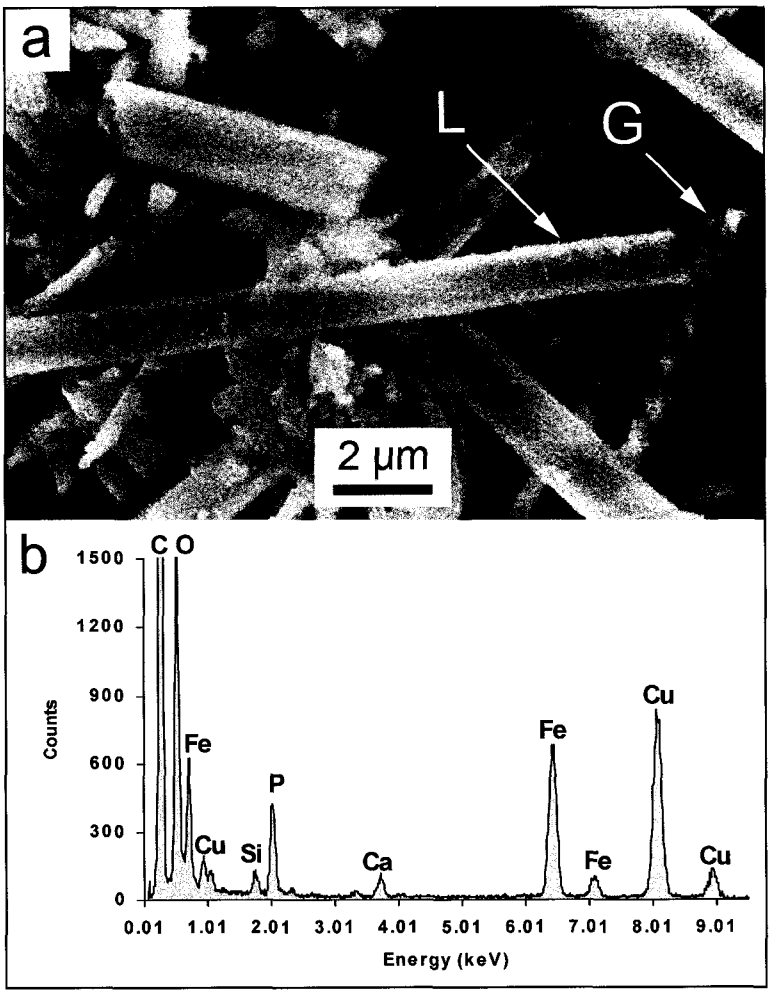

Figure S2

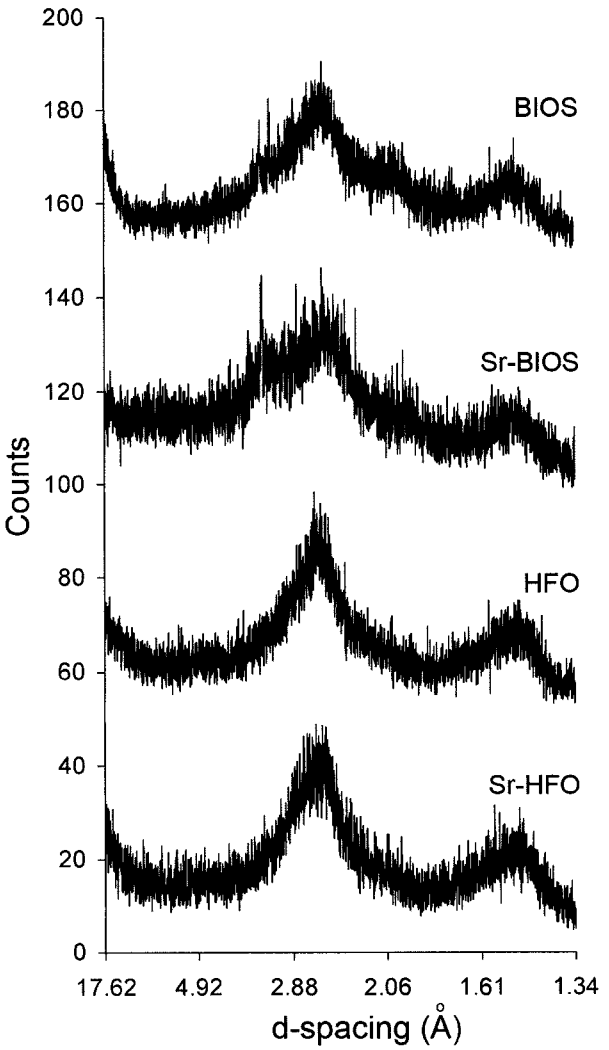

From the data presented in Section 2, BIOS appear to be effective sorbents of dissolved Sr^{2+}. However, the finding of sorption via outer-sphere complexation has important implications for immobilization of Sr by BIOS, since outer-sphere complexation is reversible and will be affected by a variety of environmental factors such as pH and ionic strength of the groundwater. Furthermore, as the BIOS are precipitated and progressively buried, they may become subjected to anaerobic microbial Fe(III) reduction. This will likely also affect the sorptive capacity of the BIOS, especially if Sr is sorbed to the iron oxide component that is being reduced.

Unfortunately, no literature is available on the microbial reduction of BIOS and, therefore, its stability under reducing conditions was unknown. In the following section, the susceptibility of BIOS to microbial reduction was examined using the well-characterized, dissimilatory iron-reducing bacterium (DIRB), *Shewanella putrefaciens* CN32. The reduction experiments were carefully designed to mimic previous studies of iron reduction using the same DIRB and growth medium, but with a synthetic, hydrated ferric oxide (HFO) serving as terminal electron acceptor. The rate and extent of iron reduction in BIOS were calculated and compared to established values of reduction for mineralogically similar HFO. Samples of BIOS from two other sites were also included, with the intent of allowing for a more general interpretation of the reducibility of BIOS compared to synthetic analogs. The results of this research are detailed, below, in Section 3.

Section 3

A comparison of the rates of Fe(III) reduction in synthetic and bacteriogenic iron oxides by *Shewanella putrefaciens* CN32

A revised version of this manuscript has been accepted for publication in *Geomicrobiology Journal*[1]

[1] Langley, S., Gault, A.G., Ibrahim, A., Renaud, R., Fortin, D., Clark, I.D., Ferris, F.G. 2008. A comparison of the rates of Fe(III) reduction in synthetic and bacteriogenic iron oxides by *Shewanella putrefaciens* CN32. Geomicrobiol. J. In press.

ABSTRACT

The susceptibility of various bacteriogenic iron oxides (BIOS) to bacterial Fe(III) reduction was examined. Reduction resulted in complete dissolution of the iron mineral from the surfaces of the Fe-oxidizing consortium. Reduction rates were compared to that of synthetic ferrihydrite (HFO). The reduction rate of HFO (0.162 day^{-1}) was significantly lower than that of Äspö (*Gallionella* dominated) BIOS (0.269 day^{-1}). Two Canadian (*Leptothrix* dominated) BIOS samples showed statistically equivalent rates of reduction (0.541 day^{-1} and 0.467 day^{-1}), which were higher than both Äspö BIOS and HFO. BIOS produced by different iron-oxidizing genera have different susceptibilities to microbial reduction.

INTRODUCTION

Iron oxides are ubiquitous minerals at the Earth's surface, due to the abundance of both iron and atmospheric oxygen and the circumneutral pH of most surface waters. Under such conditions, ferrous iron is chemically unstable and is readily oxidized to insoluble ferric oxides. However, even in acidic environments, where the low pH increases the stability of the ferrous ion, iron oxidation can still occur as a result of bacterial and archaeal metabolism. For example, acidophiles such as *Acidithiobacillus ferrooxidans*, *Leptospirillum ferrooxidans*, and *Ferroplasma* spp. (Edwards et al. 2000; Golyshina et al. 2000; Baker and Banfield 2003) derive their metabolic energy from the oxidation of Fe^{2+} and promote the precipitation of ferric minerals. Certain bacteria (e.g., *Gallionella* spp., *Leptothrix* spp., *Mariprofundus* spp.) also play a role in the active oxidation of iron in circumneutral environments (Hallbeck and Pedersen 1991; Emerson and Ghiorse 1993; Emerson et al.

2007). However, in these instances, the organisms are essentially in competition with dissolved O_2 for available ferrous ions. In order to survive, they must occupy a very limited ecological niche where Fe^{2+} is supplied at a rate that exceeds its rate of conversion to Fe^{3+} by molecular oxygen. For example, *Gallionella ferruginea* requires oxygen concentrations of around 0.1 to 1% of air saturation, with neutral or slightly alkaline pH, and an Eh in the range of +200 to +380 mV (Hallbeck and Pedersen 1990, 1991). As a result, neutrophilic iron oxidizers are often found growing in anoxic-oxic gradient zones near groundwater springs, seeps and even oceanic hydrothermal systems (Hallberg and Ferris 2004; James and Ferris 2004; Edwards et al. 2003; Emerson et al. 2007), where chemically reduced waters, enriched in Fe^{2+}, emerge to oxygenated environments. Whether taking place in acidic or neutral environments, the combination of chemical and microbial iron oxidation in the presence of bacterial cells results in the precipitation of fine-grained iron oxides in close association with microbial surfaces. To distinguish them from purely geogenic or synthetic minerals, these iron precipitates have been termed bacteriogenic iron oxides (BIOS; Ferris et al. 1999).

In circumneutral solutions, the poorly ordered mineral ferrihydrite ($FeOH_3.nH_2O$) is often one of the first solid phases to precipitate following oxidation of ferrous iron (Cornell and Schwertmann 2003), however, it is highly hydrated and not very stable. Consequently, it is usually subject to continued oxidation/hydrolysis and dehydration reactions, which form the more ordered iron oxides goethite (α-FeOOH) and lepidocrocite (γ-FeOOH; Cornell and Schwertmann 2003). Continued dehydration and subsequent re-ordering of internal atomic structure can yield even more crystalline oxides such as hematite (Fe_2O_3), which is typically the most stable end-member under pH-neutral, oxic conditions (Cornell and Schwertmann

2003). Ferrihydrite is also a common component of BIOS (Kennedy et al. 2003a, 2003b; Langley et al. 2008, unpublished data), occurring as nanometre and micrometre-scale aggregates of iron mineral, coating the surfaces of the microbial cells and cellular structures. Over time, this iron-encrusted cell debris can accumulate in sedimentary layers, occasionally forming extensive deposits that can cover thousands of square metres (Stoffers et al. 2006; Langley et al. 2008, unpublished data).

As precipitation of BIOS proceeds, underlying layers of the oxide sediment become progressively buried. With sufficient depth, or when aerobic microbial respiration rates are high, diffusion of atmospheric O_2 into the BIOS is limited and the BIOS can become anoxic, permitting anaerobic microbial respiration to proceed, with the ferric iron of the sediments acting as a potential terminal electron acceptor. The dissimilatory iron reducing bacterium (DIRB) *Rhodoferax ferrireducens* and both of the more commonly studied DIRB genera *Geobacter* and *Shewanella* have all been identified as part of the microbial consortia within some BIOS (Anderson et al. 2006). These organisms couple oxidation of organic molecules and detrital matter within the BIOS to reduction of the ferric iron, generating metabolic energy and releasing Fe^{2+} back into solution (Lovley and Phillips 1988; Myers and Nealson 1990). The newly solubilized Fe^{2+} can sorb onto available reactive sites within the BIOS where it may undergo rapid solid-phase reactions. Alternatively, the ferrous iron may diffuse upward to be re-oxidized (either chemically or biologically) in surficial BIOS layers. The combined roles of the iron-oxidizing and iron-reducing bacteria thus constitutes a redox loop that is important not only for the cycling of iron, but for the co-precipitation/solubilization of any chemical species bound to the iron oxide phase.

The ability of DIRB to reduce iron oxides is dependent on several factors including mineral particle size, surface area, and crystallinity. Typically, the rate of reduction is increased with increasing surface area, but is inversely related to the particle size and crystallinity of the oxide (Roden and Zachara 1996; Roden 2003). While the available literature is replete with information on the reduction of iron oxides, much of this work has used synthetic minerals as analogs for natural systems. These synthetic iron oxides are most often formed from the hydrolysis of reagent grade iron compounds from aqueous solution, often in ultra-pure water. The result is a chemically pure, hydrated ferric oxide (HFO). The surface area and degree of crystallinity of the HFO can vary from a poorly ordered phase such as ferrihydrite (several hundred m^2/g), to more crystalline iron oxides such as nano- and micro-scale goethite and hematite (tens to hundreds of m^2/g) (Roden and Zachara 1996). As chemically pure minerals, however, they are not truly analogous to natural systems, where such minerals are precipitated in the presence of a wide variety of organic and inorganic moieties (Fortin et al. 1993). In particular, they will be very poorly analogous to a BIOS system, where the iron is precipitated directly on the surfaces of microbial cells and cellular structures. It has been speculated that precipitation on such surfaces may act to decrease the interfacial free energy and thereby provide stability to more poorly ordered mineral phases (Warren and Ferris 1998). In addition, precipitation on cellular structures such as sheaths and stalks (which are tens of micrometres long) would likely act to decrease the effective surface area of a mineral. If this is the case, then the iron oxides within BIOS deposits should be more stable, and hence less reactive than the synthetic HFO that is often used in laboratory examinations of microbial iron reduction.

Our goal in this research was to characterize the BIOS from three separate sites with respect to iron mineralogy, and to determine the *in vitro* reactivity and susceptibility of the iron oxides from each site to microbial reduction when subjected to anaerobic conditions in the presence of *Shewanella putrefaciens* CN32, a well-characterized iron-reducing bacterium. Because the iron oxides in BIOS were originally precipitated in association with cell surfaces and a wide variety of environmental ions, we hypothesized that the stability of the mineral phase would be increased, thereby decreasing its susceptibility to bacterial reduction when compared to synthetic, but mineralogically similar, iron oxides prepared by precipitation from chemically pure solution.

MATERIALS AND METHODS

Iron Oxide Collection and Preparation

BIOS samples were obtained from Deep River (latitude: 46°09'56"N, longitude: 77°37'23"W) and Chalk River (latitude: 46°03'04"N, longitude: 77°25'11"W), Ontario, Canada, and from the Hardrock Laboratory BIOS Reactor *In Situ* Continuous Flow (BRIC) Device, in Äspö, Sweden (latitude: 57°16'02"N, longitude: 16°26'55"E; Table 1). Acid-washed, 1 L plastic bottles were immersed within the BIOS deposits, to completely fill the bottles with mineral suspension. Samples were stored at 4°C until return to the laboratory where they were decanted after settling of the solid phase. The solid suspension was then sieved (200-mesh) to remove any leaf litter and larger detrital material. The sieved suspensions were centrifuged at 14,000 × g for 10 minutes, and decanted to remove most of the remaining water. Centrifugation resulted in a thick, mud-like suspension of iron oxides, which were then gamma-irradiated using a Nordion Gammacell 220 to a final dose of

approximately 14 kGray. Irradiated samples were stored in the dark at 4°C until use. Previous studies (McNamara et al. 2003) have shown that gamma-irradiation induces little physical and mineralogical change in natural sediments and, therefore, would represent a suitable technique for the sterilization of the BIOS prior to the reduction experiments.

To allow comparison of measured iron reduction rates to established values, a synthetic hydrous ferric oxide (HFO) was also prepared as described previously (Glasauer et al. 2003). Briefly, 1 M NaOH was rapidly added to 2 M $FeCl_3 \cdot 6H_2O$ to a final pH of 7.0. The resulting iron oxide precipitate was washed 10 times in ultrapure (18 MΩ·cm) water (UPW). It was then irradiated, as described above, and stored in the dark at 4°C prior to use.

Inductively Coupled Plasma – Optical Emission Spectrometry

In order to determine the total Fe content within the BIOS and HFO samples, small aliquots (0.1 g) of each were suspended into 6 mL UPW, and fully digested by addition of 4 mL 30% H_2O_2 and 2 mL trace metal grade HNO_3, followed by heating at 70°C for 12 hours (Kulczycki et al. 2005). Digested samples were diluted (1:100) into 1% trace metal grade HNO_3 and analyzed for major element composition by inductively coupled plasma – optical emission spectroscopy using a Varian Vista-PRO CCD Simultaneous ICP-OES, operating under standard conditions.

BIOS Mineralogy

Mineralogy of the BIOS and HFO samples was determined by powder X-ray diffraction (XRD) analysis. For XRD, untreated and irradiated samples were freeze-dried, then ground to a fine powder using a standard mortar-and-pestle. Analysis was performed

using a Philips PW 1830 X-ray diffractometer, with a Cu-Kα X-ray source, operating at a tension of 45 kV and a current of 40 mA. Continuous scans were run from a start angle of 5° to an end angle of 70° (2θ) with a step size of 0.02°, and a count time of 2.5 seconds per step.

Bacterial Culture and Microcosm Growth Conditions

The dissimilatory iron-reducing bacterium (DIRB) *Shewanella putrefaciens* CN32 was kindly donated by Dr. Terry Beveridge (Department of Molecular and Cellular Biology, University of Guelph, Ontario, Canada) and maintained on tryptic soy agar at 22°C. Microcosm reduction experiments were carried out in a liquid, chemically-defined medium (CDM) with the following composition (Glasauer et al. 2003): 20 mM sodium lactate, 3.5 mM sodium phosphate, and 4 mM 1,4-piperazinediethanesulfonic acid (PIPES) buffer, and trace element salts, at pH 7.0 prior to autoclaving. For transfer into the CDM, cells were first inoculated into 50 mL of tryptic soy broth (TSB) at 22°C on a rotary shaker set to 125 rpm. After 24 hours growth, the cells were passaged (1% inoculum) through a series of TSB:CDM mixtures (50:50, 5:95, 1:99, at 125 rpm, for 24 hours at 22°C in each 50 mL mixture), in order to acclimate the cells to the depleted nutrient conditions of the CDM. After 2% inoculation into 200 mL of 100% CDM, cells were grown for 36 hours at 22°C, prior to harvesting by centrifugation at 14,000 × g for 5 minutes. The resulting cell pellet was re-suspended into 2 mL of fresh, sterile CDM, and this concentrated cell suspension was used to inoculate the experimental cultures. A commercial protein assay (BioRad Protein Assay II) was used to standardize the inoculum, such that the final experimental cultures each contained 0.5 μg/mL total protein, following established procedures (Glasauer et al. 2002, 2003).

The experimental Fe(III)-reduction systems consisted of 700 mL sterile CDM in 1 L acid-washed Kimax bottles, amended with 4 mM total iron in the form of either irradiated BIOS or HFO. Abiotic control systems were identical to the biotic ones, but did not contain *S. putrefaciens* CN32. Inoculation, incubation and sampling of the culture vessels was performed at 22°C, at all times inside a Coy Labs anaerobic chamber operating with an atmosphere of 5% H_2:95% N_2. All reduction experiments were conducted in triplicate, from three separate preparations of growth medium, cells, and iron oxides. Sampling of each system was performed immediately following addition of the cells (time 0), at 6 hours, 12 hours and 24 hours post-inoculation, followed by once daily for a total of 7 days.

Microcosm Sampling Procedures

At each sampling point, culture vessels were shaken vigorously and 20 mL aliquots were immediately removed (aseptically) while any solid phase material remained in suspension. The aliquots were placed in sterile, acid-washed borosilicate scintillation vials. All sub-samples were then taken from this aliquot (immediately following shaking), in order to minimize the possibility of contaminating the larger culture. Standard laboratory meters and probes were used for measuring pH and Eh.

For determination of culture viability, 0.5 mL of suspension was removed, serially diluted (1:10 per dilution) in sterile, fresh CDM, and plated onto sterile TSA plates for enumeration of cells using viable plate counts. Previous studies have shown this technique to be a reliable method for culture enumeration under these conditions (Glasauer et al. 2002, 2003). The remaining 0.4 mL of undiluted culture was used to prepare samples for electron microscopy, as described below.

For determination of total ferrous Fe concentration, 0.5 mL of unfiltered culture suspension was added to 4.5 mL of 0.5 M HCl (trace metal grade), and allowed to equilibrate for 24 hours prior to removal from the anaerobic chamber and analysis via the ferrozine method (Stookey 1975; Viollier et al. 2000). For analysis of soluble phase Fe (both ferrous and total Fe), 6.5 mL of culture suspension was first filtered through a 0.22 μm nylon syringe filter. For soluble ferrous Fe, 0.5 mL of the filtered suspension was added to 4.5 mL of 0.5 M HCl for analysis by ferrozine as described above. The remaining 6 mL of filtered suspension was acid digested and analyzed for total soluble Fe and P by ICP-OES as described above. An identical procedure, using 6 mL of unfiltered suspension, allowed for determination of total Fe and P concentration.

Electron Microscopy

0.4 mL of culture suspension was chemically fixed by addition of 20 μL of 50% (aq) glutaraldehyde (electron microscopy grade). Fixed samples were used for the preparation of whole mounts and thin sections, as described previously (Langley and Beveridge 1999). Transmission electron microscopy, energy-dispersive X-ray spectroscopy (EDS) and selected area electron diffraction (SAED) of whole mounts and thin sections were performed at the Guelph Regional Integrated Imaging Facility (University of Guelph, Ontario, Canada) on a Philips CM-10 electron microscope operating at 80 kV. The microscope was coupled to a Soft-imaging Systems (SiS) Morada CCD camera, controlled by SiS iTEM software, and an EDAX Sapphire X-ray detector which collected X-ray spectra over 100 seconds (live count time) at a beam diameter of approximately 200 nm. Scanning electron microscopy of whole mounts was performed at the Department of Earth Science (Carleton University,

Ottawa, Ontario, Canada) on a JEOL JSM-6400 scanning electron microscope operating at 20 kV.

RESULTS

X-Ray Diffraction

X-ray diffraction patterns are presented in Figure 1a, with significant peaks listed in Table 2. Generally, the patterns contained two broad reflections, centred at d-spacings of approximatley 2.5 and 1.5 Å, which are indicative of the poorly ordered iron oxide mineral, 2-line ferrihydrite. The sharper reflections apparent in the BIOS patterns likely corresponded to silicate minerals such as quartz, feldspar, and mica (Table 2). Following gamma-irradiation, the diffraction patterns were not significantly altered (Figure 1B), indicating that irradiation under the conditions described did not adversely affect the mineralogy of the samples.

Electron Microscopy

Scanning electron microscopy revealed that the BIOS from Deep River and Chalk River were dominated by filamentous, tubular structures approximately 1 μm wide by tens of micrometres long, which resembled the sheaths produced by the iron-oxidizing bacteria *Leptothrix* spp. (Figure 2A). Occasionally, helical structures were also observed that were similar in appearance to the twisted stalks produced by the iron-oxidizing bacteria *Gallionella* spp. (Figure 2A). In contrast, the Äspö BIOS were dominated by *Gallionella*-like structures, with a smaller proportion of the filamentous *Leptothrix*-like structures also present. Relative abundances of the two main iron-oxidizing genera within the samples are

summarized in Table 1. In thin section, the structures described above were coated with an electron-dense precipitate approximately 100-200 nm thick (Figure 2B). Analysis of the precipitate using EDS generated spectra with strong signals corresponding to Fe, O, and other trace elements common to biological materials (Figure 2C). Selected area electron diffraction (SAED) of the iron-rich precipitate generated two diffuse rings, indicative of a poorly ordered mineral, but failed to indicate the presence of any crystalline mineral phases (data not shown).

Electron microscopic examination and EDS analysis of the synthetic HFO revealed aggregates of roughly spherical particles (approximately 100 nm in diameter) which were rich in Fe and O. No microbial structures were observed and selected area electron diffraction did not reveal the presence of any crystalline phases (data not shown).

Reduction Experiments

All reduction data and lines of best fit were plotted using SigmaPlot 2001 statistical graphing software. In all abiotic controls, there was no microbial growth detected and there were no significant changes in any of the variables measured, with the exception of Eh. Within the first 24 hours following addition of the culture vessels to the anaerobic chamber, there was a gradual decrease in Eh (of approximately 70 mV, on average, for all systems), followed by a plateau at the lower level for the duration of the experiments (data not shown). This decrease likely represented out-gassing of oxygen from the medium following equilibration with the chamber atmosphere.

Synthetic HFO Reduction

Within the first 24 hours after inoculation of the HFO systems, the Eh value decreased from an average of 475 mV to 108 mV, at which point it remained level for the duration of the experiment (data not shown). Cell counts remained constant at approximately 3.1×10^7 CFU/mL for the duration of the experiment (data not shown). There was an initial decrease in Fe(II) followed by a recovery back to initial levels after 1 day. From Day 1 to Day 5, total Fe(II) increased gradually, from approximately 10% to 78% (the maximum measured, Table 3) of the total Fe available (Figure 3a). Fe(II) remained at this level for the duration of the experiment. Over the same time span, soluble phosphorus decreased from approximately 85% to 65% of the total (Figure 3a). The pH of the system increased, from 6.66 to 6.82, over the length of the experiment (data not shown).

Äspö BIOS Reduction

Immediately after addition of the DIRB, the Eh of the Äspö BIOS systems decreased from approximately 434 mV to –9 mV over the first two days, at which point it remained at this level for the duration of the experiment (data not shown). Cell counts remained constant at approximately 2.0×10^7 CFU/mL for the duration of the experiment. There was a rapid increase in the percentage of total Fe(II) in this system, immediately following addition of the DIRB (at approximately 10% of total Fe), tailing off around Day 2 (at approximately 61%) and finally levelling at about Day 4 (approximately 80%; Figure 3b). The maximum percentage of Fe reduced was 83% (Table 3). Soluble phosphorus decreased from approximately 83% of total P to 40% during the same period of time (Figure 3b). Also during the span of Fe(II) production, the pH increased, from 6.65 to 6.91 (data not shown).

Deep River BIOS Reduction

Upon addition of the DIRB, the Eh of the Deep River BIOS systems dropped from approximately 479 mV to 39 mV within 24 hours. From Day 1 to Day 4 it increased, gradually, back up to 87 mV, at which point it remained constant for the duration of the experiment (data not shown). The DIRB remained viable, at approximately 4.0×10^7 CFU/mL, until Day 3, at which point they began to die off steadily throughout the remainder of the experiment (data not shown). The percentage of total Fe(II) increased rapidly, from approximately 20% of the total Fe (at the start of the experiment) up to approximately 69%, 1 day following inoculation (Figure 3c). After 1 day, the Fe(II) concentration began to level off, reaching a plateau (at approximately 90%) after Day 3. The maximum percentage of reduced Fe measured was 92% (Table 3). During the same period of time, soluble phosphorus decreased from approximately 75% of total P to 50% (Figure 3c), while the pH increased from 6.63 to 6.90 (data not shown).

Chalk River BIOS Reduction

After addition of the DIRB, the Eh of the Chalk River BIOS systems decreased from approximately 402 mV to 71 mV at Day 6 (data not shown). There was an initial increase in cell numbers for the DIRB, from 5.5×10^7 CFU/mL at inoculation to 1.2×10^8 CFU/mL at Day 1. After 2 days, however, the culture began to decline, steadily, over the course of the experiment (data not shown). Total Fe(II) increased rapidly from approximately 26% of the total Fe at inoculation to approximately 70% at Day 1 (Figure 3d). This was followed by a rapid decline in the rate of Fe(II) accumulation between Day 1 and Day 2, with a plateau in Fe(II) proportion of approximately 95% achieved around Day 3. The maximum percentage

of reduced Fe recorded was 98% (Table 3). During the same period, soluble phosphorus decreased from 67% of the total P to 44%. However, there was an additional decrease in soluble P observed, from 44% at Day 4 to approximately 31% at termination of the experiment (Figure 3d). The pH increased in from 6.53 to 6.71 during the first 12 hours of incubation, at which point it remained at this level for the duration of the experiment (data not shown).

During the reduction, TEM of unstained thin sections revealed that the iron precipitate surrounding the microbial structures of the BIOS was completely degraded by the DIRB (Figure 4a-d). Within 12 hours after inoculation, significant depletion of the iron precipitate was observed, with continued loss of electron density in the sections representing a loss of iron from the surrounding precipitate. Finally, at termination of the experiment, the original iron-encrusted microbial structure could barely be seen in unstained TEM thin sections. EDS analysis of the precipitates at the same time intervals confirmed a steady decrease in the mass of iron surrounding the structures (Figure 4e-h).

Mineral Transformations

Following incubation with the DIRB, the iron oxide samples were transformed from their normal rust-brown appearance to a more green-white precipitate. Analysis of the precipitates with XRD revealed transformation of the poorly ordered iron oxides to a more crystalline phase (Figure 5). Computer analysis of the diffraction pattern indicated the presence of numerous hydrated ferrous phosphates of varying stoichiometries as well as the mineral, vivianite ($Fe_3(PO4)_2 \cdot 8H_2O$). Results from the microbial reduction of all BIOS samples and the HFO were identical to that described above (data not shown). This was not

unexpected, since vivianite has been reported previously in similar studies using HFO (Glasauer et al. 2003) and was also predicted from modeling of the present data using geochemical computer software (PHREEQ-C). In all of the abiotic control experiments, no similar increase in crystallinity was observed for either of the BIOS samples or the HFO (data not shown).

Reduction Rates

To obtain a measure of reduction that could be compared to established literature values for similar systems, a series of linear plots was constructed, encompassing the period of maximum Fe(II) accumulation rate observed in each system. From the linear plots (Figure 6), rate data and correlation coefficients were calculated and reported in Table 3. Statistical analyses (using t-tests, $p<0.05$) of the data indicated no significant differences in the maximum percentages of Fe reduced, nor the rates of reduction for the Deep River and Chalk River BIOS. However, their values were significantly higher than those of Äspö BIOS, which in turn were significantly higher than those of the synthetic HFO.

DISCUSSION

Mineralogical and Biological Characterization of BIOS

The presence of silicate peaks in the XRD patterns of the Deep River and Chalk River BIOS is not surprising. The Chalk River BIOS is generated within groundwater that flows through a 10,000 year-old aeolian sand aquifer prior to discharging into a wetland environment. Previous studies of the aquifer material have classified it as loosely consolidated micaceous sand (Inch and Killey 1987). Flakes of mica also can be seen

intermixed with the sand at the site. Similarly, the Deep River BIOS is fed by an artesian spring in an area underlain by gneiss bedrock (James and Ferris 2004). As seen in Table 2, the positions of the peaks in the BIOS diffractograms corresponded closely to expected reflections from quartz, feldspar (albite) and possibly mica (muscovite) (Klein 2002). The silicate components of the Deep River and Chalk River BIOS are, therefore, simply weathering products of the aquifer material through which the respective groundwater is flowing. In contrast, the Äspö BIOS did not show significant levels of silicate minerals. This is likely because the Äspö BIOS was obtained from an artificial reactor vessel (BRIC). The BRIC is essentially a flow-through growth chamber, which is fed by groundwater delivered from boreholes. The Fe-oxidizing bacteria (FeOB) responsible for BIOS production at Äspö grow within plastic growth tubes inside the BRIC (Anderson and Pedersen 2003). As such, inputs of particulate weathering material into the BIOS (either naturally, or as a result of sampling) are likely not as high as in the more natural systems.

With respect to iron mineralogy, samples from all sources in the present study were dominated by the iron oxyhydroxide 2-line ferrihydrite, as indicated by the broad features centred at d-spacings of 2.5 Å and 1.5 Å in the XRD patterns (Cornell and Schwertmann 2003). This is consistent with numerous reports that document 2-line ferrihydrite as one of the most commonly observed products of microbial iron oxidation in circumneutral environments (Kasama and Marakami 2001; Châtellier et al. 2004; James and Ferris 2004; Langley et al 2008, unpublished data). Additional work in our laboratory (manuscripts in preparation) has also analyzed the Deep River and Chalk River BIOS using Fe K-edge extended X-ray absorption fine structure (EXAFS), and no Fe-bearing mineral more ordered than 2-line ferrihydrite could be detected. Selected area electron diffraction (SAED) is more

sensitive to small-scale heterogeneities and may have provided better characterization of the BIOS mineralogy. However, SAED is somewhat limited by being a spot analysis technique, and the production of an electron diffraction pattern is dependent upon crystals being optimally aligned to the incident electron beam. Therefore, the failure of electron diffraction to identify any crystalline phases in the present study may simply reflect the sampling difficulties associated with the technique, rather than a definite lack of crystallinity within the BIOS. Work is currently underway in our laboratory to better define the relative proportions of any crystalline iron oxides using sequential chemical extractions of the BIOS from Chalk River. Nevertheless, it seems clear that (on a bulk scale) BIOS are dominated by amorphous and poorly ordered iron precipitates. However, it is still possible (and likely) that nanometre or micrometre-scale heterogeneities exist, such that localized areas of higher crystallinity are present within the BIOS, and which are undetectable by bulk-phase analyses. For example, despite the dominance of the 2-line ferrihydrite signal in the present study, Hallberg and Ferris (2004) have reported that iron mineralization in Äspö BIOS appears to proceed by a multi-step process, whereby crystalline iron (possibly hematite) is first deposited within the inner regions of the *Gallionella* stalk fibres. These initial precipitates act as templates for the continued precipitation of more iron. However, subsequent precipitation outside of the stalk fibres is marked by a shift in crystallinity, such that outer regions of the stalk are coated with a mixture of ferrihydrite and goethite (Hallberg and Ferris 2004). It is likely, therefore, that 2-line ferrihydrite represents only the most abundant iron oxide component of BIOS, with more ordered phases being present at levels that are below the limits of detection for bulk analytical techniques (e.g., ~ 5% by weight, for XRD). Interestingly, similar crystalline iron phases were not observed in the Chalk River

and Deep River BIOS in the present study. While it is possible that they simply were not observed in any of the sub-samples examined, it nevertheless raises the possibility that the type of iron oxide produced in a particular BIOS deposit may, to some extent, depend on the type of FeOB involved in its formation.

The abundance of microbial structures resembling *Leptothrix* sheaths and *Gallionella* stalks indicates that BIOS at all three sites are being formed through a combination of both passive (i.e., chemical) and active (i.e., enzymatic or metabolic) Fe oxidation. With respect to structural morphology, the samples are striking in their near-uniformity, being composed overwhelmingly of only these two morphologically distinct organisms. Indeed, James and Ferris (2004) have noted that Deep River BIOS contained only about 4% morphologically indistinct microbial forms, such as rods and cocci (presumably indicative primarily of heterotrophs), and that these forms increased in proportion (up to 70% of total) only when sampling distance from the spring was increased to several metres downstream. Presumably, this is due to the fact that *Leptothrix* might be able to out-compete other organisms for available nutrients so long as microaerophilic conditions persist to allow for metabolic Fe oxidation (James and Ferris 2004). The fact that we collected BIOS immediately adjacent to the spring would therefore explain the marked lack of indistinct cellular forms observed in the present study. The same explanation may also hold for the Chalk River site, where samples were taken from sites proximal to the point of groundwater discharge. While we are aware that morphology alone is insufficient to assign definitive microbial identifications, the distinctive twisted stalks produced by *Gallionella* spp. are often taken as presumptive evidence that the organism is indeed present within the microbial consortia (James and Ferris 2004; Anderson et al. 2006). This may be a reasonable assumption, as to date only one other

organism has been described as producing a similar, twisted-stalk structure. This organism (*Mariprofundus ferrooxydans*) is also an obligate iron oxidizer (Emerson et al. 2007), and its presence would only serve to confirm the role of FeOB in the formation of BIOS at these sites. With respect to the Äspö BIOS, definitive 16S rRNA gene sequencing has been performed, identifying *Gallionella* as the dominant iron-oxidizing genus at that site (Hallbeck et al. 1993), with the most likely species being *G. filamenta*, based on the number of fibres comprising the stalk (Hallberg and Ferris 2004). In an effort to explore the microbial community structure and identify key species within the BIOS, we are currently in the process of performing 16S rRNA gene sequencing analyses of samples collected seasonally from Chalk River. Preliminary data from this work has indeed indicated the presence of both *Gallionella* spp. and *Leptothrix* spp., as well as other iron-oxidizing genera (manuscript in preparation).

Electron Microscopy and Elemental Analysis

In thin sections, the coating of an electron-dense mineral phase on the surfaces of remnant microbial structures within the BIOS supports the notion that the iron oxides are precipitated directly on the surfaces of the FeOB, through a combination of both biotic and abiotic oxidation of Fe^{2+}. Glasauer et al. (2001) have cautioned that observation of microbial cell surface-associated minerals does not necessarily imply precipitation of the mineral on the surface, but may rather imply passive sorption of pre-existing (abiotic) minerals to reactive sites within cell wall polymers. If this were the case, it could be argued that the iron oxides within the BIOS are essentially the same as their abiotic counterparts. However, the dense, compact and uniform nature of the mineral crust observed in the present study would

seem to support the notion of direct, surface-associated precipitation in this case. Regardless, even if the mineral phase were largely abiotic in origin, the presence of such a tightly-bound microbial surface would likely act to alter the reactivity of the associated mineral (Warren and Ferris 1998).

Energy dispersive X-ray analysis of the mineral crust confirmed that it was rich in Fe and O (Figure 2c). The presence of low-atomic number elements in the spectra (such as Na, K, Ca, etc) is to be expected in biological samples, but in the case of the Chalk River and Deep River BIOS they likely also represent a contribution from the weathered silicate aquifer minerals, discussed earlier, which are rich in these lighter elements (Table 1; Klein 2002). As EDS is also a semi-quantitative technique, it can be used to establish the relative proportions of elements within a mineral sample, from which a putative stoichiometry of the mineral can be established (Fortin et al. 2008). The process was used effectively by Hallberg and Ferris (2004) to establish the presence of hematite within stalk fibres during the initial phases of iron mineralization by *Gallionella*. However, efforts at quantifying the Fe and O ratios of the BIOS in the present study did not yield any meaningful and reproducible results. Given the variable chemical composition of amorphous and poorly ordered iron oxyhydroxides (Cornell and Schwertmann 2003), it is perhaps not surprising that no precise stoichiometry could be determined. TEM-electron energy loss spectroscopy (TEM-EELS) has also been successfully used to quantify the Fe/O ratios of various abiotic and biotic iron oxides (Mavrocordatos and Fortin 2002) and should be considered for future analyses of this type of BIOS. Nevertheless, from the available data, it seems clear that the iron oxide component of BIOS is composed primarily of 2-line ferrihydrite, formed in direct association with microbial structural surfaces as 100-200 nm thick mineral precipitates.

Anaerobic Reduction of HFO

In previous studies, using similar procedures (Glasauer et al. 2002, 2003), the reduction of synthetic HFO by *S. putrefaciens* CN32 was first noticed after an initial lag phase, during which time the facultative DIRB are presumably adjusting to the anaerobic conditions imposed by the growth medium. Once adjusted, the period of measurable Fe^{2+} production was typically gradual and protracted, lasting for a period of several days or even several weeks (Glasauer et al. 2003), and was followed by a subsequent plateau in the Fe^{2+} concentration (i.e., a decline in the rate of net Fe^{2+} production). This decline was likely representative of a number of factors, all occurring simultaneously within the culture vessel. The first is a concurrent decline in the viability of the DIRB culture as nutrients become depleted. The second is saturation of the mineral surface sites with sorbed Fe^{2+}, which has a high affinity for solid-phase ferric iron (particularly ferrihydrite; Hansel et al. 2004). This coating of the mineral surface could possibly result in decreased availability of the remaining ferric iron to the enzymatic system of the DIRB (Roden and Urrutia 2002). Finally, as the Fe^{2+} concentration increases, the solution becomes saturated with respect to the ferrous phosphate mineral, vivianite (Glasauer et al. 2003), due to the high concentration (4 mM) of dissolved phosphate in the growth medium. Continued precipitation of the vivianite as a secondary mineral phase removes aqueous Fe^{2+} and phosphate from solution and results in an apparent decrease in the Fe^{2+} production rate.

Ferrous iron production has been expressed as the ratio of Fe(II):total Fe, in order to better account for potential error (inherently introduced by sampling of a suspended solid phase). Using this methodology, we observed the expected trends in growth of CN32 using HFO as the sole terminal electron acceptor. The DIRB reduced 78% of the total available

iron, with ferrous iron production resulting in the removal of phosphorus from the soluble phase (Figure 3a) as vivianite precipitation occurred (Figure 6). During this time, the rate of Fe(II) production was calculated at 0.162 day^{-1} (Table 3). Both the rate of Fe(II) production and the total percentage of Fe reduced were higher than have been reported previously. For example, Glasauer et al. (2002, 2003) have reported total percentages of 40 to 60%, at rates of approximately 0.02 and 0.04 day^{-1}. These are large discrepancies, however it is important to note that we observed an abbreviated period of Fe(II) production (on the order of days, rather than weeks). This fact, combined with the overall higher percentage of Fe(II) produced, would lead to increased values for the rates of Fe(II) production. However, at present we are unable to explain the increase in percentage of total Fe reduced, nor the abbreviated period of Fe(II) accumulation, since all culture conditions (and the DIRB culture itself) were identical to those used in previous studies.

Anaerobic Reduction of BIOS

Cultures of *S. putrefaciens* CN32 grown using BIOS as the sole terminal electron acceptor showed the same general patterns of growth as with HFO, with some important differences. The initial lag phase between culture inoculation and the onset of iron reduction was either abbreviated or absent entirely (Figure 3). This suggests that the cells were able to initiate Fe(III) reduction more easily within the BIOS than the HFO. Further, the extent of Fe(III) reduction and the rates of Fe(II) accumulation in all BIOS systems were significantly higher than for HFO (Table 3). This finding runs counter to our original hypothesis (i.e., that the presence of the microbial surfaces would act to lower the interfacial free energy of the mineral, thereby stabilizing the BIOS and making it less susceptible to reduction by DIRB),

and suggests that the Fe(III) in BIOS is in fact more reducible than that of synthetic iron oxides, even when the bulk phase mineralogy is the same. This notion is supported by the complete dissolution of the mineral precipitate surrounding the FeOB structures observed by EM (Figure 4). Previous studies have shown that (III) reduction proceeds more rapidly and completely when the ratio of DIRB concentration to available Fe(III) is increased over orders of magnitude (Roden and Zachara 1996; Glasauer et al 2002). However, the amount of total Fe added and the initial DIRB concentrations used in the present study were carefully standardized to minimize the possibility that large discrepancies in DIRB concentration might affect the measured reduction rates. Microbial Fe(III) reduction is also closely linked to mineral surface area, such that increases in surface area generally tend to promote reduction (Roden and Zachara 1996; Glasauer et al. 2003). However, this again does not explain the findings of the BIOS reduction. We have attempted to measure BIOS surface area using BET analyses but the results are inconsistent, likely due to the highly variable proportions of organic matter present within the samples. Regardless, precipitation of the BIOS along surfaces that measure tens of microns in length would tend to decrease the total available surface area of the iron oxide, relative to the small (100 nm), roughly spherical aggregates of HFO. As a result, one might expect the BIOS to be less reducible than the HFO, based solely on mineral surface area considerations, although this is clearly not the case. It is possible that the organic phase of the BIOS is somehow responsible for promoting Fe(III) reduction in these samples. For example, various organic compounds may serve as electron shuttles or additional nutrient sources for the DIRB, which might act to increase metabolic rates. However no significant differences in culture growth or viability were noted, other than a small initial increase in DIRB concentration in the Chalk River

system (which may only represent sampling error). Organic components of the BIOS might also complex the Fe(II) and prevent it from binding to, and saturating, surface sites on the remaining ferric oxide. Organic complexation would thereby leave the oxide surface free, promoting continued reduction by the DIRB. Because synthetic HFO does not contain similar organic compounds, this type of complexation would not occur, which would explain the lower reduction rates observed for those systems. Alternatively, the cell wall fabric on which the iron oxide was precipitated may somehow be maintaining the mineral in a structural form that is more readily susceptible to reduction, perhaps by preventing continued crystallization of the iron following its initial precipitation, as has been suggested for marine BIOS (Kennedy et al. 2004).

Finally, the rates of production and amounts of Fe(II) produced in the Chalk River and Deep River BIOS systems were significantly higher than that of the Äspö system. One possible explanation for this may be the presence of crystalline iron oxide phases in the Äspö BIOS. In contrast to Deep River and Chalk River, the Äspö BIOS is dominated by the FeOB *Gallionella*, such that the bulk of the biomass within the system is stalk material produced by the organism (Anderson et al. 2006). As discussed earlier, Hallberg and Ferris (2004) have reported the presence of goethite (as well as ferrihydrite) in the outer layers of the iron oxides coating the *Gallionella* stalk fibres. The presence of this more crystalline Fe phase in the outermost layers might act to slow the initial rate of reduction for this type of BIOS (compared to the Chalk River and Deep River BIOS, which have not been shown to contain any Fe oxides more crystalline than ferrihydrite). As the outer grains of goethite and ferrihydrite are eventually dissolved, the DIRB would encounter the more crystalline hematite "core" of the *Gallionella* stalks, and reduction might again be slowed. Further,

since the stalk is comprised of a tight bundle of twisted fibres (Balashova 1968; Hallberg and Ferris 2004), steric effects may have limited the ability of the *Shewanella* cells to contact the iron oxides within inner regions of the mineralized stalks, resulting in a smaller amount of the total iron being physically available for reduction. Similar steric hindrances would not be encountered with the Deep River or Chalk River BIOS because those oxides are precipitated primarily on long, straight filaments, whose surfaces would be more readily accessible to the DIRB, even as dissolution of the mineral progressed to deeper layers.

In summary, bacteriogenic iron oxides are readily susceptible to reductive dissolution by dissimilatory iron-oxidizing bacteria. Both the rate and the extent to which they are reduced are higher than those measured for mineralogically similar, synthetic iron oxides. The presence of microbial surfaces as potential stabilizing features within the BIOS appears to offer little resistance to, and may in fact promote, the reduction and dissolution of the mineral phase. This indicates that minerals formed in the presence of organic moieties exhibit fundamentally different reactive properties to synthetic or geogenic minerals. Further, the common use of synthetic iron oxides as analogs to environmental systems may significantly underestimate the reactivity of those phases in natural settings. This has important implications in areas such as contaminant modeling in groundwater systems, where sorption onto iron oxides is often considered to exert a major control on the migration of dissolved contaminants.

ACKNOWLEDGMENTS

SL was supported by scholarships from the Natural Sciences and Engineering Research Council of Canada (NSERC), the Ontario Graduate Scholarship (OGS) program,

and the University of Ottawa. Chalk River samples were obtained as part of an NSERC Strategic Project grant awarded to GF. Special thanks go to Dr. Kartsen Pedersen (University of Gothenburg, Sweden), for hosting DF and providing us with samples of Äspö BIOS. The authors are also grateful to Dragica Bogdanovic (National HIV and Retrovirology Laboratories, Health Canada) for her assistance with sample irradiation, to Dianne Moyles and Bob Harris (Department of Molecular and Cellular Biology, University of Guelph), for their assistance with the TEM, and to Xavier Châtellier (Géosciences, Université de Rennes, France) for his assistance with SEM.

REFERENCES

Anderson, CR, Pedersen, K. 2003. *In situ* growth of *Gallionella* biofilms and partitioning of lanthanides and actinides between biological material and ferric oxyhydroxides. Geobiology 1:169-178.

Anderson, CR, James, RE, Fru, EC, Kennedy, CB, Pedersen, K. 2006. *In situ* ecological development of a bacteriogenic iron oxide-producing microbial community from a subsurface granitic rock environment. Geobiology 4:29-42.

Balashova, VV. 1968. Taxonomy of the genus *Gallionella*. Microbiologiya 37:590-598.

Baker, BJ, Banfield, JF. 2003. Microbial communities in acid mine drainage. FEMS Microbiol Ecol 44:139-152.

Châtellier, X, West, MM, Rose, J, Fortin, D, Leppard, GG, Ferris, FG. 2004. Characterization of iron-oxides formed by oxidation of ferrous ions in the presence of various bacterial species and inorganic ligands. Geomicrobiol J 21:99-112.

Cornell, RM, Schwertmann, U. 2003. In: The Iron Oxides: Structure, Properties, Reactions, Occurrence and Uses, 2nd ed. Weinheim, Germany: Wiley-VCH.

Edwards, KJ, Bond, PL, Gihring, TM, Banfield, JF. 2000. An archaeal iron-oxidizing extreme acidophile important in acid mine drainage. Science 287:1796-1799.

Edwards, KJ, Rogers, DR, Wirsen, CO, McCollom, TM. 2003. Isolation and characterization of novel psychrophilic, neutrophilic, Fe-oxidizing, chemolithoautotrophic α- and γ-*proteobacteria* from the deep sea. Appl Environ Microbiol 69:2906-2913.

Emerson, D, Ghiorse, WC. 1993. Ultrastructure and chemical composition of the sheath of *Leptothrix discophora* SP-6. J Bacteriol 175:7808-7818.

Emerson, D, Rentz, JA, Lilburn, TG, Davis, RE, Aldrich, H, Chan, C, Moyer, CL. 2007. A novel lineage of Proteobacteria involved in formation of marine Fe-oxidizing microbial mat communities. PLoS ONE 2(8): e667.

Ferris, FG, Konhauser, KO, Lyvén, B, Pedersen, K. 1999. Accumulation of metals by bacteriogenic iron oxides in a subterranean environment. Geomicrobiol J 16:181-192.

Fortin, D, Leppard, GC, Tessier, A. 1993. Characteristics of lacustrine iron oxyhydroxides. Geochim Cosmochim Acta 57:4391-4404.

Fortin, D, Langley, S, Glasauer, S. 2008. Biominerals: recorders of the past? Met Ions Life Sci 4:377-411.

Glasauer, S, Langley, S, Beveridge, TJ. 2001. Sorption of Fe (hydr)oxides to the surface of *Shewanella putrefaciens*: cell-bound fine-grained minerals are not always formed de novo. Appl Environ Microbiol 67:5544-5550.

Glasauer, S, Langley, S, Beveridge, TJ. 2002. Intracellular iron minerals in a dissimilatory iron-reducing bacterium. Science 295:117-119.

Glasauer, S, Weidler, PG, Langley, S, Beveridge, TJ. 2003. Controls on Fe reduction and mineral formation by a subsurface bacterium. Geochim Cosmochim Acta 67:1277-1288.

Golyshina, OV, Pivovarova, TA, Karavaiko, GI, Kondrat'eva, TF, Moore, ERB, Abraham, WR, Lunsdorf, H, Timmins, KN, Yakimov, MM, Golyshin, PM. 2000. *Ferroplasma acidiphilum* gen. nov., spec. nov., an acidophilic, autotrophic, ferrous-iron oxidizing, cell-wall lacking, mesophilic member of the *Ferroplasmaceae* fam. nov., comprising a distinct lineage of the Archaea. Int J Syst Evol Microbiol 50:997-1006.

Hallbeck, L, Pedersen, K. 1990. Culture parameters regulating stalk formation and growth rate of *Gallionella ferruginea*. J Gen Microbiol 136:1675-1680.

Hallbeck, L, Pedersen, K. 1991. Autotrophic and mixotrophic growth of *Gallionella ferruginea*. J Gen Microbiol 137:2657-2661.

Hallbeck, L, Ståhl, F, Pedersen, K. 1993. Phylogeny and phenotypic characterization of the stalk-forming and iron-oxidizing bacterium *Gallionella ferruginea*. J Gen Microbiol 136:1675-1680.

Hallberg, R, Ferris, FG. 2004. Biomineralization by *Gallionella*. Geomicrobiol J 21:325-330.

Hansel, CM, Benner, SG, Nico, P, Fendorf, S. 2004. Structural constraints of ferric (hydr)oxides on dissimilatory iron reduction and the fate of Fe(II). Geochim Cosmochim Acta 68:3217-3229.

Inch, KJ, Killey, RWD. 1987. Surface area and radionuclide sorption in contaminated aquifers. Water Poll Res J Canada 22:85-98.

James, RE, Ferris, FG. 2004. Evidence for microbial-mediated iron oxidation at a neutrophilic groundwater spring. Chem Geol 212:301-311.

Kasama, T, Marakami, T. 2001. The effect of microorganisms on Fe precipitation rates at neutral pH. Chem Geol 180:117-128.

Kennedy, CB, Scott, SD, Ferris, FG. 2003a. Characterization of bacteriogenic iron oxide deposits from Axial Volcano, Juan de Fuca Ridge, northeast Pacific Ocean. Geomicrobiol J 20:199-214.

Kennedy, CB, Martinez, RE, Scott, SD, Ferris, FG. 2003b. Surface chemistry and reactivity of bacteriogenic iron oxides from Axial Volcano, Juan de Fuca Ridge, north-east Pacific Ocean. Geobiology 1:59-69.

Kennedy, CB, Scott, SD, Ferris, FG. 2004. Hydrothermal phase stabilization of 2-line ferrihydrite by bacteria. Chem Geol 212:269-277.

Klein, C. 2002. In: The Manual of Mineral Science, 22nd ed. Chichester, England: John Wiley & Sons.

Kulczycki, E, Fowle, DA, Fortin, D, Ferris, FG. 2005. Sorption of cadmium and lead by bacteria-ferrihydrite composites. Geomicrobiol J 22:299-310

Langley, S, Beveridge, TJ. 1999. Effect of O-side-chain-lipopolysaccharide chemistry on metal binding. Appl Environ Microbiol 65:489-498.

Lovley, D, Phillips, EJP. 1988. Novel mode of microbial energy metabolism: organic carbon oxidation coupled to dissimilatory reduction of iron or manganese. Appl Environ Microbiol 54:1472-1480.

Mavrocordatos, D, Fortin, D. 2002. Quantitative characterization of iron oxides formed onto bacterial cell walls using TEM-electron energy loss spectroscopy. Am Mineral 87:940-946.

McNamara, NP, Black, HIJ, Beresford, NA, Parekh, NR. 2003. Effects of acute gamma irradiation on chemical, physical and biological properties of soils. Appl Soil Ecol 24:117-132.

Myers, CR, Nealson, KH. 1990. Respiration-linked proton translocation coupled to anaerobic reduction of manganese(IV) and iron(III) in *Shewanella putrefaciens* MR-1. J Bacteriol 172:6232-6238.

Roden, EE, Zachara, JM. 1996. Microbial reduction of crystalline Fe(III) oxides: influence of oxide surface area and potential for cell growth. Environ Sci Technol 30:1618-1628.

Roden, EE, Urrutia, MM (2002) Influence of biogenic Fe(II) on bacterial crystalline Fe(III) oxide reduction. Geomicrobiol J 19:209-251.

Roden, EE. 2003. Fe(III) oxide reactivity toward biological versus chemical reduction. Environ Sci Technol 37:1319-1324.

Stoffers, P, Worthington, TJ, Schwarz-Schampera, U, Hannington, MD, Massoth, GJ, Heknian, R, Schmidt, M, Lundsten, LJ, Evans, LJ, Vaiomo'unga, R, Kerby, T. 2006. Submarine volcanoes and high-temperature hydrothermal venting on the Tonga Arc, southwest Pacific. Geology 34:453-456.

Stookey, LL. 1970. Ferrozine – a new spectrophotometric reagent for iron. Anal Chem 42:779-781.

Viollier E., Inglett PW, Hunter K., Roychoudhury AN, Van Cappellen P. 2000. The ferrozine method revisited: Fe(II)/Fe(III) determination in natural waters. Appl Geochem, 15: 785-790.

Warren, LA, Ferris, FG. 1998. Continuum between sorption and precipitation of Fe(III) on microbial surfaces. Environ Sci Technol 32:2331-2337.

Table 1. Sources of BIOS and relative abundances of iron-oxidizing genera observed within each BIOS type

Sample Site	BIOS Source	Fe(II)-oxidizing bacteria[a]	References
Deep River, Ontario, Canada	pH-neutral; fresh artesian spring; perennial, natural flow	93-95% *Leptothrix* spp. 2-3% *Gallionella* spp.	James and Ferris, 2004; present study
Chalk River, Ontario, Canada	pH-neutral; fresh groundwater seep; perennial, natural flow	>99% *Leptothrix* spp. <1% *Gallionella* spp.	Langley et al., 2008 (unpublished data); present study
Äspö, Sweden	pH-neutral; fresh groundwater; artificial growth device; manually-controlled flow	85% *Gallionella* spp. 15% *Leptothrix* spp.	Anderson and Pedersen, 2003; James, 2008 (personal communication)

[a] putative identifications, based on distinct cellular morphologies

Table 2. XRD reflections (d-spacing, Å) measured for BIOS, and the expected reflections (with relative intensities, I/I_0) for 2-line ferrihydrite, as well as some common silicate weathering minerals (Klein 2002).

Deep River BIOS	**Chalk River BIOS**	**Äspö BIOS**	**2-line Ferrihydrite**	**Quartz (SiO_2)**	**Albite ($NaAlSi_3O_8$)**	**Orthoclase ($KAlSi_3O_8$)**	**Muscovite ($KAl_2(Si_3Al)O_{10}(OH,F)_2$)**
4.23	4.24			4.26 (0.22)			9.95 (0.95)[a]
4.03						4.02 (0.9)	
3.32	3.35			3.34 (1)	3.76 (0.3)[a]	3.8 (0.8)[a]	3.32 (1)
3.19	3.19				3.21 (0.3)	3.18 (1)	
3.17					3.18 (1)		
2.51	2.56	2.57	2.50 (1)				2.57 (0.55)
1.81				1.82 (0.14)			
1.49	1.51	1.50	1.51 (0.7)				

[a] no potential matches seen in the XRD patterns from BIOS

Table 3. Maximum percentage of total Fe reduced, linear rates of increase in the proportion of total Fe(II)/total Fe, and correlation coefficients of the linear rates, for each iron oxide source. Rates were calculated from linear plots shown in Figure 6. Data represent means ± standard deviations for three separate replicates of each system.

Iron Oxide	**Maximum % Fe Reduced**	**Linear Reduction Rate (day^{-1})[a]**	**R^2**
HFO	78.08 ± 0.68	0.162 ± 0.009	0.970
Äspö BIOS	83.34 ± 1.75	0.269 ± 0.019	0.963
Deep River BIOS	92.36 ± 0.76[b]	0.541 ± 0.029[b]	0.961
Chalk River BIOS	97.98 ± 2.55[b]	0.467 ± 0.023[b]	0.942

[a] based on increases in the ratio of Fe(II):total Fe

[b] no significant difference ($p<0.05$)

Figure 1

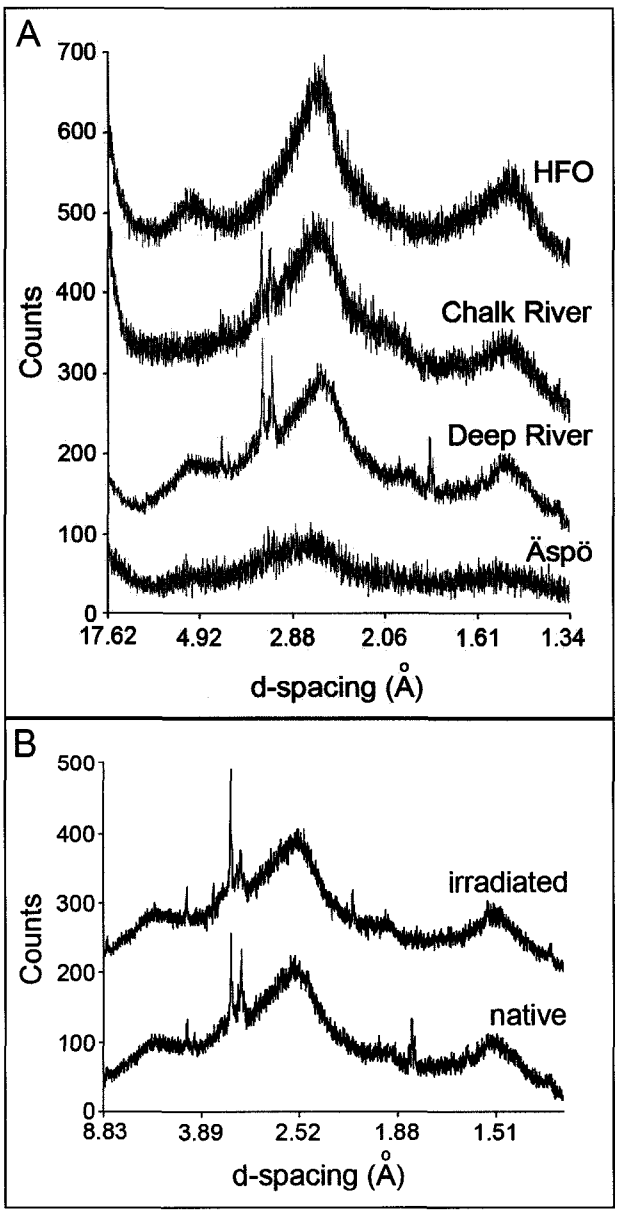

Figure 2

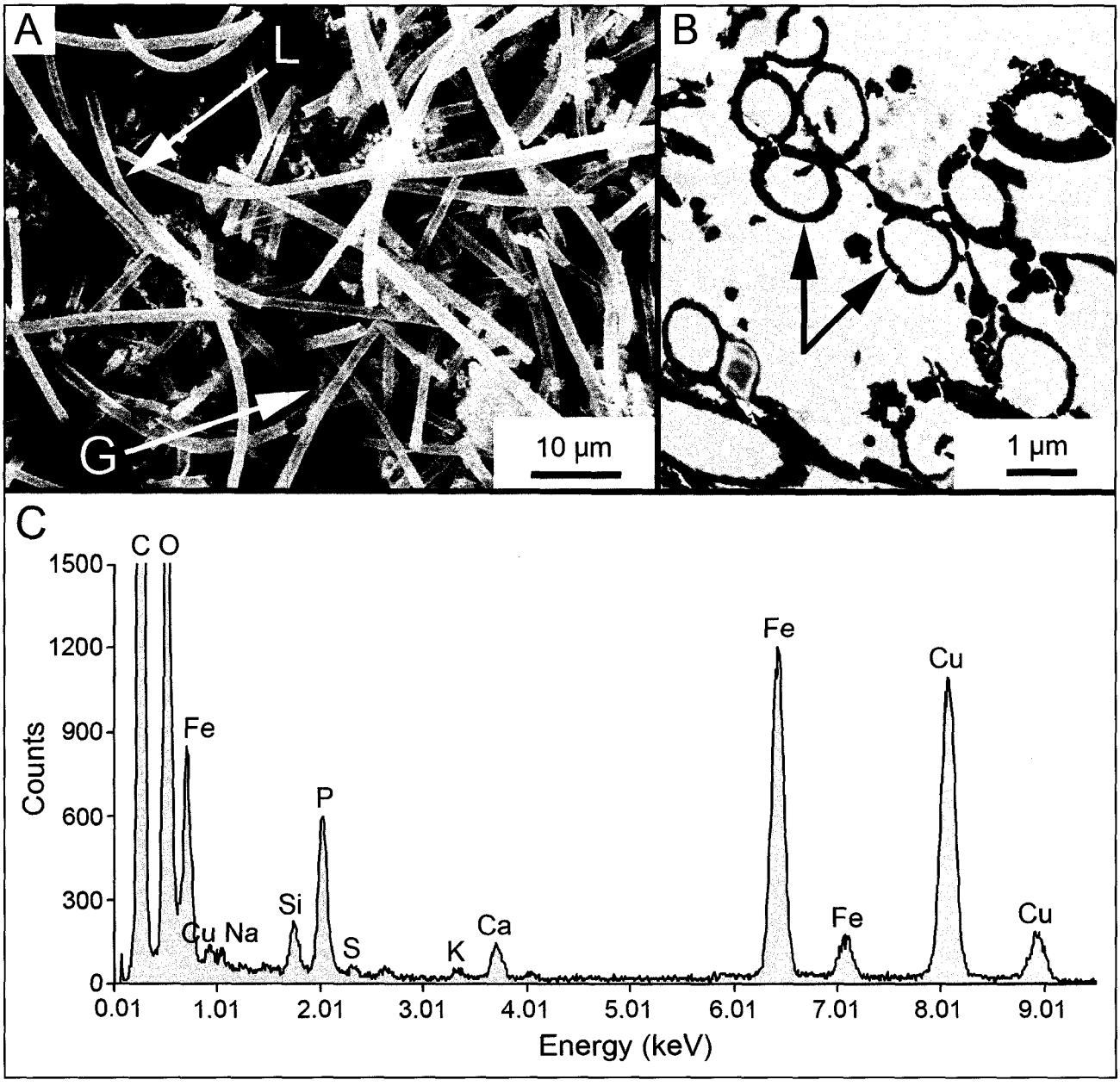

Figure 3

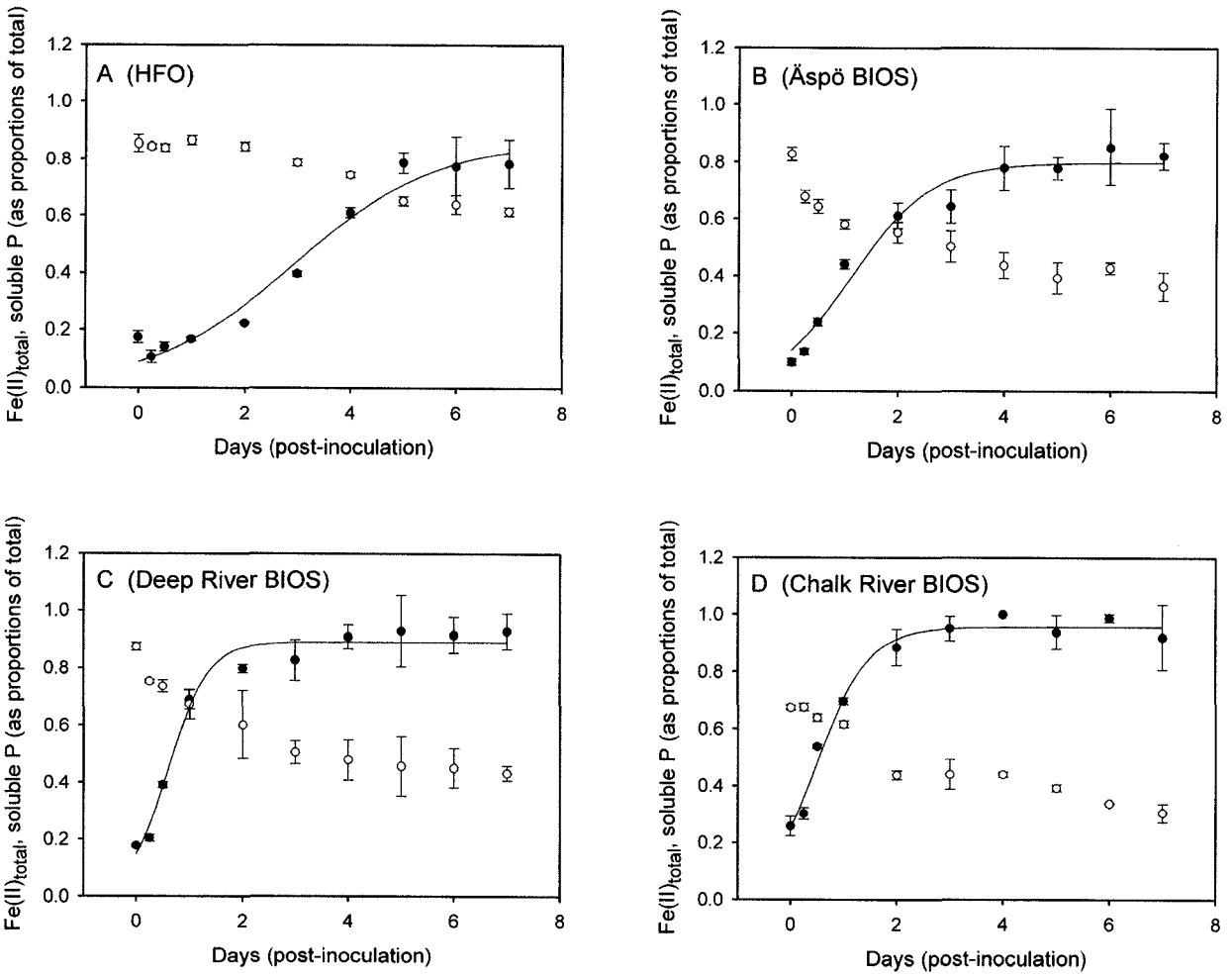

Figure 4

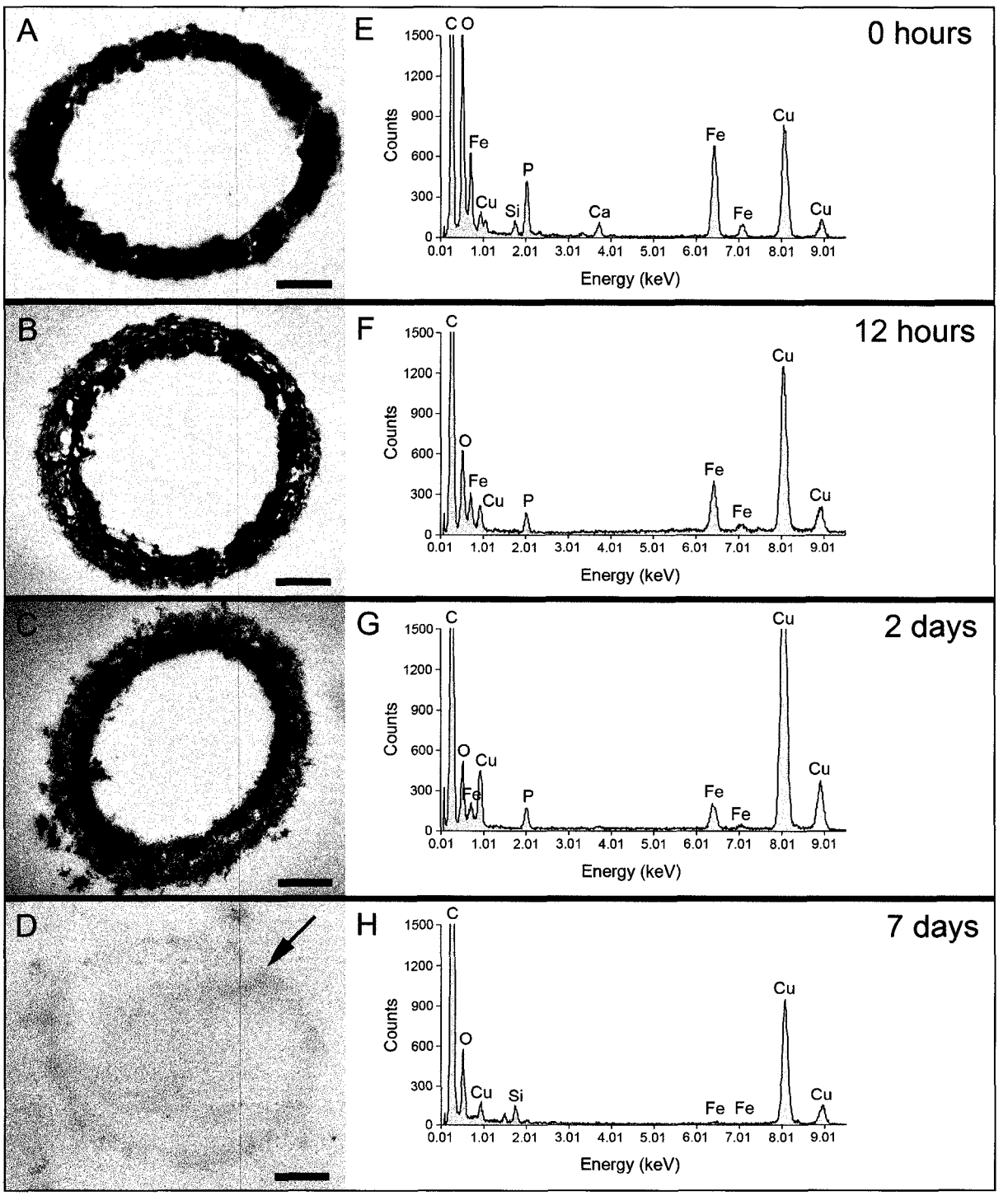

Figure 5

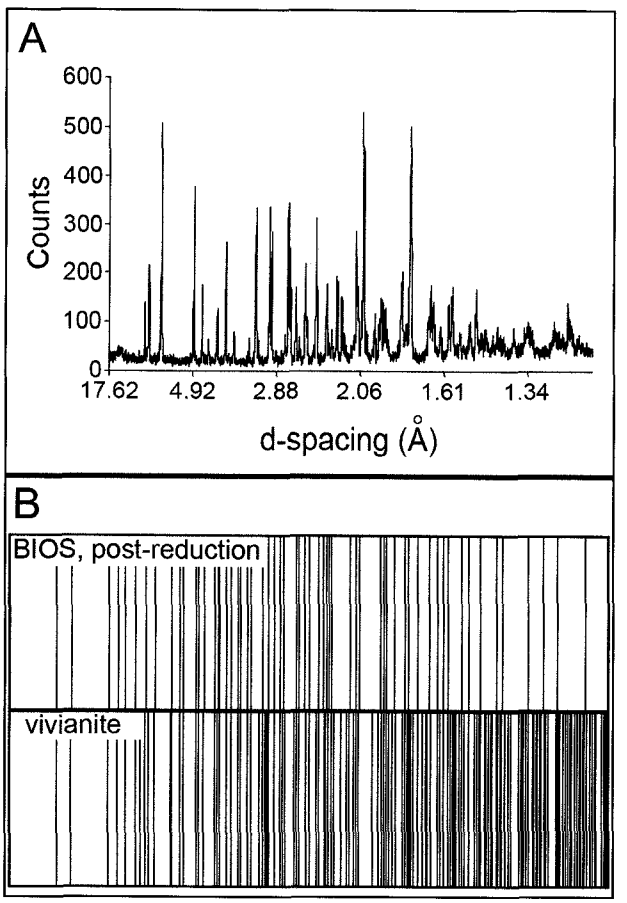

Figure 6

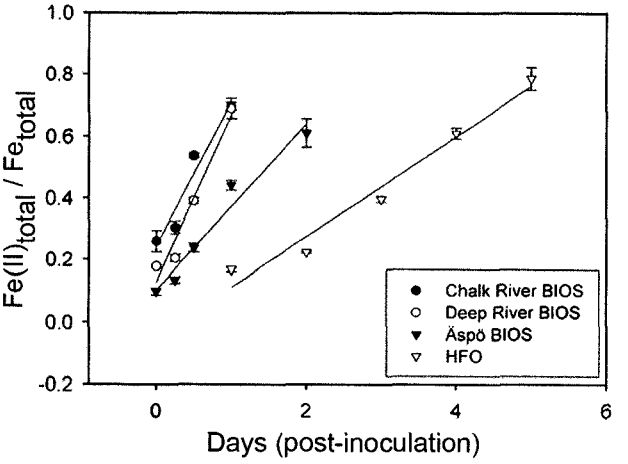

Figure captions

Figure 1. **A)** X-ray diffraction patterns generated by three different BIOS samples and HFO, showing broad features centred at approximately 2.5 Å and 1.5 Å, indicating poorly ordered, 2-line ferrihydrite. The sharper peaks in the BIOS samples are derived from silicate weathering products within the BIOS (see Table 2). The broad features centred around 5.1 Å were generated by the sample holder. **B)** X-ray diffraction patterns generated by native and γ-irradiated Deep River BIOS samples, showing no significant mineralogical alteration to the BIOS as a result of irradiation. All patterns have been vertically separated on an arbitrary y-axis, for clarity.

Figure 2. **A)** Scanning electron micrograph showing the two most abundant microbial structures observed in the Äspö, Deep River and Chalk River BIOS: *Leptothrix*-like sheaths (L) and *Gallionella*-like helical stalks (G). Relative abundances of each are detailed in Table 1. **B)** Unstained transmission electron micrograph of BIOS in thin section. A crust of electron-dense material is precipitated directly on the surfaces of remnant microbial structures (arrows). **C)** Energy-dispersive X-ray spectrograph generated by the encrusting material indicated in (B), showing that it is rich in Fe, O, and contains trace amounts of lighter elements common to both silicate weathering minerals and biological samples. The large carbon and copper peaks were generated by the specimen support grid.

Figure 3. Changes in $Fe(II)_{total}/Fe_{total}$ (solid symbols) and $P_{soluble}/P_{total}$ (open symbols) for each of the 4 iron oxide systems during anaerobic reduction by *S. putrefaciens* CN32. Data markers represent means and standard deviations derived from three

experimental replicates of each system. Solid lines indicate 3-parameter sigmoid lines of best fit to the data. Correlation coefficients (R^2) of the fitted lines are 0.971 (HFO), 0.969 (Äspö BIOS), 0.980 (Deep River BIOS), and 0.984 (Chalk River BIOS).

Figure 4. **A-D)** Unstained, thin section transmission electron micrographs showing the deterioration of the iron oxide mineral surrounding remnant microbial structures in BIOS during reduction of the material by *S. putrefaciens* CN32. Note the gradual loss of compactness and electron density over the first 2 days. After 7 days, the mineral crust is completely depleted and the surface of the microbial structure is barely visible (arrow). All scale bars = 250 nm. **E-H)** corresponding EDS spectra showing a gradual loss of iron as structural degradation of the mineral crust progresses. All times indicated are post-inoculation. The large carbon and copper peaks were generated by the specimen support grid.

Figure 5. **A)** X-ray diffraction pattern of the mineral phase remaining after the reduction of HFO and all BIOS samples by *S. putrefaciens* CN32, showing an increase in crystallinity of the mineral, compared to the starting material (Figure 1). **B)** Peaks identified within the diffraction pattern correspond to the ferrous phosphate mineral, vivianite ($Fe_3(PO4)_2 \cdot 8H_2O$).

Figure 6. Changes in the proportion of $Fe(II)_{total}/Fe_{total}$ in each system during the periods of maximum Fe(III) reduction by *S. putrefaciens* CN32. Data markers represent means and standard deviations derived from three experimental replicates of each system. Data follow linear relationships as indicated by the solid lines of

best fit. Reduction rates and correlation coefficients calculated for the respective plots are presented in Table 3.

From the data presented in Section 3, it is clear that BIOS are more susceptible to microbial Fe(III) reduction than was originally hypothesized, and that they are even more biologically reducible than a synthetic analog of the same mineral. The complete dissolution of the iron mineral phase was particularly striking. As highlighted in Section 2, the sorption of Sr to BIOS occurs via reversible outer-sphere complexation. The reduction data from Section 3 suggest that any sorption of Sr that may occur within the surface layers of a BIOS deposit may be rapidly reversed should the Sr-loaded material become subjected to reducing conditions. This would be particularly true if Sr sorption occurs primarily to the mineral phase, and not to the organic fraction of the BIOS (although, the EXAFS data from Section 2 failed to elucidate the precise Sr sorption sites). Release of the Sr back into solution would obviously increase the mobility of the contaminant, thereby negating the prior sorptive effect of the BIOS.

To examine the effect of iron reduction on the retention of Sr by BIOS, reduction experiments were performed using native and Sr-loaded BIOS samples from two different sites, as well as a Sr-loaded, synthetic HFO. This in vitro work allowed an examination of the release of Sr over time as the BIOS was reduced, but was inadequate in determining how reduction of BIOS might affect Sr mobility in a natural setting. Therefore, a series of experiments were performed, in situ, using porewater dialysis membrane devices (peepers) to monitor Fe(II) and Sr concentrations with increasing depth within the natural BIOS deposit. This approach allowed an examination of the effect of solid BIOS on soluble Sr concentrations, as well as the effect of iron reduction at depth on the release of Sr to the surrounding porewater. The results of this research are detailed, below, in Section 4.

Section 4

Strontium desorption from bacteriogenic iron oxides (BIOS) subjected to microbial Fe(III) reduction

A revised version of this manuscript has been accepted for publication in *Chemical Geology*[1]

[1] Langley, S., Gault, A.G., Ibrahim, A., Takahashi, Y., Renaud, R., Fortin, D., Clark, I.D., Ferris, F.G. 2008. Strontium desorption from bacteriogenic iron oxides (BIOS) subjected to microbial Fe(III) reduction. Chem. Geol. In press.

Abstract

The effect of microbial reduction of bacteriogenic iron oxides (BIOS) on the release of sorbed Sr was examined using a naturally low-Sr BIOS (n-BIOS) collected from Chalk River, Canada, and a naturally high-Sr BIOS (Äspö-BIOS) collected from Äspö, Sweden. EXAFS analysis suggested that Sr was bound to the Äspö-BIOS as an outer-sphere complex of hydrated Sr^{2+}. During reduction, Sr desorption from n-BIOS was concomitant with the production of Fe(II), resulting in solubilization of 80% of the total Sr. In contrast, nearly 100% of the Sr was solubilized from Äspö-BIOS, although Sr desorption was delayed, relative to Fe(II) production. When n-BIOS were artificially saturated with Sr, there was a significant decrease in the rate and extent of Fe(III) reduction and an induced delay in Sr desorption (similar to that observed for Äspö-BIOS). Saturation of synthetic hydrous ferric oxide with Sr had no such effect on Fe(III) reduction rate, although a delay in Sr desorption was again observed. In all instances, the levels of desorbed aqueous Sr remained constant, suggesting that re-sorption or co-precipitation of Sr with secondary mineral precipitates (vivianite) did not occur under the experimental conditions. In situ porewater analysis of the Chalk River BIOS indicated positive correlations between soluble-phase concentrations of Fe(II) and Sr at depth, suggesting that anaerobic reduction of Fe(III) releases Sr back into the groundwater flow at the site. Further, in areas where BIOS deposition is occurring within the groundwater discharge zone, levels of soluble Sr are 2 to 3 times lower than in areas where BIOS is absent. The data indicate that phase partitioning of Sr within BIOS is governed largely by Fe oxidation state, and that BIOS will act as effective sorbents of Sr as long as oxidizing conditions are maintained. However reduction of the BIOS will likely result in significant desorption and remobilization of the bound Sr.

1. Introduction

Fine-grained iron oxides display large surface area-to-mass ratios, as high as several hundred m^2/g (Roden and Zachara, 1996; Glasauer et al., 2003; Bonneville et al., 2004). They are also highly reactive, due to pH-dependent protonation and de-protonation of hydroxyl residues on the mineral surface (Cornell and Schwertmann, 2003). These two factors make them adsorptive of a variety of aqueous chemical species including organic compounds, heavy metals, and radionuclides (Clausen and Fabricius, 2001; Hansen et al., 2001; Dixit and Hering, 2003). As a result, in most freshwater environments at the Earth's surface, nanometre- and micrometre-scale iron oxides in soils and sediments can exert a major control on the migration of dissolved contaminants (Anderson and Lovley, 1999; Roden and Edmonds, 1997). By comparison, bacteriogenic iron oxides (BIOS) are similar, fine-grained (2 to 500 nm) iron minerals that form in association with bacterial cells and related cellular structures, such as membranes, s-layers, stalks and sheaths. (Fortin and Langley, 2005). Their formation can arise by either passive (i.e., chemical) or active (i.e., metabolic) oxidation of ferrous iron, typically resulting in a highly hydrated, amorphous, or poorly ordered precipitate such as 2-line ferrihydrite (perhaps the most commonly identified mineral component of BIOS) (Kasama and Marakami, 2001; Châtellier et al., 2004; Langley et al., 2008a). As their formation is dependent on the continued influx of ferrous iron-rich water, BIOS deposits are most often found in association with groundwater and hydrothermal flow systems (James and Ferris, 2004; Stoffers et al., 2006; Langley et al., 2008b). Over time, continued precipitation of BIOS can lead to the formation of extensive deposits that can cover several thousand m^2 to a depth of 1 m or more (Stoffers et al., 2006; Langley et al., 2008c). The iron minerals in BIOS display the same high degree of reactivity

and large surface area as other fine-grained iron oxides. However, due to the presence of abundant microbial cells and cellular debris, intermixed with the mineral phase, there is an additional sorptive component to BIOS that is not present in purely synthetic or geogenic minerals. This organic component can significantly affect sorption by altering the surface potential of the composite material, typically leading to increases in the solid-phase partitioning of dissolved metals (Ferris et al., 1999, 2000). BIOS may, therefore, represent a natural mechanism for the sorption, and removal from solution, of large quantities of dissolved metal cations.

Of particular concern to the nuclear industry is the radioactive metal, ^{90}Sr. This radioisotope is produced through fission reactions occurring during atomic weapons detonations and nuclear energy production. As a result, it is most often a contaminant of importance in areas surrounding weapons development and detonation sites, nuclear reactors and waste storage facilities (Um and Papelis, 2003; Bruno and Ewing, 2006). It has a half-life of approximately 29 years and is capable of substituting for Ca in bone. Ingestion of ^{90}Sr can lead to bone cancer, soft-tissue cancers, leukemia and anaemia (Nielsen, 2004). Removal of the isotope from groundwaters is, therefore, important. However, it is one of the more mobile radioisotopes, occurring in most ground and surface waters as the hydrated divalent ion, Sr^{2+} (Sahai et al., 2000). In circumneutral pH waters, migration of Sr is strongly influenced by sorption onto a variety of minerals including silicates and oxides (Axe et al., 1998; Parkman et al., 1998; Palmer and Gunter, 2001; Solecki, 2005). Recently, BIOS have also been examined for their ability to bind aqueous Sr. Ferris et al. (2000) reported distribution coefficients (K_d) of $10^{3.0}$ to $10^{3.1}$ for Sr sorption onto BIOS from the Strássa Mine (Sweden). Langley et al. (2008b) studied Sr sorption onto BIOS from Chalk River

(Canada) and reported a maximum sorption capacity (S_{max}) of 3.41 mol Sr/g Fe under low ionic strength. In addition to sorption, Andersson et al. (1994) reported that Sr also can be removed from the overlying water column as a result of becoming "trapped" during the precipitation of Fe oxyhydroxides. These data suggest that BIOS should be an effective material for the removal of aqueous Sr. However, examinations of sorption at higher ionic strength revealed a significant decrease in the S_{max} (to 1.06 mol Sr/g Fe), indicating that sorption occurs primarily via reversible, outer-sphere complexation, a finding which was further confirmed using EXAFS spectroscopy (Langley et al., 2008b). This fact means that Sr sorbed to BIOS likely will be easily re-mobilized due to changes in the aqueous geochemistry of the system.

One of the factors governing the impact of BIOS on Sr mobility will be the tendency for the BIOS to be exposed to anoxic conditions through continued precipitation of the mineral at the surface, forcing underlying layers of sediment to become progressively buried and allowing for anaerobic reduction of Fe(III) to proceed. Recent work has demonstrated that BIOS are particularly susceptible to microbial Fe(III) reduction, and are more readily reduced in batch experiments than mineralogically similar, synthetic hydrous ferric oxide (Langley et al., 2008a). Reductive dissolution of abiotic iron oxyhydroxides has been shown to release "trapped" Sr back into solution (Andersson et al., 1994). Similar release of Sr has also been demonstrated during the dissolution of abiotic jarosite (Welch et al., 2007). While these studies dealt with Sr incorporated into the atomic lattice of the iron mineral, it is likely that dissolution would also lead to the release of any sorbed Sr from the surface of the dissolving solid. There is currently very little literature available on the release of Sr from iron oxides during microbial Fe(III) reduction, and no literature on the process with respect

to BIOS in particular. Therefore, our aims in this research were: 1) to examine the in vitro release of Sr from BIOS (and a synthetic hydrous ferric oxide, HFO) using the well-characterized iron-reducing bacterium, *Shewanella putrefaciens* CN32, 2) to determine the effect of Sr saturation of the BIOS and HFO on subsequent rates of Fe(III) reduction and Sr desorption, and 3) to determine the in situ effect of BIOS oxidation state on the control of aqueous Sr concentrations in a natural environment.

2. Materials and methods

2.1 Site description

Low-Sr BIOS samples were collected from the grounds of Chalk River Laboratories (Atomic Energy of Canada, Limited) in Chalk River, Ontario, Canada (latitude: 46°03'04"N, longitude: 77°25'11"W). The source of Fe^{2+} for the BIOS is a groundwater seep, which flows through a 10,000 year-old aeolian sand aquifer prior to discharging into a wetland ecosystem along the base of a 20 m high dune. The primary source of recharge for the aquifer is a nearby freshwater lake. Several points of groundwater discharge are apparent and nearly all are producing BIOS, perennially, at some point along their surface flow paths (Fig. 1). A total of 10 sample sites (spaced throughout the BIOS depositional zone) comprise the study area. One point of discharge, located approximately 10 m from the nearest zone of iron precipitation, was found to be free of BIOS. Subsequent to its discovery, this site was selected for use as a 'natural control' for all in situ analyses of Fe and Sr at the site (see section 2.9). Physicochemical measurements of the groundwater (that has come to surface) at the BIOS site and at the control site are detailed in Table 1. Physical data were obtained using a YSI 650MDS datalogger with 600QS probe. To minimize the possibility of chemical

oxidation by atmospheric O_2, ferrous iron concentrations were measured immediately on-site using a HACH portable spectrophotometer and colourimetric reagent packets, according to the manufacturers instructions. Remaining samples were acidified (to 0.02 M HCl) on-site and stored at 4°C prior to return to the laboratory where they were analyzed by inductively-coupled plasma – optical emission spectrometry (ICP-OES), using a Varian Vista-PRO CCD Simultaneous ICP-OES, operating under standard conditions.

2.2 Iron oxide collection and preparation

BIOS are composed of primarily flocculent precipitates with a gelatinous consistency. For sample collection, acid-washed 1 L plastic bottles were fully immersed into the BIOS allowing the suspension to flow into, and completely fill the bottle, devoid of any remaining headspace. Samples were stored at 4°C prior to subsequent preparation. Upon return to the laboratory, the BIOS were allowed to settle, and the overlying water was carefully decanted. The remaining gel was sieved (200 mesh) to remove any large detrital material such as leaf litter, which may have been inadvertently collected. The sieved gel was then centrifuged at 14,000 × g for 10 minutes and the supernatant fluid decanted and discarded. This sample is subsequently referred to as native BIOS (n-BIOS).

To examine any potential effects of Sr-loading of the BIOS on the subsequent microbial reduction of the iron oxides, sub-samples of the centrifuged material were artificially saturated with Sr by re-suspension of the gel in 0.5 M $Sr(NO_3)_2$, (dissolved in 0.001 M KNO_3, pH 8.0), for 2 hours at 22°C. Excess $Sr(NO_3)_2$ was removed by washing the material 5 times in 18 MΩ·cm ultra-pure water (UPW). To control for the effects of this procedure, a second sub-sample of BIOS was subjected to the same conditions, without the

addition of the $Sr(NO_3)_2$. These two samples are subsequently referred to as Sr-loaded BIOS (Sr-BIOS) and washed BIOS (w-BIOS), respectively.

Finally, in order to compare the Fe(III) reduction rates of the BIOS to reported literature, a synthetic hydrated ferric oxide (HFO) was prepared following the method of Glasauer et al. (2002, 2003), whereby 1 M NaOH was rapidly added to 2 M $FeCl_3 \cdot 6H_2O$ to a final pH of 7.0. The resulting iron oxide precipitate was washed 10 times in UPW. Two sub-samples of the HFO were then subjected to the same Sr-saturation and washing procedure described above. These samples are subsequently referred to as HFO (for the washed sample) and Sr-HFO (for the Sr-loaded sample).

2.3 Natural, high-Sr BIOS

The BIOS Reactor In Situ Continuous Flow (BRIC) device is an artificial growth chamber located in the subterranean Hardrock Laboratory near Äspö, Sweden (latitude: 57°16'02"N, longitude: 16°26'55"E). Within the chamber, the iron-oxidizing bacterium *Gallionella* produces BIOS from a supply of ferrous-iron rich groundwater fed from a nearby borehole (Anderson and Pedersen, 2003). Previously unpublished data from our laboratory indicated that the Äspö BIOS generally contains naturally higher levels of Sr (and other cations), relative to the Chalk River BIOS used in the present study (Table 2). This finding provided an opportunity for an examination of the effects of Sr loading on BIOS reduction in both naturally and artificially Sr-loaded samples. Äspö BIOS were collected and prepared as described in section 2.2, with the exception that they were not exposed to $Sr(NO_3)_2$, and insufficient material was available for an examination of washed BIOS from this source.

2.4 Iron oxide sterilization

To prevent the potential microbial transformation of the BIOS during storage, and to sterilize the material prior to the reduction experiments, all samples of native, washed and Sr-loaded BIOS and HFO were gamma-irradiated, using a Nordion Gammacell 220 at a total dose of 48 kGray, as this method has been shown to provide adequate sterilization of natural sediments and BIOS without affecting mineralogy (McNamara et al., 2003; Langley et al., 2008a). All irradiated samples were stored in the dark at 4°C prior to use.

2.5 Extended X-ray absorption fine structure (EXAFS)

EXAFS was used to determine how Sr sorption to Äspö BIOS occurs. Similar work in our laboratory has already demonstrated that Sr sorption to HFO and Chalk River BIOS occurs via outer-sphere complexation of hydrated Sr^{2+} (Langley et al., 2008b). Strontium acetate and hydrated Sr^{2+} ion (in the form of a $Sr(NO_3)_2$ solution; 1000 ppm Sr) served as reference standards for the analysis. Approximately 200 mg of each sample were packaged into small (2 cm × 2 cm) polyethylene bags for measurement. For the Äspö BIOS, as much water as possible was removed, thereby minimizing the possibility of detection of any Sr^{2+} in solution. Strontium K-edge (16.105 keV) spectra were collected at beamline BL01B1 of SPring-8 (Hyogo, Japan). The SPring-8 storage ring was operated at 8.0 GeV electron energy with an electron current of 100 mA. A Si(111) double-crystal monochromator was used to obtain the incident X-ray beam. All the spectra were measured in fluorescence mode using a 19-element Ge semiconductor detector. EXAFS data analysis was performed using REX2000 ver.2.3 (Rigaku) with parameters generated by FEFF7.02 (Zavinsky et al., 1995; Ankudinov and Rehr, 1997). The background absorption (other than that of Sr) was subtracted using a linear function estimated from pre-edge region. After subtraction of

background absorption and normalization, the smooth Sr K-edge absorption of the free atom (μ_0) was removed using a spline smoothing curve method. The energy unit was transformed from keV to $Å^{-1}$ to produce the EXAFS function $\chi(k)$, where k ($Å^{-1}$) is the photoelectron wave vector given by $\sqrt{2m(E-E_0/\hbar^2)}$ (where E = the energy of the incident X-ray; E_0 = the threshold energy for liberation of the photoelectron wave). In the present study, the E_0 value was initially determined from the maximum value in the derivative of $\chi(k)$ in the absorption region, which was optimized finally in the EXAFS simulation. The k^3-weighted $\chi(k)$ values were Fourier transformed from k (1/Å) space into R (Å) space to give a radial structural function (RSF). The theoretical EXAFS function was fitted to the back transformed k^3-weighted $\chi(k)$ functions using parameters including theoretical backscattering amplitudes and phase shifts generated by FEFF 7.02. Initial structural data of $SrCO_3$ by ATOMS (Ravel, 2001) were utilized to make FEFF parameters for Sr-O pair. The EXAFS analysis gives the coordination number (CN), the interatomic distance (R) between absorber and scatterer atoms, the Debye-Waller term (σ^2), and energy offset (ΔE_0).

2.6 Sample mineralogy

Powder X-ray diffraction (XRD) was used to determine the mineralogy of the various iron oxides. Prior to analysis, samples were freeze-dried and ground to a fine powder using a mortar-and-pestle. All XRD was performed with a Philips PW 1830 X-ray diffractometer, with a Cu-Kα X-ray source, operating at a tension of 45 kV and a current of 40 mA. Continuous scans were run from a start angle of 5° to an end angle of 70° (2θ).

2.7 Bacterial culture and growth conditions

The dissimilatory iron-reducing bacterium (DIRB), *Shewanella putrefaciens* CN32, was kindly donated by Dr. Terry Beveridge (Department of Molecular and Cellular Biology,

University of Guelph, Ontario, Canada). The organism was maintained on tryptic soy agar (TSA) at 22°C. Microcosm reduction experiments were carried out in a liquid, chemically-defined medium (CDM; Glasauer et al., 2003): 20 mM sodium lactate, 3.5 mM sodium phosphate, 4 mM 1,4-piperazinediethanesulfonic acid (PIPES) buffer, and trace element salts, at pH 7.0 prior to autoclaving. For transfer into the CDM, cells were transferred from the TSA into 50 mL of tryptic soy broth (TSB) at 22°C on a rotary shaker (125 rpm). After 24 hours, the cells were sub-cultured (1% inoculum) through a series of TSB:CDM mixtures (50:50, 5:95, 1:99, at 125 rpm, for 24 hours, 22°C, in each 50 mL mixture), in order to acclimate the cells to the nutrient conditions of the CDM. Following a 2% inoculation into 200 mL of 100% CDM, cells were grown for 36 hours at 22°C, prior to harvesting by centrifugation at 14,000 × g for 5 minutes. The cell pellet was re-suspended into 2 mL of sterile, fresh CDM, and the concentrated cell suspension was used to inoculate the microcosm cultures. A commercial protein assay (BioRad Protein Assay II) was used to standardize the inoculum. The final experimental cultures each contained 0.5 μg/mL total protein, following established procedures (Glasauer et al., 2002, 2003).

The microcosm Fe(III)-reduction systems consisted of 700 mL sterile CDM in 1 L acid-washed Kimax bottles. Each bottle was amended with 4 mM total Fe in the form of either irradiated BIOS or HFO (native, and Sr-loaded for each). Abiotic control systems were identical to the biotic ones, but did not contain *S. putrefaciens* CN32. Incubation and sampling of the cultures was performed at 22°C inside a Coy Labs anaerobic chamber (atmosphere of 5% H_2:95% N_2). All experiments were conducted in triplicate, from three separate preparations of CDM, cells, and iron oxides. Sampling of each system was

performed immediately after addition of the cells (time 0), then at 6 hours, 12 hours and 24 hours post-inoculation, followed by once daily for a total of 7 days.

2.8 Microcosm sampling

Culture vessels were shaken vigorously and 20 mL aliquots were immediately removed while the solid phase material remained suspended. The aliquots were placed into sterile, acid-washed glass scintillation vials. Sub-samples were removed from this aliquot to minimize the possibility of contaminating the larger vessel. All sub-sampling was performed while solid material was suspended in the vial. Standard laboratory meters and probes were used for measuring pH and Eh. For determination of DIRB culture viability, 0.5 mL of suspension was removed and serially diluted (1:10 per dilution) into sterile, fresh CDM for enumeration of cells using viable plate counts (on TSA). For determination of total ferrous Fe concentration, 0.5 mL of unfiltered suspension was added to 4.5 mL of 0.5 M trace metal grade HCl, and reacted for 24 hours inside the anaerobic chamber. Reacted samples were analyzed using ferrozine reagent (Stookey, 1975; Viollier et al., 2000). For determination of soluble phase Sr and Fe concentration (both ferrous and total Fe), 6.5 mL of suspension were filtered through a 0.22 μm nylon syringe filter. For soluble ferrous Fe, 0.5 mL of filtered suspension was reacted in 4.5 mL of 0.5 M HCl for analysis with ferrozine as described above. The remaining 6 mL was acid digested by addition of 4 mL 30% H_2O_2 and 2 mL trace metal grade HNO_3, followed by heating to 70°C for 12 hours (Kulczycki et al., 2005). Digested samples were diluted 1:10 (in UPW) and analyzed for total soluble Sr and Fe by ICP-OES as described above. The same procedure, using 6 mL of unfiltered suspension, was used for the determination of total Sr and Fe concentration.

2.9 In situ Fe and Sr analyses

To determine the effect of BIOS reduction on Sr phase partitioning within the sediments, in situ porewater dialysis devices (peepers) were installed into the BIOS (Fig. 1b) and control site sediments. Prior to deployment, the peepers were filled with UPW and de-oxygenated for 2 days in the laboratory, using 100% N_2. They were then placed in sealed boxes (flushed with N_2) for delivery to the sample site. After installation into the BIOS, the peepers were allowed to equilibrate with the sediment porewater for 2 weeks prior to their removal. As noted above, all oxygen-sensitive measurements were analyzed on-site, immediately following removal of the peepers from the sediment. Remaining samples were acidified (to 0.02 M HCl), stored at 4°C, and returned to the laboratory for analysis by ICP-OES as described above. Peepers were deployed 4 times in a year (once in each season) to monitor seasonal variations.

3. Results

3.1 Sample site measurements

The physicochemical data from the Chalk River BIOS deposit (Table 1) indicate a dilute, freshwater aquifer system with few differences observed for most variables between the sample site and the control site. The minor differences seen for some measurements may be indicative of the more abundant microbial growth present at the BIOS site.

3.2 Sample mineralogy

Representative X-ray diffractograms of the various iron oxides are presented in Figure 2. All of the BIOS samples generated two broad features centred at 1.5 Å and 2.5 Å, indicative of the iron oxide mineral, 2-line ferrihydrite. In addition, Chalk River BIOS

generated several sharper reflections at d-spacings of 4.25 Å, 3.34 Å, and 3.19 Å (Fig. 2), indicating the presence of silicate weathering minerals (such as quartz, feldspar, and mica) which, in contrast, were the dominant mineral phases detected in control site samples (data not shown). When compared to the untreated samples, sorption of Sr onto the HFO and Chalk River BIOS did not result in significant alteration of mineralogy.

Over the course of the incubations, there were no changes in mineralogy for any of the abiotic systems. However, all of the iron oxide microcosms displayed a shift in mineralogy towards the ferrous phosphate mineral, vivianite ($Fe_3(PO4)_2 \cdot 8H_2O$; data not shown).

3.3 EXAFS analysis of Sr in Äspö BIOS

Figure 3 shows the EXAFS spectra and associated radial structure functions (RSF) for Sr-acetate, hydrated Sr^{2+} and Äspö BIOS. The EXAFS spectrum for Äspö BIOS was essentially identical to that of hydrated Sr^{2+}, suggesting that Sr^{2+} was sorbed primarily as a hydrated ion to Äspö BIOS. The peak at $R + \Delta R = 2.0$ Å in the RSF (Fig. 3) corresponds to the distance between Sr^{2+} and oxygen as the first neighbouring atom. By simulation based on parameters generated by FEFF, the interatomic distance between Sr and O was determined as $R_{Sr\text{-}O} = 2.56 \pm 0.02$ Å, in close agreement with that of hydrated Sr^{2+} species with $R_{Sr\text{-}O} = 2.58 \pm 0.02$ Å (Table 3).

3.4 Microcosm reduction of BIOS and HFO

3.4.1 Abiotic controls

In all abiotic incubations, there were no significant changes in any of the variables measured, except for a slight reduction in Eh (of approximately 70 mV, on average) which occurred during the first 24 hours of incubation, most likely due to out-gassing of oxygen

following equilibration of the culture vessels with the anaerobic atmosphere (data not shown).

3.4.2 Reduction of native, washed, and Sr-loaded Chalk River BIOS

In all three Chalk River BIOS systems, there was a significant drop in Eh (of approximately 340 mV, on average), which commenced immediately after addition of the DIRB and progressed until about 4 days post-inoculation, at which point equilibrium was again restored (data not shown). Due to the presence of the PIPES buffer in the CDM, the pH in all 3 systems remained stable, showing only minor fluctuations (within ± 0.1 pH unit), centred at approximately 6.8 (data not shown). Plate counts indicated that the DIRB were viable throughout the incubation period. Initial counts ranged from 5.5 to 7.6 × 10^7 colony-forming units (CFU)/mL. Over the first day, there was a rise (of approximately 2.0 × 10^7 CFU/mL, on average) in cell concentration in all systems, after which time the cultures gradually began to decline, reaching final concentrations of 1.3 to 6.5 × 10^7 CFU/mL (data not shown). Soluble-phase phosphorus concentration declined in all systems (data not shown), due to the precipitation of vivianite, as detected by XRD (see section 3.2).

Changes in the proportions of total Fe(II) and soluble-phase Sr for the n-BIOS, w-BIOS and Sr-BIOS microcosms are shown in Figure 4. Reduction of the n-BIOS commenced immediately after addition of the DIRB to the growth medium, reaching a maximum of approximately 98% of the total Fe being reduced by Day 4 (Table 4). Reduction rates were highest through the first 24 hours, but started to decrease by Day 2. The rate of increase in the proportion of total Fe(II):total Fe over the first 24 hours was linear (Fig. 5), at a rate of 0.467 day^{-1} (Table 4). The rate of production of total Fe(II) in n-BIOS was nearly exactly mirrored by the accumulation of Sr in the soluble phase as Fe reduction

progressed (Fig. 4). Relative to total Fe(II) production, Sr release was delayed by approximately 12 hours, reaching a maximum of approximately 85% of the total Sr in the system by Day 4 (Table 4).

Reduction of the w-BIOS also commenced immediately following addition of the DIRB, progressing through the first 24 hours, before slowing around Day 2. Both the rate (0.306 day^{-1}) and the extent (approximately 62%) to which total Fe(II) accumulated in this system were significantly lower than measured for n-BIOS (Table 4). Interestingly, the concentrations of Sr in the w-BIOS samples were undetectable by ICP-OES, and so no Sr release data could be generated.

For Sr-loaded BIOS, the period of maximal reduction rate was protracted, from about 1 day (in the case of n-BIOS and w-BIOS) to 2 days. During this time, the rate of total Fe(II) accumulation was still linear (Fig. 5), however at a rate (0.227 day^{-1}) that was significantly lower than that measured for n-BIOS and w-BIOS (Table 4). The delay in Sr release was also protracted in this system, from about 12 hours (as seen for n-BIOS) to *ca.* 2 days. The maximum percentage of Sr released to solution for Sr-BIOS was approximately 61%, again significantly lower than that measured for n-BIOS (Table 4).

3.4.3 Reduction of HFO and Sr-loaded HFO

Immediately following inoculation of the synthetic oxides with the DIRB, there was a significant decrease in Eh (of approximately 380 mV) measured in both systems over the span of the first 3 days, followed by an equilibrium at the new, lower level for the duration of the incubation (data not shown). Throughout the incubation, the pH of the two systems fluctuated between 6.6 and 6.8 (data not shown). DIRB cell counts for the HFO system started at approximately 2.0×10^7 CFU/mL and remained at this level for the first 2 days,

followed by a slight increase (up to 5.0×10^7) between Day 3 and Day 5. Cell concentration then declined to approximately 4.0×10^7 at termination of the experiment. In contrast, cell numbers in the Sr-HFO system remained relatively constant, fluctuating between 1.6 and 3.0 $\times 10^7$ CFU/mL throughout the incubation (data not shown). Soluble-phase phosphorus concentration in both systems decreased steadily throughout the incubation as vivianite precipitated (data not shown).

Following addition of the DIRB to the HFO microcosm, there was an initial lag in the production of total Fe(II), such that significant increases in the proportion of total Fe(II) were not noticed until after Day 1 of the incubation. However, between Day 1 and Day 5, the proportion of total Fe(II) increased from approximately 20%, reaching a maximum value of approximately 78% by Day 5. During this time, the rate of total Fe(II) accumulation could be expressed by a linear plot (Fig. 5) with a rate of 0.162 day^{-1} , significantly lower than either of the rates measured for the Chalk River BIOS systems (Table 4). As the HFO was prepared in the absence of any Sr compounds, the concentration of Sr was undetectable in this system.

As detailed in Table 4, subsequent loading of the HFO with Sr did not result in any significant changes to the rate (0.106 day-1) or extent (approximately 70%) of total Fe(II) production, relative to un-treated HFO. Strontium in solution for this system increased from approximately 20% to 73%. However (as was the case for Sr-loaded BIOS) there was a substantial delay (of about 2 days) observed in the release of Sr, relative to the production of total Fe(II) in this system (Fig. 4).

3.4.4 Reduction of Äspö BIOS

Following inoculation of the Äspö BIOS systems with DIRB, the Eh decreased by approximately 450 mV (on average) over the first 4 days, remaining at the lower level for

the remainder of the incubation (data not shown). The pH gradually increased (from 6.6 to 6.9 on average), while soluble-phase phosphorus gradually decreased (due to vivianite precipitation) throughout the duration of the incubation (data not shown). DIRB cell concentrations showed an initial increase (from 1.5 to 5.0 × 10^7 CFU/mL, on average) over the first 24 hours, followed by gradual decline (to approximately 4.6 × 10^6 CFU/mL, on average) throughout the remainder of the incubation (data not shown).

Reduction of Fe(III) commenced immediately following addition of the DIRB (Fig. 4). Accumulation of total Fe(II) in the system continued at a linear rate (Fig. 5) until Day 2, at which point the rate of increase slowed, eventually reaching a maximum at approximately 83%. The rate of total Fe(II) production was measured at 0.269 day-1 (Table 4). Strontium release from the Äspö BIOS showed the same 2-day delay (relative to total Fe(II) production) as observed in the Sr-loaded HFO and Sr-loaded Chalk River BIOS systems, however, nearly all (>99%) of the total Sr was released upon reduction of the Äspö BIOS, a significantly higher fraction than was measured in any of the other systems (Table 4).

3.5 In situ, soluble-phase Fe and Sr at the Chalk River Study Site

Seasonal depth profiles of soluble-phase Fe(II) and Sr concentration within the BIOS site pore-waters are shown in Fig. 6. Increases in dissolved Fe(II) were observed at increasing depths below the sediment-water interface, indicating potential zones of in situ Fe(III) reduction within the BIOS. Generally, these zones of increased aqueous Fe(II) were positively correlated with measured increases in the concentration of soluble Sr, suggesting that in situ Fe oxidation state impacts Sr mobilization at the site. Seasonal comparisons of soluble-phase [Sr] between the BIOS site and the control site are shown in Fig. 7. In all seasons, and at most depths, the levels of soluble [Sr] are 2-3 times lower when BIOS is

present, than when BIOS is absent. Further, the only instances when [Sr] at the BIOS site approached that of the control site, were at depths within the BIOS that also displayed increased [Fe(II)].

4. Discussion

4.1 Mineralogy

The finding of 2-line ferrihydrite as the dominant mineral phase in the Chalk River and Äspö BIOS was not surprising, since ferrihydrite has been previously identified in the BIOS from these two sources, using a variety of analytical techniques such as XRD, selected area electron diffraction (Langley et al., 2008a) and EXAFS spectroscopy (unpublished data). Further, ferrihydrite has been identified as the main mineral component in BIOS from a variety of different sources, including both freshwater and marine environments (James and Ferris, 2004; Emerson and Moyer, 2002; Kennedy et al., 2003; Langley et al., 2008c), so its predominance in the samples was expected. The presence of silicates in the Chalk River BIOS is likewise not surprising, because they have been reported previously in samples from this source (Inch and Killey, 1987; Langley et al., 2008a) and, as is evident from the control site diffractogram (Fig. 2), the material underlying the deposits is comprised of the same quartz sand through which the groundwater flows prior to its discharge. Nevertheless, XRD did prove useful in demonstrating that saturation of the HFO and BIOS with Sr did not significantly alter the mineralogy of either sample, an effect that (had it occurred) might have had an impact on the subsequent reduction of the iron oxides and confounded interpretation of the reduction data. We are confident, therefore, that differences in the rates

of reduction discussed below are not due to bulk mineralogical alterations of the iron oxides as a result of their treatment with Sr.

Conversion of the ferrihydrite to vivianite during reduction in these systems is largely artefactual, representative of the high concentration of dissolved phosphate in the growth medium. In natural environments, increasing Fe(II) concentrations would more likely lead to saturation with respect to magnetite (Fe_3O_4) or siderite ($FeCO_3$). Interestingly, however, ongoing work in our laboratory, studying the mineralogy of the Chalk River BIOS, has failed to clearly identify any reduced-iron minerals (unpublished data). This suggests the possibility that Fe(II) generated by microbial reduction at depth within the deposits may be rapidly converted back into Fe(III), either by chemical or microbial pathways. Alternatively, Fe(II) may be sorbed back onto the remaining BIOS, where it can undergo electron transfer resulting in dissolution or solid-phase conversion of the Fe(III). In a natural setting, it seems reasonable to suggest that both processes would be at work, leading to a continual cycle of Fe reduction and re-oxidation within the deposit.

4.2 EXAFS analysis of Sr in Äspö BIOS

As indicated in Table 2, the naturally occurring Sr concentration in the Äspö BIOS is a full order of magnitude higher than in the Chalk River BIOS. The Äspö BIOS, therefore, represents a natural analog for the Sr-BIOS, which was prepared in vitro. Previous work in our laboratory (Langley et al., 2008b) has demonstrated that Sr sorbs to Chalk River BIOS through outer-sphere complexation of hydrated Sr^{2+}. However, despite the fact that it has been used previously in metal sorption and retention studies (Ferris et al., 1999, 2000), no data have yet been reported on the mechanism by which Sr sorbs to Äspö BIOS. The Äspö EXAFS data were fitted to a Sr-O shell model (as indicated by the dotted line in Fig. 3). The

interatomic distance (R_{Sr-O}) and coordination number (CN) for the Äspö BIOS were most similar to that of hydrated Sr^{2+} (Table 3), such that the interatomic distance between Sr and O measured for Äspö BIOS (2.56 ± 0.02 Å) was virtually identical to that of hydrated Sr^{2+} (R_{Sr-O} = 2.58 ± 0.02 Å). These R_{Sr-O} values are similar to those reported by Sahai et al. (2000) for Sr^{2+} sorbed onto HFO, clay, and silica by outer-sphere complexation, and by Langley et al. (2008b) for Sr^{2+} sorbed onto HFO, bacterial cells, and Chalk River BIOS (also by outer-sphere complexation). Precipitation of Sr as a carbonate surface complex (as reported by Sahai et al., 2000) does not appear to be a factor in the case of Äspö BIOS, since a peak corresponding to a Sr-Sr shell, identifiable at 3.7 Å in the RSF of the Sr acetate standard, could not be resolved in that of the Äspö BIOS (Fig. 3). That this peak was absent further suggests that Sr sorption to BIOS does not occur via carbonate precipitation (Langley et al., 2008b). On the basis of these data, therefore, we believe that Sr^{2+} is sorbed to Äspö BIOS as a hydrated ion, through outer-sphere complexation. As such, the factors governing Sr desorption during BIOS reduction should be similar for both the Äspö and Chalk River samples.

4.3 Fe(III) reduction and release of Sr

The Fe and Sr curves displayed in Fig. 4, and the data presented in Table 4 highlight some interesting aspects of Sr desorption coupled to Fe reduction. The first, and most obvious, is that Sr release is closely linked to Fe oxidation state, such that reduction of Fe(III) leads to Sr solubilization. In all of the cultures, the soluble-phase Sr (Sr_{sol}) concentration was never observed to increase prior to an increase in the concentration of Fe(II). Previous spectroscopic studies in our laboratory have attempted to determine whether Sr might sorb preferentially to sites within the mineral component or the microbial

component of BIOS, however, no differences in the EXAFS spectra could be detected between Sr sorbed to iron oxides alone, bacterial cells alone, or a mixture of the two, as occurs in BIOS (Langley et al., 2008b). This indicated that Sr sorbed as a hydrated complex regardless of its sorption site, but failed to elucidate the actual binding site within BIOS (Langley et al., 2008b). In the present study, the fact that Sr desorption mirrored Fe(III) reduction suggests that sorption of Sr occurs primarily, but not exclusively, to sites within the iron mineral component of the BIOS, and not to sites within the microbial component. This may be due to the fact that most of the reactive surface sites within the microbial component are already saturated with Fe and are, therefore, unavailable for sorption.

The second clear feature of the reduction/desorption curves (Fig. 4) is that, once desorbed, a large proportion of the Sr remained in solution (Table 4), despite the presence of remaining solid phases (e.g., organic detritus, remaining solid-phase BIOS, secondary precipitates of vivianite, etc), which could have served as potential sites of re-sorption. There are several possible explanations for this finding. First, since Sr_{sol} never reached 100% of Sr_{total} in any of the cultures, it may be that a proportion of the Sr released was, in fact, re-sorbed onto the remaining solid phases. Saturation of those sorption sites would have prevented more Sr from sorbing, resulting in the observed accumulation of Sr_{sol}. Alternatively, a proportion of the Sr_{total} may not have been sorbed, initially, to the iron oxide component and would, therefore, not have been affected by the dissolution of that phase during reduction. Finally, competition between $Fe(II)_{sol}$ and Sr_{sol} for available sorption sites may have prevented re-sorption of Sr, particularly for reactive sites within remaining iron oxide material, since the affinity of Fe(II) for Fe(III) is known to be high (Hansel et al., 2004). Sorption of soluble Fe(II) and Sr^{2+} onto the organic fraction was difficult to estimate,

due to the unknown (and variable) composition of the BIOS. However sorption data for both Fe(II) and Sr^{2+} are available for *Shewanella putrefaciens*. Maximum binding capacities have been reported as 4.19 mmol/g for Fe(II) (Liu et al., 2001) and 75 μmol/g for Sr^{2+} (Small et al., 1999). Assuming a mass of 10^{-12} g per cell (DiChristina, 1989; Haas et al., 2001), the average total sorptive capacity of the *Shewanella* cultures was 0.05 mmol for Fe(II) and 1.03 μmol for Sr^{2+}. With respect to the total Fe(II) produced, the fraction of Fe(II) that may have been sorbed onto the *Shewanella* cells is insignificant as a control on the removal of Fe(II) from solution. However, the total sorptive capacity of the *Shewanella* culture was high enough to have potentially sorbed all of the released Sr^{2+}. Therefore, the fact that most Sr^{2+} remained in the soluble phase suggests that sorption onto the *Shewanella* cells did not occur. It has been clearly documented that *Shewanella oneidensis* MR-1 adheres tightly to solid phase iron during reduction experiments (Lower et al., 2001) and that individual cells of *S. putrefaciens* CN32 often become coated with solid material shortly after their inoculation (Glasauer et al., 2001). Furthermore, saturation of the mineral and cell surfaces with Fe(II) complexes occurs (Roden and Zachara, 1996; Roden and Urrutia, 2002) as reduction proceeds. It is possible, therefore, that the cell surface reactive sites of the *Shewanella* culture were unavailable for sorption and removal of Sr^{2+} under the experimental conditions.

With respect to mineral precipitation, strontium has been shown to become incorporated into secondary ankerite [$CaFe(CO_3)_2$] precipitates during the reduction of synthetic HFO (Roden et al., 2002), by substituting for Ca^{2+} in the metal moiety of the mineral. However, the lack of carbonate in the present study precluded the formation of siderite and ankerite. It seems clear that the Sr was not incorporated into, or sorbed onto, the secondary vivianite, as such associations would have lowered the concentration of Sr_{sol}.

Whether Sr might be removed from solution during formation of other secondary iron minerals (perhaps by re-sorption onto magnetite) remains to be studied, but is an important factor for consideration of the fate of Sr in more natural, low-phosphate environments, where precipitation of other secondary phases is favoured over vivianite. Using the experimental data, computer modeling of the aqueous chemistry within each of the microcosms was performed using PHREEQC Interactive software (v. 2.15.0.2697) and the minteq (v.4) component database. In all systems, the dominant form (>90%) of Sr predicted was the divalent ion. Various phosphate (8-9%) and hydroxide (<1%) complexes accounted for the balance of the total Sr, however saturation with respect to $SrHPO_4$ was never achieved, confirming that precipitation did not exert a major control on Sr speciation in these systems. Conversely, precipitation was the dominant control over soluble Fe(II). In all systems, the medium was saturated with respect to magnetite and vivianite immediately after addition of the cells. However, by the second day (and for the duration of the incubations), only saturation with respect to vivianite was maintained.

With Chalk River BIOS, saturation of the material with Sr resulted in several changes to the subsequent reduction, when compared to native BIOS. The first was a decrease in the maximum percentage of Sr released (from approximately 85% to 60%; Table 4). This may be due simply to the larger initial concentration of Sr_{total} in the Sr-BIOS. Alternatively, the high-concentration $Sr(NO_3)_2$ solution used to prepare the Sr-BIOS may have forced some inner-sphere sorption of Sr onto high-affinity sites within the BIOS. Such inner-sphere complexation would be less susceptible to the effects of Fe reduction than the readily-reversible, outer-sphere complexation which normally governs sorption between these two moieties. Stronger binding of the Sr may also explain why washing of the Sr-BIOS

did not result in a loss of Sr from the system, whereas washing of untreated BIOS decreased the total Sr concentration to levels which were below detection (Fig. 4). As a final consideration, since Sr sorption to BIOS is influenced by ionic strength (Langley et al., 2008b), equilibration of the w-BIOS with the KNO_3 electrolyte (prior to washing) may have caused the desorption.

The second effect of Sr-loading was to cause a significant decrease in both the rate and extent of Fe(III) reduction, relative to n-BIOS (Table 4). Poisoning of the DIRB cells due to Sr toxicity was one possible explanation for this effect. However, DIRB cell concentrations in the Sr-BIOS system were comparable to those of the n-BIOS and w-BIOS systems, so Sr toxicity does not appear to be a factor. However, if saturation of the Sr-BIOS resulted in stronger complexation between the Sr and Fe(III) in this system, then the availability of Fe(III) to the DIRB might be decreased. Interestingly, however, similar Sr-loading of synthetic HFO (Sr-HFO) had no significant effect on either the rate or extent of Fe(III) reduction, relative to untreated HFO (Table 4), so stronger complexation of Sr in the Sr-BIOS also appears to be inadequate in explaining the observed decreases in the reduction measurements. A remaining possibility may be that washing of the Sr-BIOS (following the saturation procedure) removed compounds within the BIOS that are advantageous to the growth of DIRB. This possible explanation is based on two findings. The first is that w-BIOS displayed a similar decrease in the rate and extent of Fe(III) reduction (Table 4), again indicating that washing may remove potential nutrients from the system. The second is that n-BIOS were consistently reduced faster, and to a greater extent than synthetic 2-line ferrihydrite (HFO) (Table 4; Langley et al., 2008a), suggesting that Fe(III) reduction in

BIOS is promoted by an as-yet unknown factor, perhaps contributed by the organic fraction of the BIOS itself (Langley et al., 2008a).

Finally, while saturation of the iron oxides with Sr did not have any effect on the onset of Fe(III) reduction, it did appear to delay the onset of Sr release. Comparison of the two natural samples (n-BIOS and Äspö BIOS) demonstrated that Sr desorption in the Äspö sample was significantly delayed (by about 2 days) following the onset of Fe(III) reduction. Subsequent saturation of native BIOS with Sr resulted in a change in the reduction profile, such that the delay in Sr desorption for the Sr-BIOS was identical to that of the naturally-high-Sr Äspö BIOS (Fig. 4). Interestingly, a similar 2-day delay in Sr desorption was also noted for Sr-HFO. Reports on the sorption of Sr to HFO have indicated that sorption appears to be governed more by inner-sphere complexation (Small et al., 2001), whereas sorption to BIOS is governed largely by outer-sphere complexation, until Sr concentrations become elevated (Langley et al., 2008b). The fact that the Sr-saturated BIOS samples display desorption profiles which are similar to that of Sr-HFO again suggests the possibility that Sr saturation may promote inner-sphere complexation of Sr to higher affinity sorption sites within the BIOS. Those high affinity sites would bind the Sr more strongly, thereby delaying its release into solution. This may have important implications because it suggests that a BIOS deposit intersecting a groundwater Sr plume might actually become more resistant to the release of Sr during reduction as the material becomes progressively saturated with the metal. Given the chemical heterogeneities within BIOS, it is also possible that Sr saturation promotes sorption onto reactive sites within the BIOS that are relatively unaffected by iron reduction (e.g., onto minor phases of Mn-oxides). If this were the case, however, then

similar delays in Sr desorption would not have been observed for the chemically pure Sr-HFO.

4.4 In situ attenuation of Sr by BIOS

The in vitro experiments clearly demonstrated that significant desorption of Sr can occur when BIOS is subjected to reducing conditions, due largely to the reversible nature of outer-sphere complexation, which governs Sr sorption to iron oxides of this type (Langley et al., 2008b). However, the microcosm experiments are poor analogs for the natural system, where desorbed Sr would likely be carried upward by the groundwater flow to encounter overlying layers of solid phase BIOS, likely resulting in re-sorption of the aqueous Sr. Such a process would not have been observed in the microcosm experiments, due to the nearly complete dissolution of the BIOS in the closed, batch systems. Examination of the depth profiles presented in Fig. 6 shows a positive correlation of soluble-phase Sr with soluble-phase Fe(II) in the porewaters of the BIOS (R^2 values ranging from 0.48 in the spring to 0.87 in the winter). Furthermore, the concentrations of both species generally tend to increase with increasing depth. These profiles suggest that Sr desorption is indeed linked (at least to some extent) to Fe(III) reduction in situ. Also, the fact that soluble-phase Sr concentration decreases above potential zones of Fe(III) reduction suggests that upward flow of the groundwater does result in removal from the porewaters of a large proportion of the solubilized Sr (i.e., soluble Sr concentrations in the oxidized BIOS zone are lower). Whether the Sr is simply re-sorbed to the existing overlying BIOS, or is co-precipitated as the Fe(II) is re-oxidized, is unclear at this point. As mentioned earlier, co-precipitation with a mineral phase might be advantageous in limiting Sr migration, if the Sr were to become bound within the mineral structure (Andersson et al., 1994), rather than simply sorbed as a hydrated

complex. However, the fact that Sr was easily desorbed from n-BIOS samples in the microcosm experiments suggests that most of the Sr in the (at least within the surficial sediment layers) is naturally present as a sorbed species, rather than as a co-precipitate.

Finally, in areas where no BIOS are being formed, the levels of soluble Sr in the porewaters are 2 to 3 times higher than in areas where BIOS are present (Fig. 7). The only apparent exception appears to occur at depths within the BIOS that are correlated with increased Fe(II) concentration, suggesting that in situ reduction and dissolution of the BIOS is sufficient to return most of the bound Sr back into solution. It seems reasonable to suggest that in a natural setting, in the presence of BIOS, the residence time of Sr within the deposit will be extended (relative to a similar system lacking BIOS). As groundwater discharges to the surface, the dissolved Sr encounters the solid BIOS, becomes sorbed and so is removed from solution. However, as BIOS deposition proceeds, the Sr-loaded material is progressively buried, until such time as anaerobic processes result in the reduction and dissolution of the iron oxides. Dissolution releases the Sr back into solution, where it is again transported by groundwater flow into the upper layers of the BIOS where re-sorption and/or co-precipitation with Fe(II) might occur, at which point the cycle begins again. Such an hypothesis is dependent on an upward flow of groundwater, and future studies planned for this site will focus on determination of the direction of groundwater flow.

5. Conclusions

Sr sorption to BIOS is not only governed by outer-sphere complexation, but is also closely linked to Fe oxidation state, such that oxidized BIOS are efficient sorbents of dissolved Sr^{2+} while reduced Fe(II) phosphates and, specifically, vivianite are not. Sorbed Sr

does not appear to affect the mineralogy of BIOS, however, the relative ease with which all BIOS are reduced by DIRB means that significant Sr desorption will occur when Sr-loaded BIOS are subjected to anoxic conditions. Saturation of BIOS with Sr decreases the rate and extent to which the iron oxide phases are reduced, but significant release of the sorbed Sr still occurs. Once desorbed, a large proportion of the total Sr remains in solution and does not appear to re-sorb readily to secondary mineral phases under anoxic conditions, but may become re-sorbed following exposure to fresh oxide surfaces *in situ*. BIOS in natural groundwater flow systems display the ability to significantly decrease the level of dissolved Sr in porewaters, relative to similar flow systems without BIOS. Release of the sorbed Sr (due to Fe reduction at depth) appears to be counteracted by re-sorption of the Sr following upward flow into more oxic layers of the deposit. BIOS may, therefore, represent a natural and efficient means of Sr attenuation in groundwater systems affected by this contaminant.

Acknowledgements

SL was supported by scholarships from the Natural Sciences and Engineering Research Council of Canada (NSERC), the Ontario Graduate Scholarship (OGS) program, and the University of Ottawa. This project was supported by an NSERC Strategic Project grant awarded to GF. We are indebted to Kristen Feige, Danielle Denis, Sara Cowell, Ivy Liu, Sun Hungfu, and Yuan Linxi for their assistance with the seasonal peeper sampling. We are also grateful to Dragica Bogdanovic (National HIV and Retrovirology Laboratories, Health Canada) for her kind assistance with sample irradiation.

References

Anderson, R.T., Lovley, D.R., 1999. Naphthalene and benzene degradation under Fe(III)-reducing conditions in petroleum-contaminated aquifers. Biorem. J. 3, 121–135.

Anderson, C.R., Pedersen, K., 2003. *In situ* growth of *Gallionella* biofilms and partitioning of lanthanides and actinides between biological material and ferric oxyhydroxides. Geobiology. 1, 169-178.

Andersson, P.S., Wasserburg, G.J., Ingri, J., Stordal, M.C., 1994. Strontium, dissolved and particulate loads in fresh and brackish waters: the Baltic Sea and Mississippi Delta. Earth Planet. Sci. Lett. 124, 195-210.

Ankudinov, A.L., Rehr, J.J., 1997. Relativistic calculations of spin-dependent x-ray absorption spectra. Phys. Rev. B56, 1712-1716.

Axe, L., Bunker, G.B., Anderson, P.R., Tyson, T.A., 1998. An XAFS analysis of strontium at the hydrous ferric oxide surface. J. Colloid. Interface Sci. 199, 44-52.

Bonneville, S., Van Cappellen, P., Behrends, T., 2004. Microbial reduction of iron(III) oxyhydroxides: effects of mineral solubility and availability. Chem. Geol. 212, 255-268.

Bruno, J., Ewing, R.C., 2006. Spent nuclear fuel. Elements. 2, 343-349.

Châtellier, X., West, M.M., Rose, J., Fortin, D., Leppard, G.G., Ferris, F.G., 2004. Characterization of iron-oxides formed by oxidation of ferrous ions in the presence of various bacterial species and inorganic ligands. Geomicrobiol J. 21, 99-112.

Clausen, L., Fabricius, I., 2001. Atrazine, isoproturon, mecoprop, 2,4-D, and bentazone adsorption onto iron oxides. J. Environ. Qual. 30, 858-869.

Cornell, R.M., Schwertmann, U., 2003. The Iron Oxides: Structure, Properties, Reactions, Occurrence and Uses. VCH, Germany.

DiChristina, T.J., 1989. Dissimilative Fe(III) reduction by *Alteromonas putrefaciens* strain 200. PhD dissertation. California Institute of Technology, Pasadena, CA, USA.

Dixit, S., Hering, J.G., 2003. Comparison of arsenic(V) and arsenic(III) sorption onto iron oxide minerals: implications for arsenic mobility. Environ. Sci. Technol. 37, 4182-4189.

Emerson, D., Moyer, C.L., 2002. Neutrophilic Fe-oxidizing bacteria are abundant at the Loihi seamount hydrothermal vents and play a major role in Fe oxide deposition. Appl. Environ. Microbiol. 68, 3085-3093.

Ferris, F.G., Konhauser, K.O., Lyvén, B., Pedersen, K., 1999. Accumulation of metals by bacteriogenic iron oxides in a subterranean environment. Geomicrobiol. J. 16, 181-192.

Ferris, F.G., Hallberg, R.O., Lyvén, B., Pedersen, K., 2000. Retention of strontium, cesium, lead and uranium by bacterial iron oxides from a subterranean environment. Appl. Geochem. 15, 1035-1042.

Fortin, D., Langley, S., 2005. Formation and occurrence of biogenic iron-rich minerals. Earth Sci. Rev. 72, 1-19.

Glasauer, S., Langley, S., Beveridge, T.J., 2001. Sorption of Fe (hydr)oxides to the surface of *Shewanella putrefaciens*: cell-bound fine-grained minerals are not always formed de novo. Appl. Environ. Microbiol. 67, 5544-5550.

Glasauer, S., Langley, S., Beveridge, T.J., 2002. Intracellular iron minerals in a dissimilatory iron-reducing bacterium. Science. 295, 117-119.

Glasauer, S., Weidler, P.G., Langley, S., Beveridge, T.J., 2003. Controls on Fe reduction and mineral formation by a subsurface bacterium. Geochim. Cosmochim. Acta. 67, 1277-1288.

Haas, J.R., DiChristina, T.J., Wade, Jr., R., 2001. Thermodynamics of U(VI) sorption onto *Shewanella putrefaciens*. Chem. Geol. 180, 33-54.

Hansel, C.M., Benner, S.G., Nico, P., Fendorf, S., 2004. Structural constraints of ferric (hydr)oxides on dissimilatory iron reduction and the fate of Fe(II). Geochim. Cosmochim. Acta. 68, 3217-3229.

Hansen, B., Kwan, P., Benjamin, M.M., Li, C-W., Korshin, G.V., 2001. Use of iron oxide-coated sand to remove strontium from simulated Hanford tank wastes. Environ. Sci. Technol. 35, 4905-4909.

Inch, K.J., Killey, R.W.D., 1987. Surface area and radionuclide sorption in contaminated aquifers. Water Poll. Res. J. Canada. 22, 85-98.

James, R.E., Ferris, F.G., 2004. Evidence for microbial-mediated iron oxidation at a neutrophilic groundwater spring. Chem. Geol. 212, 301-311.

Kasama, T., Marakami, T., 2001. The effect of microorganisms on Fe precipitation rates at neutral pH. Chem. Geol. 180, 117-128.

Kennedy, C.B., Scott, S.D., Ferris, F.G., 2003. Characterization of bacteriogenic iron oxide deposits from Axial Volcano, Juan de Fuca Ridge, northeast Pacific Ocean. Geomicrobiol. J. 20, 199-214.

Kulczycki, E., Fowle, D.A., Fortin, D., Ferris, F.G., 2005. Sorption of cadmium and lead by bacteria-ferrihydrite composites. Geomicrobiol. J. 22, 299-310.

Langley, S., Gault, A.G., Ibrahim, A., Renaud, R., Fortin, D., Clark, I.D., Ferris, F.G., 2008a. A comparison of the rates of Fe(III) reduction in synthetic and bacteriogenic iron oxides by *Shewanella putrefaciens* CN32. Geomicrobiol. J. submitted.

Langley, S., Takahashi, Y., Gault, A.G., Ibrahim, A., Renaud, R., Fortin, D., Clark, I.D., Ferris, F.G., 2008b. Sorption of strontium onto bacteriogenic iron oxides. Environ. Sci. Technol. submitted.

Langley, S., Igric, P., Takahashi, Y., Sakai, Y., Fortin, D., Hannington, M.D., Schwarz-Schampera, U., 2008c. Preliminary characterization and biological reduction of putative biogenic iron oxides (BIOS) from the Tonga-Kermadec Arc, southwest Pacific Ocean Geobiology. In press.

Liu, C., Zachara, J.M., Gorby, Y.A., Szecsody, J.E., Brown, C.F., 2001. Microbial reduction of Fe(III) and sorption/precipitation of Fe(II) on *Shewanella putrefaciens* strain CN32. Environ. Sci. Technol. 35, 1385-1393.

Lower, S.K., Hochella, M.F., Beveridge, T.J., 2001. Bacterial recognition of mineral surfaces: nanoscale interactions between *Shewanella* and α-FeOOH. Science. 292, 1360-1363.

McNamara, N.P., Black, H.I.J., Beresford, N.A., Parekh, N.R., 2003. Effects of acute gamma irradiation on chemical, physical and biological properties of soils. Appl. Soil. Ecol. 24, 117-132.

Nielsen, P., 2004. The biological role of strontium. Bone. 35, 583-588.

Palmer, J.L., Gunter, M.E., 2001. The effects of time, temperature, and concentration on Sr^{2+} exchange in clinoptilolite in aqueous solutions. Amer. Mineral. 86, 431-437.

Parkman, R.H., Charnock, J.M., Livens, F.R., Vaughan, D.J., 1998. A study of the interaction of strontium ions in aqueous solution with the surfaces of calcite and kaolinite. Geochim. Cosmochim. Acta. 62, 1481-1492.

Ravel, B., 2001. ATOMS: crystallography for the X-ray absorption spectroscopy. J. Synchrotron Radiat. 8, 314-316.

Roden, E.E., Zachara, J.M., 1996. Microbial reduction of crystalline Fe(III) oxides: influence of oxide surface area and potential for cell growth. Environ. Sci. Technol. 30, 1618-1628.

Roden, E.E., Edmonds, J.W., 1997. Phosphate mobilization in iron-rich anaerobic sediments. Microbial Fe(III) oxide reduction versus iron-sulfide formation. Arch. Hydrobiol. 139, 347-378.

Roden, E.E., Urrutia, M.M., 2002. Influence of biogenic Fe(II) on bacterial crystalline Fe(III) oxide reduction. Geomicrobiol. J. 19, 209-251.

Roden, E.E., Leonardo, M.R., Ferris, F.G., 2002. Immobilization of strontium during iron biomineralization coupled to dissimilatory hydrous ferric oxide reduction. Geochim. Cosmochim. Acta. 66, 2823-2839.

Sahai, N., Carroll, S.A., Roberts, S., O'Day, P.A., 2000. X-ray absorption spectroscopy of strontium(II) coordination II: sorption and precipitation at kaolinite, amorphous silica and goethite surfaces. J. Colloid. Interface Sci. 222, 198-212.

Small, T.D., Warren, L.A., Roden, E.E., Ferris, F.G., 1999. Sorption of strontium by bacteria, Fe(III) oxide, and bacteria-Fe(III) oxide composites. Environ. Sci. Technol. 33, 4465-4470.

Small, T.D., Warren, L.A., Ferris, F.G., 2001. Influence of ionic strength on strontium sorption to bacteria, Fe(III) oxide, and composite bacteria-Fe(III) oxide surfaces. Appl. Geochem. 16, 939-946.

Solecki, J., 2005. Investigation of ^{85}Sr adsorption on selected soils of different horizons. J. Environ. Radioact. 82, 303-320.

Stoffers, P., Worthington, T.J., Schwarz-Schampera, U., Hannington, M.D., Massoth, G.J., Heknian, R., Schmidt, M., Lundsten, L.J., Evans, L.J., Vaiomo'unga, R., Kerby, T., 2006. Submarine volcanoes and high-temperature hydrothermal venting on the Tonga Arc, southwest Pacific. Geology 34:453-456.

Stookey, L.L., 1970. Ferrozine – a new spectrophotometric reagent for iron. Anal. Chem. 42, 779-781.

Um, W., Papelis, C., 2003. Sorption mechanisms of Sr and Pb on zeolitized tuffs from the Nevada test site as a function of pH and ionic strength. Amer. Mineral. 88, 2028-2039.

Viollier E., Inglett P.W., Hunter K., Roychoudhury A.N., Van Cappellen P., 2000. The ferrozine method revisited: Fe(II)/Fe(III) determination in natural waters. Appl. Geochem. 15, 785-790.

Welch, S.A., Christy, A.G., Kirste, D., Beavis, S.G., Beavis, F., 2007. Jarosite dissolution I - trace cation flux in acid sulfate soils. Chem. Geol. 245, 183-197.

Zavinsky, S.I., Rehr, J.J., Ankudinov, A., Albers, R.C., Eller, M.J., 1995. Multiple scattering calculations of X-ray absorption spectra. Phys. Rev. B52, 2995-3009.

Figure captions

Figure 1. Perennial BIOS deposition at the Chalk River site. **a)** approximately 1 m wide groundwater discharge point, showing rust-coloured BIOS in the winter. The base of the sand dune aquifer is in the background. **b)** downstream BIOS deposit in the summer showing installation of an in situ pore-water dialysis membrane device (peeper), in front of the yellow marker flag. The peeper is approximately 20 cm wide.

Figure 2. **a)** X-ray diffractograms of iron oxides showing broad reflections at 2.5 Å and 1.5 Å, characteristic of 2-line ferrihydrite. **b)** X-ray diffractograms of Chalk River BIOS and HFO following artificial Sr-loading and washing, indicating no significant alterations to mineralogy as a result of sample treatment. Äspö BIOS was untreated. The sharper peaks in the n-BIOS, Sr-BIOS, and w-BIOS patterns are derived from silicate weathering minerals such as quartz and feldspar, which comprise the bulk of the aquifer material, as shown in the control site diffractogram (**c**). For clarity, patterns in panels a and b have been vertically separated on an arbitrary y-axis.

Figure 3. Strontium EXAFS spectra and radial structure functions (RSFs) of hydrated Sr^{2+}, Sr-acetate, and Äspö BIOS. Solid lines are non-linear least-squares fits with a k-range of 2.0 to 12.0 $Å^{-1}$.

Figure 4. Changes in the proportions of total ferrous iron ($Fe(II)_{total}$) and soluble-phase Sr (Sr_{sol}), relative to total Fe and total Sr, respectively, during each of the iron oxide reductions with *S. putrefaciens* CN32. No Sr could be detected in either the washed BIOS (w-BIOS) or HFO preparations. Data represent means and

standard deviations from three separate replicates of each system. Maximum values for $Fe(II)_{total}$ and Sr_{sol} produced in each system are detailed in Table 4.

Figure 5. Changes in the proportion of $Fe(II)_{total}/Fe_{total}$ for each iron oxide during periods of maximum Fe(III) reduction by *S. putrefaciens* CN32. Data markers represent means and standard deviations from three separate replicates of each system. The data follow linear relationships, as indicated by the lines of best fit. Reduction rates and linear correlation coefficients calculated for the respective plots are presented in Table 4.

Figure 6. Seasonal, in situ, pore-water Fe(II) and Sr concentration depth profiles at a site showing BIOS deposition. Depths are shown relative to the sediment-water interface (0 cm). Spikes in soluble-phase [Sr] are positively correlated (R^2 values indicated in each panel) with spikes in [Fe(II)], indicating that Sr is released from the solid phase at depths where Fe(III) reduction is elevated. Note the different scales for [Fe(II)] and [Sr].

Figure 7. Seasonal comparisons of in situ pore-water Sr concentration between a site showing BIOS deposition and a natural control site (fed by the same groundwater but lacking BIOS). Depths are shown relative to the sediment-water interface (0 cm). In the absence of BIOS, Sr concentrations in the soluble phase are generally 2 to 3 times higher. In the presence of BIOS, soluble-phase Sr only reaches comparable levels at depths where Fe(III) reduction occurs, thereby releasing Sr back into solution.

Table 1. Physicochemical variables measured at Chalk River for a sample site with active BIOS deposition, compared to those for a control site (fed by the same groundwater, but lacking BIOS deposition). Values presented are means, derived from seasonal samplings at the same site, with ranges (minimum – maximum) indicated in parentheses.

Measurement	**BIOS Site**	**Control Site**
T (°C)	7.89 (4.20 – 9.64)	7.81 (5.96 – 8.86)
pH	5.73 (5.60 – 5.87)	5.77 (5.41 – 5.95)
Eh (mV)	328.5 (284 – 377)	345.3 (295 – 405)
Dissolved O_2 (mg/L)	3.88 (0.31 – 7.65)	5.38 (0.65 – 8.64)
Conductivity (μS/cm)	42.3 (39.0 – 45.0)	24.0 (8.0 – 40.0)
Total Fe_{sol} (mg/L)[a]	2.68 (2.62 – 2.76)	0.025 (0.02 – 0.03)
Total Fe (mg/L)	4.38 (3.14 – 5.36)	0.60 (0.50 – 0.69)
Sr_{sol} (mg/L)[a]	0.042 (0.040 – 0.044)	0.057 (0.053 – 0.060)
Sr_{total} (mg/L)	0.045 (0.040 – 0.055)	0.056 (0.052 – 0.060)
$Fe(II)_{sol}$ (mg/L)[a,b]	2.18 (0.76 – 3.00)	0.005 (ND – 0.02)[c]
Total Fe(II) (mg/L)[b]	2.44 (0.80 – 3.10)	0.085 (ND – 0.34)[c]

[a] soluble Fe and soluble Sr samples were filtered (0.22 μm, nylon filter) prior to analysis.

[b] Fe(II) was measured by the ferrozine method (Stookey, 1970).

[c] ND = none detected.

Table 2. Major and selected trace element composition of Chalk River and Äspö BIOS following acid digestion. Note the elevated levels of many cations (in particular Sr), which are naturally present within the Äspö BIOS. All values are mg/L.

Element[a]	Chalk River BIOS	Äspö BIOS
Ba	0.04	0.28
Ca	2.48	13.64
Fe	136.94	171.38
K	0.31	0.40
Mg	0.47	1.77
Mn	0.06	1.01
Na	4.14	12.16
P	1.79	2.70
S	1.17	2.36
Sr	0.03	0.48

[a] values for Al were artificially over range, due to inadvertent corrosion of Al-foil cap liners during the digestion procedure. Values for Cd, Co, Cr, Cu, Mo, Ni and Zn were all below the limits of detection by ICP-OES.

Table 3. Measurements obtained from fitting Sr K-edge EXAFS spectra.

Sample	Shell	N	R (Å)	ΔE_0 (eV)	σ^2 (Å^2)
Sr^{2+} (aq.)	Sr-O	8.0 ± 1.3	2.580 ± 0.015	-2.6 ± 1.5	0.013 ± 0.001
Sr-acetate	Sr-O	6.5 ± 1.6	2.550 ± 0.021	-1.9 ± 2.3	0.013 ± 0.001
	Sr-C	1.9 ± 0.1	3.476 ± 0.364		0.015 ± 0.001
	Sr-Sr	2.9 ± 1.0	4.266 ± 0.022		0.01[a]
Äspö BIOS	Sr-O	8.9 ± 1.9	2.561 ± 0.023	-0.4 ± 1.9	0.016 ± 0.001

[a] fixed

Table 4. Maximum Fe(II) produced (as a percentage of total Fe), linear reduction rates and correlation coefficients, and maximum Sr released (as a percentage of total Sr), calculated for the various iron oxides when reduced by *S. putrefaciens* CN32. Data represent means ± standard deviations taken from 3 separate replicates of each experiment.

Iron Oxide	Maximum % Fe Reduced	Linear Reduction Rate (day^{-1})[a]	R^2	Maximum % Sr Released
n-BIOS	97.98 ± 2.55[b]	0.467 ± 0.023[b]	0.942	85.48 ± 1.93
w-BIOS	61.91 ± 8.38[c]	0.306 ± 0.022[c]	0.977	ND[g]
Sr-BIOS	67.34 ± 4.41[c]	0.227 ± 0.016[e]	0.952	61.26 ± 0.44
HFO	78.08 ± 0.68[c]	0.162 ± 0.009[f]	0.970	ND[g]
Sr-HFO	70.41 ± 7.31[c]	0.106 ± 0.025[f]	0.989	73.32 ± 4.41
Äspö BIOS	83.34 ± 1.75[d]	0.269 ± 0.019[e]	0.963	99.45 ± 0.95

[a] based on increases in the ratio of Fe(II):total Fe in each system

[b] Maximum % Fe reduced and linear reduction rate for n-BIOS were significantly higher than for all other systems ($p<0.05$)

[c,f] No significant difference ($p<0.05$)

[d] Maximum % Fe reduced for Äspö BIOS was significantly different from all other systems ($p<0.05$)

[e] Linear reduction rate for Sr-BIOS was significantly lower than for w-BIOS but not significantly different from Äspö BIOS ($p<0.05$)

[g] ND = none detected

Figure 1

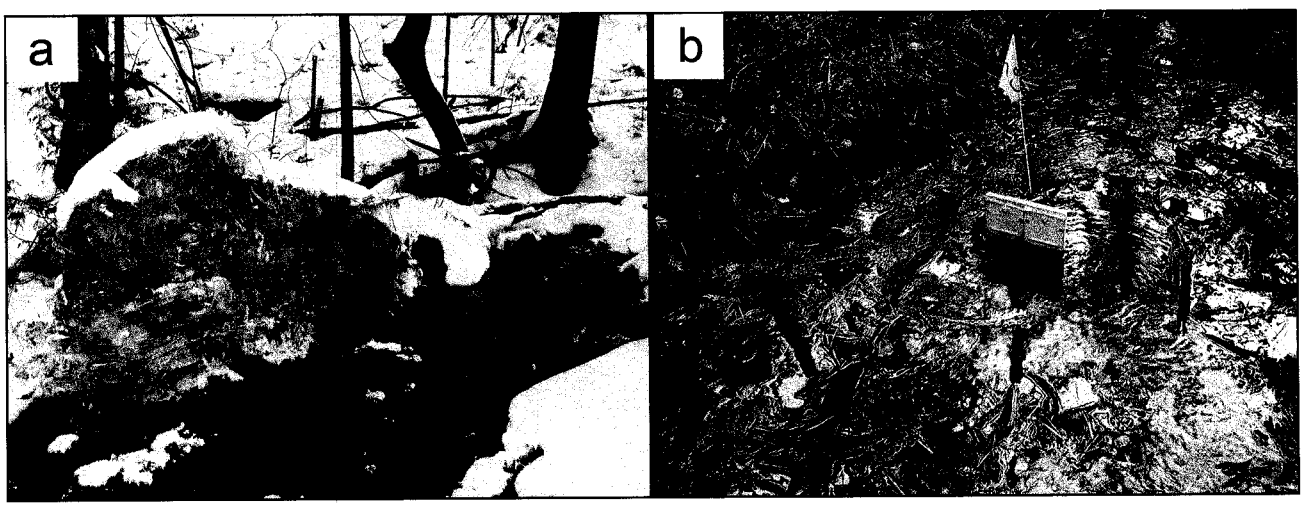

Figure 2

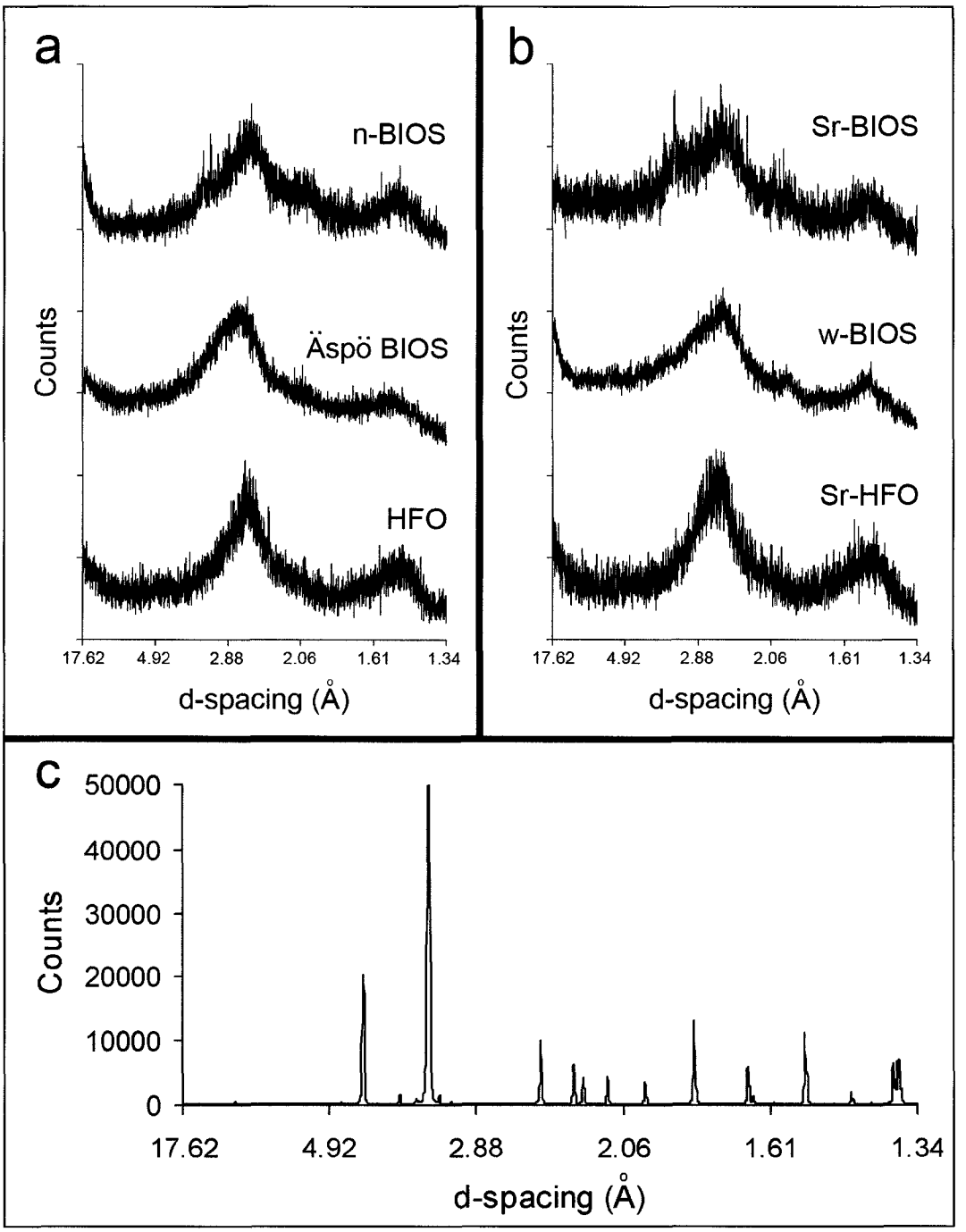

Figure 3

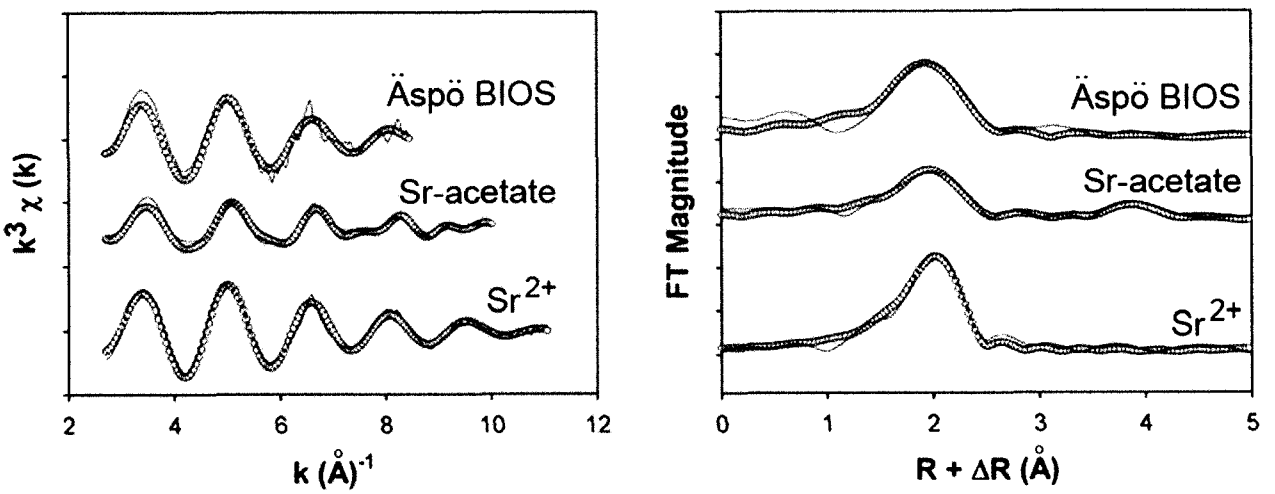

Figure 4

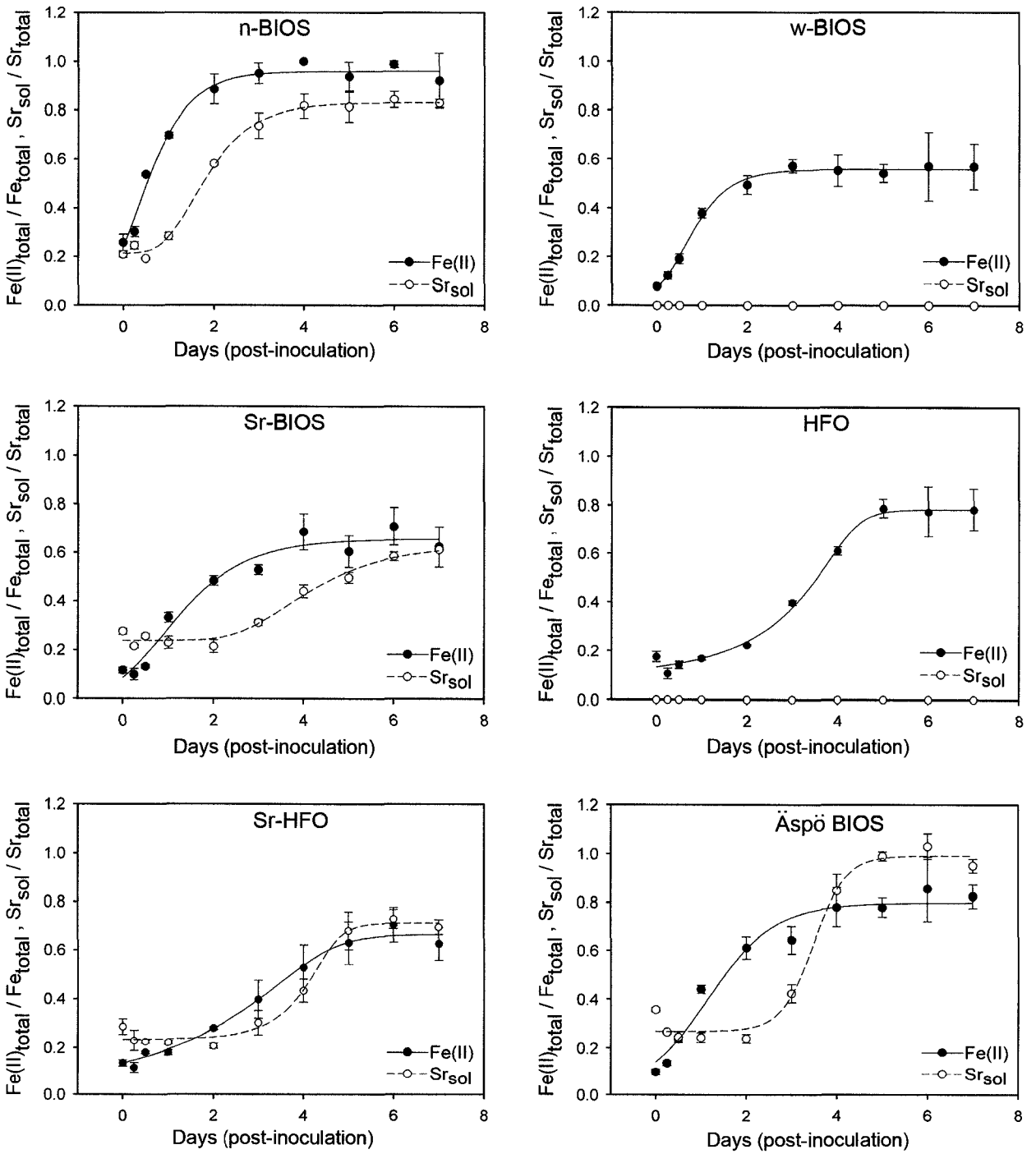

Figure 5

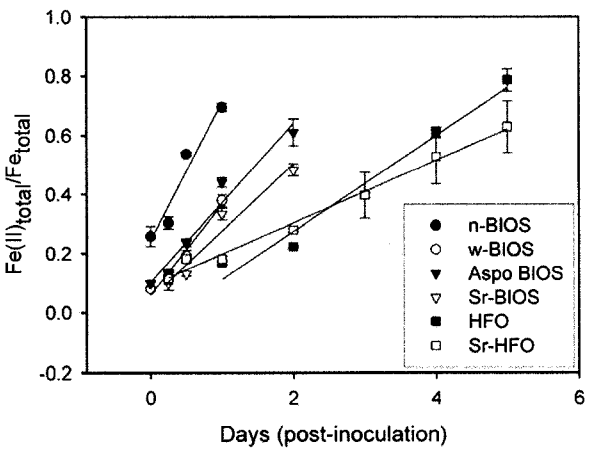

Figure 6

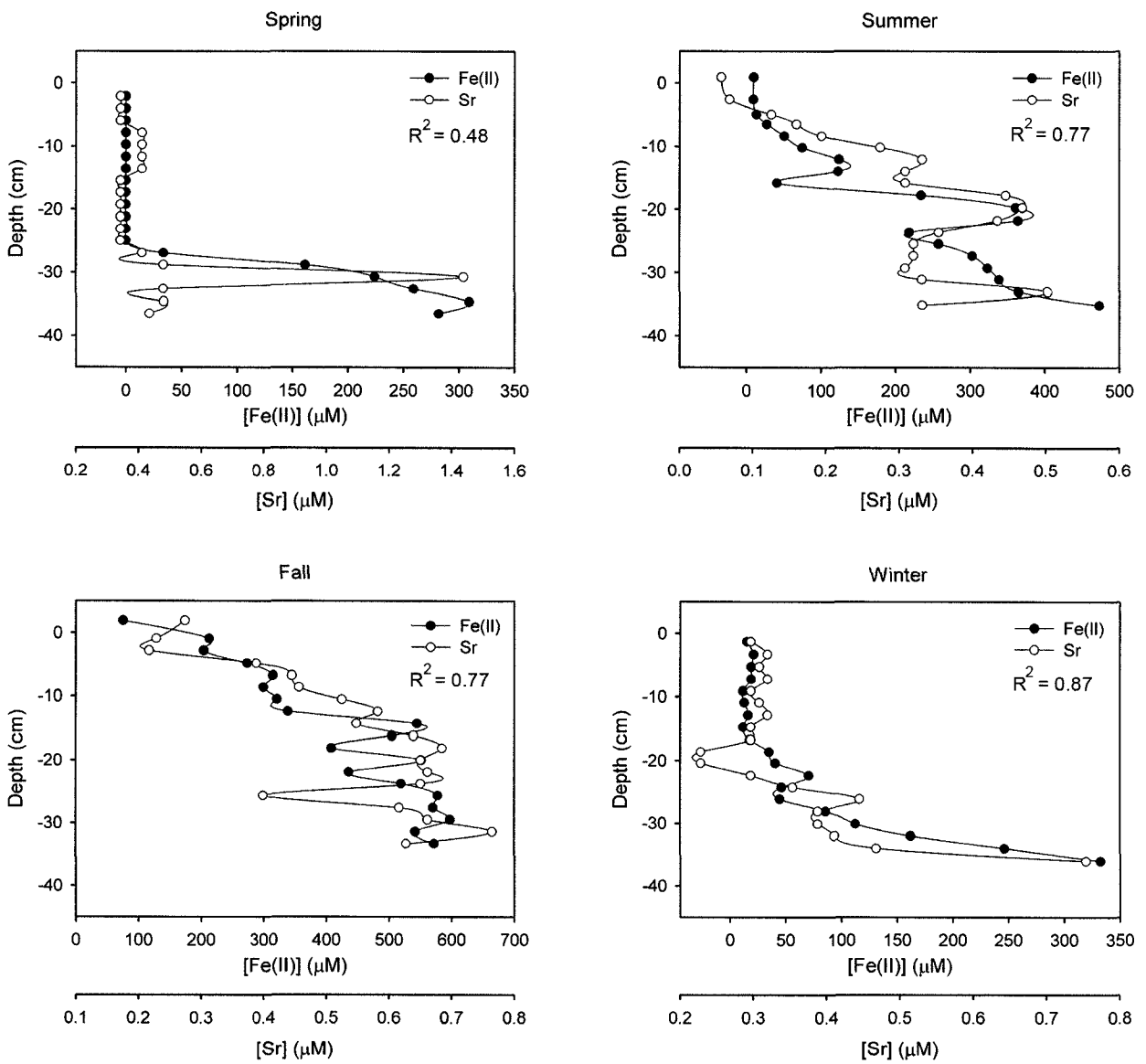

Figure 7

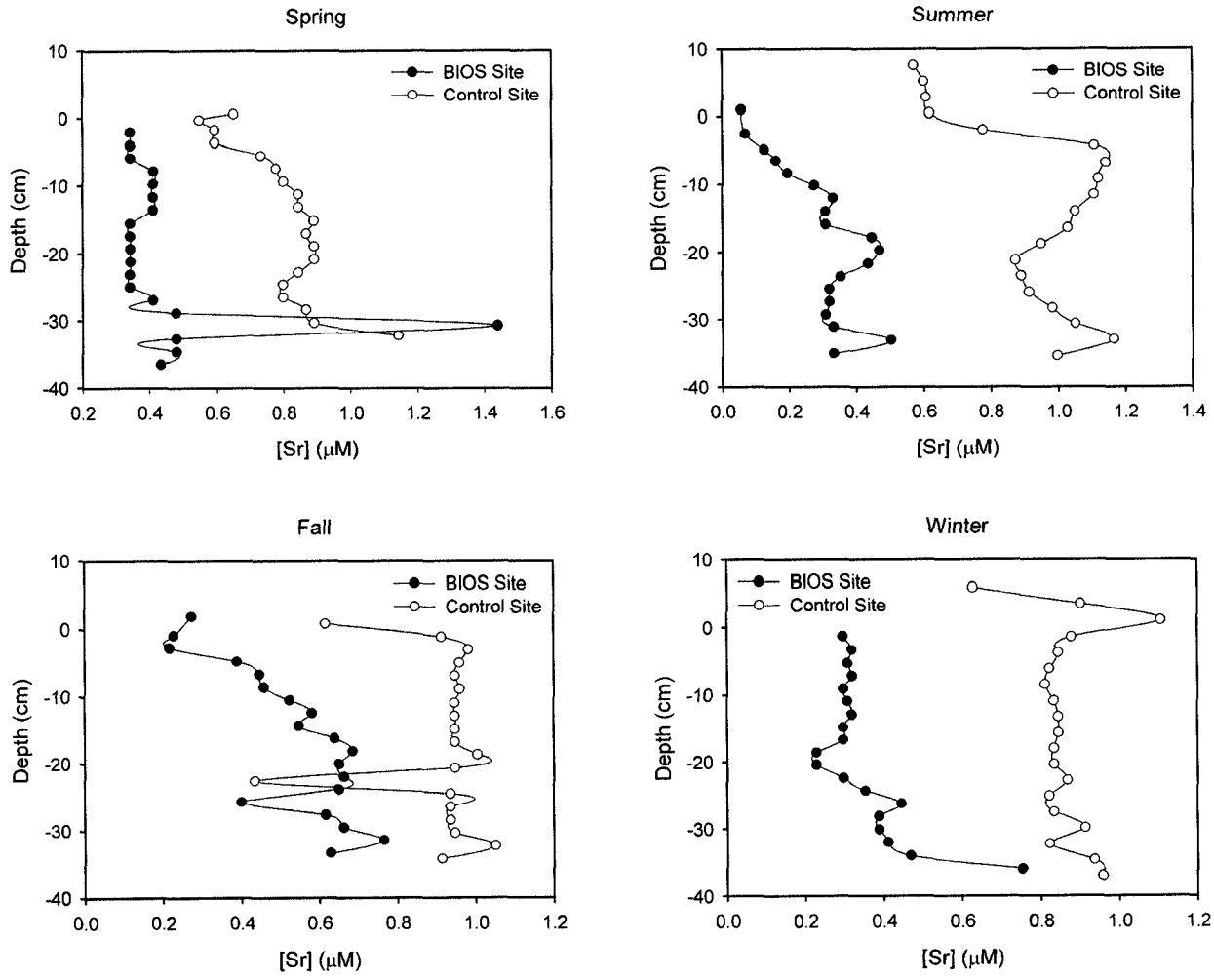

From the data presented in the previous three sections (and from the literature cited therein), it is clear that all natural BIOS deposits described to date consist of amorphous or poorly ordered iron oxyhydroxides. Most of the available literature on these deposits deals with freshwater environments and, by contrast, relatively little is known about the formation and reactivity of BIOS from marine environments. Most studies of marine BIOS have focused on elucidating the microbial community structure, and have only briefly characterized the iron oxide component of the sediments. Furthermore, the available literature deals only with BIOS from two areas (sites along the Juan de Fuca Ridge and Loihi Seamount), although this is likely only due to the expense and technical difficulty associated with seafloor exploration and sampling.

In 2005, exploratory dives along the Tonga-Kermadec Arc in the south-west Pacific Ocean discovered large fields of columnar structures, tentatively identified as iron oxyhydroxides. Filamentous microbial mats were observed in association with the structures, leading to speculation that they were biogenic in origin. Three samples were retrieved and preliminary investigations confirmed a mixture of microbial cells and iron oxides, although the small volume of sample precluded the possibility of extensive testing. A subsequent research cruise to the same area in 2007 permitted the recovery of larger volumes of the material. These samples were used for a more extensive analysis of the iron oxides and microbial structures associated with the sediments from two different hydrothermal fields. The larger sample volume also permitted preliminary investigations into the microbial reduction of these putative marine BIOS samples. The results of these investigations are presented, below, in Section 5.

Section 5

Preliminary characterization and biological reduction of putative biogenic iron oxides (BIOS) from the Tonga-Kermadec Arc, southwest Pacific Ocean

This manuscript has been accepted for publication in *Geobiology*[1]

[1] Langley, S., Igric, P., Takahashi, Y., Sakai, Y., Fortin, D., Hannington, M.D., Schwarz-Schampera, U. 2008. Preliminary characterization and biological reduction of putative biogenic iron oxides (BIOS) from the Tonga-Kermadec Arc, southwest Pacific Ocean. Geobiology. In press.

ABSTRACT

Sediment samples were obtained from areas of diffuse hydrothermal venting along the seabed in the Tonga sector of the Tonga-Kermadec Arc, southwest Pacific Ocean. Sediments from Volcano 1 and Volcano 19 were analyzed by X-ray diffraction (XRD) and found to be composed primarily of the iron oxyhydroxide mineral, 2-line ferrihydrite. XRD also suggested the possible presence of minor amounts of more ordered iron (hydr)oxides (including 6-line ferrihydrite, goethite/lepidocrocite and magnetite) in the biogenic iron oxides (BIOS) from Volcano 1, however Mössbauer spectroscopy failed to detect any mineral phases more crystalline than 2-line ferrihydrite. The minerals were precipitated on the surfaces of abundant filamentous microbial structures. Morphologically, some of these structures were similar in appearance to the known iron-oxidizing genus *Mariprofundus* spp., suggesting that the sediments are composed of biogenic iron oxides. At Volcano 19, an areally extensive, active vent field, the microbial cells appeared to be responsible for the formation of cohesive chimney-like structures of iron oxyhydroxide, 2 to 3 metres in height, whereas at Volcano 1, an older vent field, no chimney-like structures were apparent. Iron reduction of the sediment material (i.e., BIOS) by *Shewanella putrefaciens* CN32 was measured, in vitro, as the ratio of [total Fe(II)]:[total Fe]. From these measurements, reduction rates were calculated for Volcano 1 BIOS (0.0521 day^{-1}), Volcano 19 BIOS (0.0473 day^{-1}), and HFO, a synthetic 2-line ferrihydrite (0.0224 day^{-1}). Sediments from both BIOS sites were more rapidly reduced than synthetic ferrihydrite, which suggests that the decrease in effective surface area of the minerals within the sediments (due to the presence of the organic component) does not inhibit subsequent microbial reduction. These results indicate that natural, marine BIOS are easily reduced in the presence of dissimilatory iron-

reducing bacteria, and that the use of common synthetic iron minerals to model their reduction may lead to a significant underestimation of their biological reactivity.

INTRODUCTION

The Tonga-Kermadec Arc is a submarine arc-backarc system, which extends 2500-3000 km northeastward, from New Zealand to Tonga, in the Pacific Ocean (Regelous *et al.*, 1997; de Ronde *et al.*, 2003). It is an area of active volcanism and hydrothermal activity, due to subduction occurring as a result of the convergence between the Pacific and Australian tectonic plates. Approximately 90-94 submarine volcanoes lie along the span of the entire arc, the majority of which are located within the 1220 km long Kermadec sector (de Ronde *et al.*, 2003, 2005). In addition to volcanic activity, the system is known to produce at least one instance of black smokers, as well as areas of both low- and high-temperature diffuse venting of hydrothermal fluids (Stoffers *et al.*, 2006). Analysis of various vent plume samples has shown that the fluids being ejected at these sites can have a highly varied chemical composition. However, in several instances, the concentrations of dissolved and particulate iron were distinctively high (de Ronde *et al.*, 2001), indicating a large influx of this metal into the surrounding water.

It is well known that ferrous iron can serve as an electron donor in the metabolic pathways of a wide variety of bacterial and archaeal species. For example, in terrestrial environments, acidophilic iron oxidizers such as *Acidithiobacillus ferrooxidans*, *Leptospirillum ferrooxidans*, *Ferroplasma* spp. and many others couple iron oxidation to the reduction of a variety of terminal electron acceptors in acidic environments such as mining sites and tailings empoundments (Edwards *et al.*, 2000; Baker and Banfield, 2003 and

references therein). Neutrophilic iron oxidizers such as *Gallionella ferruginea* and *Leptothrix ochracea* can form large iron oxide deposits (e.g., red ochres) in circumneutral pH environments such as springs and groundwater seeps (Hallberg and Ferris, 2004; James and Ferris, 2004). These organisms catalyze the oxidation of ferrous to ferric iron. The electrons released by the oxidation are channelled into the cells' electron transport chains to drive the production of metabolic energy needed for growth and reproduction (Hallbeck and Pedersen, 1990, 1991). As they grow, the specialized appendages produced by the cells (stalks/sheaths) become encrusted in iron oxide. Once encrusted, they are discarded by the cells as detrital material that precipitates as flocs of fine-grained (2-500 nm), poorly ordered mineral, termed biogenic (or bacteriogenic) iron oxides (BIOS; Hallberg and Ferris, 2004). Once formed, the BIOS can settle into sedimentary layers and undergo typical diagenesis and transformation reactions towards more crystalline phases such as goethite or hematite, which (under oxic conditions) are the most stable end members in a variety of possible transformation pathways (Cornell and Schwertmann, 2003).

While much is known about these terrestrial systems, the abundance and role of iron-oxidizing microbes in marine environments is less understood. Known and suspected iron oxidizers have been found in association with certain submarine hydrothermal and volcanic systems including the Loihi Seamount (Emerson and Moyer, 2002; Emerson *et al.*, 2007), Juan de Fuca Ridge axis (Edwards *et al.*, 2003), and Axial Volcano (Kennedy *et al.*, 2003b). In 2005, manned submersible dives along the Tonga sector of the Tonga-Kermadec Arc revealed the presence of filamentous microbial mats in the vicinity of the southern cone of Volcano 1. Underlying the mats were extensive crusts of iron oxyhydroxide (Stoffers *et al.*, 2006). The same research cruise also discovered the presence of unusual, iron oxyhydroxide

chimney-like structures surrounding Volcano 19 (Stoffers *et al.*, 2006). The chimneys covered a large area (60,000 m^2) and were composed of unconsolidated sedimentary material. White, filamentous, microbial mats were often observed at the tops of the chimneys (Stoffers *et al.*, 2006), suggesting a possible microbial role in their formation.

Perhaps less well understood is the role of microbes in the cycling of iron within deep-sea sedimentary environments. Iron cycling is dependent upon the oxidation and reduction of iron, by both biotic and abiotic pathways. In oceanic sediments, where localized regions of anoxia may develop, dissimilatory iron reducing bacteria (DIRB) can couple the oxidation of available organic matter to the reduction of ferric iron, thereby generating metabolic energy and releasing Fe^{2+} back into solution (Lovley and Phillips, 1988; Myers and Nealson, 1990). The aqueous Fe^{2+} can adsorb onto available reactive sites on the surfaces of the remaining solid iron, or onto the microbial cells themselves. Alternatively, it can be re-oxidized, either chemically or by the action of iron-oxidizing microbes, thus completing the redox cycle. The ability of DIRB to reduce iron oxides is dependent on a variety of factors including nutrient concentration and mineral particle size, surface area, and crystallinity. Generally, the more crystalline the iron oxide, the slower it's rate of reduction by DIRB (Roden and Zachara, 1996; Roden, 2003). However, most studies on the reduction of iron oxides by DIRB have used synthetic iron oxides manufactured from pure chemicals. In contrast, very little is known about the rates of reduction of naturally formed BIOS and the effect of the various organic and inorganic impurities on the rate of its reduction.

Here we present the initial characterization of putative BIOS retrieved from two sites along the Tonga-Kermadec Arc, and provide the first evidence of a possible microbial role in their formation. This study is also one of the first to examine the biological reactivity of

environmental iron oxides subjected to in vitro reduction by a previously cultivated iron-reducing bacterium under anoxic conditions. We hypothesized that differences in the crystallinity of the BIOS obtained from the two sites would result in different reduction rates. Further, we hypothesized that the stabilizing influence of the microbial surfaces would act to make the BIOS less reducible than the chemically pure, synthetic ferric oxides typically used in studies of microbial iron reduction rates.

MATERIALS AND METHODS

Site descriptions

Putative BIOS samples were obtained from two sites along the Tonga-Kermadec Arc, Pacific Ocean: Volcano 19 and Volcano 1. The floor of the western caldera, and the west flank of the central cone of Volcano 19 were areas of diffuse, active venting. No shimmering water or bubbling was observed, however some significant temperature anomalies were noted (Table 1). Numerous chimney-like structures were visible throughout the site (Fig. 1a), however they were extremely unstable, composed of unconsolidated sedimentary material. They were predominantly brown or rust-coloured, with lighter beige-coloured tops, suggestive of the iron oxides ferrihydrite and goethite. The chimneys in the western caldera measured up to 2 to 3 m in height, whereas those along the west flank of the central cone were much shorter, approximately 60 cm high. The beige-coloured material covering the chimneys appeared to be dominated by a filamentous microbial mat. It is possible that the bacteria are, at least in part, responsible for forming the chimney-like structures and providing some stability to the otherwise flocculent, sedimentary material.

At Volcano 1 there was extensive deposition of iron oxides with microbial mat material and ash deposits on the sediment surface (Fig. 1b). The mat material was approximately the same rust colour as that seen in the Western caldera of Volcano 19, however no chimney-like structures were present. Immediately below the surface layer, the iron oxides were a much darker, red-brown colour, suggestive of a shift towards a more crystalline form of iron oxide (e.g., hematite). In addition, the sediments were more coarse than those of Volcano 19 and tended to settle more rapidly from suspension. There were no obvious signs of venting such as shimmering water or bubbles, however subtle temperature anomalies were noted (Table 1). This site may represent an area where active venting has slowed or ceased, likely affecting both the microbial community structure and processes of iron oxide formation and diagenesis within the sediment.

Dive sampling procedure

The Canadian submersible, *ROPOS*, a remotely-operated vehicle (ROV), was used to retrieve sediment samples using an automated vacuum system attached to one of the ROV robotic manipulator arms. The sediments were filtered (200 mesh) onboard the ROV to remove large particles prior to return to surface. Temperature probes onboard the ROV recorded temperatures of both the ambient seawater, and the sediment porewater (at the point of insertion of the vacuum nozzle). Onboard the research vessel, aqueous phase samples were analyzed for pH and total Fe(II) concentration (Table 1). Fe(II) in the seawater was determined by the phenanthroline method using a HACH portable commercial spectrophotometer and reagent packets. pH was measured using a standard laboratory pH meter and probe.

Sterilization of sediments

In order to ensure that the observed rates of reduction were not affected by members of the native microbial communities, the sediments were sterilized prior to use by gamma irradiation (^{60}Co source) using a Nordion Gammacell 220. Total exposure was 48 kGray. According to McNamara *et al.* (2003), gamma-radiation causes little physical and mineralogical changes and therefore represents a suitable technique to sterilize natural sediments.

Culturing of iron-reducing bacteria

A pure culture of *Shewanella putrefaciens* CN32 was kindly donated by professor Terry Beveridge of the Department of Molecular and Cellular Biology, University of Guelph, Ontario, Canada. The culture was maintained, aerobically, on tryptic soy agar (TSA) plates at 22°C. BIOS reductions were performed in an artificial seawater medium (ASM) with the following composition, per L (Park *et al.*, 2001): NH_4NO_3 2 mg, H_3BO_3 27 mg, $CaCl_2$ 1.14 g, $FePO_4$ 1 mg, $MgCl_2$ 5.143 g, KBr 0.1 g, KCl 0.69 g, $NaHCO_3$ 0.2 g, NaF 3 mg, Na_2SiO_3 2 mg, Na_2SO_4 4.06 g, SrCl, 26 mg, and NaCl 25 g, pH 7.0. The ASM was modified to include 20 mM sodium lactate, and 3.9 mM $NaH_2PO_4 \cdot H_2O$ in order to support growth of the organism at levels comparable to previously published reports (Glasauer *et al.*, 2002, 2003).

For reduction experiments, a single colony of the bacteria was transferred, aseptically, from TSA into a flask containing 50 mL of tryptic soy broth (TSB) and grown, aerobically, for 24 hours at 22°C on a rotary shaker set to 150 rpm. The cells were then subcultured in a series of liquid media mixtures in which the concentration of TSB was gradually reduced to 0%, while the concentration of ASM was gradually increased to 100%.

100 mL of cells grown in 100% ASM for 36 hours were concentrated by centrifugation (14,000 × g) and resuspension in a small volume (2-3 mL) of sterile, fresh ASM. This concentrated cell suspension was used to inoculate the experimental biotic systems to an initial cell concentration of 10^7 colony-forming units (CFU)/mL, following established protocols (Glasauer *et al.*, 2002).

The experimental biotic systems consisted of 700 mL sterile ASM in 1 L acid-washed Kimax bottles, amended with 4 mM total iron in the form of either irradiated BIOS or a synthetic hydrous ferric oxide (HFO), which was prepared, aseptically, as described previously (Glasauer *et al.*, 2002). Abiotic control systems were identical to the biotic ones, but they did not contain *S. putrefaciens* CN32.

Laboratory sampling procedure

Eh and pH

Eh measurements were performed on a 3 mL subsample from each Kimax bottle inside the anaerobic chamber, using a standard portable Eh meter and probe (Corning). The same subsample was then removed from the anaerobic chamber for measurement of pH using a standard laboratory pH meter and probe (VWR).

Culture enumeration

A 0.5 mL subsample was removed, aseptically, from each Kimax bottle. From this subsample, 0.1 mL was used to prepare a dilution series for enumeration of live bacteria by the viable plate count technique. Cells were plated onto sterile TSA plates and incubated at 22°C for 24 to 48 hours, until the colonies could be counted.

Determination of Fe(II)

Inside the anaerobic chamber, a 0.5 mL subsample from each bottle was removed and added directly to 4.5 mL of 0.5 M HCl (trace-metal grade) for extraction of total Fe(II). Extraction was performed for a minimum of 24 hours prior to analysis of the sample. An additional 10 mL subsample was withdrawn from each bottle and immediately filtered (using a 0.2 μm nylon syringe filter) inside the anaerobic chamber. 0.5 mL of the filtered solution was added to 4.5 mL of 0.5 M HCl, as described above, for extraction of soluble Fe(II). Total and soluble Fe(II) extracts were analyzed for Fe(II) concentration according to the ferrozine method of Stookey (1970).

Determination of total Fe and P

Samples meant for determination of total Fe and P were digested according to the method of Kulczycki *et al.* (2002), as follows. 6 mL of unfiltered sample were removed from each bottle and added to acid-washed, 20 mL glass scintillation vials. 4 mL of 30% H_2O_2 and 2 mL of concentrated HNO_3 acid (trace metal grade) were added to each 6 mL sample, and the mixture heated to 70°C overnight. This treatment resulted in the complete solubilization of the sample and represented the total Fe and P in each system. The process was repeated using 6 mL of filtered sample taken from each bottle, representing the total soluble Fe and total soluble P.

Digested samples were diluted (1:10) into 1% trace metal grade HNO_3 and analyzed for Fe and P by inductively coupled plasma optical emission spectroscopy using a Varian Vista-PRO CCD Simultaneous ICP-OES, operating under standard conditions.

Electron microscopy

0.5 mL of sample was removed from each bottle for electron microscopy. The samples were chemically fixed by addition of 15 μL of 50% (aq) glutaraldehyde (electron microscopy grade). Fixed samples were washed 5 times in ultrapure water (to remove any salt) prior to being used for the preparation of whole mounts and thin sections, as described previously (Langley and Beveridge, 1999).

Transmission electron microscopy (TEM), selected area electron diffraction (SAED) and energy-dispersive X-ray spectroscopy (EDS) were performed at the Guelph Regional Integrated Imaging Facility (University of Guelph, Guelph, Ontario, Canada) on a Philips CM-10 electron microscope operating at 80 kV. The microscope was coupled to a Soft-imaging Systems (SiS) Morada CCD camera, controlled by SiS iTEM software, and an EDAX Sapphire X-ray detector which collected X-ray spectra over 100 seconds (live count time) at a beam diameter of approximately 200 nm.

Scanning electron microscopy (SEM) with EDS was performed at the Department of Earth Science (Carleton University, Ottawa, Ontario, Canada) on a JEOL JSM-6400 scanning electron microscope operating at 20 kV. This instrument was coupled to a Link Analytical Pentafet X-ray detector, which collected spectra for 80 seconds (live count time).

X-ray diffraction (XRD)

Samples of each iron oxide type were washed 5 times in ultrapure water (to remove any salt) and freeze-dried to preserve their mineral structure (Cornell and Schwertmann, 2003). They were then ground to a fine powder, using a mortar and pestle. Mineral samples remaining in the culture bottles following iron reduction by *S. putrefaciens* CN32 were washed 5 times using de-oxygenated ultrapure water. They were then dried and ground,

using a mortar and pestle, inside the anaerobic chamber to prevent the possible chemical re-oxidation of any reduced iron. An anoxic sample holder was loaded inside the anaerobic chamber and transported inside a sealed jar to the X-ray diffractometer, where the jar was opened and the sample loaded into the machine under a stream of 100% nitrogen. All XRD was performed using a Philips PW 1830 X-ray diffractometer, with a Cu-Kα X-ray source, operating at a tension of 45 kV and a current of 40 mA. Continuous scans were run from a start angle of 5° to an end angle of 80° (2θ).

Mössbauer spectroscopy

The ^{57}Fe Mössbauer spectra were measured at room temperature (293 K) and 78 K in transmission mode using Topologic Systems MD-222B Mössbauer spectrometer against 370-MBq or 925-MBq ^{57}Co in Rh foil. The cryogenic measurements were performed at 78 K using a liquid nitrogen cryostat DN1726 (Oxford Instruments). Each sample was mounted to an Al holder with a 1.0 cm diameter window. The spectra were not corrected for thickness effects (Rancourt *et al.*, 1993). Spectra were analyzed by MossWinn 3.0i (Klencsár *et al.*, 1996), and the curve fitting of spectra was performed by a nonlinear least-squares method assuming that all spectra were composed of Lorentzian-shaped peaks. The isomer shift (IS) was calibrated with respect to the centroid of the sextet of α-iron at room temperature. Each relative peak area of the Fe components was calculated using peak intensity, and the line-width (LW) of the peak as fitting variables. All errors in the fitting parameters are one-SD (1σ) errors, as calculated by MossWinn 3.0i.

Mineral Surface Area

Surface areas were determined by N_2 BET analysis using a BELSORP-mini (BEL Japan). Samples were dried under vacuum for 17 hours at 22°C prior to the analysis (Cornell and Schwertmann, 2003).

RESULTS

X-ray diffraction (XRD)

Representative XRD patterns for the different oxides (prior to reduction) are shown in Figure 2 (a). In each case, the diffraction pattern was dominated by two broad features, approximately centred at d-spacing values of 2.5 Å and 1.5 Å, which are representative of 2-line ferrihydrite. Computer analysis of the patterns generated by the synthetic HFO and the Volcano 19 BIOS failed to indicate the presence of any additional peaks (relative to the background noise of the instrument). In the case of the BIOS from Volcano 1, however, the two reflections appeared less broad, and computer analysis of the pattern indicated numerous additional (although very minor) peaks, including reflections at 4.18, 3.78, 3.19, 2.70, 1.48, and 1.42 Å which suggested the possible presence of small quantities of 6-line ferrihydrite, goethite/lepidocrocite, and magnetite (Figure 2b).

There were no changes in the XRD pattern of either oxide (BIOS or HFO) following incubation under abiotic conditions (data not shown). Following reduction of the oxides by *S. putrefaciens* CN32, however, there was a marked increase in both the number and sharpness of the peaks, indicating mineral transformation as a result of reduction (Fig. 2c). Results were similar for all three iron oxide types (BIOS and HFO). Computer analysis of

the diffractograms (Figure 2d) revealed numerous peaks corresponding to the reduced-iron phosphate mineral vivianite ($Fe_3(PO4)_2 \cdot 8H_2O$).

Mössbauer spectroscopy

The Fe Mössbauer spectra of the BIOS samples recorded at 293 K and 78 K are shown in Figure 3. The RT spectra were simulated by one spectral component with a single doublet. Based on the IS and the quadruple splitting (QS) shown in Table 2, the doublet can be ascribed to high-spin Fe(III) species. Assuming that the first neighbouring atom is oxygen, the IS value can indicate whether the Fe is in octahedral (IS/(mm/s) = 0.3-0.5) or tetrahedral (0.1–0.3) coordination (Menil, 1985). The IS values (0.36 and 0.38 mm/s relative to α-Fe for Volcano 1 and 19, respectively) show that Fe atoms in the samples are in octahedral coordination. There were no Fe(II) doublets observed in the spectra, showing that the amount of Fe(II) species in the BIOS was negligible compared to Fe(III). The IS (0.36 and 0.38 mm/s for Volcano 1 and 19, respectively) and QS (0.79 and 0.85 mm/s) values were similar to those of ferrihydrite reported in previous studies (e.g., Murad and Schwertmann, 1980; Rancourt *et al.*, 2001; Mikutta *et al.*, 2008).

Surface Area

BET analysis of the Volcano 1 and Volcano 19 BIOS yielded surface area measurements of 207 and 92.6 m^2/g, respectively.

Electron microscopy

Transmission electron micrographs and EDS spectra of whole mounts and thin sections taken from the BIOS are presented in Figure 4. In both cases, the samples were dominated by numerous filamentous structures. The surfaces of the filaments appeared to be heavily encrusted in an electron-dense precipitate, and EDS analysis of the precipitate

revealed large peaks corresponding to iron. In the BIOS retrieved from Volcano 19, a distinctly twisted (spiral) stalk was evident in whole mount preparations, also encrusted with an iron-rich precipitate (Figure 5). Selected area electron diffraction of whole mount material did not indicate the presence of any well-ordered mineral phases in either sample.

Scanning electron microscopy of the BIOS from Volcano 19 revealed poorly ordered mineral phases and filamentous structures (Figure 6). In the BIOS from Volcano 1, filamentous structures were again observed and there was a predominance of poorly ordered mineral phases. But also evident were some crystalline habits including plates, needles and some octahedra (Figure 7). In all cases, the mineral phases generated strong iron and oxygen signals when analyzed by EDS (data not shown).

Iron reduction experiments

Eh, pH and cell enumerations

In all abiotic systems, no viable cells were detected and no significant changes in pH were observed for the entire duration of the experiment. There was an initial drop in Eh (from approximately +80 mV to -50 mV) over the first day, followed by a plateau and recovery phase throughout the remainder of the experiment (data not shown).

Cell numbers in the biotic reduction systems showed an initial plateau (at approximately 2×10^6 CFU/mL) over the first 6-12 hours, followed by an increase to approximately 4.5×10^7 CFU/mL by the end of day 1. Cell density remained at this level until between day 4 and day 5, at which point a slight decrease in cell density (to approximately 2.5×10^7 CFU/mL) was observed in all three systems until termination of the experiment at day 7 (data not shown). Over the course of the experiment, there were no significant changes in the pH. The redox potential (Eh) dropped dramatically in all three

systems during the first day following inoculation, decreasing to a minimum (approximately –295 mV) well below that of the abiotic control systems (data not shown).

Fe(II) and phosphorus concentrations

Data for the production of ferrous iron during anaerobic reduction of the various oxides is summarized in Table 3 and Figure 8. The data are presented as the ratio of [total Fe(II)] to [total Fe], so as to account for both soluble and sorbed ferrous iron and particulate Fe(II). Following an initial lag of approximately 1 day, the concentration of Fe(II) in each of the systems increased steadily, reaching a maximum at approximately 4 days following initial inoculation of the cultures. Beyond 4 days, the levels of Fe(II) in each of the systems remained essentially unchanged, represented by a plateau in the graph. In anaerobic systems that were not inoculated with *S. putrefaciens* CN32, no detectable levels of Fe(II) were observed for the entire length of incubation (data not shown).

Because iron reduction (as indicated by an increase in Fe(II) concentration) appeared to take place only over a restricted time frame (i.e., 1 day to 4 days, post-inoculation), rates of iron reduction for each of the oxide mineral types were calculated based solely on the data from this range. Linear reduction rates for each system are presented in Figure 9. Reduction rates for all three oxides displayed linearity, as determined by R^2 values of the fitted regression lines. Rate data and R^2 values are presented in Table 3. Statistical analysis (using t-tests) of the rate data revealed no significant difference in the rates of reduction of BIOS from either volcano ($p < 0.05$). However, rates of BIOS reduction were significantly higher than the rate of reduction of synthetic HFO ($p < 0.05$). In all three systems, there was an overall decrease in soluble phosphorus, while concentrations of total phosphorus remained

constant (data not shown). In abiotic controls, no decrease in either soluble or total phosphorus was observed over the entire length of the experiment (data not shown).

DISCUSSION

The presence of two broad features centred at approximately 1.5 Å and 2.5 Å in the XRD patterns is characteristic of the iron mineral, 2-line ferrihydrite (Cornell and Schwertmann, 2003), which is a poorly ordered iron oxyhydroxide ($Fe_2O_3.nH_2O$). It is reported that ferrihydrite is often superparamagnetic (SP) at RT (273K) (van der Zee *et al.*, 2003), which means that no magnetic splitting (MS) is observed due to the fast relaxation of magnetization for the nanoparticles of ferrihydrite at higher temperature (Murad and Cashion, 2004; Mitsunobu *et al.*, 2008). This fact is also consistent with our results that the magnetic component was absent in the Mössbauer spectra of the BIOS samples collected at RT. In addition, sextet magnetic splitting was not shown in the spectra at 78K. It has been reported that the blocking temperature where MS appears can reveal information on the crystallinity and average particle size of the ferrihydrite (Murad and Cashion, 2004). Although the spectra at lower than 78K are not available (which cannot provide the blocking temperature), the absence of the MS at 78K shows that the crystallinity of the Volcano 1 and Volcano 19 BIOS is less than that of 6-line ferrihydrite (Johnston and Lewis, 1983). Together, the XRD and Mössbauer data presented here indicate that the iron oxide sediments of Volcano 1 and Volcano 19 are dominated by poorly ordered, 2-line ferrihydrite.

Ferrihydrite is often one of the first solid phases to form upon oxidation of ferrous iron in pH-neutral solutions. It is also, typically, the dominant mineral phase associated with microbial iron oxidation in circumneutral surface environments such as springs (James and

Ferris, 2004) and groundwater seeps (Hallberg and Ferris, 2004). With respect to marine hydrothermal systems in particular, Kennedy *et al.* (2003b) have described a BIOS system occurring at Axial Volcano (northeast Pacific Ocean) which was dominated by microbes and mineral particles consistent with biologically-produced iron oxides. The authors identified 2-line ferrihydrite occurring in both blanket deposits and small (0.5 m high) mounds (Kennedy *et al.*, 2004). In addition, Emerson *et al.* (2007) have described similar microbial structures (composed of Fe-oxyhydroxides) in their studies of iron-rich microbial mats occurring at sites of hydrothermal venting near Loihi Seamount in the Hawaiian archipelago (Emerson and Moyer, 2002). Therefore, ferrihydrite and other poorly ordered iron oxyhydroxides appear also to be the dominant phase of iron mineral produced in submarine BIOS systems.

Ferrihydrite commonly undergoes transformation toward goethite and/or lepidocrocite (via continued oxidation and hydrolysis reactions), and hematite (via internal arrangement of atomic structure) (Cornell and Schwertmann, 2003). However, the dominance of the ferrihydrite signal (and lack of peaks for either goethite/lepidocrocite) in the XRD patterns and Mössbauer spectra suggests that, in the Volcano 19 BIOS, the ferrihydrite structure is stabilized, likely due to the presence of the microbial cells and detrital organic material, as described by Kennedy *et al.* (2004) for similar BIOS obtained from the caldera of Axial Volcano. Additionally, silica from the seawater, adsorbed to the ferrihydrite or substituted for Fe within the atomic structure (Fig. 4c), would act to further stabilize it's structure and inhibit transformation to a more crystalline phase (Zhao *et al.*, 1994; Kukkadapu *et al.*, 2003). Alternatively, the rate of production of the ferrihydrite (catalyzed by the microbial metabolism) might simply have exceeded the rate of conversion,

thereby decreasing the percentage of more crystalline forms within the sample to a level that was undetectable by the technique (< ~5 wt %).

The filamentous structures observed by SEM and TEM in the present study are morphologically similar to those described by Kennedy *et al.* (2004) and Emerson *et al.* (2007) for BIOS deposits at Axial and Loihi Seamounts, and the coating of iron oxide on the structures (confirmed by EDS) suggests that the organisms within the Kermadec BIOS may be precipitating the ferrihydrite in a manner similar to that occurring at other submarine hydrothermal sites. However, it is important to note that all microbial cells (and cellular structures) present reactive surfaces that are particularly efficient at binding and precipitating dissolved metals. At saturating concentrations, these reactive surface sites can nucleate the precipitation of a variety of mineral phases, including poorly ordered iron oxyhydroxides (Langley and Beveridge, 1999; Châtellier and Fortin, 2004; Châtellier *et al.*, 2004). In addition, microbial cell surfaces are also effective adsorbents of pre-existing nano- and micro-phase iron oxide crystals, so a coating of such minerals does not necessarily imply active precipitation on the cell surface (Glasauer *et al.*, 2001). Therefore, on the basis of microscopy and cellular morphology alone, we cannot state definitively that the microorganisms are actively precipitating the iron oxide (as opposed to passively binding and/or nucleating iron oxides from the surrounding seawater). However, a more compelling case for active microbial iron oxidation can be made based on the structural features of the iron-oxidizing genus *Mariprofundus*. This organism is a newly described member of the proposed ζ-class of *Proteobacteria*. The cells produce a stalk structure of Fe-oxyhydroxide similar to that shown in Figure 5 (Emerson *et al.*, 2007). The type species, *M. ferrooxydans*, was isolated from iron mats surrounding Loihi Seamount and it's growth is limited to iron

oxidation, with Fe^{2+} (or Fe^{0}) serving as the sole energy source. The presence of morphologically similar structures in the Volcano 19 samples suggests at least a partial active microbial role in the production of the mineral at this site, since *Mariprofundus* is not known to use any electron donors other than reduced forms of Fe. Molecular biological studies are currently underway to fully elucidate the microbial community structure (and identify any iron oxidizers) within the Volcano 1 and Volcano 19 sediments using 16S ribosomal RNA gene sequencing.

The chimney-like structures observed at the Volcano 19 site are unusual, in that no known hydrothermal or volcanic process accounts for the formation of such structures from unconsolidated sedimentary material. Similar structures (e.g., barite/anhydrite chimneys and black/white smokers) along the Tonga-Kermadec arc are formed, chemically, from the interaction of metal-loaded hydrothermal fluid with cold seawater (de Ronde *et al.*, 2005), however these structures are composed of hard rock and mineral assemblages that are structurally resilient. In contrast, the chimney-like structures at Volcano 19 had a gelatinous consistency, and were extremely fragile. Any major disturbance of the structure itself or the surrounding water resulted in the total collapse of the "chimney" and a clouding of the water with flocs of the sedimentary material. We therefore believe that the structures are composed of a mixture of microbial material and associated sediments. The presence of filamentous microbial mats capping the structures, combined with the results of our microscopic examinations, would seem to support this conclusion. The presence of a significant temperature differential (up to 40°C in some instances) between the surface and the interior of the "chimneys" suggests a potential upward flow of hydrothermal fluid within the structure. We therefore propose a process whereby the microbes oxidize ferrous iron from

the hydrothermal fluid to generate energy. As the microbes grow and become mineralized, newly formed cells are produced at the upper surface of the sediment. In this way, the sediments are cemented together in a meshwork of microbial cells and filaments that, over time, grows vertically due to the up-welling of nutrient-laden fluid within the "chimney".

In contrast, at Volcano 1, there was little evidence for active venting. For example, no shimmering water or bubbling, and no significant temperature anomalies were observed. The lack of chimney-like structures at the Volcano 1 site may also be indicative of a lack of significant microbial activity, if chimney formation is dependent on active microbial growth, as we have proposed for Volcano 19. It was therefore believed that the Volcano 1 site is, perhaps, representative of an extinct vent field where microbial activity has slowed or ceased. If this is the case, the continued production of ferrihydrite (and its potential stabilization by the microbiota) would also be decreased, possibly allowing conversion of the mineral towards more crystalline forms. While computer analysis of the XRD pattern generated by Volcano 1 BIOS (prior to reduction) did suggest minor reflections corresponding to the more crystalline iron oxides goethite and magnetite, the reflections from these phases were overwhelmed by the predominance of the ferrihydrite contribution, making accurate identification of the minerals nearly impossible. SEM imaging of the Volcano 1 BIOS revealed the presence of small crystals corresponding to the expected habits of crystalline iron oxides, which were not observed in the Volcano 19 sample by either XRD or SEM. Washing of the samples prior to imaging precludes the possibility that these minerals were evaporites (e.g., halite, sylvite, etc) derived from the growth medium. In addition, EDS revealed that the minerals were rich in Fe and O and were therefore likely not salts, but part of the iron oxide component. While we are aware that SEM alone is

insufficient for determining mineralogy, the presence of iron- and oxygen-rich crystals does tend to corroborate the XRD data for this sample. However, since both SAED and Mössbauer spectroscopy failed to detect the presence of any iron mineral more crystalline than 2-line ferrihydrite, it is likely that the crystals observed by SEM (if they are iron oxides) constitute only a very minor fraction of the overall sediment mass, at or below the limits of detection of the techniques we have used (~ 2 to 5% by weight). Our current supply of samples has been fully depleted, but EXAFS analysis and sequential chemical extractions performed on samples obtained from any future dives should no doubt prove useful in determining the presence and relative proportions of any crystalline phases present. However, until such time as these analyses can be performed, we must assume that the iron oxides at both sites are nearly identical with respect to their mineralogy, at least with respect to their bulk composition.

The overall trends in the growth of *Shewanella putrefaciens* CN32 seen in this study mirror previous findings from freshwater studies using HFO (Glasauer *et al.*, 2002, 2003) and freshwater BIOS (unpublished data), and suggest that cell growth and metabolism were proceeding normally within the various systems. There was an initial lag phase in cell growth and Fe(II) production, likely due to the time required for the cells to adapt to anaerobic conditions. This was followed by an increase in cell numbers, concurrent with an increase in Fe(II) concentration and a decrease in Eh, as anaerobic respiration by the cells drove down the reduction potential of the cultures. The drop in Eh measured for the abiotic systems was not as large as for the biotic cultures and likely represented out-gassing of oxygen from the culture bottles after equilibration with the anoxic atmosphere. The fact that Fe(II) production increased from day 1 to day 5, while cell numbers remained constant,

suggests that the cells were able to derive sufficient energy from the reduction of the BIOS to support limited reproduction. This is confirmed by the fact that when Fe(II) production ceased, the cell numbers began to decline.

The growth pattern described above leads to a roughly sigmoidal curve of Fe(II) concentration (see Figure 8), with the majority of Fe(III) reduction occurring within a restricted space of time, preceded by a lag and followed by a plateau in Fe(II) production. Previous Fe(III) reduction studies (Glasauer *et al.*, 2002, 2003) using *S. putrefaciens* CN32 in a freshwater growth medium have measured continual increases in Fe(II) production over large time spans (e.g., 14 to 20 days). However, we have not observed continual Fe(II) production in any of our marine systems beyond about 4 days, post-inoculation. Using this time frame, reduction rates were calculated and found to be linear (R^2 values ranging from approximately 0.87 to 0.96). The rate reported for HFO reduction in the present study (0.0224 day^{-1}) is within range of those reported for HFO in freshwater reduction experiments (e.g., 0.021 to 0.0357 day^{-1}; Glasauer *et al.*, 2003), and suggests that while the reduction proceeds over a shorter period of time in the marine system, the total percentage of iron reduced is lower than in comparable freshwater studies using HFO. The salinity of the medium is an obvious potential reason for this discrepancy, however on-going studies in our laboratory using freshwater systems also indicates an abbreviated span of iron reduction, usually between 1 to 3 days (unpublished data). At present, we are unable to explain these differences, as all variables and culture conditions have been replicated according to established protocols.

There was no statistically significant difference in the reduction rates obtained for the two volcanic BIOS samples (Table 3), however both BIOS reduction rates were significantly

higher than that obtained for fresh synthetic HFO. This finding runs contrary to both of our original hypotheses. The first hypothesis was that Volcano 1 BIOS should be less reducible than Volcano 19 BIOS, based on presumed sediment aging and potential diagenesis at the Volcano 1 site (which should act to increase the crystallinity of the iron oxides present in those sediments). As both sites were shown to be nearly identical with respect to their bulk mineralogy, however, this finding is not surprising. In addition, rates of microbial iron reduction are typically considered to be proportional to the surface area of the mineral, such that the greater the reactive surface area of the mineral, the more readily it is reduced (Roden and Zachara, 1996; Roden, 2003). Generally, increases in surface area tend to be inversely related to the crystallinity of the mineral (i.e., the more crystalline the iron oxide, the less reactive surface area is available to the microbe). Therefore, based solely on the BET measurements, rates of reduction in the Volcano 1 BIOS should actually have exceeded those of Volcano 19. However, since all BIOS contain both organic and inorganic components, BET measurements of BIOS surface area are often highly variable (Châtellier and Fortin, unpublished data) and may not be a reliable indicator of the actual mineral surface area. It is therefore possible that the Volcano 1 BIOS simply contained a larger fraction of organic material, which led to a higher total measured surface area, even though the mineral surface area might be identical to that of Volcano 19.

An alternative explanation for the identical reduction rates is saturation of the cell and oxide surfaces with Fe(II). Saturation of either surface may have effectively poisoned enzymatic reduction of the Fe(III) by the microbes, thereby halting iron reduction at levels which were similar for both BIOS systems (Roden and Urrutia, 2002). However, while the affinity of Fe(II) for solid-phase ferrihydrite is high (Hansel et al., 2004), electron transfer

between the sorbed Fe(II) and solid-phase iron is rapid (Williams and Scherer, 2004), likely leading to re-oxidation or sequestration of the ferrous iron in secondary minerals such as magnetite (Hansel et al., 2004). Consequently, saturation of the cell surfaces (Roden and Urrutia, 2002) is likely a more important factor in the cessation of iron reduction.

The second hypothesis was that the presence of microbial surfaces within the BIOS samples should act to decrease the interfacial free energy for nucleation of iron oxides (when compared to synthetic iron oxides arising from homogeneous nucleation in solution) and chemically stabilize the nanoparticles of iron oxides (Warren and Ferris, 1998). The fact that the reduction rates of the BIOS were higher than that of the pure HFO suggests the possibility that the organic component of the BIOS may in fact promote its reduction. One possibility is that the organic material might be used by the iron reducing cells as a nutrient source, thereby increasing metabolic activity and, hence, iron reduction. However, no differences in culture growth rate or sustainability were observed in our systems, suggesting that the BIOS did not provide any metabolic advantage to the cells.

Post-reduction XRD analysis of the remaining sediments indicated conversion of the minerals from poorly ordered to crystalline mineral phases. Modeling of the aqueous geochemistry of the growth medium (using PHREEQ-C software) predicted saturation with respect to the reduced-iron phosphate mineral, vivianite. Similar reduction experiments using *S. putrefaciens* CN32 and HFO or BIOS in freshwater systems have produced a variety of reduced and mixed-valence iron mineral phases, including magnetite, maghemite, and vivianite (Fredrickson *et al.*, 1998; Zachara *et al.*, 2002; Glasauer *et al.*, 2002, 2003). Pattern analysis of the post-reduction X-ray diffractograms generated in the present study generated matches for a variety of poorly ordered, hydrated ferrous phosphates of varying

stoichiometry as well as for vivianite. This represents the high concentration of phosphate in the medium, which was observed to decrease over time, as the secondary mineral phosphates precipitated. Typical seawater phosphate concentration is about 1.7 μM (Miyazaki *et al.*, 1981, 1982; Yang *et al.*, 2001). However, sediment porewater phosphate concentrations typically increase with increasing depth in the sediment and can range from 1 to 30 μM (Dahllöf *et al.*, 1997). The natural sediments would, therefore, be undersaturated with respect to vivianite and its formation in this study is essentially artefactual. In the natural system, Fe^{2+} released during microbial reduction would likely be re-oxidized (either chemically or by the microbial consortia), or become sorbed to the surrounding ferric mineral phase and bacterial surfaces, as discussed earlier. Such continued dissolution and re-precipitation of ferrihydrite can lead to increases in the ordering of the mineral phase (Cornell and Schwertmann, 2003). This may explain the slightly increased crystallinity seen in the Volcano 1 sediments, which included weak XRD reflections for goethite and magnetite. Kennedy *et al.* (2003a) found goethite in BIOS sediment samples obtained from Axial Volcano (Juan de Fuca Ridge) and proposed a "localized geological event" which resulted in the production of goethite from the more typical ferrihydrite found at the site. The present study has revealed the susceptibility of marine BIOS to rapid microbial reduction and dissolution. Hence, the cycling of iron between members of the microbial consortia may be responsible for the phase shift noted by Kennedy *et al.* (2003a) at Axial Volcano.

In summary, the iron oxyhydroxide sediments of Volcanoes 1 and 19 on the Tonga-Kermadec Arc appear to be precipitated (at least in part) due to the presence of abundant microbial life, morphologically similar to known iron-oxidizing genera. The mineral phase is precipitated on the cell surfaces, primarily as 2-line ferrihydrite. In the more microbially and

hydrothermally active zone (Volcano 19), the microbes contribute to the formation of chimney-like structures by binding together the otherwise loose sedimentary material into a cohesive columnar structure, possibly fed by internal up-welling of nutrient-laden hydrothermal fluid. In both zones, the presence of the cellular interface and other organic detritus appears to stabilize the ferrihydrite and slow its conversion to more crystalline mineral phases. However, the sediments are readily reduced under anoxic conditions by dissimilatory iron-reducing bacteria, potentially leading to cycles of iron reduction and oxidation that may slowly re-work the poorly ordered ferrihydrite into goethite and mixed valence oxides such as magnetite.

Finally, it is worth noting that the financial costs involved in retrieving samples from any deep-sea environment is extremely high. Furthermore, the MANGO research cruise was a multi-disciplinary excursion, with dives servicing research groups in the fields of microbiology, zoology, geology, geochemistry, hydrothermal fluid chemistry and volcanology. The unavoidable consequence is that the number of samples which could be reasonably obtained for any particular field of interest were somewhat limited. We would, therefore, like to acknowledge that the present study is statistically limited, by having samples from only two sites. However, future dives along the Tonga-Kermadec Arc may yet provide the opportunity for more intensive sampling and analyses.

ACKNOWLEDGMENTS

SL is supported by graduate scholarships from NSERC, the Government of Ontario, and the University of Ottawa. The MANGO research cruise (SO-192/2) was funded by BMBF Project No. 03G0192 (Bundesministerium fur Bildung) awarded to Dr. J. Scholten

(University of Kiel), Dr. R. Botz (University of Kiel), and Dr. U. Schwarz-Schampera (BGR). Canadian participation was made possible by a Natural Sciences and Engineering Research Council of Canada (NSERC) Discovery Grant to MDH, and ROPOS operations were funded by an NSERC Shiptime allocation and Major Facilities Grant. We thank Captain Lutz Mallon and the officers and crew of *FS Sonne*, and Keith Shepherd and his support crew of the Canadian Scientific Submersible Facility. We are grateful to the governments of New Zealand and the Kingdom of Tonga for giving us permission to work in their territorial waters. On-board determination of pH and [Fe(II)] were performed with the assistance of Dr. Matt Leybourne (GNS Science, Lower Hutt, New Zealand). Gamma irradiation was performed at the Public Health Agency of Canada's National HIV and Retrovirology Laboratories (Ottawa, Ontario, Canada). We would like to thank Dragica Bogdanovich for her kind assistance with irradiating the samples, and Dianne Moyles (Department of Molecular and Cellular Biology, University of Guelph) for her expertise with thin sectioning for TEM.

REFERENCES

Baker, BJ, Banfield, JF (2003) Microbial communities in acid mine drainage. *FEMS Microbiology Ecology*, **44**, 139-152.

Châtellier, X, Fortin, D (2004) Adsorption of ferrous ions onto *Bacillus subtilis* cells. *Chemical Geology*, **212**, 209-228.

Châtellier, X, West, M, Rose, J, Fortin, D, Leppard, GG, Ferris, FG (2004) Oxidation of ferrous ions in the presence of various bacterial strains and inorganic ligands. *Geomicrobiology Journal*, **21**, 99-112.

Cornell, RM, and Schwertmann, U (2003) *The iron oxides: structure, properties, reactions, occurrence and uses*. VCH, Weinheim, Germany.

Dahllöf, I, Svensson, O, Torstensson, C (1997) Optimising the determination of nitrate and phosphate in sea water with ion chromatography using experimental design. *Journal of Chromatography A*, **771**, 163-169.

de Ronde, CEJ, Baker, ET, Massoth, GJ, Lupton, JE, Wright, IC, Feely, RA, Greene, RR (2001) Intra-oceanic subduction-related hydrothermal venting, Kermadec volcanic arc, New Zealand. *Earth and Planetary Science Letters*, **193**, 359-369.

de Ronde, CEJ, Faure, K, Bray, CJ, Chappell, DA, Wright, IC (2003) Hyrdrothermal fluids associated with seafloor mineralization at two southern Kermadec Arc volcanoes, offshore New Zealand. *Mineralium Deposita*, **38**, 217-233.

de Ronde, CEJ, Hannington, MD, Stoffers, P, Wright IC, Ditchburn, RG, Reyes, AG, Baker, ET, Massoth, GJ, Lupton, JE, Walker, SL, Greene, RR, Soong, CWR, Ishibashi, J, Lebon, GT, Bray, CJ, Resing, JA (2005) Evolution of a submarine magmatic-hydrothermal system: Brothers Volcano, southern Kermadec Arc, New Zealand. *Economic Geology*, **100**, 1097-1133.

Edwards, KJ, Bond, PL, Gihring, TM, Banfield, JF (2000) An archaeal iron-oxidizing extreme acidophile important in acid mine drainage. *Science*, **287**, 1796-1799.

Edwards, KJ, Rogers, DR, Wirsen, CO, McCollom, TM (2003) Isolation and characterization of novel psychrophilic, neutrophilic, Fe-oxidizing, chemolithoautotrophic α- and γ-*proteobacteria* from the deep sea. *Applied and Environmental Microbiology*, **69**, 2906-2913.

Emerson, D, Moyer, CL (2002) Neutrophilic Fe-oxidizing bacteria are abundant at the Loihi seamount hydrothermal vents and play a major role in Fe oxide deposition. *Applied and Environmental Microbiology*, **68**, 3085-3093.

Emerson D, Rentz, JA, Lilburn, TG, Davis, RE, Aldrich H, Chan, C, Moyer, CL (2007) A novel lineage of Proteobacteria involved in formation of marine Fe-oxidizing microbial mat communities. *PLoS ONE*, **2**, e667.

Fortin, D, Langley, S, Glasauer, S (2008) Biominerals. Recorders of the past? In *Metal Ions in Life Sciences 4: Biomineralization. From Nature to Application* (eds. Sigel, A, Sigel, H, Sigel, RKO). John Wiley & Sons Limited, Chichester, England, p. 391.

Fredrickson, JK, Zachara, JM, Kennedy, DW, Li, S-M, Hinman, NW (1998) Biogenic iron mineralization accompanying the dissimilatory reduction of hydrous ferric oxide by a groundwater bacterium. *Geochimica et Cosmochimica Acta*, **62**, 3239–3257.

Glasauer, S, Langley, S, Beveridge, TJ (2001) Sorption of Fe (hydr)oxides to the surface of *Shewanella putrefaciens*: cell-bound fine-grained minerals are not always formed *de novo*. *Applied and Environmental Microbiology*, **67**, 5544-5550.

Glasauer, S, Langley, S, Beveridge, TJ (2002) Intracellular iron minerals in a dissimilatory iron-reducing bacterium. *Science*, **295**, 117-119.

Glasauer, S, Weidler, PG, Langley, S, Beveridge, TJ (2003) Controls on Fe reduction and mineral formation by a subsurface bacterium. *Geochimica et Cosmochimica Acta*, **67**, 1277-1288.

Hallbeck, L, Pedersen, K (1990) Culture parameters regulating stalk formation and growth rate of *Gallionella ferruginea*. *Journal of General Microbiology*, **136**, 1675-1680.

Hallbeck, L, Pedersen, K (1991) Autotrophic and mixotrophic growth of *Gallionella ferruginea*. *Journal of General Microbiology*, **137**, 2657-2661.

Hallberg, R, Ferris, FG (2004) Biomineralization by *Gallionella*. *Geomicrobiology Journal*, **21**, 325-330.

Hansel, CM, Benner, SG, Nico, P, Fendorf, S (2004) Structural constraints of ferric (hydr)oxides on dissimilatory iron reduction and the fate of Fe(II). *Geochimica et Cosmochimica Acta*, *68*, 3217-3229.

James, R, Ferris, FG (2004) Evidence for microbial-mediated iron oxidation at a neutrophilic groundwater spring. *Chemical Geology*, **212**, 301-311.

Johnston, JH, Lewis, DG (1983) A detailed study of the transformation of ferrihydrite to hematite in an aqueous medium at 92°C. *Geochimica et Cosmochimica Acta*, **47**, 1823–1831.

Kennedy, CB, Martinez, RE, Scott, SD, Ferris, FG (2003a) Surface chemistry and reactivity of bacteriogenic iron oxides from Axial Volcano, Juan de Fuca Ridge, north-east Pacific Ocean. *Geobiology*, **1**, 59-69.

Kennedy, CB, Scott, SD, Ferris, FG (2003b) Characterization of bacteriogenic iron oxide deposits from Axial Volcano, Juan de Fuca Ridge, Northeast Pacific Ocean. *Geomicrobiology Journal*, **20**, 199-214.

Kennedy, CB, Scott, SD, Ferris, FG (2004) Hydrothermal phase stabilization of 2-line ferrihydrite by bacteria. *Chemical Geology*, **212**, 269-277.

Klencsár, Z, Kuzmann, E, Vértes, A (1996) User-friendly software for Mössbauer spectrum analysis. *Journal of Radioanalytical and Nuclear Chemistry*, **210**, 105-118.

Kukkadapu, RK, Zachara, JM, Fredrickson, JK, Smith, SC, Dohnalkova, AC, Russell, CK (2003) Transformation of 2-line ferrihydrite to 6-line ferrihydrite under oxic and anoxic conditions. *American Mineralogist*, **88**, 1903-1914.

Kulczycki, E, Ferris, FG, Fortin, D (2002). Impact of cell wall structure on the behaviour of bacterial cells as sorbents of cadmium and lead. *Geomicrobiology Journal*, **19**, 553-565.

Langley, S, Beveridge, TJ (1999) Effect of O-side-chain-lipopolysaccharide chemistry on metal binding. *Applied and Environmental Microbiology*, **65**, 489-498.

Lovley, D, Phillips, EJP (1988) Novel mode of microbial energy metabolism: organic carbon oxidation coupled to dissimilatory reduction of iron or manganese. *Applied and Environmental Microbiology*, **54**, 1472-1480.

McNamara, NP, Black, HIJ, Beresford, NA, Parekh, NR (2003) Effects of acute gamma irradiation on chemical, physical and biological properties of soils. *Applied Soil Ecology*, **24**, 117-132.

Menil, F (1985) Systematic trends of the ^{57}Fe Mössbauer isomer shifts in (FeO_n) and (FeF_n) polyhedra. Evidence of a new correlation between the isomer shift and the inductive effect of the competing bond T-X (→Fe) (where X is O or F and T any element with a formal positive charge). *Journal of Physics and Chemistry of Solids*, **46**, 763-789.

Mikutta, C, Mikutta, R, Bonneville, S, Wagner, F, Voegelin, A, Christl, I, Kretzschmar, R (2008) Synthetic coprecipitates of exopolysaccharides and ferrihydrite. Part I: Characterization. *Geochimica et Cosmochimica Acta*, **72**, 1111–1127.

Mitsunobu, S, Sakai, Y, Takahashi, Y (2008) Characterization of Fe(III) (hydr)oxides in arsenic contaminated soil under various redox conditions by XAFS and Mössbauer spectroscopies. *Applied Geochemistry*, in press.

Miyazaki, A, Kimura, A, Umezaki, Y (1981) Determination of ng ml^{-1} levels of phosphorus in waters by diisobutyl ketone extraction and inductively coupled plasma atomic emission spectrometry. *Analytica Chimica Acta*, **127**, 93-101.

Miyazaki, A, Kimura, A, Umezaki, Y (1982) Indirect determination of sub-ng ml^{-1} levels of phosphorus in waters by di-isobutyl ketone extraction of reduced molybdoantimonylphosphoric acid and inductively-coupled plasma emission spectrometry. *Analytica Chimica Acta*, **138**, 121-127.

Murad, E, Schwertmann, U (1980) The Mössbauer spectrum of ferrihydrite and its relations to those of other iron oxides. *American Mineralogist*, **65**, 1044–1049.

Murad, E, Cashion, J (2004) *Mössbauer Spectroscopy of Environmental Materials and their Industrial Utilization.* Kluwer Academic Publishers, Boston, USA.

Myers, CR, Nealson, KH (1990) Respiration-linked proton translocation coupled to anaerobic reduction of manganese(IV) and iron(III) in *Shewanella putrefaciens* MR-1. *Journal of Bacteriology*, **172**, 6232-6238.

Park, SH, Lee, HS, Lee, HK (2001) Preservation of marine heterotrophic bacteria by using a deep-freezing method. *Journal of Microbiology*, **39**, 240-243.

Rancourt, DG, Fortin, D, Pichler, T, Thibault, P-J, Lamarche, G, Morris, RV, Mercier, PHJ (2001) Mineralogy of a natural As-rich hydrous ferric oxide coprecipitate formed by mixing of hydrothermal fluid and seawater: Implications regarding surface complexation and color banding in ferrihydrite deposits. *American Mineralogist*, **86**, 834-851.

Rancourt, DG, Mcdonald, AM, Lalonde, AE, Ping, JY (1993) Mössbauer absorber thickness for accurate site population in Fe bearing minerals. *American Mineralogist*, **78**, 1-7.

Rancourt, DG (1998) Mössbauer spectroscopy in clay science. *Hyperfine Interactions*, **117**, 3-38.

Regelous, M, Collerson, KD, Ewart, A, Wendt, JI (1997) Trace element transport rates in subduction zones: evidence from Th, Sr and Pb isotope data for Tonga-Kermdec arc lavas. *Earth and Planetary Science Letters*, **150**, 291-302.

Roden, EE, Zachara, JM (1996) Microbial reduction of crystalline Fe(III) oxides: influence of oxide surface area and potential for cell growth. *Environmental Science and Technology*, **30**, 1618-1628.

Roden, EE, Urrutia, MM (2002) Influence of biogenic Fe(II) on bacterial crystalline Fe(III) oxide reduction. *Geomicrobiology Journal*, **19**, 209-251.

Roden, EE (2003) Fe(III) oxide reactivity toward biological versus chemical reduction. *Environmental Science and Technology*, **37**, 1319-1324.

Stoffers, P, Worthington, TJ, Schwarz-Schampera, U, Hannington, MD, Massoth, GJ, Heknian, R, Schmidt, M, Lundsten, LJ, Evans, LJ, Vaiomo'unga, R, Kerby, T (2006) Submarine volcanoes and high-temperature hydrothermal venting on the Tonga Arc, southwest Pacific. *Geology*, **34**, 453-456.

Stookey, LL (1970) Ferrozine – a new spectrophotometric reagent for iron. *Analytical Chemistry*, **42**, 779-781.

Warren, LA, Ferris, FG (1998) Continuum between sorption and precipitation of Fe(III) on microbial surfaces. *Environmental Science and Technology*, **32**, 2331-2337.

Williams, AGB, Scherer, MM (2004) Spectroscopic evidence for Fe(II)-Fe(III) electron transfer at the iron oxide-water interface. *Environmental Science and Technology*, **38**, 4782-4790.

van der Zee, C, Roberts, D, Rancourt, DG, Slomp, CP (2003) Nanogoethite is the dominant reactive oxyhydroxide phase in lake and marine sediments. *Geology*, **31**, 993-996.

Yang, L, Sturgeon, RE, Lam, JWH (2001) On-line determination of dissolved phosphate in sea-water by ion-exclusion chromatography inductively coupled plasma mass spectrometry. *Journal of Analytical Atomic Spectrometry*, **16**, 1302-1306.

Zachara, JM, Kukkadapu, RK, Fredrickson, JK, Gorby, YA, Smith, SC (2002) Biomineralization of poorly crystalline Fe(III) oxides by dissimilatory metal reducing bacteria (DMRB). *Geomicrobiology Journal*, **19**, 179-207.

Zhao, JM, Huggings, FE, Feng, Z, Huffman, GP (1994) Ferrihydrite surface structure and its effects on phase transformation. *Clays and Clay Minerals*, **42**, 737-746.

Table 1. Sample site data for putative biogenic iron oxides at Volcano 1 and Volcano 19, Tonga Arc, Pacific Ocean

Volcano	Latitude	Longitude	Depth (m)	Ambient water T (°C)	Sediment T (°C)	[Fe(II)] (ppm)	pH
1	21°, 9.2034' S	175°, 44.7600' W	197.8	19	23	0.02	7.25
1	21°, 9.2046' S	175°, 44.7636' W	197.0	16	17.2	0.11	7.50
19	24°, 48.2712' S	177°, 1.1352' W	986.6	5.2	25	0.47	6.10
19	24°, 48.3528' S	177°, 0.1644' W	503	6.9	42	0.09	6.63

Table 2. Mössbauer measurements obtained for Volcanoes 1 and 19.

Sample	**IS[a] (mm/s)**	**QS[b] (mm/s)**	**LW[c] (mm/s)**
Volcano 1	0.362 (1)[d]	0.785 (1)	0.516 (1)
Volcano 19	0.379 (1)	0.852 (1)	0.540 (1)

[a] isomer shift with respect to that of α-Fe foil
[b] quadrupole splitting
[c] full width at half maximum
[d] errors (in parentheses) are in scientific notation (e.g., 1.24 (5) = 1.24 ± 0.05)

Table 3. Reduction data for each of the iron oxide types during the period of active reduction (1 to 4 days, post-inoculation).

Iron Oxide Type	**Maximum [$Fe(II)_{total}$] (mM)**	**Maximum % Fe reduced**	**Linear Reduction Rate**	**R^2**
Synthetic HFO	1.201	24.99	0.0224 d^{-1}	0.87
Volcano 1 BIOS[a]	1.243	31.47	0.0521 d^{-1}	0.94
Volcano 19 BIOS[a]	1.659	32.62	0.0473 d^{-1}	0.96

[a] no statistically significant difference between the reduction rates for the two BIOS samples, however both were significantly higher than the reduction rate for synthetic HFO ($p < 0.05$).

Figure Legends

Figure 1. a) iron oxide "chimneys" at Volcano 19. The structures measure 2 to 3 m in height. Note the lighter coloured mats capping each structure, and the flocculent nature of the material after it has been disturbed by the robotic arm of the ROV. **b)** iron oxide sediments at Volcano 1. Note the absence of chimney-like structures at this site. The darker brown patches are ash deposits overlying the rust coloured iron oxide sediments.

Figure 2. a) X-ray diffraction patterns generated by the HFO and BIOS prior to reduction, showing broad reflections at 1.5 and 2.5 Å, indicative of 2-line ferrihydrite **b)** computer analysis of the Volcano 1 BIOS indicated several additional minor reflections above background, some of which correspond with more ordered iron oxides such as 6-line ferrihydrite, goethite/lepidocrocite and magnetite **c)** X-ray diffraction patterns generated by the mineral phases produced during reduction of the HFO and BIOS by *S. putrefaciens* CN32 **d)** computer analysis of all post-reduction mineral phases indicated the presence of vivianite. Patterns in a) and c) have been vertically separated on an arbitrary y-axis, for clarity.

Figure 3. Mössbauer spectra of Volcanoes 1 and 19 recorded at 293 K (left) and 78 K (right), where the circles indicate the measured vales, while the curves are the simulation results by the methods written in the text.

Figure 4. a) Transmission electron micrograph (unstained whole mount) of BIOS material from Volcano 19 showing filamentous microbial structures. Similar results were obtained for

Volcano 1 BIOS. **b)** Transmission electron micrograph (unstained thin section) of BIOS material from Volcano 1, showing a filament in cross section. An electron-dense mineral crust is obvious surrounding the structure. Similar results were obtained for Volcano 19 BIOS. **c)** EDS spectrum of the encrusting material from b), showing the elemental composition of the crust. The C and Cu peaks are generated by the specimen support grid.

Figure 5. Transmission electron micrograph (whole mount) of a twisted microbial stalk structure observed in the Volcano 19 BIOS. The structure is typical of the iron-oxidizing genus *Mariprofundus*. The sample is unstained and electron density is provided solely by the iron oxide coating precipitated on the stalk.

Figure 6. Scanning electron micrograph of BIOS from Volcano 19, showing filamentous structures and poorly defined mineral precipitates.

Figure 7. Scanning electron micrograph of BIOS from Volcano 1, showing numerous filamentous structures, poorly defined mineral phases, and a variety of well-defined crystal habits including plates, needles and small octahedra (inset). Portions of this figure appear in Fortin *et al.*, 2008 (reproduced with permission).

Figure 8. Increases in [total Fe(II)] as a function of [total Fe] for HFO and BIOS samples during anaerobic reduction by *S. putrefaciens* CN32. The plateau in Fe(II) production after Day 4 represents the end of the reduction period. Both BIOS samples were reduced to a

greater extent than the synthetic HFO. Data represent means ± standard deviations for three individual replicates.

Figure 9. Reduction rates for the three iron oxides were linear during the period of reduction occurring between 1 and 4 days post-inoculation. Correlation coefficients and rate data for the plots are provided in Table 3.

Figure 1

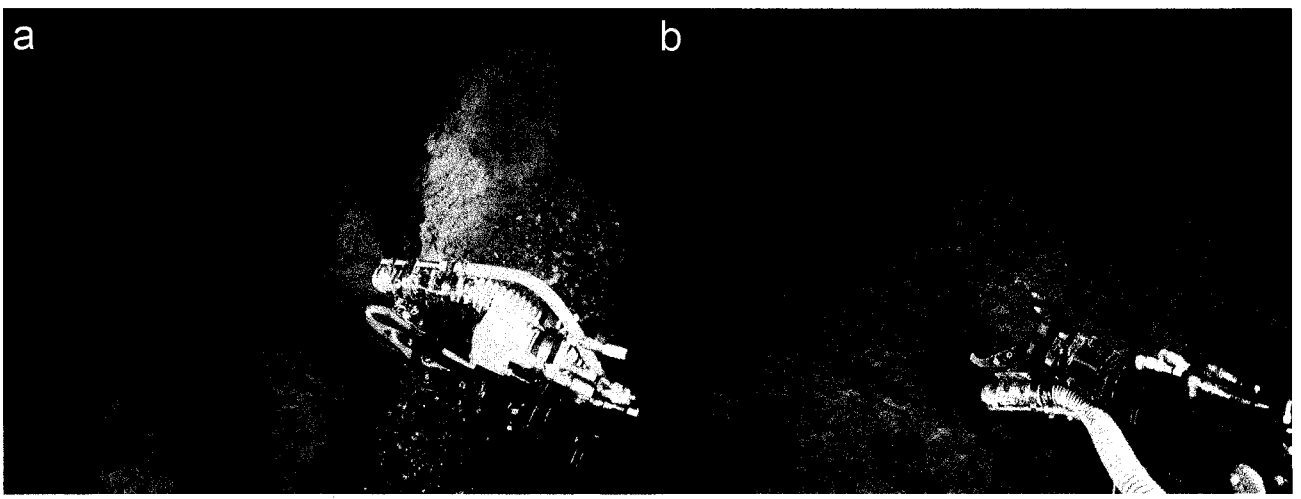

Figure 2

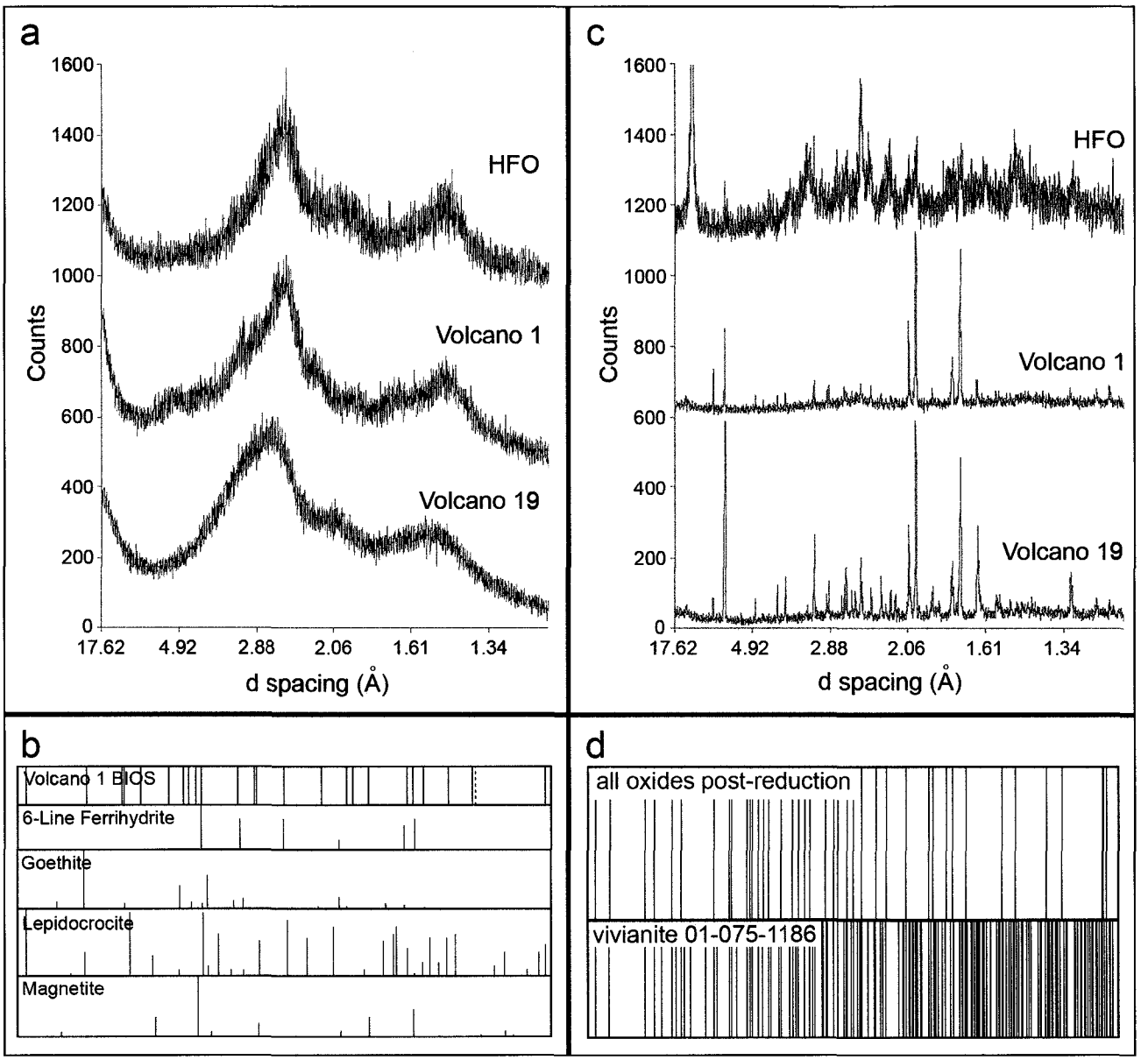

Figure 3

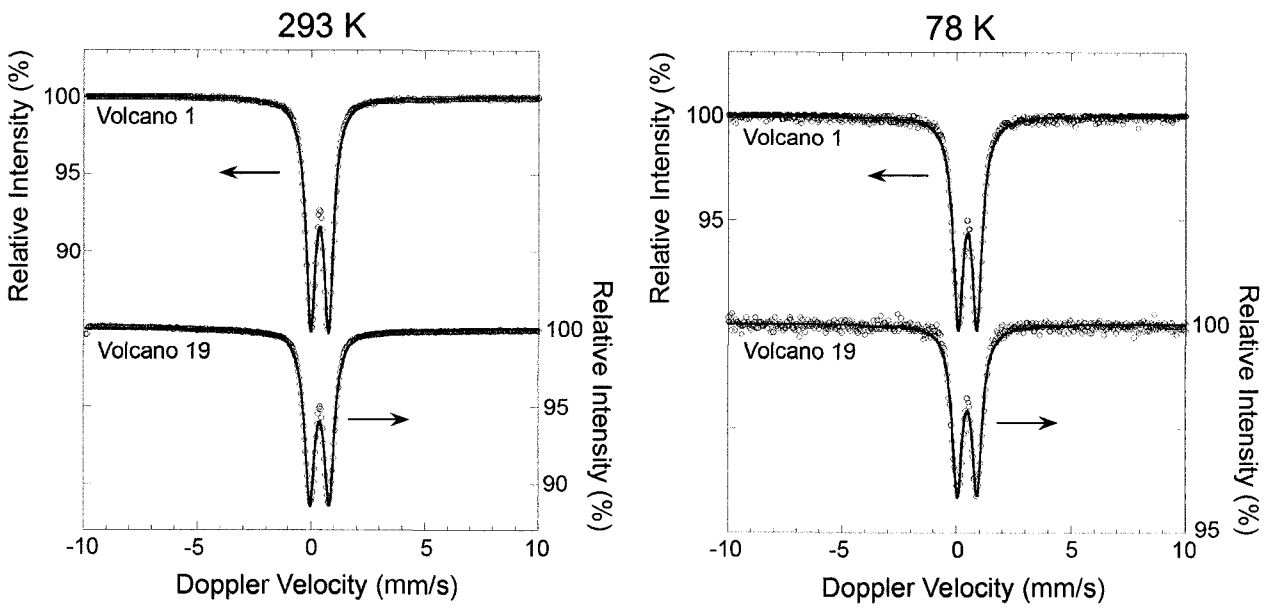

Figure 4

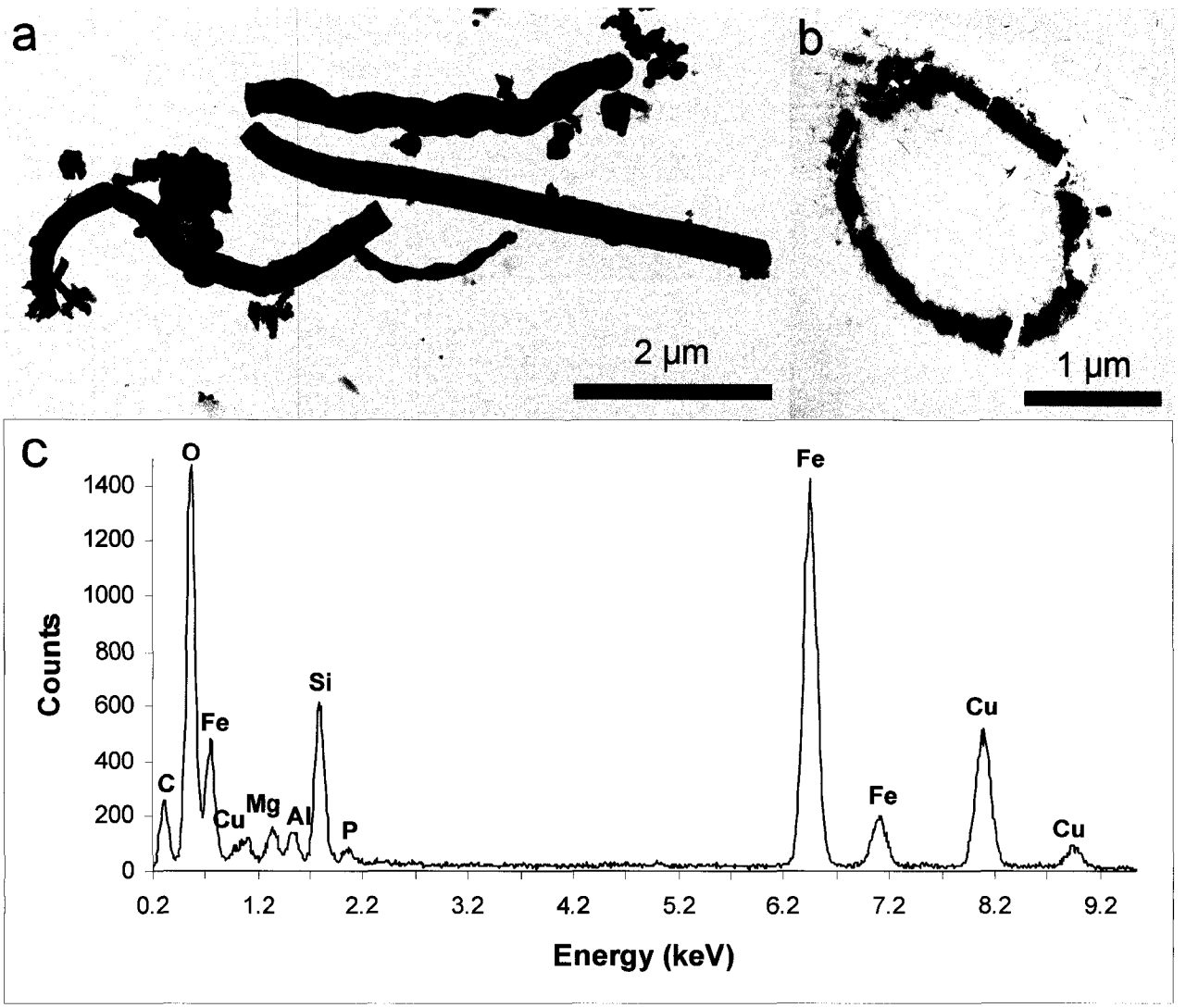

Figure 5

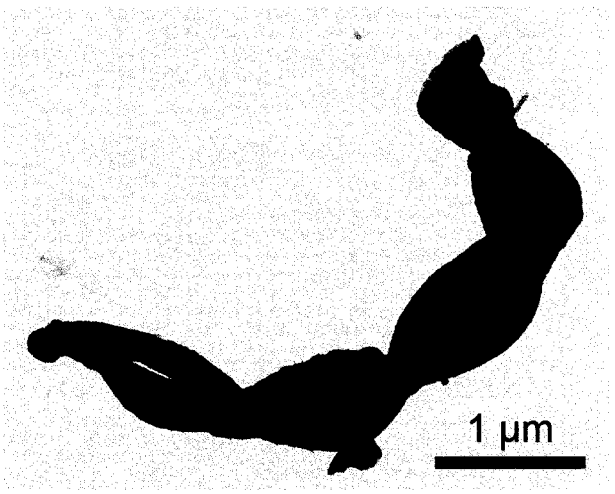

Figure 6

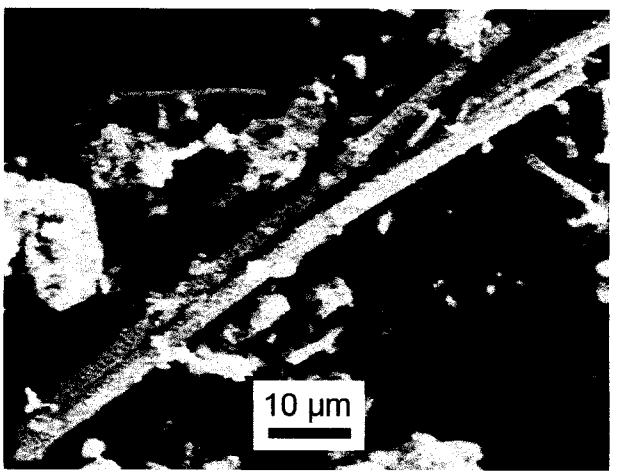

Figure 7

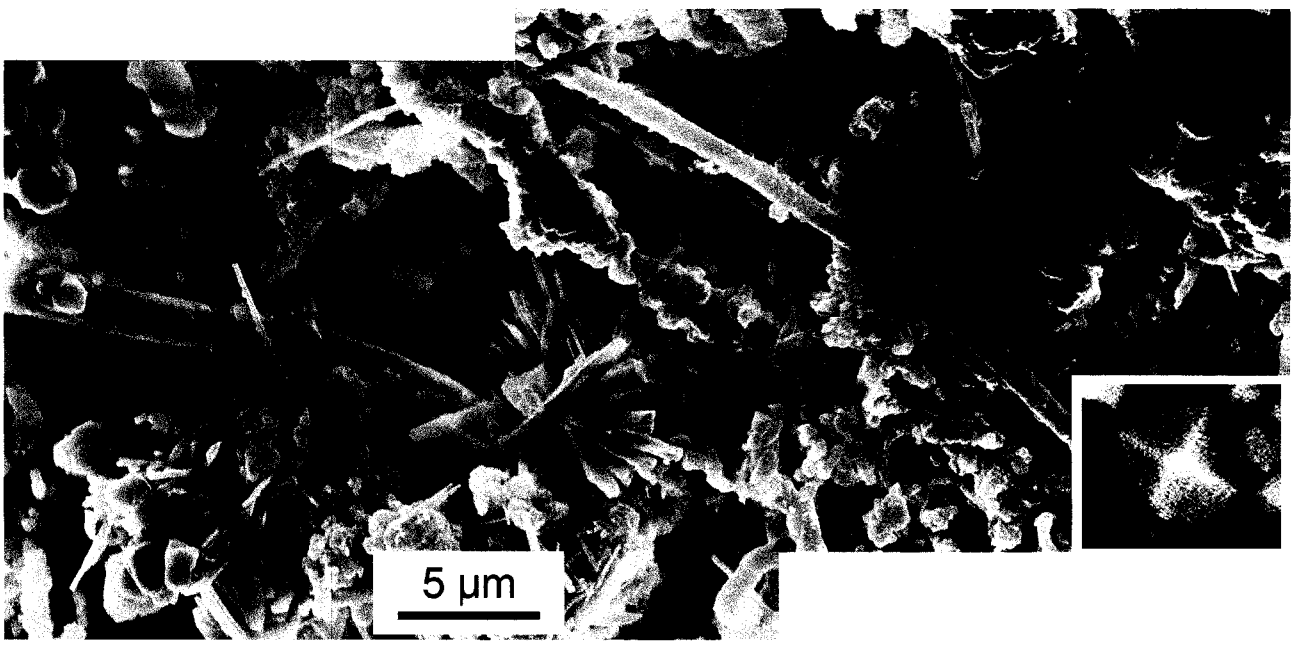

Figure 8

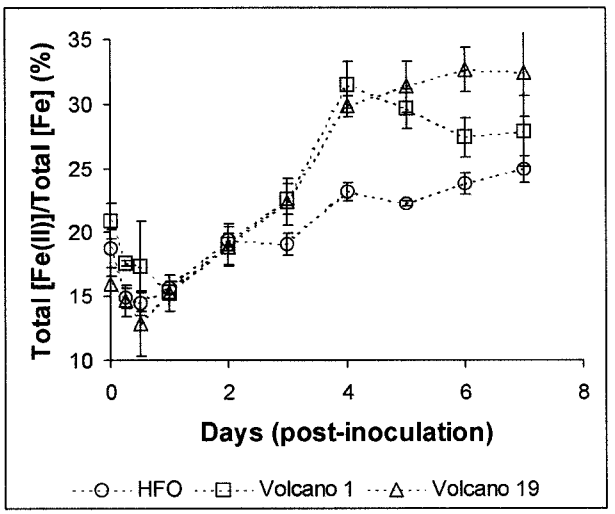

Figure 9

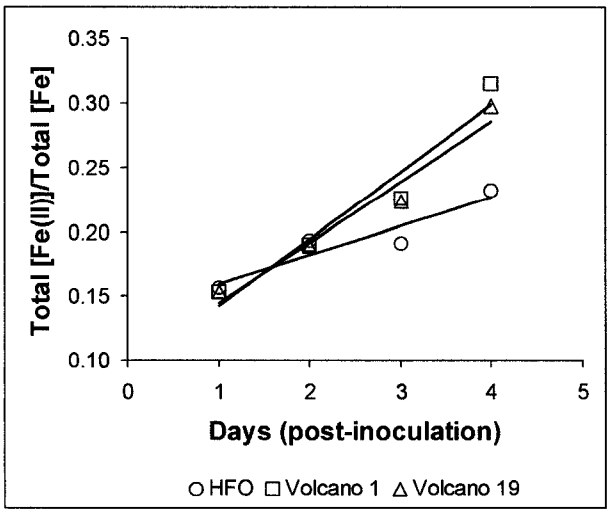

Conclusions

With respect to the specific objectives outlined in the Introduction to this thesis, the following general conclusions can be made:

1) BIOS from both the freshwater and marine environments reported in this study were dominated by the poorly ordered iron mineral, 2-line ferrihydrite, as determined by XRD, electron diffraction, and Mössbauer spectroscopy. This confirms the hypothesis that BIOS are comprised of amorphous or poorly ordered iron oxyhydroxides. Surface area-to-mass ratios were variable, likely due to variations in the mass of the associated organic fraction. However, values were still high, indicative of their small particle size. The mineral was usually in direct association with the surfaces of microbial structures. Often, these structures were morphologically distinct, being associated with known or suspected iron-oxidizing microbes such as *Gallionella* spp., *Mariprofundus* spp., or *Leptothrix* spp. Identification of these organisms through 16S rRNA gene sequencing has conclusively demonstrated their presence in the microbial consortia, and indicate an active microbial role in the precipitation of the ferrihydrite at these sites.

2) BIOS from the Chalk River aquifer and Äspö BRIC bind significant quantities of aqueous strontium. Sorption to Chalk River BIOS is maximal at pH values of 7.5 or higher, and is significantly inhibited by increases in the ionic strength of the aqueous milieu. Sorption occurs via reversible, outer-sphere complexation between hydrated Sr^{2+} and sites within the BIOS (however, the precise binding site could not be accurately determined using EXAFS). In a natural setting, the presence of BIOS within the groundwater flow path is correlated to a decrease in

the concentration of soluble-phase Sr. These data confirm the hypothesis that BIOS are effective sorbents of dissolved Sr, and suggest that BIOS may be an effective means of natural attenuation in aquifers impacted by this contaminant.

3) BIOS are highly susceptible to Fe(III) reduction by dissimilatory iron-reducing bacteria. Both the rate and extent of iron reduction in BIOS are higher than for mineralogically similar, synthetic ferrihydrite. The mineral precipitates which coat the surfaces of the iron-oxidizing cells are completely dissolved within days following the onset of iron reduction. These data are contrary to the hypothesis that the precipitation of ferrihydrite along microbial surfaces might act to stabilize the mineral and make it less susceptible to microbial reduction. This is an important conclusion, as it implies that synthetic fine-grained, hydrous ferrous oxides are not suitable analogs for the study of BIOS. Further, the iron reduction rates measured in vitro for such analogs, while perhaps adequate for some soils and sediments, cannot be extrapolated to a BIOS system, where the iron oxide fraction appears to be significantly more reactive.

4) Microbial reduction of Sr-loaded BIOS results in solubilization of nearly all of the sorbed Sr, which suggests that Sr sorption is linked to Fe oxidation state and that Sr sorbs primarily to sites within the iron oxide component of the BIOS, and not the organic component. In natural BIOS deposits, increased soluble-phase [Sr] is positively correlated with increased [Fe(II)] at depth, confirming a release of Sr coupled to reduction of the Fe(III). This confirms the hypothesis that reductive dissolution of the solid-phase BIOS results in Sr desorption. In vitro data indicate that desorbed Sr remains in solution and does not become sorbed to,

or co-precipitated with, secondary mineral phases (specifically, vivianite). However, in situ data suggest that desorbed Sr will likely sorb back onto the abundant solid-phase BIOS which surrounds zones of Fe(III) reduction.

5) Iron oxyhydroxides from hydrothermal fields at Volcano 1 and Volcano 19 of the Tonga-Kermadec Arc are likely bacteriogenic. As with other BIOS deposits (marine and freshwater), they are composed primarily of 2-line ferrihydrite, encrusting abundant microbial cells and cellular debris. Distinctive microbial morphologies are present within the BIOS, including that of the known, obligate iron-oxidizing bacterium, *Mariprofundus ferrooxydans*. Differences in crystallinity between the two depositional sites (hypothesized) are difficult to elucidate, but BIOS from Volcano 1 may contain iron oxides of increased crystallinity (such as 6-line ferrihydrite, goethite and magnetite). Rates of Fe(III) reduction in the BIOS were higher than measured for synthetic ferrihydrite, again indicating that BIOS are more susceptible to microbial reduction than synthetic and geogenic analogs. However, rates of reduction are identical for both sites, suggesting that any differences in bulk crystallinity between the two sites are insufficient to affect microbial reduction.

Future research

This thesis represents some of the first available data on the reactivity of natural BIOS, and is the only report currently available on the microbial reduction of either freshwater or marine BIOS. As such, it is merely a starting point in the study of these systems. The microcosms used to examine reduction were artificial, being composed of a

well-defined growth medium to support the iron-reducing bacteria. Despite being a minimal medium, it is likely more nutritionally rich than the aqueous environments in which the BIOS are naturally forming. In particular, the high levels of lactate and phosphate seem unreasonably high with respect to mimicking the natural environment. However, the use of the medium was warranted, in order to allow comparison of reduction rate data to previously established values. Also, given that this research was intended to be the first step towards a better characterization of BIOS reactivity, it was reasonable to start with a clearly defined set of experimental parameters. Outlined below are some ideas for future experiments, designed to build upon the current data and, perhaps, move toward a more realistic approximation of the natural setting.

1) Elucidate the composition of the natural groundwater in which the BIOS are forming. The groundwater discharge is likely carbonate-buffered and also likely contains a variety of organic compounds, due to decomposition of leaf litter and other detritus. DIC-DOC analysis and HPLC would prove useful in determining concentrations of carbonate and organic compounds. These concentrations would assist in developing a more realistic growth medium (see 2, below) or improving modeling of factors such as chemical speciation of Fe or trace elements. A similar approach could be taken for the construction of a more realistic artificial seawater medium.

2) Based on the data from groundwater analyses, a chemically-defined growth medium could be developed which would better mimic the natural system in future iron reduction studies. Alternatively (and, perhaps, ideally), native groundwater could be collected from the site and sterilized (e.g., by filtration or

irradiation) prior to use as an unamended growth medium. Use of such a medium would not only provide a more realistic approximation of in situ reduction rates, but the decrease in dissolved phosphate concentration would likely eliminate the artefactual production of vivianite as a secondary mineral precipitate. Consequently, a more accurate understanding of secondary mineral formation in BIOS might be gained.

3) Reduction in the presence of excess solid-phase BIOS also seems warranted. *Shewanella putrefaciens* CN32 appears to require contact with the iron mineral to carry out reduction, so a portion of solid BIOS could be sequestered from the culture during incubation (e.g., using a semi-permeable membrane such as dialysis tubing). By having excess solid-phase material present, the system would provide a better approximation of the natural environment (assuming electron shuttling compounds are not present or could not be used by CN32). This approach would prove particularly useful in elaborating upon the sorption studies. For example, as Sr is desorbed during reduction of the available BIOS fraction, it may simply become re-sorbed onto the non-reducible fraction. The same may be true for soluble-phase Fe(II). Again, examinations of secondary mineral formation may be assisted by this approach, since the excess BIOS may act to limit the accumulation of soluble-phase ferrous iron, and thereby limit saturation of the medium with respect to secondary ferrous iron minerals.

4) Analysis of the BIOS microbial consortia using 16S rRNA gene sequencing should identify iron-reducing bacteria native to the various BIOS communities. This work is currently underway in our laboratory. Re-examination of the

reduction rates using the native species would also provide a more realistic approach to modeling the dynamics of Fe cycling at play within the deposits.

5) Similarly, an examination of reduction could be performed by simply allowing untreated samples of BIOS to become anaerobic. This situation becomes more complicated, however, since preliminary studies of this type have indicated the presence of sulfate-reducing bacteria (SRB). The sulfide produced by these cells would also reduce the ferric iron, chemically, thereby confounding interpretation of the reduction data. However, to circumvent this problem, inhibition of the SRB (using sodium molybdate) could be employed.

It is clear from this research that the reactivity of BIOS is significantly different from that of the synthetic and geogenic analogs commonly used in most in vitro studies. It is also clear that BIOS deposits can become vast, holding enormous quantities of iron, and that BIOS are efficient sorbents of aqueous chemical species. In addition to sorption, precipitation of fresh BIOS may also entrap dissolved contaminants within the nascent mineral. Progressive burial of the newly formed BIOS, combined with microbial respiration of O_2, will act to drive regions of BIOS towards anoxia where iron reduction can proceed. In these regions, iron will be converted back into the ferrous form, and sorbed/co-precipitated contaminants may be released back into solution. The ferrous iron produced in these regions would likely be rapidly re-oxidized (either chemically or biologically) following diffusion into overlying regions of the deposit, thereby completing the Fe redox cycle. Re-oxidation of the iron may again entrap or re-sorb dissolved contaminants. Based on this continued cycle of oxidation and reduction, it seems reasonable to suggest that the residence time of Fe and

trace elements in a BIOS deposit may be very high. BIOS may, therefore, represent an important means of natural bio-attenuation, and their continued study is warranted.

Appendix A

Statement of Candidate's Contributions and Explanation of Manuscript Authorships

Portions of this thesis made use of BIOS obtained from the grounds of Atomic Energy of Canada Limited (AECL) – Chalk River Laboratories (CRL). Access to CRL was made available by a Strategic Project Grant awarded to Dr. Grant Ferris (PI, University of Toronto) by the Natural Sciences and Engineering Research Council of Canada (NSERC). Co-PIs on this grant were Dr. Danielle Fortin (the candidate's supervisor, University of Ottawa) and Dr. Ian Clark (University of Ottawa). On-site administrative and technical support at CRL was provided by Mr. Rob Renaud (formerly with AECL). The grant funded three separate (but related) research projects, which were conducted by the candidate, an MSc graduate student (Alex Ibrahim, University of Ottawa), and a post-doctoral fellow (Dr. Andrew Gault, University of Ottawa). All manuscripts in this thesis were written by the candidate, but all members of the NSERC grant were included in the authorship as a means of acknowledging their thoughts and suggestions from numerous discussions, as well as their comments arising from the journal submission and review process. Similarly, the marine BIOS work was funded by a German federal research grant awarded to Dr. Ulrich Schwarz-Schampera (Cruise Leader, Bundesanstalt für Geowissenschaften und Rohstoffe) and an NSERC Discovery Grant awarded to Dr. Mark Hannington (University of Ottawa), who each appear in the authorship for that manuscript.

All sample collection and preparation was performed by the candidate, with the exception of robotic retrieval of the marine BIOS (performed by the ROV team). All experiments and analyses were performed by the candidate, with the following exceptions. EXAFS analyses required access to (and operation of) a synchrotron light source and

beamline, which were managed by Dr. Yoshio Takahashi (University of Hiroshima, Japan). Mössbauer spectroscopy of marine BIOS required access to equipment that was unavailable to the candidate at the time of study. Consequently, this work was performed by Dr. Yoichi Sakai (Daido Institute, Japan). Assistance with the marine BIOS reductions was provided by Mr. Petar Igric, an undergraduate honours thesis student who worked under the co-supervision of the candidate and Dr. Danielle Fortin. The contributions of these individuals were likewise acknowledged in the authorship of the relevant manuscripts.